THE EFFECTS OF BRONZE AND COMPOSITE SLEEVES ON TRUNNION YOKE PLATE STRESS CONCENTRATIONS

A THESIS IN
Civil Engineering

Presented to the Faculty of the University
of Missouri-Kansas City in partial fulfillment of
the requirements for the degree

MASTER OF SCIENCE

by
THOMAS JOHNATHAN WALKER

B.S., Washington University in St. Louis, 2005
B.A., St. Mary's College of California, 2005

Kansas City, MO
2012

THE EFFECTS OF BRONZE AND COMPOSITE
SLEEVES ON TRUNNION YOKE PLATE
STRESS CONCENTRATIONS

Thomas Johnathan Walker, Candidate for the Master of Science Degree
University of Missouri-Kansas City, 2012

ABSTRACT

Nonlinear simulations were used to predict and further understand the load transfer between trunnion shafts and yoke plates within a tainter gate trunnion assembly. Traditionally, yoke plates have been sized for an average stress based on the projected bearing area between the trunnion shaft and the yoke plate; however, finite element analyses proved that the stress is not uniform across the thickness of the yoke plate. The non-uniform stress distribution is attributed to the transverse shaft rotations that exist at the supports, concentrating load on the inboard edges of the yoke plates. Further study showed that the installation of either a bronze or composite sleeve between the yoke plate and the trunnion shaft will reduce the magnitude of the stress concentrations.

A series of finite element models was developed to investigate the effects that shaft diameter, yoke plate thickness, and sleeve material have on the trunnion shaft to yoke plate load path. The finite element models were developed utilizing solid elements in order to capture the stress distribution across the yoke plate thickness by

including multiple solution points across the yoke plate thickness. The analyses showed that a trend can be identified between the magnitude of the edge stress and the L/D ratio (shaft clear span to shaft diameter). As the L/D ratio of the system is increased, the magnitude of the edge stress increases; however, when a sleeve with a lower modulus of elasticity is introduced into the system, it is observed that the magnitude of the edge stress is reduced. The results proved that the reduction in stress is sensitive to shaft diameter, sleeve material, yoke plate thickness and L/D ratio.

Typically for a yoke-shaft detail, the L/D ratio is designed to be close to 1.0 in order to minimize the inboard edge stress; however, trunnion assemblies with larger L/D ratios are desirable from a tainter gate design perspective. Larger clear spans (L) simplify the connection between the strut arms and the trunnion assembly, and small shaft diameters (D) reduce the trunnion pin friction moment demand on the tainter gate strut arms. By installing a low modulus sleeve between the trunnion shaft and the yoke plate, the magnitude of the edge stress is reduced; therefore, the design can accommodate L/D ratios larger than 1.0 while still keeping the stresses below an acceptable level. The simplified detailing and the reduction in strut arm demand will produce a more cost effective tainter gate design.

APPROVAL PAGE

The faculty listed below, appointed by the Dean of the School of Computing and Engineering, have examined a thesis titled "The Effects of Bronze and Composite Sleeves on Trunnion Yoke Plate Stress Concentrations" presented by Thomas J. Walker, candidate for the Master of Science degree, and certify that in their opinion it is worthy of acceptance.

Supervisory Committee

Kevin Z. Truman, Ph.D., Committee Chair
Department of Civil and Mechanical Engineering
School of Computing and Engineering, Dean

Ganesh Thiagarajan, Ph.D., P.E.
Department of Civil and Mechanical Engineering

John T. Kevern, Ph.D., P.E., LEED AP
Department of Civil and Mechanical Engineering

Michael Bluhm, Ph.D., P.E.
Federal Special Projects, Black & Veatch Corp.

TABLE OF CONTENTS

LIST OF ILLUSTRATIONS

Figure **Page**

LIST OF TABLES

Table **Page**

ACKNOWLEDGEMENTS

A special thank you is owed to Kurt Jacobs without whom this thesis would not have been possible. Kurt Jacobs is a Senior Structural Engineer with the U.S. Army Corps of Engineers, Sacramento District, and he provided the insight and motivation to help get this study off the ground.

The faculty of the University of Missouri-Kansas City's School of Computing and Engineering provided an outstanding academic environment that ensured the growth of this research. Thank you Dr. Kevin Z. Truman, Dr. Ganesh Thiagarajan, and James Mahoney, your technical ability, patience, and mentorship were vital to the success of this project. Additionally, thank you Dr. John Kevern and Dr. Michael Bluhm for your valuable comments during the defense of this thesis, they were appreciated and implemented into the final manuscript.

Most importantly, a heartfelt thank you goes out to my wife, Jessica, and my two sons Matthew and Erik. Jess, you are without a doubt the most amazing woman I have ever met, and I would not have been able to do this without you. Boys, I am looking forward to catching up on some much deserved playtime.

CHAPTER 1

INTRODUCTION

The trunnion assembly is located at the focal point of the radial gate, also known as a tainter gate. The purpose of the trunnion assembly is to transmit the reservoir loads from the tainter gate to a trunnion girder or concrete pier, while still providing a pivot point for the gate to rotate about during gate operations. Figure 1.1 shows a typical tainter gate configuration, including the trunnion assembly.

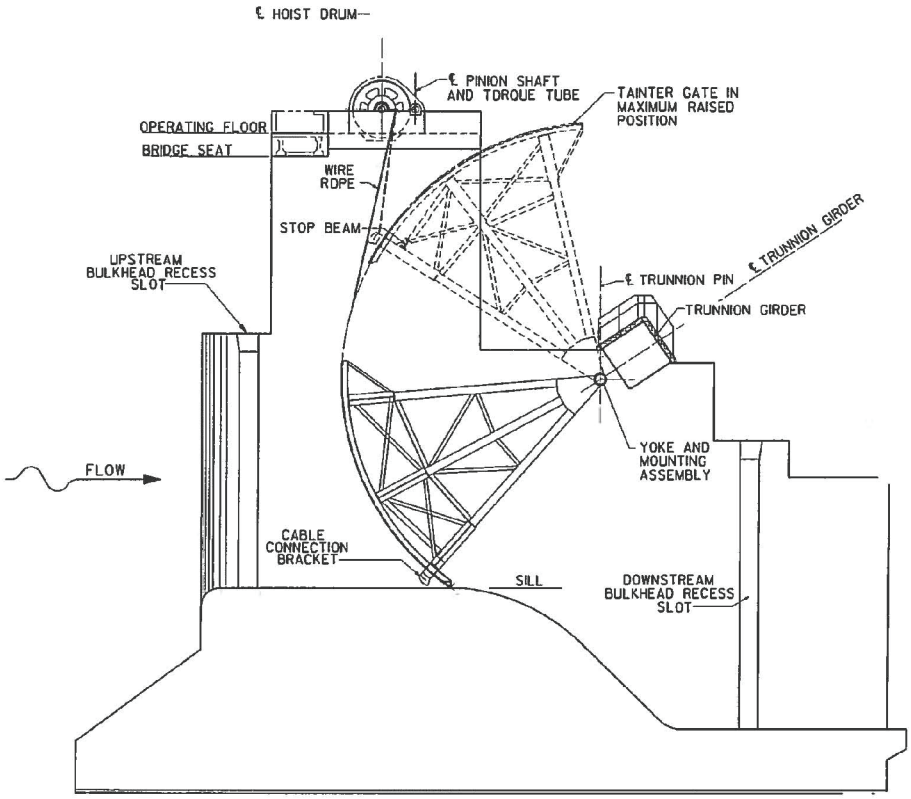

FIGURE 1.1. Typical Tainter Gate Configuration. ***Source:*** **U.S. Army Corps of Engineers *"EM 1110-2-2702, Design of Spillway Tainter Gates"*, Figure 3-6.**

Note that in Figure 1.1 the trunnion assembly is called out as the "yoke and mounting assembly." For the purposes of this document, the term "trunnion assembly" is used as the nomenclature for this structure.

The trunnion assembly is typically comprised of a shaft (also called a trunnion pin in industry) and its supporting yoke plates. The focus of this research was to examine the load transfer between the trunnion shaft and the supporting yoke plates through a series of finite element analyses. Some trunnion assemblies include a sleeve between the trunnion shaft and the yoke plate (see Figure 1.2) that is commonly fabricated from a composite or bronze material. This study focuses on the effects that sleeves have on load transfer between the trunnion shaft and supporting yoke plates.

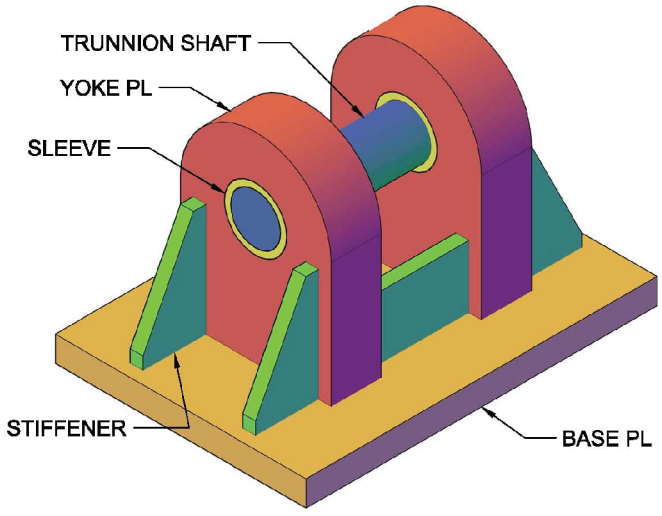

FIGURE 1.2. Typical Trunnion Assembly Configuration

1.1 Literature Survey

The U.S. Army Corps of Engineers has several Engineering Manuals (EMs) that are considered the industry standard for tainter gate design and its components, including trunnion assemblies. These EM's include *EM 1110-2-2702 Design of Spillway Tainter Gates*[1], *EM 1110-2-2105 Design of Hydraulic Steel Structures*[2], and *EM 1110-2-2610 Lock & Dam Gate Operating and Control Systems*[3]. These EMs also make reference to the *American Institute of Steel Construction Manual*[4].

EM 2702 (2000, 4-6) provides some guidance for the structural analysis and design of the trunnion yoke plates, "All components of the trunnion assembly shall be designed based on allowable stress design." In addition, EM 2702 (2000, 4-8) states, "The yoke plate shall be sized to resist trunnion pin bearing load and lateral gate loads."

EM 2105 provides additional details for design that are specific to Allowable Stress Design, including additional modification factors that are to be applied to the strength reduction factors defined by AISC 325. AISC 325 plays an important role in the trunnion assembly design; however, designers should make note that this is a building code; therefore, trunnion assembly design is outside of its scope. Although there is an abundance of relevant information in AISC 325, not everything will be

[1] Hereafter in this thesis, this standard will be referred to as **EM 2702.**
[2] Hereafter in this thesis, this standard will be referred to as **EM 2105.**
[3] Hereafter in this thesis, this standard will be referred to as **EM 2610.**
[4] Hereafter in this thesis, this standard will be referred to as **AISC 325.**

applicable to trunnion assembly design, so engineering judgment and experience is required in order to determine if a building code provision is applicable to tainter gate and trunnion assembly design.

Neither EM 2702 nor EM 2105 provide guidance for selecting an analysis method that will appropriately capture the load path between the trunnion shaft and the supporting yoke plate. EM 2610 provides some guidance that is considered relevant for the designs that include a sleeve between the trunnion shaft and supporting yoke plate. The guidance provided in EM 2610 is specific to bearings; however, this has some relevance for designs that include sleeves of similar materials. EM 2610 (2004, 5-3) states, "Plain Bearings, also identified as sleeve bearings, bushings, etc., should be designed for a maximum normal bearing pressure of 6.9 MPa (1,000 psi), except for bearings operating below five (5) revolutions per minute. Under special, slow speed, uniform load conditions, the bearing pressure may be designed for up to 27.6 MPa (4,000 psi)." For trunnion assemblies the trunnion shaft is typically fixed, so no rotation occurs between the shaft and the sleeves that are installed in the supporting yoke plates. Because there is no rotation, the 27.6 MPa (4,000 psi) is applicable for sleeve design. No reference is made to the appropriate analysis method that should be used to determine the bearing pressure in Chapter 5 of EM 2610; however, Chapter 3 of EM 2610 provides a formula for determining the bearing size:

$$\text{Maximum Load} = \frac{\text{Maximum Applied Load}}{(\text{Shaft Diameter}) \times (\text{Length of Bearing})}$$

Section 3.3 of EM 2610 is specific to wicket gate design, and is not directly applicable to the trunnion assembly design on a tainter gate; however, the simplified P/A method is the most common analysis method that is currently being utilized in industry to analyze load transfer between a trunnion shaft and the supporting yoke plates.

EM 2610 (2004, 5-4) also provides some guidance on the recommended ratio of shaft length to diameter, "The length to diameter ratio (L/D) should be designed close to unity (1.0), considering the bearing pressure required, in order to minimize wear and misalignment." For the purposes of this research, "L" is taken as the clear span of the trunnion shaft. In trunnion assembly design, it is difficult to meet a L/D ratio of 1.0 given that the span of the trunnion shaft is typically controlled by the depth of the tainter gate strut arms. Designers also try to minimize the diameter of the trunnion shaft, as the diameter of the trunnion shaft is directly related to the trunnion shaft friction moment that must be considered in the strut arm design.

1.2 Objective

The primary objective of this research is to predict the magnitude of the stress concentrations on the inboard edges of the yoke plates and the effects that composite and bronze sleeves have on these stresses. With this knowledge, designers can safely design trunnion assemblies with L/D ratios larger than 1.0, which will produce a more cost effective tainter gate design by reducing the trunnion pin friction moment

demand and simplifying the detailing between the tainter gate and the trunnion assembly (more discussion is provided in Section 1.4).

1.3 Relevance to Industry

Tainter gates are critical to a dam's ability to provide flood protection to urban and rural communities located downstream of a dam. The tainter gates allow for controlled releases from the reservoir so that levees downstream of the dam can safely pass the water through the protected region. However, in extreme flood events, tainter gates provide the dam with the capability to release enough water to protect the dam from overtopping by releasing large amounts of water in order to keep the reservoir below the dam's maximum safe elevation. If the maximum reservoir elevation is exceeded, or the dam becomes overtopped, risk of a catastrophic dam failure significantly increases. The trunnion assembly is a hydraulic steel structure that is critical to the overall performance of a tainter gate during a flood event. If the trunnion assembly becomes compromised during a flood event, the tainter gate may become inoperable, and lead to a dam failure.

According to the United States Society on Dams, "in the next five years nearly 60,000 of the more than 80,000 dams in our national inventory will have exceeded their design life." With so many dams exceeding their design life, a significant amount of rehabilitation work will need to be done in the near future in order to keep our critical flood protection infrastructure in safe working order. This effort will

include the analysis and design of tainter gate trunnion assemblies, so it is important for the industry to have a sound understanding of the structural interaction that exists between the trunnion shaft and the supporting yoke plate.

1.4 Relevance to Tainter Gate Design

Typically, the ratio of the shaft clear span to the shaft diameter (L/D) is designed to be as close to 1.0 as possible in order to prevent a significant concentration of load on the inboard edge of the supporting yoke plate; however, small L/D ratios are problematic for tainter gate design. When the clear span of the shaft is small compared to the depth of the strut arm, a custom transition piece is required to make the connection between the tainter gate and the trunnion assembly. The transition piece can be a design challenge, and requires a 3-dimensional finite element model for the structural analysis due to the unique geometry. The transition pieces are also difficult to fabricate because there is a significant amount of welding that is required to be performed in a concentrated area, and care must be taken to control distortion. A more cost effective solution for both design and fabrication is to eliminate the transition piece from the design all together. The transition piece can be eliminated if the clear span of the trunnion shaft is increased to be larger than the depth of the strut arm. The detailing becomes much simpler because the strut arm can frame directing into the trunnion assembly, eliminating the need for a custom transition piece.

Tainter gate strut arms are typically oriented with the webs spanning in the horizontal direction to simplify bracing connection details; however, the moment that develops due to trunnion pin friction introduces weak axis bending into the strut arms. Designers have an incentive to reduce the magnitude of the trunnion pin friction moment because it can control the strut arm design, leading to a larger structural section and a heavier gate. As shown in the equation below, the trunnion pin friction moment is directly proportional to the diameter of the trunnion shaft.

$$M_f = P \cdot \mu \cdot \left(\frac{D}{2}\right)$$

Where M_f is the trunnion pin friction moment, P is the resultant trunnion load, μ is the coefficient of friction between the trunnion shaft and the trunnion bearing, and D is the diameter of the trunnion shaft. Therefore, the reduction in the trunnion shaft diameter will reduce the demand on the tainter gate because the diameter of the trunnion shaft is directly related to the magnitude of the trunnion pin friction moment. The reduction in demand will allow for a lighter gate and a more cost effective design.

1.5 Scope

This scope of work for this research is outlined below:

1. Investigate the various analysis methods currently available to determine how loads are transferred from the trunnion shaft to the supporting

yoke plate and make recommendations on which analysis method is most suitable.

2. Perform a series of finite element analyses that can capture the effects that yoke plate thickness, trunnion shaft diameter, and sleeve material have on the magnitude of stress concentrations.

3. Post-process the results, and determine if any trends can be identified. If trends are identified, develop a design tool that can be utilized by designers in the future, in lieu of performing a full 3D finite element analysis.

1.6 Thesis Organization

Chapter 1 provides a general introduction to the research, including its relevance, current available guidance, objective, and scope.

Chapter 2 details the three different analysis methods that are currently available to design engineers: (1) Traditional Rigid Body (P/A), (2) Finite Element Analysis – Shell Elements, and (3) Finite Element Analysis – Solid Elements. After a description of each of the methods, an example is provided showing how the methods will produce a wide variance in the stress results.

Chapter 3 provides the general details of the finite element models, including software, boundary conditions, material properties, and contact definitions. Also included are some sensitivity analyses that were performed on load application and mesh size. Some discussion is provided on the various quality control measures that

were implemented to validate the model. The chapter ends by establishing the different parameters for each of the analysis cases that were run as a part of the parametric study.

Chapter 4 documents all of the results of the parametric study. The von Mises stress results are provided for the 3 categories of (1) No Sleeve, (2) Bronze Sleeve, and (3) Composite Sleeve.

Chapter 5 presents the analysis of the results that were presented in Chapter 4, and proposes some design aids for consideration by future trunnion assembly designers.

Conclusions and recommendations are summarized in Chapter 6. Also included is a list of topics that may be considered for future studies.

CHAPTER 2

ANALYSIS METHODS

Generally there are three different methods that have been used to quantify the load transfer between the trunnion shaft and the yoke plate: (1) Traditional Rigid Body (P/A), (2) Finite Element Analysis – Shell Elements, and (3) Finite Element Analysis – Solid Elements. This chapter provides general information about each method, as well as advantages and disadvantages of these methods as it applies to the analysis of a trunnion assembly structure.

2.1 Traditional Rigid Body (P/A)

Traditionally the supporting yoke plate thickness was designed by assuming a simple average stress between the yoke plate and the trunnion shaft

$$\sigma := \frac{P}{A}$$

where P is half of the total trunnion load and A is the projected bearing area based on the trunnion shaft diameter and the yoke plate thickness.

The advantage to this approach is that it is simple, and easy to calculate; however, this approach is considered an over simplification of the problem because is neglects true distribution in the radial direction as well as across the yoke plate thickness. This method underestimates the stresses that develop in this type of connection.

2.2 Finite Element Analysis – Shell Elements

More recently, trunnion assemblies have been modeled 3-dimensionally using shell elements. This is considered an improvement to the Traditional Rigid Body (P/A) Method because it provides a more accurate representation of the load distribution in the radial direction. Still, this analysis is limited because it only provides (1) solution point across the thickness of the yoke plate; thus it does not capture the stress distribution across the yoke plate thickness.

Typically, this method will result in higher stresses than the Traditional Rigid Body (P/A) Method; however, it will still underestimate stresses that can develop in a trunnion assembly yoke plate.

2.3 Finite Element Analysis – Solid Elements

The most appropriate analysis method is to model the trunnion assembly using 3D solid elements. This method is able to capture load distribution in the radial direction as well as the distribution across the thickness of the yoke plate. The disadvantage is that this type of analysis can be time consuming; however, the advantage of capturing the stress distribution in both the radial and longitudinal directions makes this a necessary investment. The Finite Element Analysis – Solid Elements Method was the method selected for this study.

2.4 Example

This section performs the analysis of a simplified trunnion assembly using the three methods described above to further illustrate the importance of selecting an appropriate analysis method for this type of problem. For this example problem, the assembly shown in Figure 2.1 is analyzed and the results and conclusions are presented for each case: (1) Traditional Rigid Body (P/A) Method, (2) Finite Element Analysis – Shell Elements, and (3) Finite Element Analysis – Solid Elements.

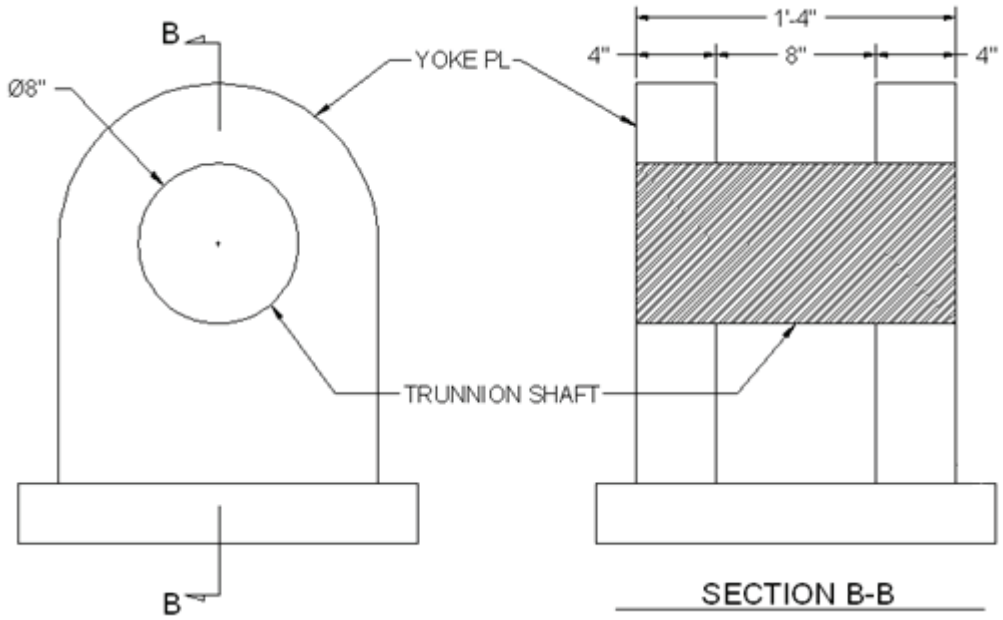

FIGURE 2.1. Trunnion assembly configuration analyzed using the three different methods: (1) Traditional Rigid Body (P/A) Method, (2) FEA – Shell Elements, and (3) FEA – Solid Elements.

The trunnion assembly consists of an 8 inch diameter shaft that spans 8 inches between two 4 inch thick supporting yoke plates. Note that this example problem assumes that no sleeve exists between the trunnion shaft and the yoke plate, and that the steel trunnion shaft bears directly on the bore through the steel yoke plate. The yoke plate is assumed to be fabricated from ASTM A36 steel, and the trunnion shaft is assumed to be a hardened stainless steel (17-4 material) with a yield strength of 100 ksi.

2.4.1 Example – Traditional Rigid Body (P/A) Method

The calculations shown in Figure 2.2 analyze the load transfer between the trunnion shaft and the supporting yoke plates assuming rigid bodies and a projected bearing area equal to the diameter of the shaft times the thickness of the yoke plate. The demand is then compared to the allowable stress as required by EM 2105.

$P := 240kip$	Maximum Resultant Load per Trunnion
$D_{trunnion\_shaft} := 8in$	Diameter of Trunnion Shaft
$t_{yoke} := 4in$	Thickness of Supporting Yoke Plate
$P_{yoke} := \frac{1}{2} \cdot P = 120.0 \cdot kip$	Assumed Load per Yoke Plate
$A_{projected} := D_{trunnion\_shaft} \cdot t_{yoke} = 32.0 \cdot in^2$	Projected Bearing Area Shaft on Yoke Plate
$f_u := \frac{P_{yoke}}{A_{projected}} = 3.8 \cdot ksi$	Bearing Stress Between Shaft and Yoke
$F_y := 36ksi$	Yield Strength of Yoke Plate
$\Omega := 1.67$	ASD Factor per AISC 325
$\alpha := 0.75$	EM 2105 HSS Factor
$F_{all} := \frac{F_y \cdot \alpha}{\Omega} = 16.2 \cdot ksi$	Allowable Stress
"PASS" if $f_u < F_{all}$ = "PASS" "FAIL" otherwise	Criteria Check

FIGURE 2.2. Example problem calculation using Traditional Rigid Body (P/A) Method.

Note that using the Traditional Rigid Body (P/A) Method, the designer is led to believe that the demands are significantly below the allowable stress. The

traditional Rigid Body (P/A) Method produces a demand of 3.8 ksi, where the allowable stress is 16.2 ksi for the material and gate classification that were specified in the example problem.

2.4.2 – Finite Element Analysis – Shell Elements

For the Finite Element Analysis – Shell Elements Method, the same shaft and the yoke plate configuration that was shown in the previous section was modeled. The model took advantage of half symmetry, and the load was applied as a uniform pressure over the top half of the shaft as shown in Figure 2.4.

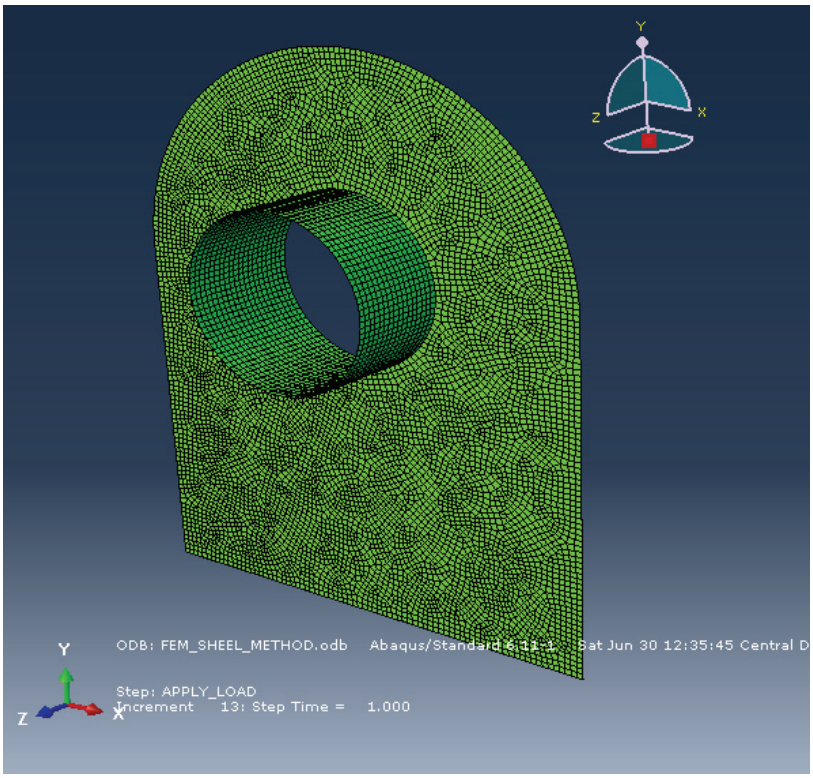

FIGURE 2.3. 0.25 inches x 0.25 inches mesh used to evaluate the example trunnion assembly using the FEA-Shell Elements Method.

Figure 2.3 above shows the mesh that was used to investigate the Finite Element Analysis – Shell Element Method. The typical mesh size was a 0.25 inches x 0.25 inches shell element, where the thickness of the shell elements was defined based on the plate thicknesses targeted. Specifically, the thickness of the yoke plate elements was defined as 4 inches and the thickness of the shaft shell elements was defined as 4 inches. The finite element was defined as a S4R element type within ABAQUS. The S4R is a 4 noded quadrilateral shell element that converges to shear flexible theory for thick shells and classical theory for thin shells (SIMULA). The shell elements were defined from the "Standard Library," the geometric order of the element was set to linear, and the membrane strains were set to finite.

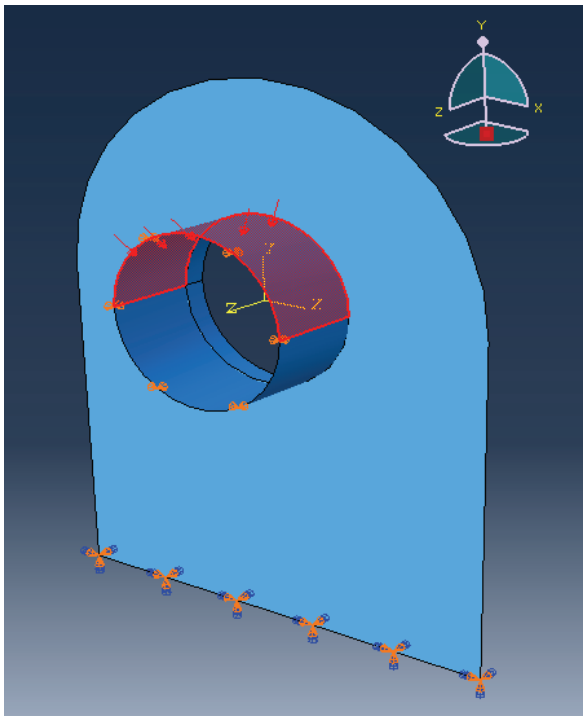

FIGURE 2.4. Load application and boundary conditions used to evaluate the example trunnion assembly using the FEA-Shell Elements Method.

The magnitude of the pressure load was defined as 3,750 psi, which corresponds to a resultant vertical load of 120 kips per yoke plate. Note that this is equivalent to the loading assumed in the Traditional Rigid Body (P/A) Method. See Figure 2.5 for a calculation on the applied loading.

ABAQUS Model Verificaiton **Check Load Input** 6/30/2012

Surface Pressure to Vertica

shaft radius (in)	4
width of loaded area (in)	4
delta theta (rad)	0.031
incremental arc length (in)	0.126
Number of increments (ea)	100
Pressure (psi)	3750
Resultant on Increment Area (kip)	1.885

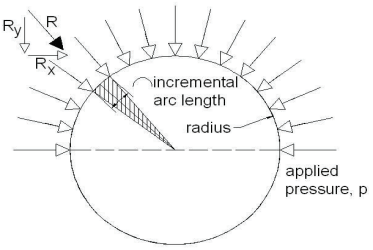

increment	R	theta	Ry	Rx
1	2.83	0.03	0.09	2.83
2	1.88	0.06	0.12	1.88
3	1.88	0.09	0.18	1.88
4	1.88	0.13	0.24	1.87
5	1.88	0.16	0.29	1.86
6	1.88	0.19	0.35	1.85
7	1.88	0.22	0.41	1.84
8	1.88	0.25	0.47	1.83
9	1.88	0.28	0.53	1.81
10	1.88	0.31	0.58	1.79
11	1.88	0.35	0.64	1.77
12	1.88	0.38	0.69	1.75
13	1.88	0.41	0.75	1.73
14	1.88	0.44	0.80	1.71
15	1.88	0.47	0.86	1.68
16	1.88	0.50	0.91	1.65
17	1.88	0.53	0.96	1.62
18	1.88	0.57	1.01	1.59
19	1.88	0.60	1.06	1.56
20	1.88	0.63	1.11	1.52
21	1.88	0.66	1.16	1.49
22	1.88	0.69	1.20	1.45
23	1.88	0.72	1.25	1.41
24	1.88	0.75	1.29	1.37
25	1.88	0.79	1.33	1.33
26	1.88	0.82	1.37	1.29
27	1.88	0.85	1.41	1.25
28	1.88	0.88	1.45	1.20
29	1.88	0.91	1.49	1.16
30	1.88	0.94	1.52	1.11
31	1.88	0.97	1.56	1.06
32	1.88	1.01	1.59	1.01
33	1.88	1.04	1.62	0.96
34	1.88	1.07	1.65	0.91
35	1.88	1.10	1.68	0.86
36	1.88	1.13	1.71	0.80
37	1.88	1.16	1.73	0.75
38	1.88	1.19	1.75	0.69
39	1.88	1.23	1.77	0.64
40	1.88	1.26	1.79	0.58
41	1.88	1.29	1.81	0.53
42	1.88	1.32	1.83	0.47
43	1.88	1.35	1.84	0.41
44	1.88	1.38	1.85	0.35
45	1.88	1.41	1.86	0.29
46	1.88	1.45	1.87	0.24
47	1.88	1.48	1.88	0.18
48	1.88	1.51	1.88	0.12
49	1.88	1.54	1.88	0.06
50	1.88	1.57	1.88	0.00
51	1.88	1.60	1.88	-0.06
52	1.88	1.63	1.88	-0.12
53	1.88	1.67	1.88	-0.18
54	1.88	1.70	1.87	-0.24
55	1.88	1.73	1.86	-0.29
56	1.88	1.76	1.85	-0.35
57	1.88	1.79	1.84	-0.41

increment	R	theta	Ry	Rx
58	1.88	1.82	1.83	-0.47
59	1.88	1.85	1.81	-0.53
60	1.88	1.88	1.79	-0.58
61	1.88	1.92	1.77	-0.64
62	1.88	1.95	1.75	-0.69
63	1.88	1.98	1.73	-0.75
64	1.88	2.01	1.71	-0.80
65	1.88	2.04	1.68	-0.86
66	1.88	2.07	1.65	-0.91
67	1.88	2.10	1.62	-0.96
68	1.88	2.14	1.59	-1.01
69	1.88	2.17	1.56	-1.06
70	1.88	2.20	1.52	-1.11
71	1.88	2.23	1.49	-1.16
72	1.88	2.26	1.45	-1.20
73	1.88	2.29	1.41	-1.25
74	1.88	2.32	1.37	-1.29
75	1.88	2.36	1.33	-1.33
76	1.88	2.39	1.29	-1.37
77	1.88	2.42	1.25	-1.41
78	1.88	2.45	1.20	-1.45
79	1.88	2.48	1.16	-1.49
80	1.88	2.51	1.11	-1.52
81	1.88	2.54	1.06	-1.56
82	1.88	2.58	1.01	-1.59
83	1.88	2.61	0.96	-1.62
84	1.88	2.64	0.91	-1.65
85	1.88	2.67	0.86	-1.68
86	1.88	2.70	0.80	-1.71
87	1.88	2.73	0.75	-1.73
88	1.88	2.76	0.69	-1.75
89	1.88	2.80	0.64	-1.77
90	1.88	2.83	0.58	-1.79
91	1.88	2.86	0.53	-1.81
92	1.88	2.89	0.47	-1.83
93	1.88	2.92	0.41	-1.84
94	1.88	2.95	0.35	-1.85
95	1.88	2.98	0.29	-1.86
96	1.88	3.02	0.24	-1.87
97	1.88	3.05	0.18	-1.88
98	1.88	3.08	0.12	-1.88
99	1.88	3.11	0.06	-1.88
100	0.94	3.14	0.00	-0.94
SUM	188.50	-	120.02	0.00

Check Total Force	188.50	OK

FIGURE 2.5. Applied load calculation that determines the vertical force that results from a pressure applied over half the shaft's surface area.

The shell model produced a peak combined stress of 6.3 ksi. A plot of the von Mises contours is shown in Figure 2.6.

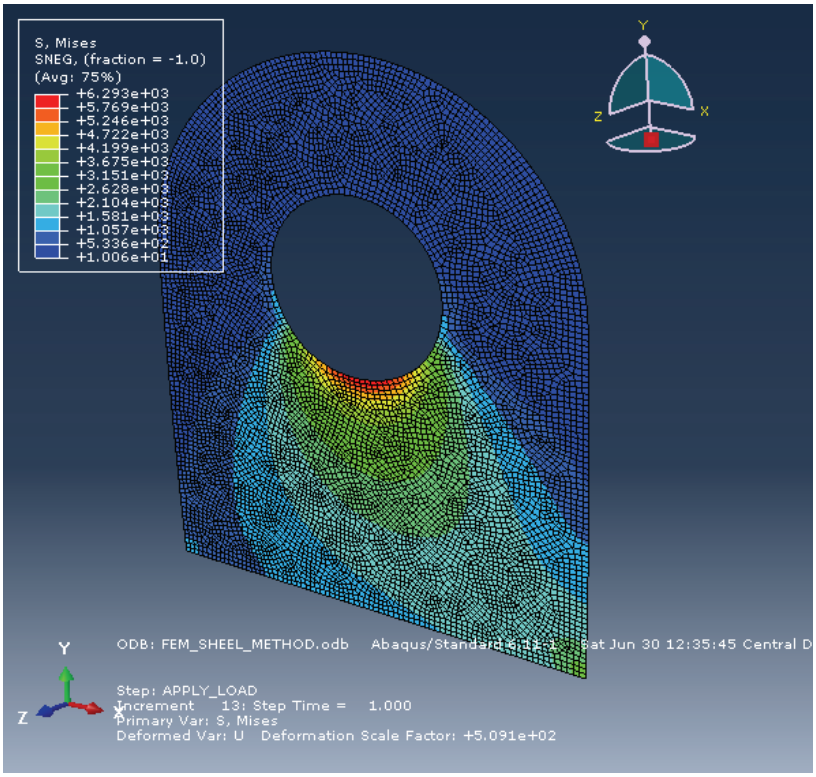

FIGURE 2.6. Von Mises stress results from the FEA-Shell Elements Method

Note that the Finite Element Analysis – Shell Elements Method produced a higher stress than what the Traditional Rigid Body (P/A) Method produced; however, the calculated demand is still well below the allowable stress limit defined by EM 2105.

The Finite Element Analysis – Shell Elements Method assumes that the yoke plate will deform uniformly across the thickness of the yoke plate. The model provides (1) solution point across the thickness of the yoke plate; thus it is assuming a uniform average stress distribution across the thickness of the yoke plate.

2.4.3 – Finite Element Analysis – Solid Elements

For the Finite Element Analysis – Solid Elements Method, the same configuration was modeled as described for the previous two methods. Again, the model took advantage of half symmetry, and the load was applied as a uniform pressure over the top half of the shaft.

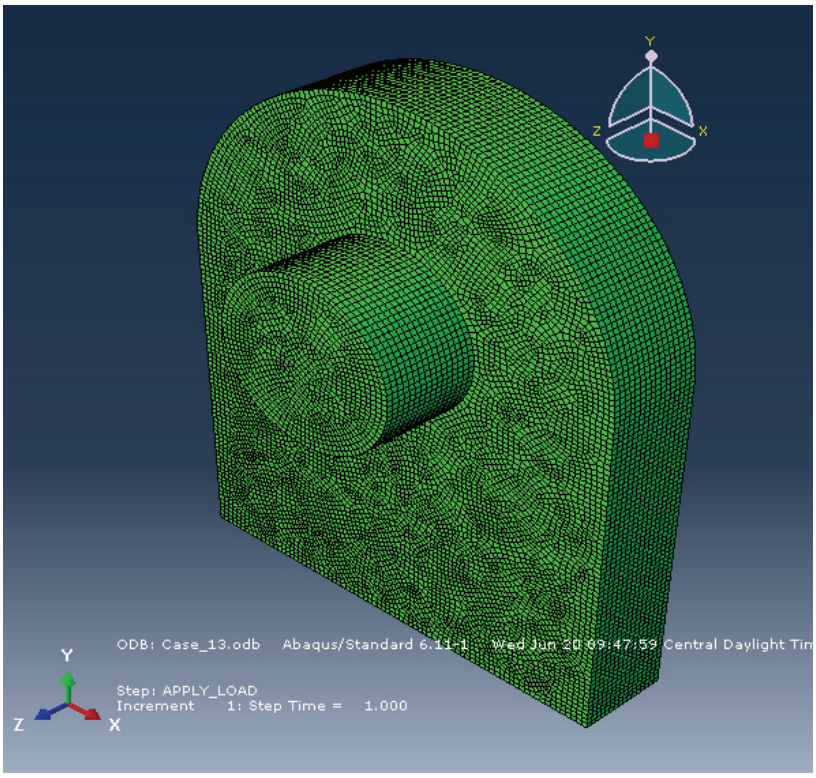

FIGURE 2.7. 0.25 inches x 0.25 inches x 0.25 inches mesh used to evaluate the example trunnion assembly using the FEA-Solid Elements Method.

Figure 2.7 shows the mesh that was used to investigate the Finite Element Analysis – Solid Elements Method. The mesh consisted of solid elements that were

typically 0.25 inches wide x 0.25 inches long x 0.25 inches high. Additional details specific to the finite element analysis using solid elements is provided in Chapter 3. The magnitude of the applied pressure was 3,750 psi, similar to the shell model because the same configuration of shaft and yoke plate was modeled. See Figure 2.5 for the calculation of the applied pressure. Figure 2.8 shows how the load was applied to the model.

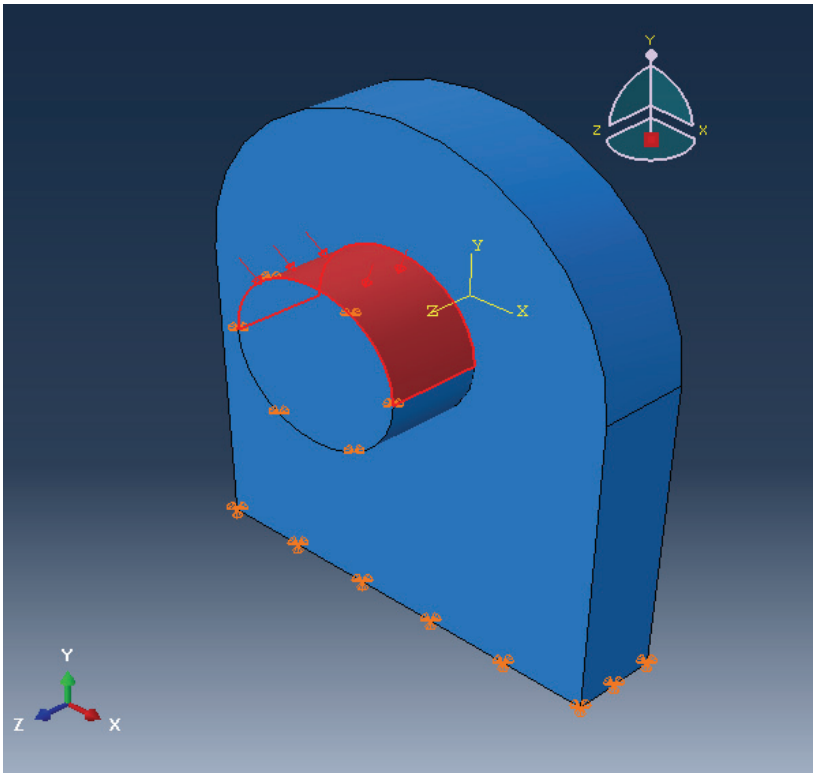

FIGURE 2.8. Load application and boundary conditions used to evaluate the example trunnion assembly using the FEA-Solid Elements Method.

The peak stress at the edge was found to be 12.8 ksi, which is significantly higher than the results produced by the Traditional Rigid Body (P/A) Method and the

FEM-Shell Elements. Note that the recorded edge stress is an average of the nodal stresses in the defined edge area (see Chapter 3).

Figure 2.9 shows that the stresses are not uniform across the thickness of the yoke plate; therefore, the nodes located at the inboard edge of the yoke plate experience more strain than the nodes located at the outboard edge of the yoke plate. This phenomenon is attributed to the small transverse shaft rotations that exist at the ends of the shaft.

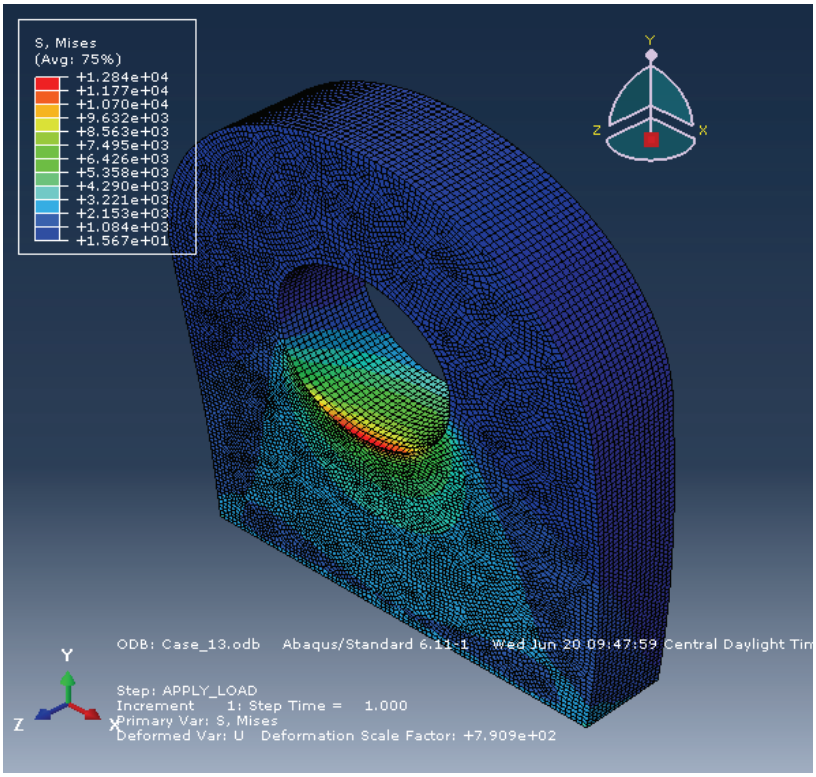

FIGURE 2.9. Von Mises stress results from the FEA-Solid Elements Method

2.4.4 – Example – Summary & Conclusions

The results of the three analysis methods are summarized in Table 2.1.

Table 2.1. Summary of von Mises Stress Results

Analysis Method	Maximum Stress (ksi)
Traditional P/A	3.8
FEM – Shell Elements	6.3
FEM Solid Elements	12.8

This example problem shows that the Traditional Rigid Body (P/A) method and the Finite Element Analysis - Shell Elements methods have the potential to produce stresses that are significantly less than those produced by the Finite Element Analysis - Solid Elements. These two analysis methods are not able to capture the stress distribution across the thickness of the yoke plate; thus when these methods are implemented, a uniform average stress is assumed across the thickness of the yoke plate. The Finite Element Analysis – Solid Element Method proved that the stress is not uniform across the thickness of the yoke plate.

The trunnion shaft is not rigid. When load is applied, the trunnion shaft will deflect, which produces a measurable transverse rotation at the supporting yoke plates. This rotation, all though small, has significant impacts to the stress distribution across the thickness of the yoke plate. The Finite Element Analysis - Solid Elements Method is able to more closely model the true load path between the trunnion shaft and the yoke plate by accounting for the distributions in both the radial direction as well as the distribution across the yoke plate thickness. This example

problem showed that although the distribution in the radial direction is important, capturing the distribution across the thickness of the yoke plate is more critical when determining the maximum stress that can develop between the yoke plate and the trunnion shaft.

2.4.5 – Example – Further Investigation

To further confirm that the conclusions that were described in the previous section, another finite element model was created using solid elements. The model was identical to the model described in the Finite Element Analysis – Solid Elements section, except the modulus of elasticity for the shaft material was increased to 1,000 times the modulus of steel. This was done to simulate a rigid trunnion shaft. Figure 2.10 is a plot of the von Mises stress contours for the rigid shaft analysis.

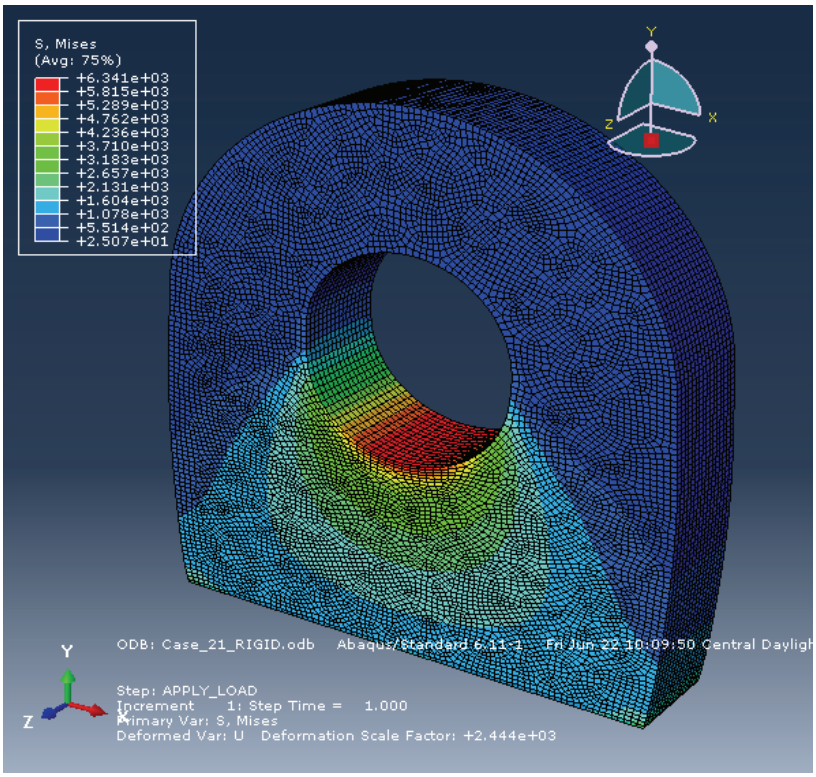

FIGURE 2.10. Von Mises stress results from the FEA-Solid Elements Method when the trunnion shaft is modeled as a rigid.

By modeling a rigid shaft, the stress distribution caused by shaft rotations is taken out of the problem; therefore, we can observe that the model shows that the stress is uniform across the thickness of the yoke plate when no shaft rotations exist. The model still captures the distribution in the radial direction, so a comparison can be made between the rigid shaft model and the flexible shaft model to determine how sensitive the yoke stresses are to the stiffness of the trunnion shaft.

Table 2.2. Comparison of FEA–Shell Elements and FEA-Solid Elements with Rigid Shaft

Analysis Method	Modulus of Shaft Material (ksi)	Von Mises Stress (ksi)
FEA – Solid Elements	29,000	12.8
FEA – Solid Elements	29,000 x 1,000	6.3

As shown in Table 2.2 the rigid shaft model produced stress results that were approximately half of those produced by the flexible shaft model. From this, we can conclude that the magnitude of the stress on the inboard edge of the yoke plate is sensitive to the stiffness of the trunnion shaft.

CHAPTER 3

PARAMETRIC STUDY

This chapter outlines the specifics of the parametric study including general modeling information, as well as sensitivity analyses that were done on the load application and mesh size.

3.1 Finite Element Software

The numerical analysis program ABAQUS was selected as an appropriate software package for performing the parametric study because of its ability to model contacts and non-linear materials using solid elements. This study was performed using ABAQUS CAE Version 6.11-1.

3.2 Boundary Conditions

All of the finite element analyses took advantage of half symmetry; therefore boundary conditions were applied at the centerline of the trunnion shaft as well as at the bottom of the yoke plate. Figure 3.1 shows an example of the boundary conditions that were applied in the models.

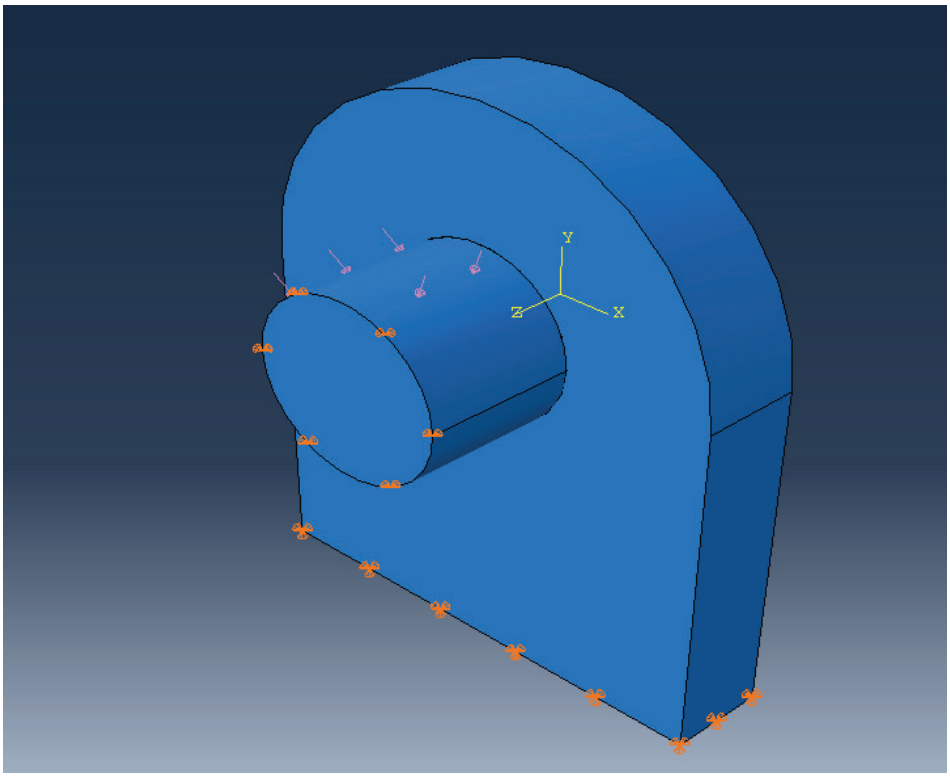

FIGURE 3.1. Typical boundary conditions and loads applied to models.

The boundary conditions applied to the trunnion shaft restrained the cross section from translation in the z-direction (longitudinal) and the x-direction (transverse). The y-direction (vertical) was released such that the cross section was free to move in the vertical direction.

The bottom of the supporting yoke plates were restrained for the three translational degrees of freedom. Since solid elements were used universally, none of the rotational degrees of freedom were restrained.

3.3 Material Properties

The models included four different materials: (1) 36 ksi steel, (2) 100 ksi steel, (3) Bronze, and (4) Composite. All of the materials were modeled with non-linear properties assumed to be elastic perfectly plastic. This simplification was identified as a potential future work topic. Table 3.1 summarizes the material properties that were used in the finite element models.

Table 3.1. Summary of material properties defined in the finite element models.

Component	Material	Modulus of Elasticity (ksi)	Poisson's Ratio	Yield Strength, F_y (ksi)
Trunnion Shaft	Steel (17-4)	29,000	0.29	100
Sleeve	Bronze	14,500	0.34	20
Sleeve	Composite	260	0.231	15
Yoke Plate	Steel (A 36)	29,000	0.29	36

All of the materials were modeled as isotropic materials. Note that the composite sleeve material is not truly isotropic; however, for the scope of this study it was determined to be acceptable because of the stresses in the areas of interest are predominately normal to the composite layers. The variance in the modulus and strength of the composite material, when oriented parallel to the composite layers, was assumed to not affect the magnitude of the stress concentrations. An analysis that includes a more detailed composite material model was identified as a future work item.

3.4 Contact Definition

The model was created by defining two parts: (1) Shaft and (2) Yoke. The interaction between the parts was modeled by specifying the 'General Contact (Standard)' within ABAQUS. The contact properties were defined such that all contacts associated with the trunnion shaft were frictionless (note this was identified as a future work item). For the analyses that modeled a sleeve between the trunnion shaft and the yoke plate, the sleeve was modeled as merged to the yoke plate.

3.5 Finite Element

The finite element analyses used the C3D8R solid element within ABAQUS, which is an 8 node linear hexahedron element from the standard library.

3.6 Load Application

Some sensitivity analyses were used to verify the load application. The load was applied to the model using three different methods: (1) traction over the centerline cross section, (2) pressure over a 90-degree surface, and (3) pressure over a 180-degree surface. Figure 3.2 shows the three different load applications that were investigated.

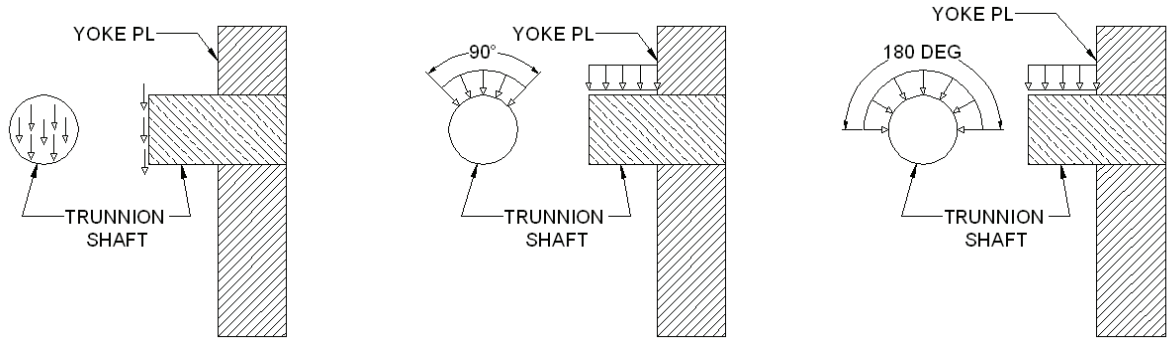

FIGURE 3.2. Sensitivity of three methods used to apply load.

As observed in Table 3.2, the recorded von Mises edge stress converged for the two cases where the load was applied over a surface area of the shaft. The case where the load was applied over the cross section produced slightly higher edge stresses due to the added rotation this loading condition produces at the support; therefore, it was not considered appropriate for this study. For ease of modeling, the load was applied as a pressure over a 180-degree surface in the parametric study.

Table 3.2. Sensitivity of load application.

Trunnion Load (kips)	Loaded Area[5]	Recorded von Mises Edge Stress (ksi)
120	Cross Section - πR^2	29.6
120	90^o Surface Area - $\frac{\pi R}{2}$ x b	25.2
120	180^o Surface Area - πR x b	25.4

[5] Note that variable "b" represents the longitudinal length (along shaft's axis) of the loaded area.

3.7 Definition of Edge

For the purposes of this research, the "edge" was defined as an area of 1 inches x ¼ inches for the configurations that include an 8 inch diameter trunnion shaft, and ½ inches x ¼ inches for the configurations that include a 4 inch diameter trunnion shaft.

The length of the edge distance was set to be a fixed percentage of the circumference of the trunnion shaft's outside diameter. After observing the stress contours of the models, ~4% was deemed appropriate.

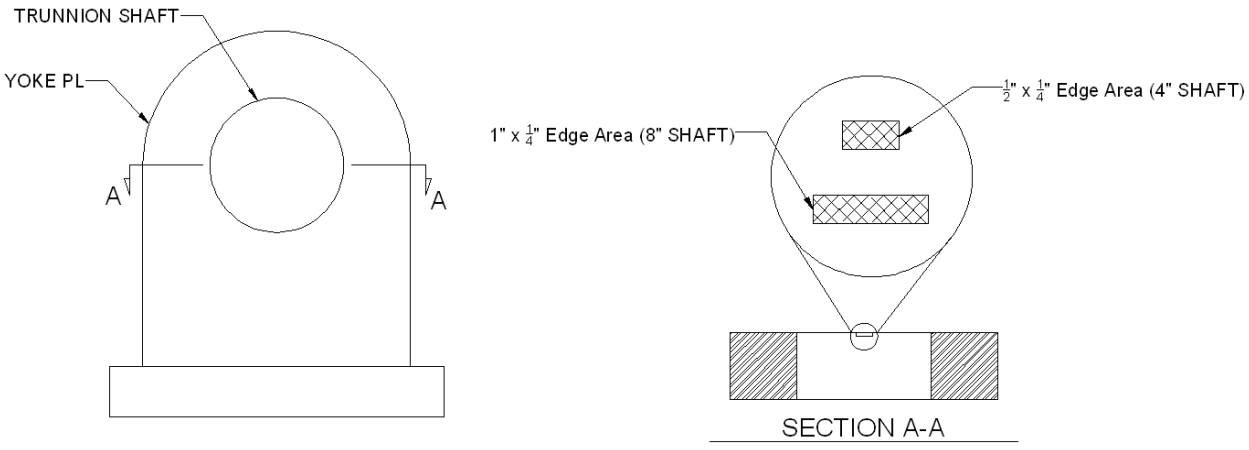

FIGURE 3.3. Location of defined edge area.

3.8 Stress Output

The von Mises stress output is commonly used in the industry to determine the overall combined effects of the different stresses acting on a particular element. In *Elasticity Theory, Applications, and Numerics,* Sadd states, "If at some point in the structure, the von Mises stress equals the yield stress, then the material is considered to be at failure condition. Based on this fact, many finite element computer codes commonly plot von Mises stress distributions based on the numerically generated stress field (SADD p. 66)." Based on this discussion provided by Sadd and the standard within the gate design industry, von Mises was the chosen stress output for models included in the parametric study.

3.9 Mesh Size

The reported edge stress is the average of the nodes that are contained within the previously defined edge area; therefore, a sensitivity analysis was performed to determine how the mesh size affected the magnitude of the stress concentrations located at the inboard edges of the yoke plates. There were two difference sensitivity cases run: (1) ¼ inches mesh size and (2) 1/8 inches mesh size. Figures 3.4 and 3.5 show the two meshes that were considered.

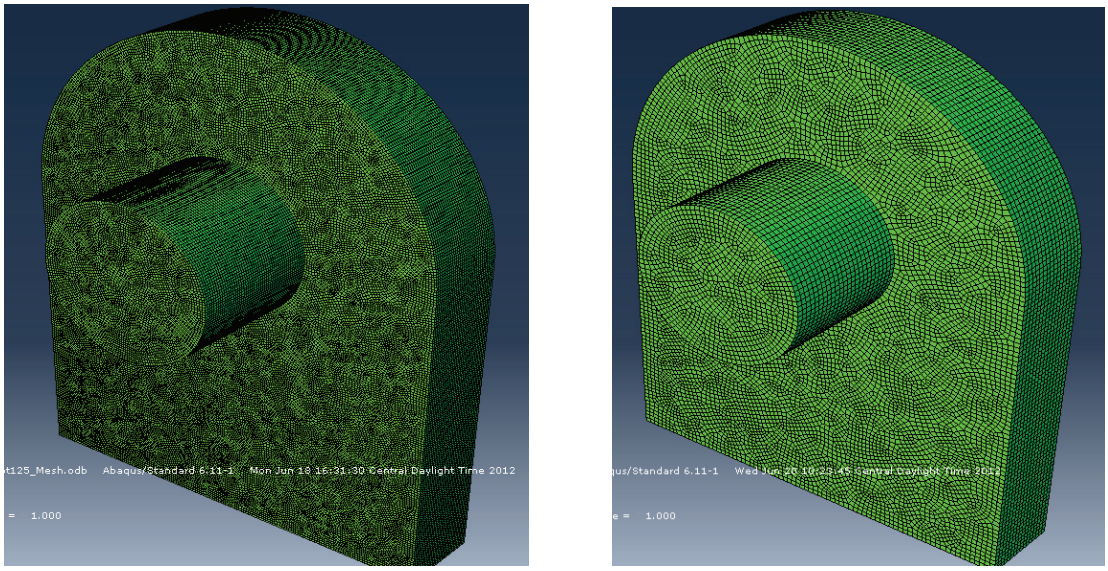

FIGURE 3.4 – Illustrations of meshes used in sensitivity analyses. 0.125 inches Mesh Size (Left) and 0.25 inches Mesh Size (Right).

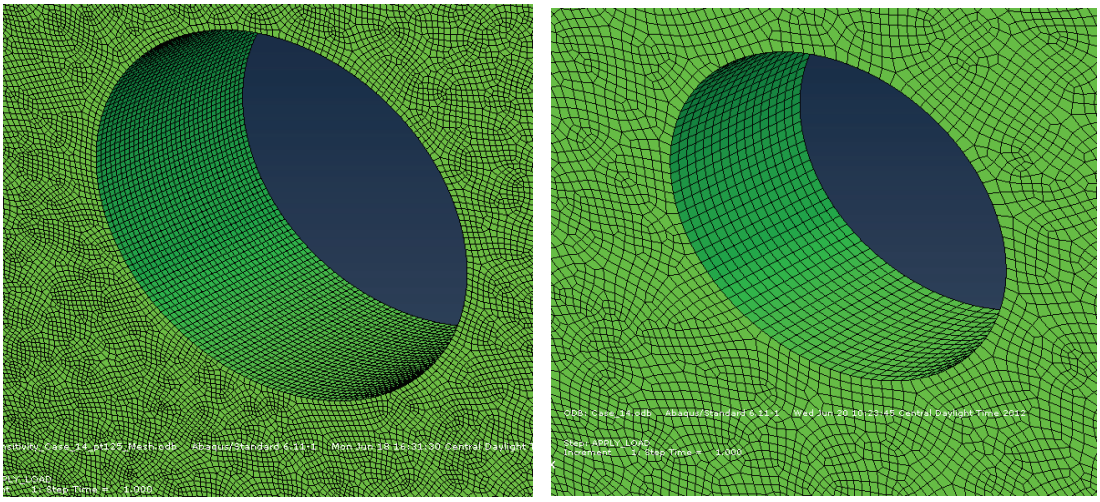

FIGURE 3.5 – Illustration of meshes used in sensitivity analyses, zoomed in on the bore through the yoke plate. 0.125 inches Mesh Size (Left) and 0.25 inches Mesh Size (Right).

The sensitivity analysis was performed on a trunnion assembly configuration that contained an 8 inch diameter trunnion shaft, a 4 inch thick yoke plate, and a clear span of 12 inches. The models were run with the ¼ inches mesh size and again with the 1/8 inches mesh size. As stated above the reported edge stress is an average of all of the nodes contained within the defined "edge" area, which for an 8 inches shaft is 1 inches x ¼ inches. For the ¼ inches mesh this resulted in the average of 10 nodes, and for the 1/8 inches mesh 27 nodes were averaged. See Figure 3.6.

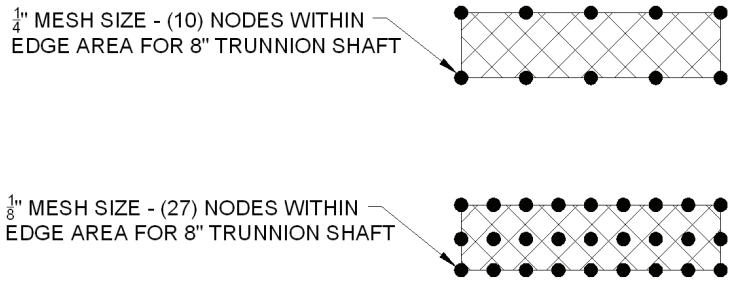

FIGURE 3.6 – Idealized sketch of the number of nodes located within the defined edge area for the two different mesh sizes included in the mesh sensitivity analysis.

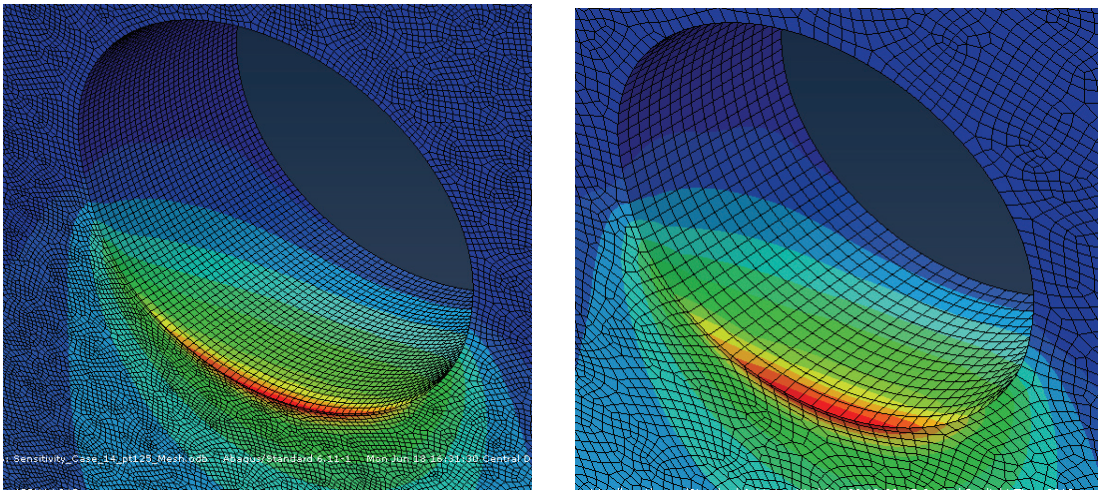

FIGURE 3.7 – Von Mises contour plots, 0.125 inches Mesh Size (Left) and 0.25 inches Mesh Size (Right).

Contour plots are shown in Figure 3.7, and the results are summarized in the Table 3.3. The two models showed that the recorded average stress was converging within 5% of each other; therefore, the ¼ inches inch mesh density was considered acceptable for the parametric study.

Table 3.3. Summary of mesh sensitivity results.

Mesh Size	Nodes within Edge Area	Average Von Mises Stress (ksi)
1/4 inches	10	14.1
1/8 inches	27	14.8

3.10 Parameters of Study

The parameters of the study include: (1) Trunnion Shaft Diameter, (2) Yoke Plate Thickness, (3) Clear Span, and (4) Sleeve Material. By varying each of these parameters, 60 different finite element models were developed. A summary of the individual cases that were analyzed as a part of the study are shown in the Tables 3.4, 3.5, and 3.6.

Table 3.4. Summary of cases without a sleeve.

Case	Sleeve	Shaft Diameter (in)	Trunnion Load (kips)	Yoke Plate Thickness (in)	Clear Span (in)
1	None	4	120	2	2
2	None	4	120	2	4
3	None	4	120	2	6
4	None	4	120	4	4
5	None	4	120	4	8
6	None	4	120	4	12
7	None	4	120	6	4
8	None	4	120	6	8
9	None	4	120	6	12
10	None	8	240	2	8
11	None	8	240	2	12
12	None	8	240	2	16
13	None	8	240	4	8
14	None	8	240	4	12
15	None	8	240	4	16
16	None	8	240	6	8
17	None	8	240	6	12
18	None	8	240	6	16
19	None	8	240	6	20
20	None	8	240	6	4

The size of the trunnion assembly components vary depending on the size of the tainter gate, so this study covered different sizes of trunnion shafts and supporting

yoke in an attempt to determine how sensitive the magnitude of the edge stress was to the overall size of the trunnion assembly components.

Table 3.5. Summary of cases with a bronze sleeve.

Case	Sleeve	Shaft Diameter (in)	Trunnion Load (kips)	Yoke Plate Thickness (in)	Clear Span (in)
101	Bronze	4	120	2	2
102	Bronze	4	120	2	4
103	Bronze	4	120	2	6
104	Bronze	4	120	4	4
105	Bronze	4	120	4	8
106	Bronze	4	120	4	12
107	Bronze	4	120	6	4
108	Bronze	4	120	6	8
109	Bronze	4	120	6	12
110	Bronze	8	240	2	8
111	Bronze	8	240	2	12
112	Bronze	8	240	2	16
113	Bronze	8	240	4	8
114	Bronze	8	240	4	12
115	Bronze	8	240	4	16
116	Bronze	8	240	6	8
117	Bronze	8	240	6	12
118	Bronze	8	240	6	16
119	Bronze	8	240	6	20
120	Bronze	8	240	6	4

The loads were established based on the industry practice to keep the projected bearing pressure near 5 ksi for bearings and sleeves, where the projected bearing area is calculated as described in the previous chapter under 'Traditional Rigid Body (P/A) Method.' The cases that were established resulted in a range of projected bearing pressures from 2.5 ksi to 7.5 ksi.

Table 3.6. Summary of cases with a composite sleeve.

Case	Sleeve	Shaft Diameter (in)	Trunnion Load (kips)	Yoke Plate Thickness (in)	Clear Span (in)
1001	Composite	4	120	2	2
1002	Composite	4	120	2	4
1003	Composite	4	120	2	6
1004	Composite	4	120	4	4
1005	Composite	4	120	4	8
1006	Composite	4	120	4	12
1007	Composite	4	120	6	4
1008	Composite	4	120	6	8
1009	Composite	4	120	6	12
1010	Composite	8	240	2	8
1011	Composite	8	240	2	12
1012	Composite	8	240	2	16
1013	Composite	8	240	4	8
1014	Composite	8	240	4	12
1015	Composite	8	240	4	16
1016	Composite	8	240	6	8
1017	Composite	8	240	6	12
1018	Composite	8	240	6	16
1019	Composite	8	240	6	20
1020	Composite	8	240	6	4

CHAPTER 4

RESULTS

Chapter 4 summarizes the results of the parametric study. The beginning of the chapter provides some discussion on the quality control measures that were implemented to validate the model.

4.1 Model Validation

In addition to the sensitivity analyses that were previously discussed in Chapter 3, the models were further validated by checking the base reactions and relative deflection of the trunnion shaft. See appendices A & B for the details of these validation checks.

4.2 Von Mises Stress – No Sleeve

The results of the analysis cases that did not include a sleeve between the trunnion shaft and the supporting yoke plate are documented in this section. Figure 4.1 shows a representative contour plot; however, the contour plots for all of the configurations that were analyzed without a sleeve are documented in Appendix C.

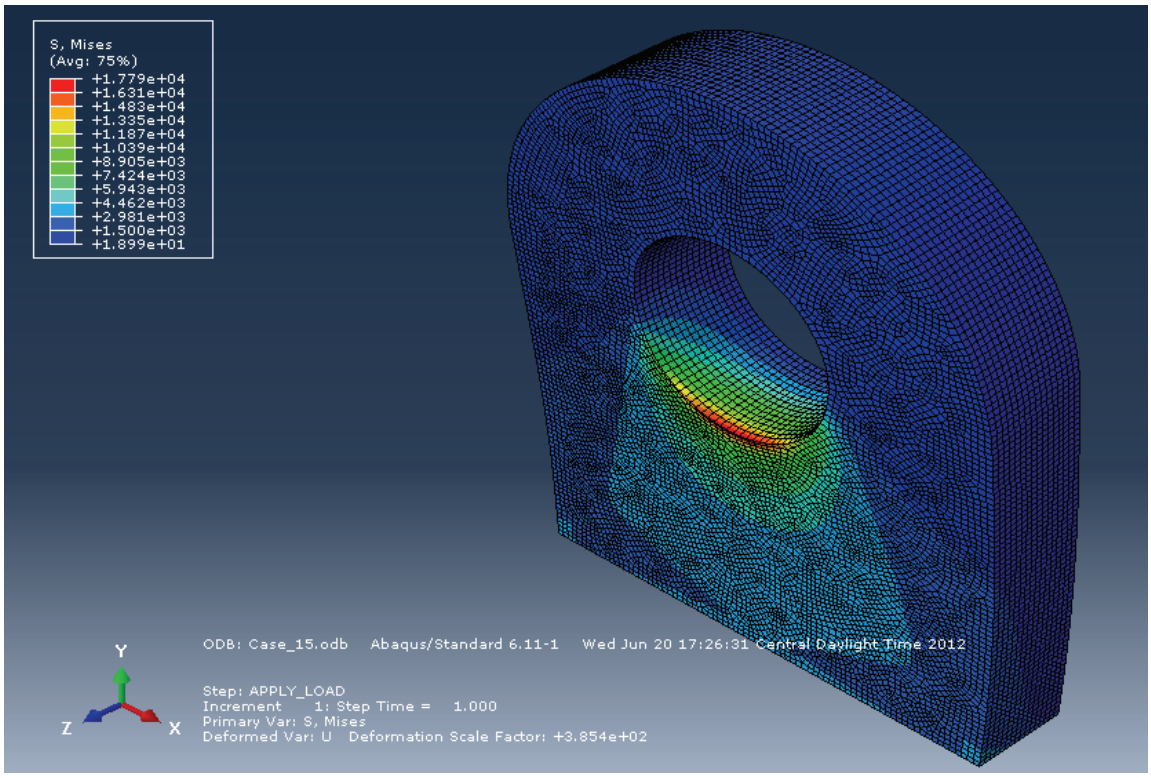

FIGURE 4.1. Case 15 Yoke Plate von Mises Contours (8 inch Diameter Shaft, 4 Inch Thick Yoke, 16 Inch Span)

Figure 4.2 shows the magnitude of the edge stress for each of the cases that did not include a sleeve between the trunnion shaft and the supporting yoke plate. The edge stress results are presented for each case. For reference, the configurations that are associated to each of the cases are repeated below the summary of results as Table 4.1.

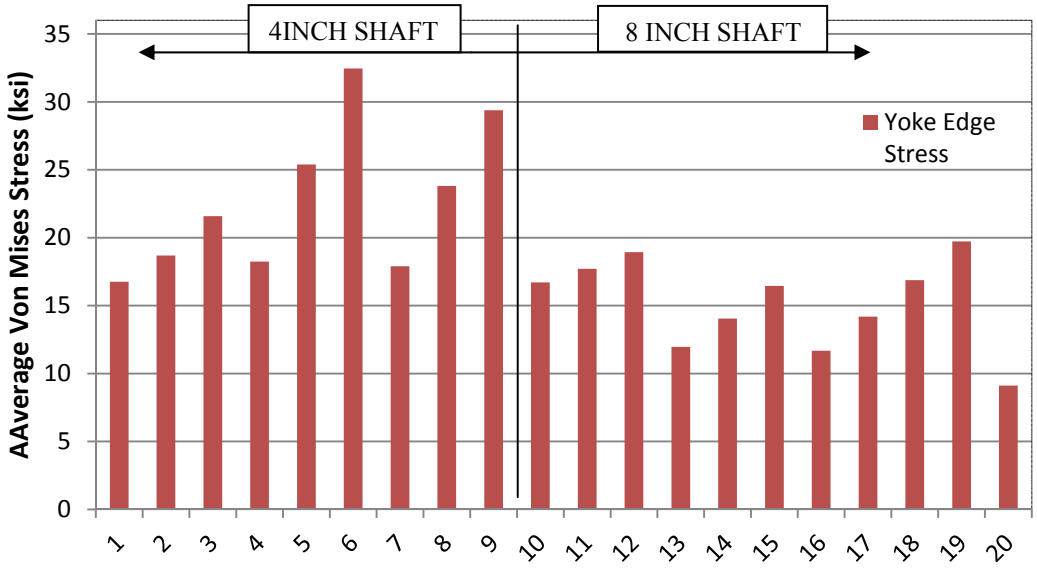

FIGURE 4.2. Summary of von Mises edge stresses in ksi for trunnion assemblies without a sleeve.

Table 4.1. Summary of cases without a sleeve.

Case	Sleeve	Shaft Diameter (in)	Trunnion Load (kips)	Yoke Plate Thickness (in)	Clear Span (in)
1	None	4	120	2	2
2	None	4	120	2	4
3	None	4	120	2	6
4	None	4	120	4	4
5	None	4	120	4	8
6	None	4	120	4	12
7	None	4	120	6	4
8	None	4	120	6	8
9	None	4	120	6	12
10	None	8	240	2	8
11	None	8	240	2	12
12	None	8	240	2	16
13	None	8	240	4	8
14	None	8	240	4	12
15	None	8	240	4	16
16	None	8	240	6	8
17	None	8	240	6	12
18	None	8	240	6	16
19	None	8	240	6	20
20	None	8	240	6	4

4.3 Von Mises Stress – Bronze Sleeve

The results of the analysis cases that included a bronze sleeve between the trunnion shaft and the supporting yoke plate are documented in this section. Below, Figures 4.3 and 4.4 show representative contour plots; however, all of the contour plots for the configurations that included a bronze sleeve are documented in Appendix D.

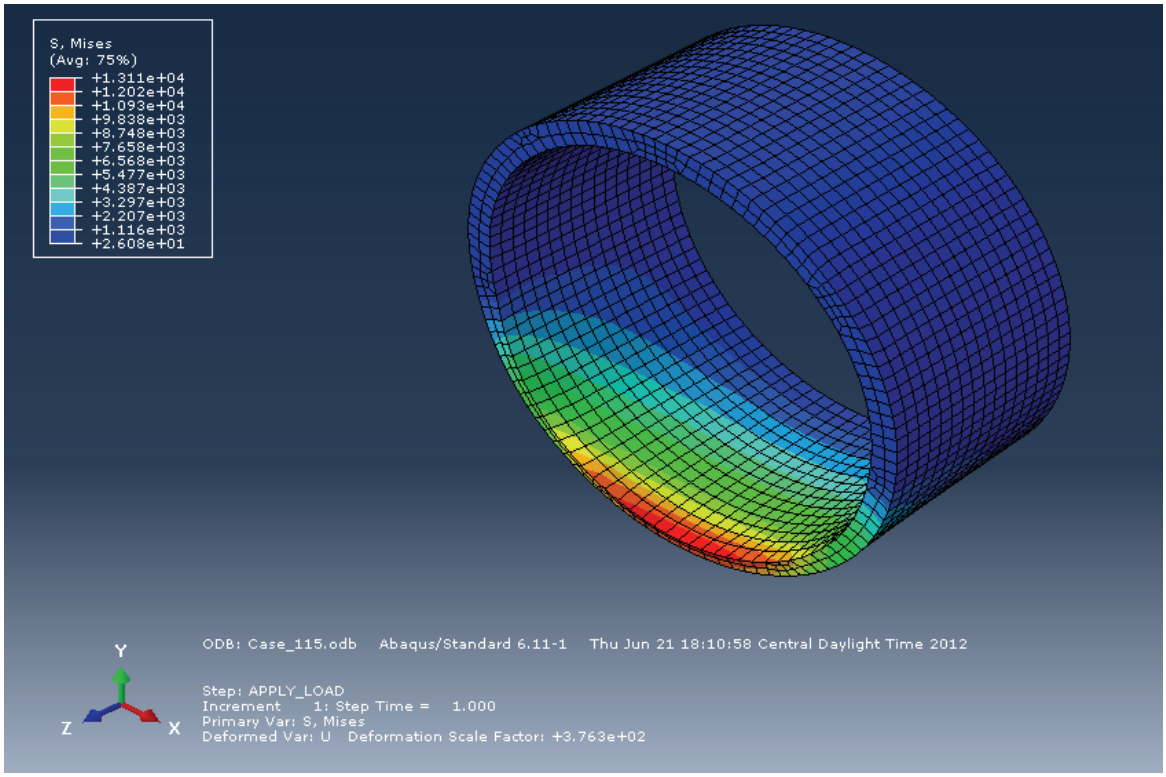

FIGURE 4.3. Case 115 Sleeve von Mises Contours (8 inch Diameter Shaft, 4 Inch Thick Yoke, 16 Inches Span)

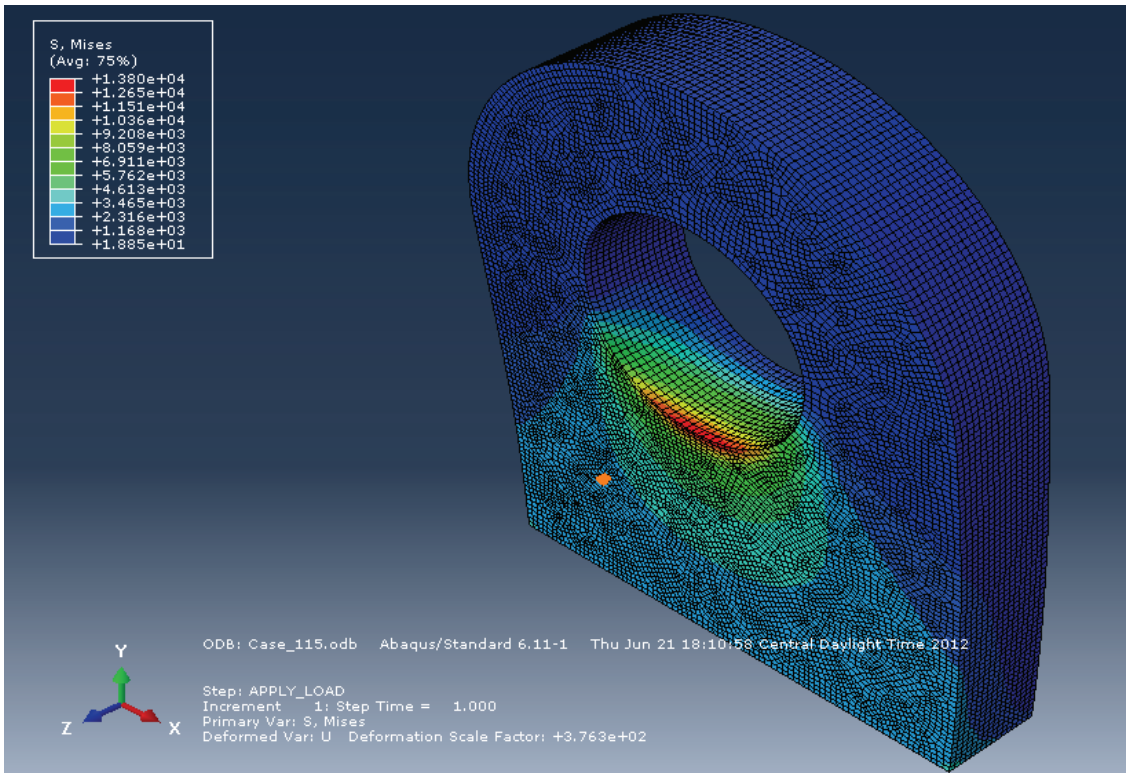

FIGURE 4.4. Case 115 Yoke Plate von Mises Contours (8 Inch Diameter Shaft, 4 Inch Thick Yoke, 16 Inch Span)

Figure 4.5 shows the magnitude of the edge stress in both the sleeve and the yoke plate for each of the cases that included a bronze sleeve between the trunnion shaft and the supporting yoke plate. Again for reference, Table 4.2 shows the configurations that are associated for each of the cases that modeled a bronze sleeve.

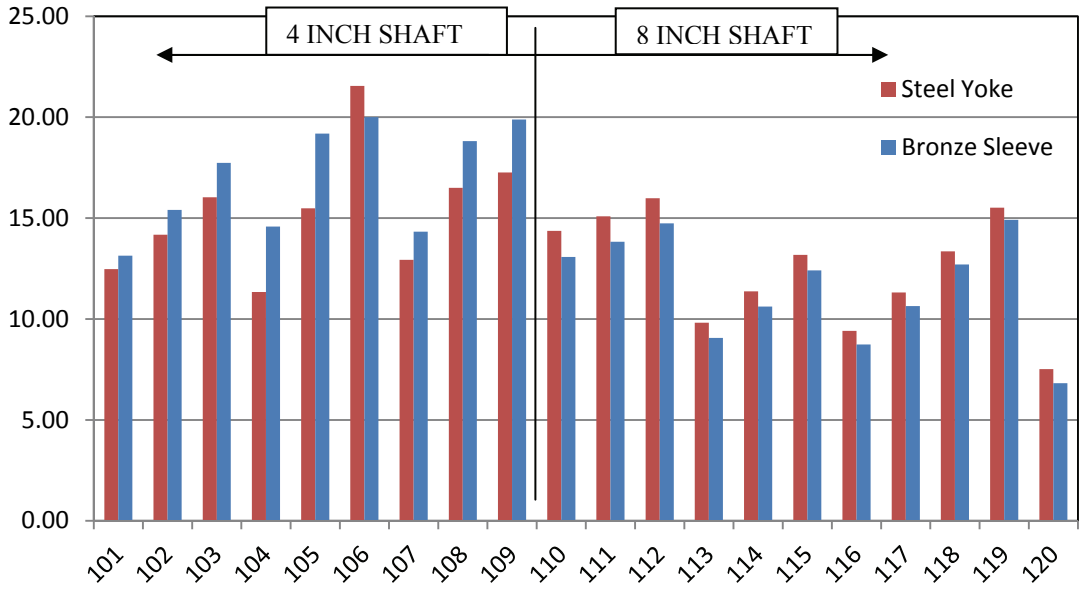

FIGURE 4.5. Summary of von Mises edge stresses in ksi for trunnion assemblies with a bronze sleeve.

Table 4.2. Summary of cases with a bronze sleeve.

Case	Sleeve	Shaft Diameter (in)	Trunnion Load (kips)	Yoke Plate Thickness (in)	Clear Span (in)
101	Bronze	4	120	2	2
102	Bronze	4	120	2	4
103	Bronze	4	120	2	6
104	Bronze	4	120	4	4
105	Bronze	4	120	4	8
106	Bronze	4	120	4	12
107	Bronze	4	120	6	4
108	Bronze	4	120	6	8
109	Bronze	4	120	6	12
110	Bronze	8	240	2	8
111	Bronze	8	240	2	12
112	Bronze	8	240	2	16
113	Bronze	8	240	4	8
114	Bronze	8	240	4	12
115	Bronze	8	240	4	16
116	Bronze	8	240	6	8
117	Bronze	8	240	6	12
118	Bronze	8	240	6	16
119	Bronze	8	240	6	20
120	Bronze	8	240	6	4

4.4 Von Mises Stress – Composite Sleeve

The results of the analysis cases that included a composite sleeve between the trunnion shaft and the supporting yoke plate are documented in this section. Figures 4.6 and 4.7 show representative contour plots; however, all of the contour plots for the configurations that included a composite sleeve are documented in Appendix F.

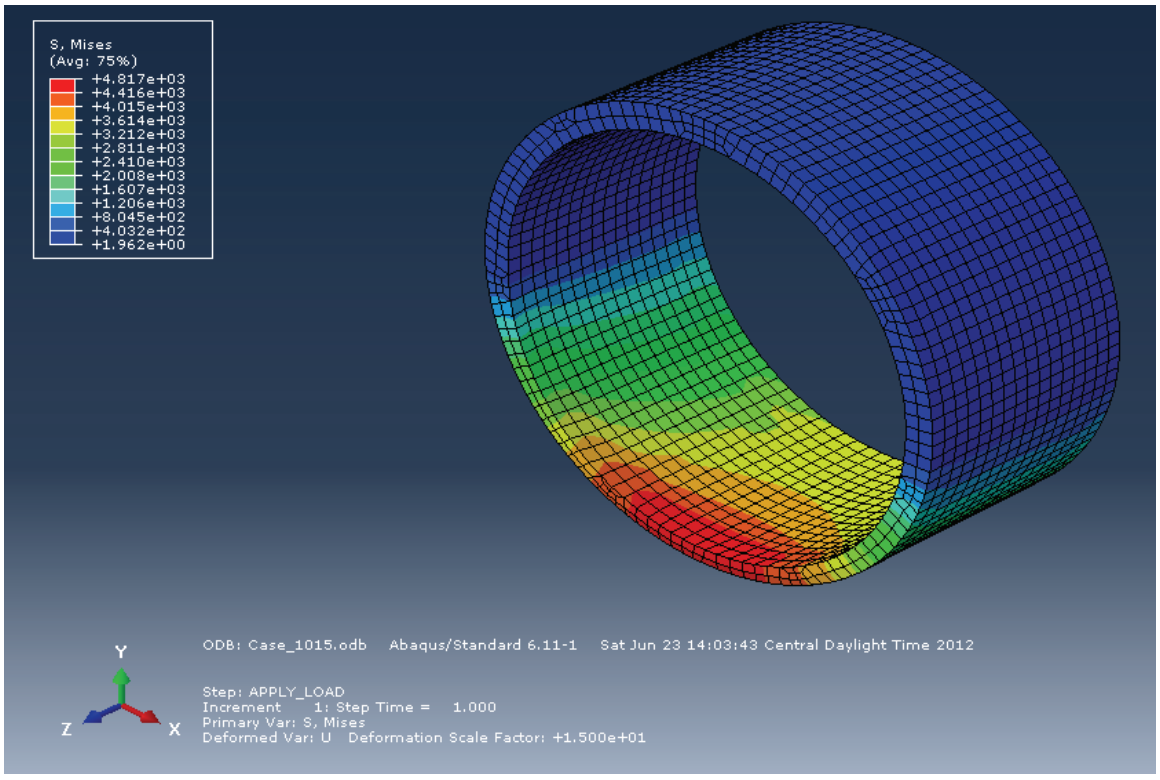

FIGURE 4.6. Case 1015 Sleeve von Mises Contours (8 Inch Diameter Shaft, 4 Inch thick Yoke, 16 Inch Span)

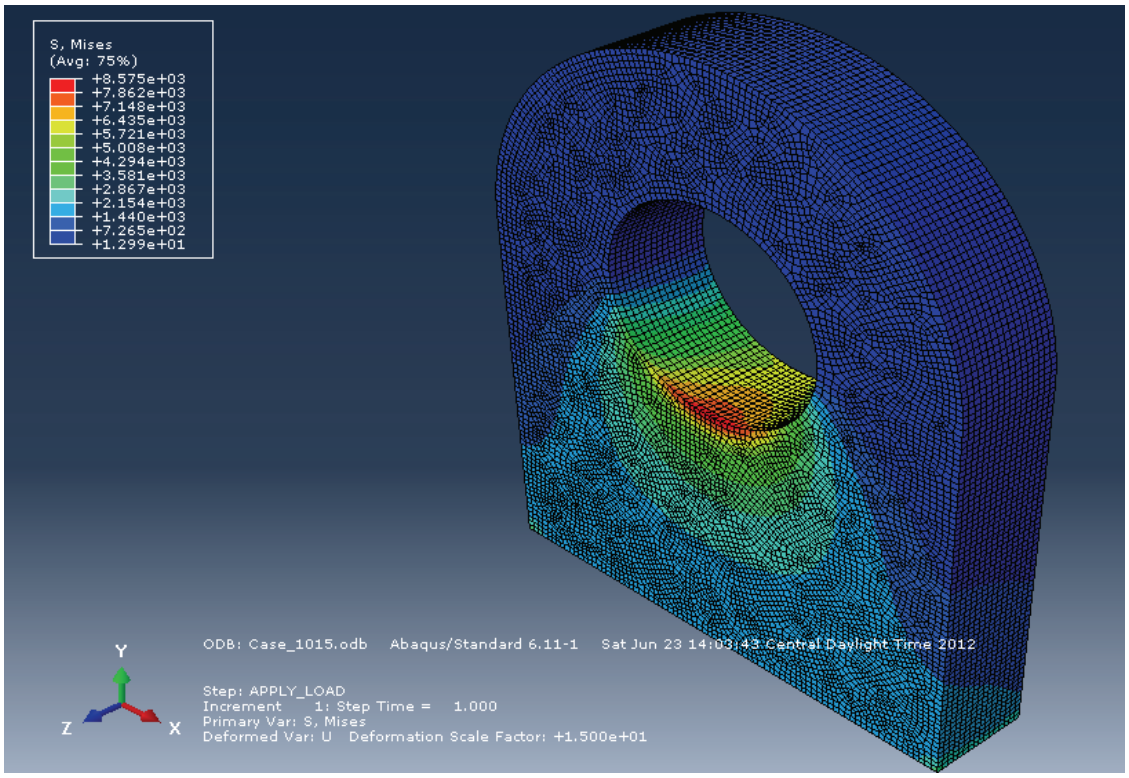

FIGURE 4.7. Case 1015 Sleeve von Mises Contours (8 Inch Diameter Shaft, 4 Inch Thick Yoke, 16 Inch Span)

Figure 4.8 shows the magnitude of the edge stress in both the sleeve and the yoke plate for each of the cases that included a composite sleeve between the trunnion shaft and the supporting yoke plate. Table 4.3 shows the configurations for each of the cases that modeled a composite sleeve for reference.

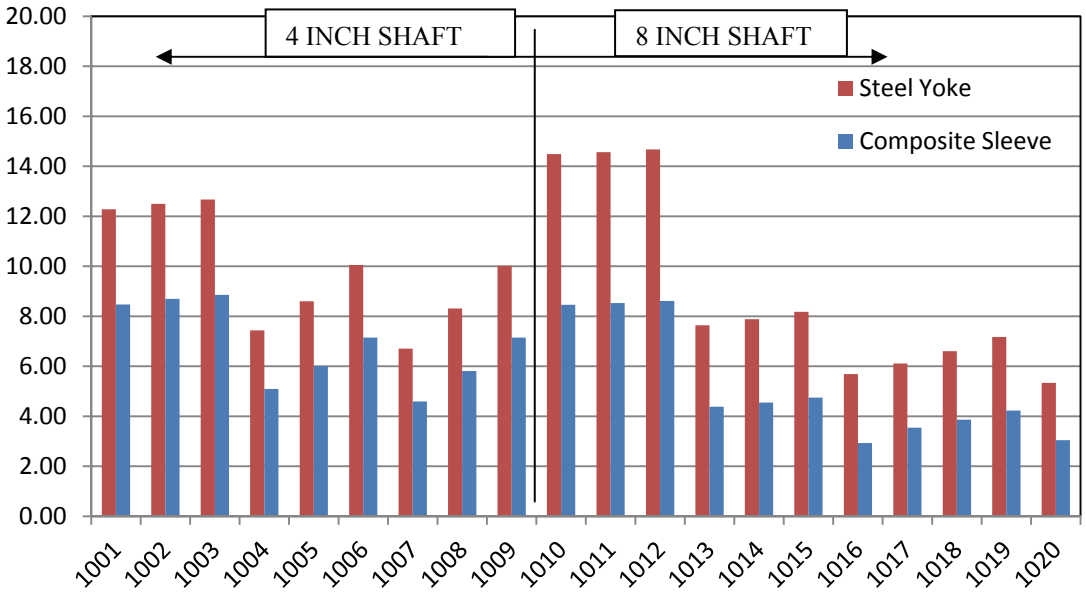

FIGURE 4.8. Summary of von Mises edge stresses for trunnion assemblies with a composite sleeve.

Table 4.3. Summary of cases with a composite sleeve.

Case	Sleeve	Shaft Diameter (in)	Trunnion Load (kips)	Yoke Plate Thickness (in)	Clear Span (in)
1001	Composite	4	120	2	2
1002	Composite	4	120	2	4
1003	Composite	4	120	2	6
1004	Composite	4	120	4	4
1005	Composite	4	120	4	8
1006	Composite	4	120	4	12
1007	Composite	4	120	6	4
1008	Composite	4	120	6	8
1009	Composite	4	120	6	12
1010	Composite	8	240	2	8
1011	Composite	8	240	2	12
1012	Composite	8	240	2	16
1013	Composite	8	240	4	8
1014	Composite	8	240	4	12
1015	Composite	8	240	4	16
1016	Composite	8	240	6	8
1017	Composite	8	240	6	12
1018	Composite	8	240	6	16
1019	Composite	8	240	6	20
1020	Composite	8	240	6	4

CHAPTER 5

ANALYSIS OF RESULTS

This chapter analyzes the results and identifies trends and relationships between the parameters that were included in the study and the magnitude of the edge stress. All edge stresses are reported as the von Mises stress.

5.1 Trends – No Sleeve

Figure 5.1 plots the magnitude of the calculated edge stress, which is the average of the nodal stresses (see Chapter 3 for details), verses the ratio between the clear span of the trunnion shaft and the trunnion shaft diameter.

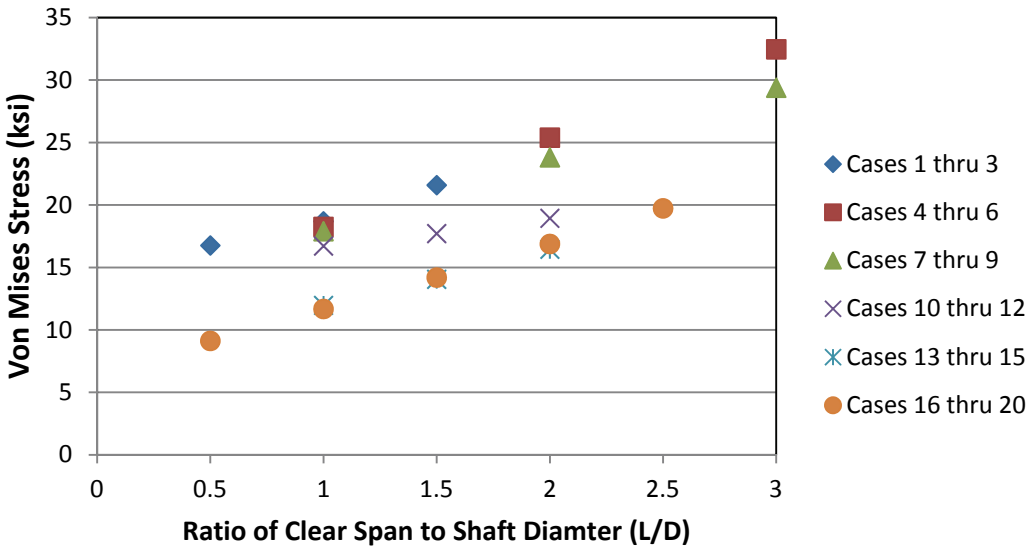

FIGURE 5.1. Scatter plot of the von Mises edge stresses vs. the ratio between the trunnion shaft clear span and trunnion shaft diameter.

With the exception of cases 10 through 12, the data demonstrates that there are two linear relationships represented on the above plot, each specific to the trunnion shaft diameter that was modeled.

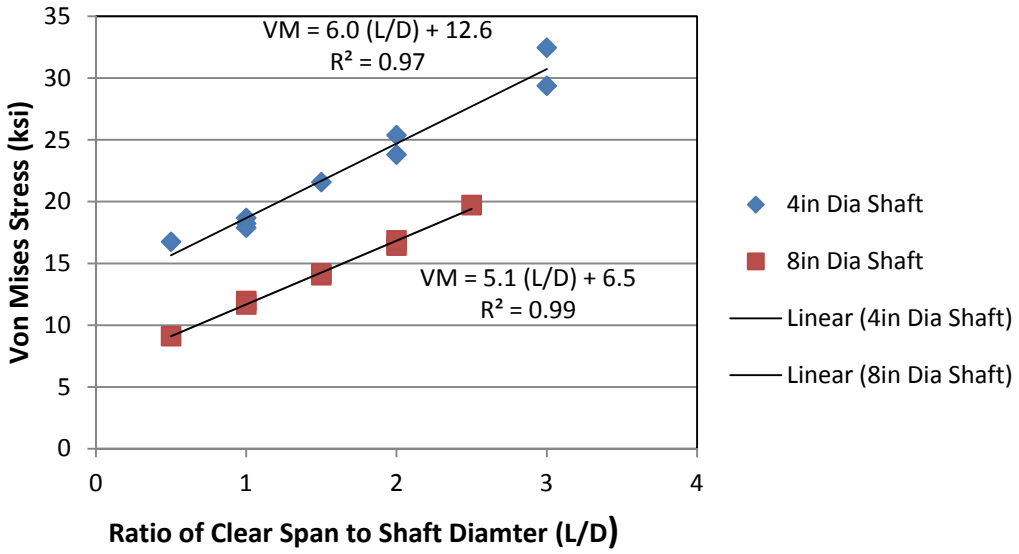

FIGURE 5.2. Trends of edge stress for trunnion assemblies that do not include a sleeve.

Figure 5.2 illustrates the two linear trends that can be identified between the von Mises edge stress and the ratio between clear span and shaft diameter for the cases that do not include a sleeve between the yoke and the trunnion shaft. Note that the trends shown in this Figure 5.2 are only valid when the yoke plate is between 0.5 and 1.5 times the trunnion shaft diameter; therefore, the data from cases 10 through 12 was not included. Based on the results of cases 10 through 12, which are shown in Figure 5.1, it is observed that the linear relationship between the magnitude of the

edge stress and the L/D ratio is only valid for yoke plate thicknesses between 0.5 and 1.5 times the trunnion shaft diameter. The data showed that when the trunnion yoke plates are small compared to the trunnion shaft diameter, the relationship between the magnitude of the edge stress and the L/D ratio is not as suggested in Figure 5.2. Cases 10 through 12 (refer back to table 3.4 for case parameters) include a yoke plate thickness that is 0.25 times the shaft diameter. Figure 5.1 shows that the relationship between the magnitude of the edge stress and the L/D ratio is still linear; however, the trend has a milder slope. More investigation of the trends for configurations with yoke plate to shaft diameter ratios less than 0.5 was identified as a future work topic. This research focuses on the trends for yoke plate to shaft diameter ratios between 0.5 and 1.5.

5.2 Trends – Bronze Sleeve

The trends for the relationship between the magnitude of the edge stress and the L/D ratio is also linear for the configurations that include bronze sleeves (for yoke plates that are between 0.5 and 1.5 times the trunnion shaft diameter).

Figure 5.3 and 5.4 show that the magnitude of the edge stresses is reduced when a bronze sleeve is included in the design. This is attributed to the difference in modulus of elasticity between the steel yoke and the bronze sleeve. The modulus of elasticity for the bronze sleeve is approximately half of the steel modulus of elasticity (see table 3.1). As shown by the results, the layer of soft material helps to reduce the

magnitude of the edge stresses caused by the small shaft rotations at the yoke supports.

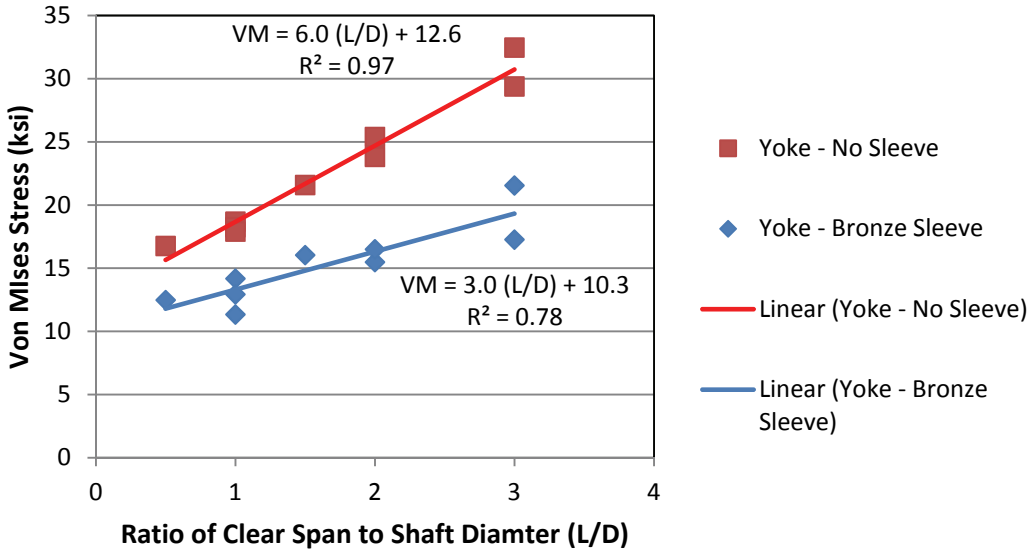

FIGURE 5.3. Von Mises edge stress in ksi vs. the L/D ratio for the 4 inches diameter shaft cases.

Figure 5.3 compares the trends of the edge stress in the steel yoke as it varies with the L/D ratio for designs with and without a bronze sleeve located between the trunnion shaft and the yoke plate. A linear trend is identified, and it is observed that the as the L/D ratio increases the sleeve becomes more effective in reducing the magnitude of the stress located on the inboard edge of the yoke plate.

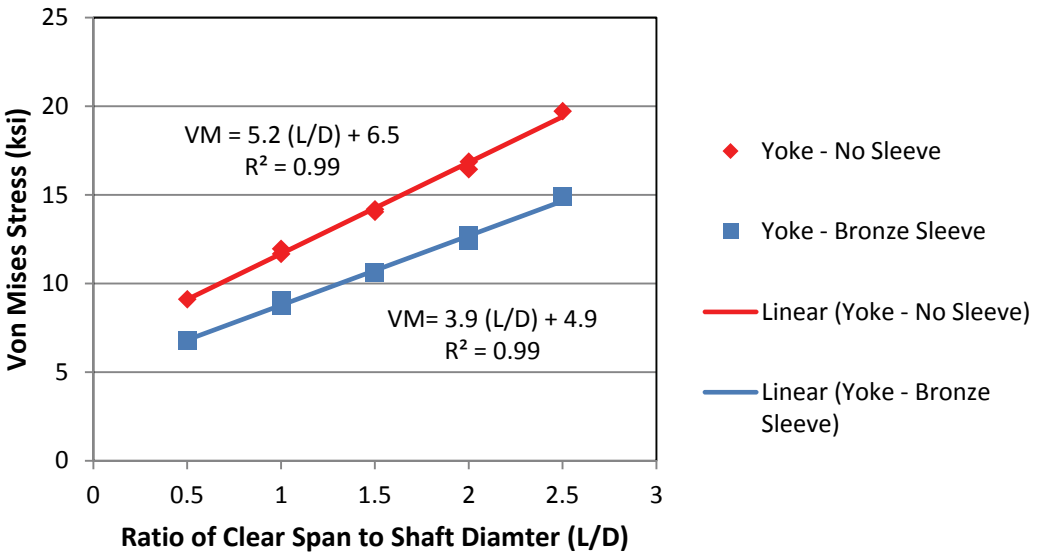

FIGURE 5.4. Von Mises edge stress in ksi vs. the L/D ratio for the 8 inch diameter shaft cases.

Figure 5.4 compares the trends of the edge stress in the steel yoke as it varies with the L/D ratio for designs with and without a bronze sleeve located between the trunnion shaft and the yoke plate. Similar to what was observed in the 4 inch shaft cases, the bronze sleeve reduced the magnitude of the edge stress. Figure 5.4 also shows that as the L/D ratio increases the sleeve becomes more effective in reducing the edge stress.

The concentration of loading is also present in the sleeve itself. Figures 5.5 and 5.6 show similar trends between the stresses in the sleeve and the L/D ratio; however, it can be seen that a polynomial better describes the relationship between the L/D ratio and the magnitude of the edge stress, especially the stresses begin to approach the yield strength of the bronze material (20 ksi for the purposes of this study).

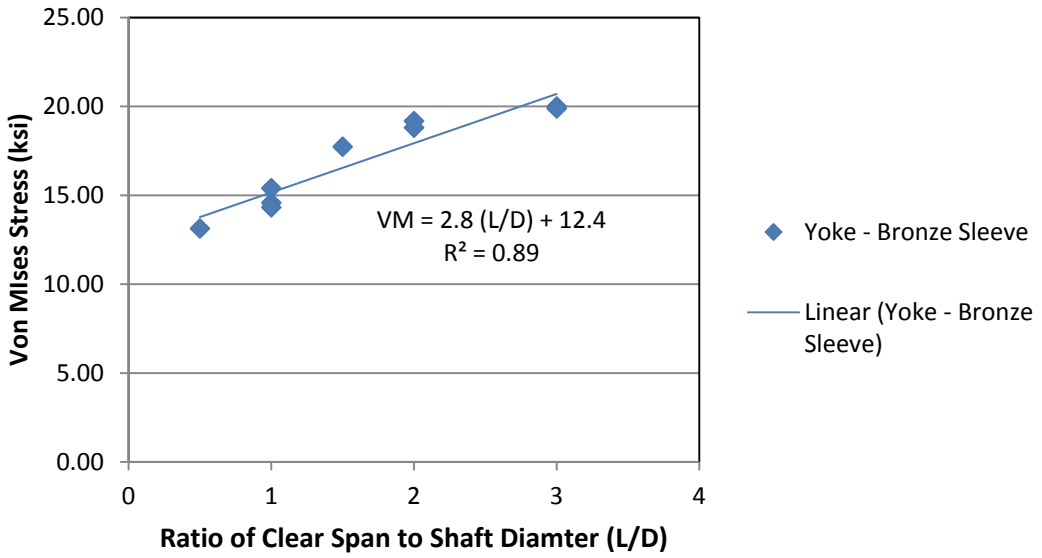

FIGURE 5.5. For the 4 inch diameter shaft cases, the relationship between the von Mises edge stress and the L/D ratio is plotted. Note that the yield strength of the bronze material was defined at 20 ksi.

The cases that included an 8 inch diameter shaft did not produce any stresses in the bronze sleeve that were approaching the 20 ksi yield stress of the bronze material. In Figure 5.6 it is observed that the relationship is linear between the magnitude of the von Mises edge stress and the L/D ratio.

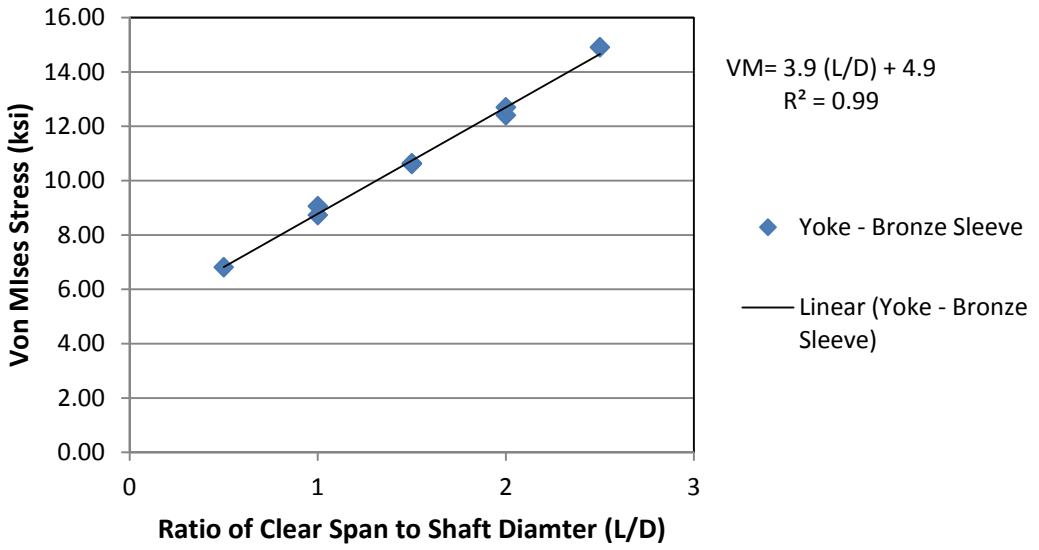

FIGURE 5.6. For the 8 inch diameter shaft cases, the relationship between the von Mises edge stress and the L/D ratio is plotted.

Based on Figures 5.5 and 5.6, we can conclude that the edge stresses in the bronze sleeve have a linear relationship with the L/D ratio until the edge stresses begin to approach yield.

5.3 Trends – Composite Sleeve

Generally, the trends for the configurations that included composite sleeves are similar to the trends previously identified, in that the magnitude of the edge stress is a function of the L/D ratio; however, the results also show that these configurations are more sensitive to the yoke plate thickness than what was observed for the configurations that did not include a sleeve, or included a bronze sleeve. Figure 5.7 plots the magnitude of the edge stress vs. the L/D ratio for the steel yoke plate.

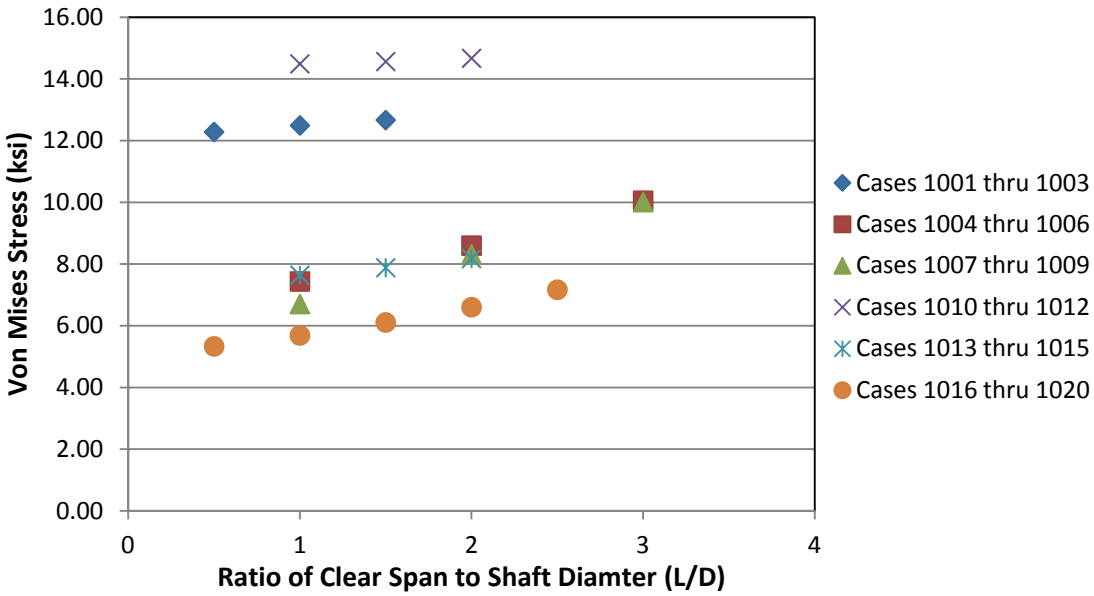

FIGURE 5.7. Plot of the edge stresses in the steel yoke plate for the configurations that include a composite sleeve.

The relationship between the edge stress in the sleeve and the L/D ratio is similar as what is observed in the steel yoke plate in that the stress increases linearly with the L/D ratio; however, the results also show that when a composite sleeve is used, the stresses become more sensitive to the thickness of the yoke plate.

Figure 5.8 plots the magnitude of the edge stress in the composite sleeve verses the L/D ratio.

Table 5.1. Summary of cases with a composite sleeve.

Case	Sleeve	Shaft Diameter (in)	Trunnion Load (kips)	Yoke Plate Thickness (in)	Clear Span (in)
1001	Composite	4	120	2	2
1002	Composite	4	120	2	4
1003	Composite	4	120	2	6
1004	Composite	4	120	4	4
1005	Composite	4	120	4	8
1006	Composite	4	120	4	12
1007	Composite	4	120	6	4
1008	Composite	4	120	6	8
1009	Composite	4	120	6	12
1010	Composite	8	240	2	8
1011	Composite	8	240	2	12
1012	Composite	8	240	2	16
1013	Composite	8	240	4	8
1014	Composite	8	240	4	12
1015	Composite	8	240	4	16
1016	Composite	8	240	6	8
1017	Composite	8	240	6	12
1018	Composite	8	240	6	16
1019	Composite	8	240	6	20
1020	Composite	8	240	6	4

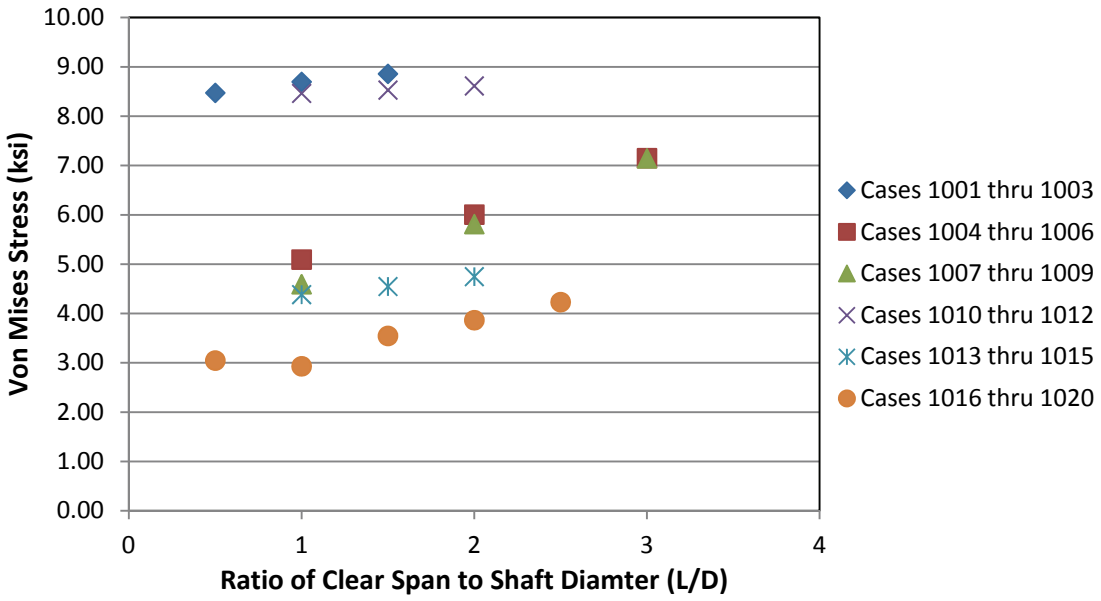

FIGURE 5.8. Plot of the edge stresses in the composite sleeve for the configurations that include a composite sleeve.

It was observed that there are linear trends that can be established for each subset of data. However, unlike what was observed in the configurations that did not include a sleeve, or included a bronze sleeve, the trends for the composite sleeve configurations are sensitive to the yoke plate thickness. This is attributed to the modulus of elasticity of the composite sleeve being low compared to the modulus of elasticity of steel (260 ksi vs. 29,000 ksi). The layer of soft material is able to better distribute the loads across the thickness of the material; thus the magnitude of the edge stress caused by the small transverse shaft rotations are reduced when compared to the configurations that did not include a sleeve, or the configurations that included the bronze sleeve.

5.4 Trends – Comparison Summary

Figure 5.9 summarizes all of the edge stress results in the steel yoke plate that were produced for the 4 inch trunnion shaft diameter cases.

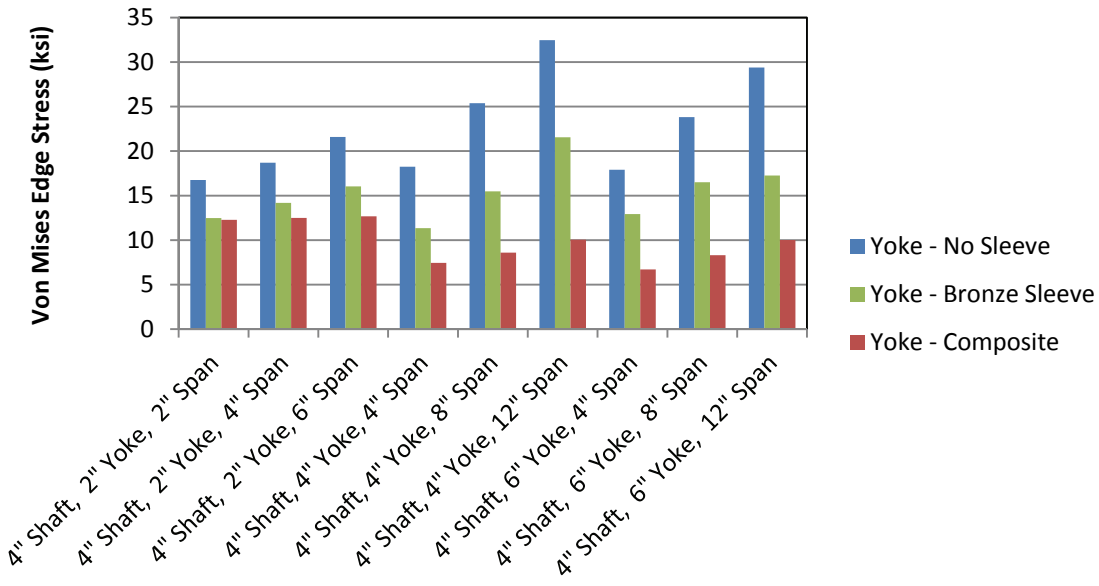

FIGURE 5.9. Comparison plot of the edge stresses for the configurations that included a 4 inches diameter trunnion shaft.

The magnitude of the edge stress is decreased when a sleeve is included between the trunnion shaft and the supporting yoke plate. For the trunnion shafts that are required to span a larger distance (L/D greater than 1.0), the composite sleeves have superior performance in terms of distributing the load across the thickness of the yoke plate, and reducing the magnitude of the edge stress.

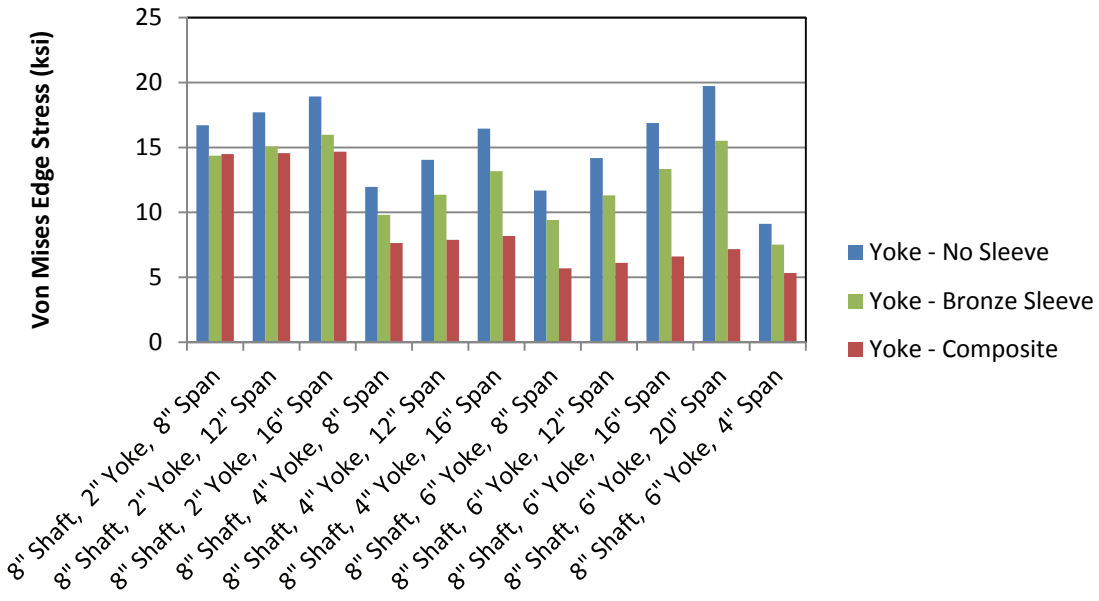

FIGURE 5.10. Comparison plot of the edge stresses for the configurations that included a 8 inches diameter trunnion shaft.

Similar to what was observed in Figure 5.9 for the 4 inch diameter shaft cases, Figure 5.10 plots the edge stresses for the 8 inch diameter trunnion shaft cases. Again, the data shows that the sleeves are able to reduce the magnitude of the edge stress.

CHAPTER 6

CONCLUSION

6.1 Conclusion

The Traditional Rigid Body (P/A) method and the Finite Element Analysis Shell Element method were concluded to be un-conservative because they are not able to capture the load distribution across the thickness of the yoke plate. As shown in the example problem, the most appropriate analysis method for a shaft-yoke assembly is the Finite Element Analysis-Solid Element Method because it can capture the load distribution in the radial direction as well as the distribution across the yoke plate thickness.

This study showed that the inboard edges of trunnion yoke plates will experience high stresses due to small load induced transverse rotations at the yoke plate supports. The magnitude of the stress is linearly related to the L/D ratio of the trunnion shaft, and can have a magnitude up to 3 to 5 times the average stress that is calculated using the Traditional Rigid Body (P/A) Method.

The study also showed that bronze and composite sleeves reduce the magnitude of the edge stress. The effectiveness of the sleeve is dependent on the modulus of the sleeve and the L/D ratio. Overall, the larger the L/D ratio, the more effective the sleeve was in reducing the magnitude of the edge stress. The sleeves with the lower modulus of elasticity (i.e. the composite sleeves) performed superior in terms of reducing the magnitude of the edge stress.

For the cases that included a bronze sleeve, it was observed that the magnitude of the edge stress was reduced by 10% to 30% depending on the L/D ratio. For the cases that included the composite sleeves, the magnitude of the edge stress was reduced by 10% to 65% depending on the L/D ratio.

Based on this research, future tainter gate designs should consider an L/D ratio within the range of 2.0 to 2.5 and include a low modulus sleeve (bronze or composite) between the trunnion shaft and the supporting yoke plate. The combination of adding sleeves to the design and increasing the L/D ratio will result in a more efficient tainter gate design because the detailing at the trunnion will be simplified and the demands on the strut arms will be reduced due to the smaller trunnion shaft diameter.

6.2 Future Work

This research focused on the effects that the bronze and composite sleeves had on the magnitude of the inboard edge stress; however, additional research should be done on to determine if the larger L/D ratio has an effect on the main trunnion bearing. Specifically, the research should be done to determine the impacts that designs with L/D ratios between 2.0 and 2.5 have on the trunnion pin friction moment and the life of the primary trunnion bearing.

There are additional parameters that could be modeled to further the understanding of the trunnion shaft to trunnion yoke plate load path: (1) edge

chamfers, (2) thickness of sleeve, (2) additional sleeve materials, (3) friction, (4) installation tolerances (5) thermal stresses due to sleeve installation (6) advanced material modeling and (7) operational loading conditions. The parameters listed above may have an effect on the magnitude of the stress concentrations in the yoke plate and sleeves; however, they were not included in this phase of the research.

While additional analyses that investigate the items identified above would be beneficial, the most significant contribution to this topic would come from a physical testing program that could record the actual edge stresses in the yoke plates. This could either be performed in a laboratory, or in the field on an actual trunnion assembly.

APPENDIX A

VALIDATION – LOAD INPUT

The loads were inputted into the ABAQUS models as a pressure applied over the top half of the trunnion shaft. In order to obtain the same resultant trunnion load on the assembly, the applied pressure must vary with shaft diameter and clear span. This appendix documents the validation calculations that were used to determine that the desired loading was inputted into the model. An excel spreadsheet was developed to calculate the resultant vertical load on a yoke plate. The results of this spreadsheet were then compared to the reaction force output from the ABAQUS models. When there was agreement between the two, we knew that the desired loading was correctly entered into the numerical model.

The total force applied in the model is calculated by multiplying the surface area by the applied load. However, because the horizontal components of the applied load act equal and opposite, the targeted trunnion load is the sum of only the vertical components (R_y in the spreadsheet calculation). The comparison for the validation check is between R_y and the targeted resultant load on the yoke plate.

The parametric study resulted in 60 different finite element models; however, due to the different parameters, there were only 10 unique loading conditions. This appendix contains an example validation check of each of the 10 different unique loading conditions.

ABAQUS Model Verificaiton **Check Load Input** 6/23/2012

Surface Pressure to Vertical Reaction Force

shaft radius (in)	2
width of loaded area (in)	1
delta theta (rad)	0.031
incremental arc length (in)	0.063
Number of increments (ea)	100
Pressure (psi)	15000
Resultant on Increment Area (kip)	0.942

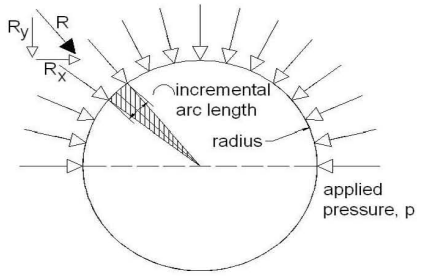

increment	R	theta	Ry	Rx
1	1.41	0.03	0.04	1.41
2	0.94	0.06	0.06	0.94
3	0.94	0.09	0.09	0.94
4	0.94	0.13	0.12	0.94
5	0.94	0.16	0.15	0.93
6	0.94	0.19	0.18	0.93
7	0.94	0.22	0.21	0.92
8	0.94	0.25	0.23	0.91
9	0.94	0.28	0.26	0.91
10	0.94	0.31	0.29	0.90
11	0.94	0.35	0.32	0.89
12	0.94	0.38	0.35	0.88
13	0.94	0.41	0.37	0.86
14	0.94	0.44	0.40	0.85
15	0.94	0.47	0.43	0.84
16	0.94	0.50	0.45	0.83
17	0.94	0.53	0.48	0.81
18	0.94	0.57	0.51	0.80
19	0.94	0.60	0.53	0.78
20	0.94	0.63	0.55	0.76
21	0.94	0.66	0.58	0.74
22	0.94	0.69	0.60	0.73
23	0.94	0.72	0.62	0.71
24	0.94	0.75	0.65	0.69
25	0.94	0.79	0.67	0.67
26	0.94	0.82	0.69	0.65
27	0.94	0.85	0.71	0.62
28	0.94	0.88	0.73	0.60
29	0.94	0.91	0.74	0.58
30	0.94	0.94	0.76	0.55
31	0.94	0.97	0.78	0.53
32	0.94	1.01	0.80	0.51
33	0.94	1.04	0.81	0.48
34	0.94	1.07	0.83	0.45
35	0.94	1.10	0.84	0.43
36	0.94	1.13	0.85	0.40
37	0.94	1.16	0.86	0.37
38	0.94	1.19	0.88	0.35
39	0.94	1.23	0.89	0.32
40	0.94	1.26	0.90	0.29
41	0.94	1.29	0.91	0.26
42	0.94	1.32	0.91	0.23
43	0.94	1.35	0.92	0.21
44	0.94	1.38	0.93	0.18
45	0.94	1.41	0.93	0.15
46	0.94	1.45	0.94	0.12
47	0.94	1.48	0.94	0.09
48	0.94	1.51	0.94	0.06
49	0.94	1.54	0.94	0.03
50	0.94	1.57	0.94	0.00
51	0.94	1.60	0.94	-0.03
52	0.94	1.63	0.94	-0.06
53	0.94	1.67	0.94	-0.09

increment	R	theta	Ry	Rx
54	0.94	1.70	0.94	-0.12
55	0.94	1.73	0.93	-0.15
56	0.94	1.76	0.93	-0.18
57	0.94	1.79	0.92	-0.21
58	0.94	1.82	0.91	-0.23
59	0.94	1.85	0.91	-0.26
60	0.94	1.88	0.90	-0.29
61	0.94	1.92	0.89	-0.32
62	0.94	1.95	0.88	-0.35
63	0.94	1.98	0.86	-0.37
64	0.94	2.01	0.85	-0.40
65	0.94	2.04	0.84	-0.43
66	0.94	2.07	0.83	-0.45
67	0.94	2.10	0.81	-0.48
68	0.94	2.14	0.80	-0.51
69	0.94	2.17	0.78	-0.53
70	0.94	2.20	0.76	-0.55
71	0.94	2.23	0.74	-0.58
72	0.94	2.26	0.73	-0.60
73	0.94	2.29	0.71	-0.62
74	0.94	2.32	0.69	-0.65
75	0.94	2.36	0.67	-0.67
76	0.94	2.39	0.65	-0.69
77	0.94	2.42	0.62	-0.71
78	0.94	2.45	0.60	-0.73
79	0.94	2.48	0.58	-0.74
80	0.94	2.51	0.55	-0.76
81	0.94	2.54	0.53	-0.78
82	0.94	2.58	0.51	-0.80
83	0.94	2.61	0.48	-0.81
84	0.94	2.64	0.45	-0.83
85	0.94	2.67	0.43	-0.84
86	0.94	2.70	0.40	-0.85
87	0.94	2.73	0.37	-0.86
88	0.94	2.76	0.35	-0.88
89	0.94	2.80	0.32	-0.89
90	0.94	2.83	0.29	-0.90
91	0.94	2.86	0.26	-0.91
92	0.94	2.89	0.23	-0.91
93	0.94	2.92	0.21	-0.92
94	0.94	2.95	0.18	-0.93
95	0.94	2.98	0.15	-0.93
96	0.94	3.02	0.12	-0.94
97	0.94	3.05	0.09	-0.94
98	0.94	3.08	0.06	-0.94
99	0.94	3.11	0.03	-0.94
100	0.47	3.14	0.00	-0.47
SUM	94.25	-	60.01	0.00

Check Total Force	94.25	OK

Figure A.1. Load input calculation - Cases 1, 101, and 1001

ABAQUS Model Verificaiton **Check Load Input** 6/23/2012

Surface Pressure to Vertical Reaction Force

shaft radius (in)	2
width of loaded area (in)	2
delta theta (rad)	0.031
incremental arc length (in)	0.063
Number of increments (ea)	100
Pressure (psi)	7500
Resultant on Increment Area (kip)	0.942

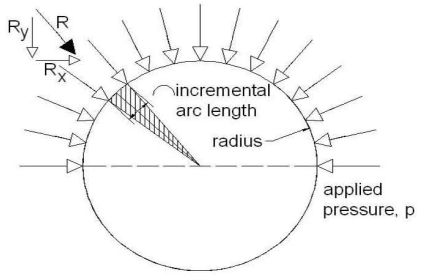

increment	R	theta	Ry	Rx
1	1.41	0.03	0.04	1.41
2	0.94	0.06	0.06	0.94
3	0.94	0.09	0.09	0.94
4	0.94	0.13	0.12	0.94
5	0.94	0.16	0.15	0.93
6	0.94	0.19	0.18	0.93
7	0.94	0.22	0.21	0.92
8	0.94	0.25	0.23	0.91
9	0.94	0.28	0.26	0.91
10	0.94	0.31	0.29	0.90
11	0.94	0.35	0.32	0.89
12	0.94	0.38	0.35	0.88
13	0.94	0.41	0.37	0.86
14	0.94	0.44	0.40	0.85
15	0.94	0.47	0.43	0.84
16	0.94	0.50	0.45	0.83
17	0.94	0.53	0.48	0.81
18	0.94	0.57	0.51	0.80
19	0.94	0.60	0.53	0.78
20	0.94	0.63	0.55	0.76
21	0.94	0.66	0.58	0.74
22	0.94	0.69	0.60	0.73
23	0.94	0.72	0.62	0.71
24	0.94	0.75	0.65	0.69
25	0.94	0.79	0.67	0.67
26	0.94	0.82	0.69	0.65
27	0.94	0.85	0.71	0.62
28	0.94	0.88	0.73	0.60
29	0.94	0.91	0.74	0.58
30	0.94	0.94	0.76	0.55
31	0.94	0.97	0.78	0.53
32	0.94	1.01	0.80	0.51
33	0.94	1.04	0.81	0.48
34	0.94	1.07	0.83	0.45
35	0.94	1.10	0.84	0.43
36	0.94	1.13	0.85	0.40
37	0.94	1.16	0.86	0.37
38	0.94	1.19	0.88	0.35
39	0.94	1.23	0.89	0.32
40	0.94	1.26	0.90	0.29
41	0.94	1.29	0.91	0.26
42	0.94	1.32	0.91	0.23
43	0.94	1.35	0.92	0.21
44	0.94	1.38	0.93	0.18
45	0.94	1.41	0.93	0.15
46	0.94	1.45	0.94	0.12
47	0.94	1.48	0.94	0.09
48	0.94	1.51	0.94	0.06
49	0.94	1.54	0.94	0.03
50	0.94	1.57	0.94	0.00
51	0.94	1.60	0.94	-0.03
52	0.94	1.63	0.94	-0.06
53	0.94	1.67	0.94	-0.09

increment	R	theta	Ry	Rx
54	0.94	1.70	0.94	-0.12
55	0.94	1.73	0.93	-0.15
56	0.94	1.76	0.93	-0.18
57	0.94	1.79	0.92	-0.21
58	0.94	1.82	0.91	-0.23
59	0.94	1.85	0.91	-0.26
60	0.94	1.88	0.90	-0.29
61	0.94	1.92	0.89	-0.32
62	0.94	1.95	0.88	-0.35
63	0.94	1.98	0.86	-0.37
64	0.94	2.01	0.85	-0.40
65	0.94	2.04	0.84	-0.43
66	0.94	2.07	0.83	-0.45
67	0.94	2.10	0.81	-0.48
68	0.94	2.14	0.80	-0.51
69	0.94	2.17	0.78	-0.53
70	0.94	2.20	0.76	-0.55
71	0.94	2.23	0.74	-0.58
72	0.94	2.26	0.73	-0.60
73	0.94	2.29	0.71	-0.62
74	0.94	2.32	0.69	-0.65
75	0.94	2.36	0.67	-0.67
76	0.94	2.39	0.65	-0.69
77	0.94	2.42	0.62	-0.71
78	0.94	2.45	0.60	-0.73
79	0.94	2.48	0.58	-0.74
80	0.94	2.51	0.55	-0.76
81	0.94	2.54	0.53	-0.78
82	0.94	2.58	0.51	-0.80
83	0.94	2.61	0.48	-0.81
84	0.94	2.64	0.45	-0.83
85	0.94	2.67	0.43	-0.84
86	0.94	2.70	0.40	-0.85
87	0.94	2.73	0.37	-0.86
88	0.94	2.76	0.35	-0.88
89	0.94	2.80	0.32	-0.89
90	0.94	2.83	0.29	-0.90
91	0.94	2.86	0.26	-0.91
92	0.94	2.89	0.23	-0.91
93	0.94	2.92	0.21	-0.92
94	0.94	2.95	0.18	-0.93
95	0.94	2.98	0.15	-0.93
96	0.94	3.02	0.12	-0.94
97	0.94	3.05	0.09	-0.94
98	0.94	3.08	0.06	-0.94
99	0.94	3.11	0.03	-0.94
100	0.47	3.14	0.00	-0.47
SUM	94.25	-	60.01	0.00

Check Total Force	94.25	OK

Figure A.2. Load input calculation - Cases 2, 4, 7, 102, 104, 107, 1002, 1004, and 1007

ABAQUS Model Verificaiton **Check Load Input** 6/23/2012

Surface Pressure to Vertical Reaction Force

shaft radius (in)	2
width of loaded area (in)	3
delta theta (rad)	0.031
incremental arc length (in)	0.063
Number of increments (ea)	100
Pressure (psi)	5000
Resultant on Increment Area (kip)	0.942

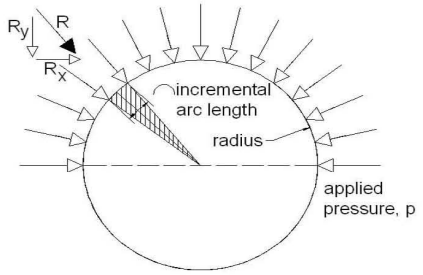

increment	R	theta	Ry	Rx
1	1.41	0.03	0.04	1.41
2	0.94	0.06	0.06	0.94
3	0.94	0.09	0.09	0.94
4	0.94	0.13	0.12	0.94
5	0.94	0.16	0.15	0.93
6	0.94	0.19	0.18	0.93
7	0.94	0.22	0.21	0.92
8	0.94	0.25	0.23	0.91
9	0.94	0.28	0.26	0.91
10	0.94	0.31	0.29	0.90
11	0.94	0.35	0.32	0.89
12	0.94	0.38	0.35	0.88
13	0.94	0.41	0.37	0.86
14	0.94	0.44	0.40	0.85
15	0.94	0.47	0.43	0.84
16	0.94	0.50	0.45	0.83
17	0.94	0.53	0.48	0.81
18	0.94	0.57	0.51	0.80
19	0.94	0.60	0.53	0.78
20	0.94	0.63	0.55	0.76
21	0.94	0.66	0.58	0.74
22	0.94	0.69	0.60	0.73
23	0.94	0.72	0.62	0.71
24	0.94	0.75	0.65	0.69
25	0.94	0.79	0.67	0.67
26	0.94	0.82	0.69	0.65
27	0.94	0.85	0.71	0.62
28	0.94	0.88	0.73	0.60
29	0.94	0.91	0.74	0.58
30	0.94	0.94	0.76	0.55
31	0.94	0.97	0.78	0.53
32	0.94	1.01	0.80	0.51
33	0.94	1.04	0.81	0.48
34	0.94	1.07	0.83	0.45
35	0.94	1.10	0.84	0.43
36	0.94	1.13	0.85	0.40
37	0.94	1.16	0.86	0.37
38	0.94	1.19	0.88	0.35
39	0.94	1.23	0.89	0.32
40	0.94	1.26	0.90	0.29
41	0.94	1.29	0.91	0.26
42	0.94	1.32	0.91	0.23
43	0.94	1.35	0.92	0.21
44	0.94	1.38	0.93	0.18
45	0.94	1.41	0.93	0.15
46	0.94	1.45	0.94	0.12
47	0.94	1.48	0.94	0.09
48	0.94	1.51	0.94	0.06
49	0.94	1.54	0.94	0.03
50	0.94	1.57	0.94	0.00
51	0.94	1.60	0.94	-0.03
52	0.94	1.63	0.94	-0.06
53	0.94	1.67	0.94	-0.09

increment	R	theta	Ry	Rx
54	0.94	1.70	0.94	-0.12
55	0.94	1.73	0.93	-0.15
56	0.94	1.76	0.93	-0.18
57	0.94	1.79	0.92	-0.21
58	0.94	1.82	0.91	-0.23
59	0.94	1.85	0.91	-0.26
60	0.94	1.88	0.90	-0.29
61	0.94	1.92	0.89	-0.32
62	0.94	1.95	0.88	-0.35
63	0.94	1.98	0.86	-0.37
64	0.94	2.01	0.85	-0.40
65	0.94	2.04	0.84	-0.43
66	0.94	2.07	0.83	-0.45
67	0.94	2.10	0.81	-0.48
68	0.94	2.14	0.80	-0.51
69	0.94	2.17	0.78	-0.53
70	0.94	2.20	0.76	-0.55
71	0.94	2.23	0.74	-0.58
72	0.94	2.26	0.73	-0.60
73	0.94	2.29	0.71	-0.62
74	0.94	2.32	0.69	-0.65
75	0.94	2.36	0.67	-0.67
76	0.94	2.39	0.65	-0.69
77	0.94	2.42	0.62	-0.71
78	0.94	2.45	0.60	-0.73
79	0.94	2.48	0.58	-0.74
80	0.94	2.51	0.55	-0.76
81	0.94	2.54	0.53	-0.78
82	0.94	2.58	0.51	-0.80
83	0.94	2.61	0.48	-0.81
84	0.94	2.64	0.45	-0.83
85	0.94	2.67	0.43	-0.84
86	0.94	2.70	0.40	-0.85
87	0.94	2.73	0.37	-0.86
88	0.94	2.76	0.35	-0.88
89	0.94	2.80	0.32	-0.89
90	0.94	2.83	0.29	-0.90
91	0.94	2.86	0.26	-0.91
92	0.94	2.89	0.23	-0.91
93	0.94	2.92	0.21	-0.92
94	0.94	2.95	0.18	-0.93
95	0.94	2.98	0.15	-0.93
96	0.94	3.02	0.12	-0.94
97	0.94	3.05	0.09	-0.94
98	0.94	3.08	0.06	-0.94
99	0.94	3.11	0.03	-0.94
100	0.47	3.14	0.00	-0.47
SUM	94.25	-	60.01	0.00

Check Total Force	94.25	OK

Figure A.3. Load input calculation - Cases 3, 103, and 1003

ABAQUS Model Verificaiton **Check Load Input** 6/23/2012

Surface Pressure to Vertical Reaction Force

shaft radius (in)	2
width of loaded area (in)	4
delta theta (rad)	0.031
incremental arc length (in)	0.063
Number of increments (ea)	100
Pressure (psi)	3750
Resultant on Increment Area (kip)	0.942

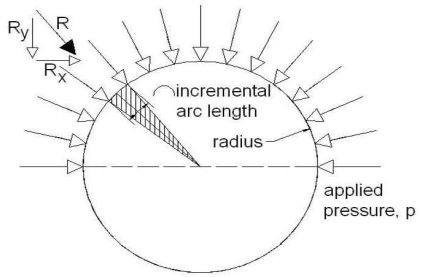

increment	R	theta	Ry	Rx
1	1.41	0.03	0.04	1.41
2	0.94	0.06	0.06	0.94
3	0.94	0.09	0.09	0.94
4	0.94	0.13	0.12	0.94
5	0.94	0.16	0.15	0.93
6	0.94	0.19	0.18	0.93
7	0.94	0.22	0.21	0.92
8	0.94	0.25	0.23	0.91
9	0.94	0.28	0.26	0.91
10	0.94	0.31	0.29	0.90
11	0.94	0.35	0.32	0.89
12	0.94	0.38	0.35	0.88
13	0.94	0.41	0.37	0.86
14	0.94	0.44	0.40	0.85
15	0.94	0.47	0.43	0.84
16	0.94	0.50	0.45	0.83
17	0.94	0.53	0.48	0.81
18	0.94	0.57	0.51	0.80
19	0.94	0.60	0.53	0.78
20	0.94	0.63	0.55	0.76
21	0.94	0.66	0.58	0.74
22	0.94	0.69	0.60	0.73
23	0.94	0.72	0.62	0.71
24	0.94	0.75	0.65	0.69
25	0.94	0.79	0.67	0.67
26	0.94	0.82	0.69	0.65
27	0.94	0.85	0.71	0.62
28	0.94	0.88	0.73	0.60
29	0.94	0.91	0.74	0.58
30	0.94	0.94	0.76	0.55
31	0.94	0.97	0.78	0.53
32	0.94	1.01	0.80	0.51
33	0.94	1.04	0.81	0.48
34	0.94	1.07	0.83	0.45
35	0.94	1.10	0.84	0.43
36	0.94	1.13	0.85	0.40
37	0.94	1.16	0.86	0.37
38	0.94	1.19	0.88	0.35
39	0.94	1.23	0.89	0.32
40	0.94	1.26	0.90	0.29
41	0.94	1.29	0.91	0.26
42	0.94	1.32	0.91	0.23
43	0.94	1.35	0.92	0.21
44	0.94	1.38	0.93	0.18
45	0.94	1.41	0.93	0.15
46	0.94	1.45	0.94	0.12
47	0.94	1.48	0.94	0.09
48	0.94	1.51	0.94	0.06
49	0.94	1.54	0.94	0.03
50	0.94	1.57	0.94	0.00
51	0.94	1.60	0.94	-0.03
52	0.94	1.63	0.94	-0.06
53	0.94	1.67	0.94	-0.09

increment	R	theta	Ry	Rx
54	0.94	1.70	0.94	-0.12
55	0.94	1.73	0.93	-0.15
56	0.94	1.76	0.93	-0.18
57	0.94	1.79	0.92	-0.21
58	0.94	1.82	0.91	-0.23
59	0.94	1.85	0.91	-0.26
60	0.94	1.88	0.90	-0.29
61	0.94	1.92	0.89	-0.32
62	0.94	1.95	0.88	-0.35
63	0.94	1.98	0.86	-0.37
64	0.94	2.01	0.85	-0.40
65	0.94	2.04	0.84	-0.43
66	0.94	2.07	0.83	-0.45
67	0.94	2.10	0.81	-0.48
68	0.94	2.14	0.80	-0.51
69	0.94	2.17	0.78	-0.53
70	0.94	2.20	0.76	-0.55
71	0.94	2.23	0.74	-0.58
72	0.94	2.26	0.73	-0.60
73	0.94	2.29	0.71	-0.62
74	0.94	2.32	0.69	-0.65
75	0.94	2.36	0.67	-0.67
76	0.94	2.39	0.65	-0.69
77	0.94	2.42	0.62	-0.71
78	0.94	2.45	0.60	-0.73
79	0.94	2.48	0.58	-0.74
80	0.94	2.51	0.55	-0.76
81	0.94	2.54	0.53	-0.78
82	0.94	2.58	0.51	-0.80
83	0.94	2.61	0.48	-0.81
84	0.94	2.64	0.45	-0.83
85	0.94	2.67	0.43	-0.84
86	0.94	2.70	0.40	-0.85
87	0.94	2.73	0.37	-0.86
88	0.94	2.76	0.35	-0.88
89	0.94	2.80	0.32	-0.89
90	0.94	2.83	0.29	-0.90
91	0.94	2.86	0.26	-0.91
92	0.94	2.89	0.23	-0.91
93	0.94	2.92	0.21	-0.92
94	0.94	2.95	0.18	-0.93
95	0.94	2.98	0.15	-0.93
96	0.94	3.02	0.12	-0.94
97	0.94	3.05	0.09	-0.94
98	0.94	3.08	0.06	-0.94
99	0.94	3.11	0.03	-0.94
100	0.47	3.14	0.00	-0.47
SUM	94.25	-	60.01	0.00

Check Total Force	94.25	OK

Figure A.4. Load input calculation - Cases 5, 8, 105, 108, 1005, and 1008

ABAQUS Model Verificaiton **Check Load Input** 6/23/2012

Surface Pressure to Vertical Reaction Force

shaft radius (in)	2
width of loaded area (in)	6
delta theta (rad)	0.031
incremental arc length (in)	0.063
Number of increments (ea)	100
Pressure (psi)	2500
Resultant on Increment Area (kip)	0.942

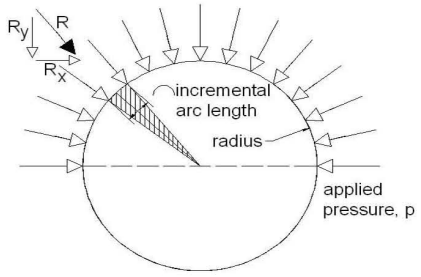

increment	R	theta	Ry	Rx
1	1.41	0.03	0.04	1.41
2	0.94	0.06	0.06	0.94
3	0.94	0.09	0.09	0.94
4	0.94	0.13	0.12	0.94
5	0.94	0.16	0.15	0.93
6	0.94	0.19	0.18	0.93
7	0.94	0.22	0.21	0.92
8	0.94	0.25	0.23	0.91
9	0.94	0.28	0.26	0.91
10	0.94	0.31	0.29	0.90
11	0.94	0.35	0.32	0.89
12	0.94	0.38	0.35	0.88
13	0.94	0.41	0.37	0.86
14	0.94	0.44	0.40	0.85
15	0.94	0.47	0.43	0.84
16	0.94	0.50	0.45	0.83
17	0.94	0.53	0.48	0.81
18	0.94	0.57	0.51	0.80
19	0.94	0.60	0.53	0.78
20	0.94	0.63	0.55	0.76
21	0.94	0.66	0.58	0.74
22	0.94	0.69	0.60	0.73
23	0.94	0.72	0.62	0.71
24	0.94	0.75	0.65	0.69
25	0.94	0.79	0.67	0.67
26	0.94	0.82	0.69	0.65
27	0.94	0.85	0.71	0.62
28	0.94	0.88	0.73	0.60
29	0.94	0.91	0.74	0.58
30	0.94	0.94	0.76	0.55
31	0.94	0.97	0.78	0.53
32	0.94	1.01	0.80	0.51
33	0.94	1.04	0.81	0.48
34	0.94	1.07	0.83	0.45
35	0.94	1.10	0.84	0.43
36	0.94	1.13	0.85	0.40
37	0.94	1.16	0.86	0.37
38	0.94	1.19	0.88	0.35
39	0.94	1.23	0.89	0.32
40	0.94	1.26	0.90	0.29
41	0.94	1.29	0.91	0.26
42	0.94	1.32	0.91	0.23
43	0.94	1.35	0.92	0.21
44	0.94	1.38	0.93	0.18
45	0.94	1.41	0.93	0.15
46	0.94	1.45	0.94	0.12
47	0.94	1.48	0.94	0.09
48	0.94	1.51	0.94	0.06
49	0.94	1.54	0.94	0.03
50	0.94	1.57	0.94	0.00
51	0.94	1.60	0.94	-0.03
52	0.94	1.63	0.94	-0.06
53	0.94	1.67	0.94	-0.09

increment	R	theta	Ry	Rx
54	0.94	1.70	0.94	-0.12
55	0.94	1.73	0.93	-0.15
56	0.94	1.76	0.93	-0.18
57	0.94	1.79	0.92	-0.21
58	0.94	1.82	0.91	-0.23
59	0.94	1.85	0.91	-0.26
60	0.94	1.88	0.90	-0.29
61	0.94	1.92	0.89	-0.32
62	0.94	1.95	0.88	-0.35
63	0.94	1.98	0.86	-0.37
64	0.94	2.01	0.85	-0.40
65	0.94	2.04	0.84	-0.43
66	0.94	2.07	0.83	-0.45
67	0.94	2.10	0.81	-0.48
68	0.94	2.14	0.80	-0.51
69	0.94	2.17	0.78	-0.53
70	0.94	2.20	0.76	-0.55
71	0.94	2.23	0.74	-0.58
72	0.94	2.26	0.73	-0.60
73	0.94	2.29	0.71	-0.62
74	0.94	2.32	0.69	-0.65
75	0.94	2.36	0.67	-0.67
76	0.94	2.39	0.65	-0.69
77	0.94	2.42	0.62	-0.71
78	0.94	2.45	0.60	-0.73
79	0.94	2.48	0.58	-0.74
80	0.94	2.51	0.55	-0.76
81	0.94	2.54	0.53	-0.78
82	0.94	2.58	0.51	-0.80
83	0.94	2.61	0.48	-0.81
84	0.94	2.64	0.45	-0.83
85	0.94	2.67	0.43	-0.84
86	0.94	2.70	0.40	-0.85
87	0.94	2.73	0.37	-0.86
88	0.94	2.76	0.35	-0.88
89	0.94	2.80	0.32	-0.89
90	0.94	2.83	0.29	-0.90
91	0.94	2.86	0.26	-0.91
92	0.94	2.89	0.23	-0.91
93	0.94	2.92	0.21	-0.92
94	0.94	2.95	0.18	-0.93
95	0.94	2.98	0.15	-0.93
96	0.94	3.02	0.12	-0.94
97	0.94	3.05	0.09	-0.94
98	0.94	3.08	0.06	-0.94
99	0.94	3.11	0.03	-0.94
100	0.47	3.14	0.00	-0.47
SUM	94.25	-	60.01	0.00

Check Total Force	94.25	OK

Figure A.5. Load input calculation - Cases 6, 9, 106, 109, 1006, and 1009

ABAQUS Model Verificaiton **Check Load Input** 6/23/2012

Surface Pressure to Vertical Reaction Force

shaft radius (in)	4
width of loaded area (in)	4
delta theta (rad)	0.031
incremental arc length (in)	0.126
Number of increments (ea)	100
Pressure (psi)	3750
Resultant on Increment Area (kip)	1.885

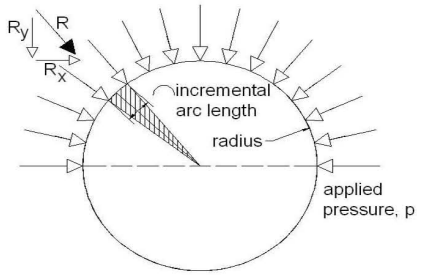

increment	R	theta	Ry	Rx
1	2.83	0.03	0.09	2.83
2	1.88	0.06	0.12	1.88
3	1.88	0.09	0.18	1.88
4	1.88	0.13	0.24	1.87
5	1.88	0.16	0.29	1.86
6	1.88	0.19	0.35	1.85
7	1.88	0.22	0.41	1.84
8	1.88	0.25	0.47	1.83
9	1.88	0.28	0.53	1.81
10	1.88	0.31	0.58	1.79
11	1.88	0.35	0.64	1.77
12	1.88	0.38	0.69	1.75
13	1.88	0.41	0.75	1.73
14	1.88	0.44	0.80	1.71
15	1.88	0.47	0.86	1.68
16	1.88	0.50	0.91	1.65
17	1.88	0.53	0.96	1.62
18	1.88	0.57	1.01	1.59
19	1.88	0.60	1.06	1.56
20	1.88	0.63	1.11	1.52
21	1.88	0.66	1.16	1.49
22	1.88	0.69	1.20	1.45
23	1.88	0.72	1.25	1.41
24	1.88	0.75	1.29	1.37
25	1.88	0.79	1.33	1.33
26	1.88	0.82	1.37	1.29
27	1.88	0.85	1.41	1.25
28	1.88	0.88	1.45	1.20
29	1.88	0.91	1.49	1.16
30	1.88	0.94	1.52	1.11
31	1.88	0.97	1.56	1.06
32	1.88	1.01	1.59	1.01
33	1.88	1.04	1.62	0.96
34	1.88	1.07	1.65	0.91
35	1.88	1.10	1.68	0.86
36	1.88	1.13	1.71	0.80
37	1.88	1.16	1.73	0.75
38	1.88	1.19	1.75	0.69
39	1.88	1.23	1.77	0.64
40	1.88	1.26	1.79	0.58
41	1.88	1.29	1.81	0.53
42	1.88	1.32	1.83	0.47
43	1.88	1.35	1.84	0.41
44	1.88	1.38	1.85	0.35
45	1.88	1.41	1.86	0.29
46	1.88	1.45	1.87	0.24
47	1.88	1.48	1.88	0.18
48	1.88	1.51	1.88	0.12
49	1.88	1.54	1.88	0.06
50	1.88	1.57	1.88	0.00
51	1.88	1.60	1.88	-0.06
52	1.88	1.63	1.88	-0.12
53	1.88	1.67	1.88	-0.18

increment	R	theta	Ry	Rx
54	1.88	1.70	1.87	-0.24
55	1.88	1.73	1.86	-0.29
56	1.88	1.76	1.85	-0.35
57	1.88	1.79	1.84	-0.41
58	1.88	1.82	1.83	-0.47
59	1.88	1.85	1.81	-0.53
60	1.88	1.88	1.79	-0.58
61	1.88	1.92	1.77	-0.64
62	1.88	1.95	1.75	-0.69
63	1.88	1.98	1.73	-0.75
64	1.88	2.01	1.71	-0.80
65	1.88	2.04	1.68	-0.86
66	1.88	2.07	1.65	-0.91
67	1.88	2.10	1.62	-0.96
68	1.88	2.14	1.59	-1.01
69	1.88	2.17	1.56	-1.06
70	1.88	2.20	1.52	-1.11
71	1.88	2.23	1.49	-1.16
72	1.88	2.26	1.45	-1.20
73	1.88	2.29	1.41	-1.25
74	1.88	2.32	1.37	-1.29
75	1.88	2.36	1.33	-1.33
76	1.88	2.39	1.29	-1.37
77	1.88	2.42	1.25	-1.41
78	1.88	2.45	1.20	-1.45
79	1.88	2.48	1.16	-1.49
80	1.88	2.51	1.11	-1.52
81	1.88	2.54	1.06	-1.56
82	1.88	2.58	1.01	-1.59
83	1.88	2.61	0.96	-1.62
84	1.88	2.64	0.91	-1.65
85	1.88	2.67	0.86	-1.68
86	1.88	2.70	0.80	-1.71
87	1.88	2.73	0.75	-1.73
88	1.88	2.76	0.69	-1.75
89	1.88	2.80	0.64	-1.77
90	1.88	2.83	0.58	-1.79
91	1.88	2.86	0.53	-1.81
92	1.88	2.89	0.47	-1.83
93	1.88	2.92	0.41	-1.84
94	1.88	2.95	0.35	-1.85
95	1.88	2.98	0.29	-1.86
96	1.88	3.02	0.24	-1.87
97	1.88	3.05	0.18	-1.88
98	1.88	3.08	0.12	-1.88
99	1.88	3.11	0.06	-1.88
100	0.94	3.14	0.00	-0.94
SUM	188.50	-	120.02	0.00

Check Total Force	188.50	OK

Figure A.6. Load input calculation - Cases 10, 13, 16, 110, 113, 116, 1010, 1013, and 1016

ABAQUS Model Verificaiton **Check Load Input** 6/23/2012

Surface Pressure to Vertical Reaction Force

shaft radius (in)	4
width of loaded area (in)	6
delta theta (rad)	0.031
incremental arc length (in)	0.126
Number of increments (ea)	100
Pressure (psi)	2500
Resultant on Increment Area (kip)	1.885

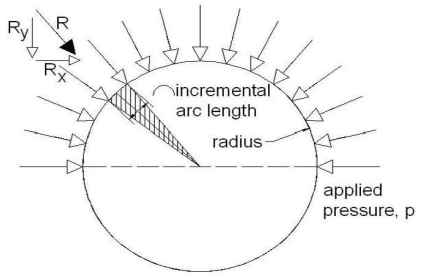

increment	R	theta	Ry	Rx
1	2.83	0.03	0.09	2.83
2	1.88	0.06	0.12	1.88
3	1.88	0.09	0.18	1.88
4	1.88	0.13	0.24	1.87
5	1.88	0.16	0.29	1.86
6	1.88	0.19	0.35	1.85
7	1.88	0.22	0.41	1.84
8	1.88	0.25	0.47	1.83
9	1.88	0.28	0.53	1.81
10	1.88	0.31	0.58	1.79
11	1.88	0.35	0.64	1.77
12	1.88	0.38	0.69	1.75
13	1.88	0.41	0.75	1.73
14	1.88	0.44	0.80	1.71
15	1.88	0.47	0.86	1.68
16	1.88	0.50	0.91	1.65
17	1.88	0.53	0.96	1.62
18	1.88	0.57	1.01	1.59
19	1.88	0.60	1.06	1.56
20	1.88	0.63	1.11	1.52
21	1.88	0.66	1.16	1.49
22	1.88	0.69	1.20	1.45
23	1.88	0.72	1.25	1.41
24	1.88	0.75	1.29	1.37
25	1.88	0.79	1.33	1.33
26	1.88	0.82	1.37	1.29
27	1.88	0.85	1.41	1.25
28	1.88	0.88	1.45	1.20
29	1.88	0.91	1.49	1.16
30	1.88	0.94	1.52	1.11
31	1.88	0.97	1.56	1.06
32	1.88	1.01	1.59	1.01
33	1.88	1.04	1.62	0.96
34	1.88	1.07	1.65	0.91
35	1.88	1.10	1.68	0.86
36	1.88	1.13	1.71	0.80
37	1.88	1.16	1.73	0.75
38	1.88	1.19	1.75	0.69
39	1.88	1.23	1.77	0.64
40	1.88	1.26	1.79	0.58
41	1.88	1.29	1.81	0.53
42	1.88	1.32	1.83	0.47
43	1.88	1.35	1.84	0.41
44	1.88	1.38	1.85	0.35
45	1.88	1.41	1.86	0.29
46	1.88	1.45	1.87	0.24
47	1.88	1.48	1.88	0.18
48	1.88	1.51	1.88	0.12
49	1.88	1.54	1.88	0.06
50	1.88	1.57	1.88	0.00
51	1.88	1.60	1.88	-0.06
52	1.88	1.63	1.88	-0.12
53	1.88	1.67	1.88	-0.18

increment	R	theta	Ry	Rx
54	1.88	1.70	1.87	-0.24
55	1.88	1.73	1.86	-0.29
56	1.88	1.76	1.85	-0.35
57	1.88	1.79	1.84	-0.41
58	1.88	1.82	1.83	-0.47
59	1.88	1.85	1.81	-0.53
60	1.88	1.88	1.79	-0.58
61	1.88	1.92	1.77	-0.64
62	1.88	1.95	1.75	-0.69
63	1.88	1.98	1.73	-0.75
64	1.88	2.01	1.71	-0.80
65	1.88	2.04	1.68	-0.86
66	1.88	2.07	1.65	-0.91
67	1.88	2.10	1.62	-0.96
68	1.88	2.14	1.59	-1.01
69	1.88	2.17	1.56	-1.06
70	1.88	2.20	1.52	-1.11
71	1.88	2.23	1.49	-1.16
72	1.88	2.26	1.45	-1.20
73	1.88	2.29	1.41	-1.25
74	1.88	2.32	1.37	-1.29
75	1.88	2.36	1.33	-1.33
76	1.88	2.39	1.29	-1.37
77	1.88	2.42	1.25	-1.41
78	1.88	2.45	1.20	-1.45
79	1.88	2.48	1.16	-1.49
80	1.88	2.51	1.11	-1.52
81	1.88	2.54	1.06	-1.56
82	1.88	2.58	1.01	-1.59
83	1.88	2.61	0.96	-1.62
84	1.88	2.64	0.91	-1.65
85	1.88	2.67	0.86	-1.68
86	1.88	2.70	0.80	-1.71
87	1.88	2.73	0.75	-1.73
88	1.88	2.76	0.69	-1.75
89	1.88	2.80	0.64	-1.77
90	1.88	2.83	0.58	-1.79
91	1.88	2.86	0.53	-1.81
92	1.88	2.89	0.47	-1.83
93	1.88	2.92	0.41	-1.84
94	1.88	2.95	0.35	-1.85
95	1.88	2.98	0.29	-1.86
96	1.88	3.02	0.24	-1.87
97	1.88	3.05	0.18	-1.88
98	1.88	3.08	0.12	-1.88
99	1.88	3.11	0.06	-1.88
100	0.94	3.14	0.00	-0.94
SUM	188.50	-	120.02	0.00

Check Total Force	188.50	OK

Figure A.7. Load input calculation - Cases 11, 14, 17, 111, 114, 117, 1011, 1014, and 1017

ABAQUS Model Verificaiton **Check Load Input** 6/23/2012

Surface Pressure to Vertical Reaction Force

shaft radius (in)	4
width of loaded area (in)	8
delta theta (rad)	0.031
incremental arc length (in)	0.126
Number of increments (ea)	100
Pressure (psi)	1875
Resultant on Increment Area (kip)	1.885

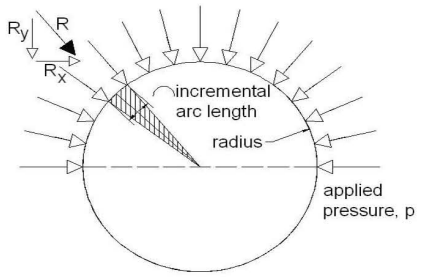

increment	R	theta	Ry	Rx
1	2.83	0.03	0.09	2.83
2	1.88	0.06	0.12	1.88
3	1.88	0.09	0.18	1.88
4	1.88	0.13	0.24	1.87
5	1.88	0.16	0.29	1.86
6	1.88	0.19	0.35	1.85
7	1.88	0.22	0.41	1.84
8	1.88	0.25	0.47	1.83
9	1.88	0.28	0.53	1.81
10	1.88	0.31	0.58	1.79
11	1.88	0.35	0.64	1.77
12	1.88	0.38	0.69	1.75
13	1.88	0.41	0.75	1.73
14	1.88	0.44	0.80	1.71
15	1.88	0.47	0.86	1.68
16	1.88	0.50	0.91	1.65
17	1.88	0.53	0.96	1.62
18	1.88	0.57	1.01	1.59
19	1.88	0.60	1.06	1.56
20	1.88	0.63	1.11	1.52
21	1.88	0.66	1.16	1.49
22	1.88	0.69	1.20	1.45
23	1.88	0.72	1.25	1.41
24	1.88	0.75	1.29	1.37
25	1.88	0.79	1.33	1.33
26	1.88	0.82	1.37	1.29
27	1.88	0.85	1.41	1.25
28	1.88	0.88	1.45	1.20
29	1.88	0.91	1.49	1.16
30	1.88	0.94	1.52	1.11
31	1.88	0.97	1.56	1.06
32	1.88	1.01	1.59	1.01
33	1.88	1.04	1.62	0.96
34	1.88	1.07	1.65	0.91
35	1.88	1.10	1.68	0.86
36	1.88	1.13	1.71	0.80
37	1.88	1.16	1.73	0.75
38	1.88	1.19	1.75	0.69
39	1.88	1.23	1.77	0.64
40	1.88	1.26	1.79	0.58
41	1.88	1.29	1.81	0.53
42	1.88	1.32	1.83	0.47
43	1.88	1.35	1.84	0.41
44	1.88	1.38	1.85	0.35
45	1.88	1.41	1.86	0.29
46	1.88	1.45	1.87	0.24
47	1.88	1.48	1.88	0.18
48	1.88	1.51	1.88	0.12
49	1.88	1.54	1.88	0.06
50	1.88	1.57	1.88	0.00
51	1.88	1.60	1.88	-0.06
52	1.88	1.63	1.88	-0.12
53	1.88	1.67	1.88	-0.18

increment	R	theta	Ry	Rx
54	1.88	1.70	1.87	-0.24
55	1.88	1.73	1.86	-0.29
56	1.88	1.76	1.85	-0.35
57	1.88	1.79	1.84	-0.41
58	1.88	1.82	1.83	-0.47
59	1.88	1.85	1.81	-0.53
60	1.88	1.88	1.79	-0.58
61	1.88	1.92	1.77	-0.64
62	1.88	1.95	1.75	-0.69
63	1.88	1.98	1.73	-0.75
64	1.88	2.01	1.71	-0.80
65	1.88	2.04	1.68	-0.86
66	1.88	2.07	1.65	-0.91
67	1.88	2.10	1.62	-0.96
68	1.88	2.14	1.59	-1.01
69	1.88	2.17	1.56	-1.06
70	1.88	2.20	1.52	-1.11
71	1.88	2.23	1.49	-1.16
72	1.88	2.26	1.45	-1.20
73	1.88	2.29	1.41	-1.25
74	1.88	2.32	1.37	-1.29
75	1.88	2.36	1.33	-1.33
76	1.88	2.39	1.29	-1.37
77	1.88	2.42	1.25	-1.41
78	1.88	2.45	1.20	-1.45
79	1.88	2.48	1.16	-1.49
80	1.88	2.51	1.11	-1.52
81	1.88	2.54	1.06	-1.56
82	1.88	2.58	1.01	-1.59
83	1.88	2.61	0.96	-1.62
84	1.88	2.64	0.91	-1.65
85	1.88	2.67	0.86	-1.68
86	1.88	2.70	0.80	-1.71
87	1.88	2.73	0.75	-1.73
88	1.88	2.76	0.69	-1.75
89	1.88	2.80	0.64	-1.77
90	1.88	2.83	0.58	-1.79
91	1.88	2.86	0.53	-1.81
92	1.88	2.89	0.47	-1.83
93	1.88	2.92	0.41	-1.84
94	1.88	2.95	0.35	-1.85
95	1.88	2.98	0.29	-1.86
96	1.88	3.02	0.24	-1.87
97	1.88	3.05	0.18	-1.88
98	1.88	3.08	0.12	-1.88
99	1.88	3.11	0.06	-1.88
100	0.94	3.14	0.00	-0.94
SUM	188.50	-	120.02	0.00

Check Total Force	188.50	OK

Figure A.8. Load input calculation - Cases 12, 15, 18, 112, 115, 118, 1012, 1015, and 1018

ABAQUS Model Verificaiton **Check Load Input** 6/23/2012

Surface Pressure to Vertical Reaction Force

shaft radius (in)	4
width of loaded area (in)	10
delta theta (rad)	0.031
incremental arc length (in)	0.126
Number of increments (ea)	100
Pressure (psi)	955
Resultant on Increment Area (kip)	1.200

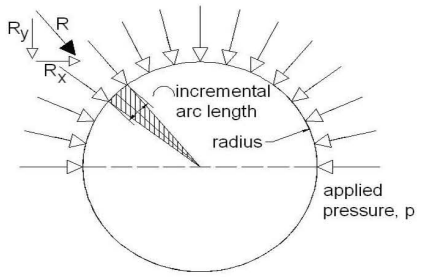

increment	R	theta	Ry	Rx
1	1.80	0.03	0.06	1.80
2	1.20	0.06	0.08	1.20
3	1.20	0.09	0.11	1.19
4	1.20	0.13	0.15	1.19
5	1.20	0.16	0.19	1.19
6	1.20	0.19	0.22	1.18
7	1.20	0.22	0.26	1.17
8	1.20	0.25	0.30	1.16
9	1.20	0.28	0.33	1.15
10	1.20	0.31	0.37	1.14
11	1.20	0.35	0.41	1.13
12	1.20	0.38	0.44	1.12
13	1.20	0.41	0.48	1.10
14	1.20	0.44	0.51	1.09
15	1.20	0.47	0.54	1.07
16	1.20	0.50	0.58	1.05
17	1.20	0.53	0.61	1.03
18	1.20	0.57	0.64	1.01
19	1.20	0.60	0.67	0.99
20	1.20	0.63	0.71	0.97
21	1.20	0.66	0.74	0.95
22	1.20	0.69	0.76	0.92
23	1.20	0.72	0.79	0.90
24	1.20	0.75	0.82	0.87
25	1.20	0.79	0.85	0.85
26	1.20	0.82	0.87	0.82
27	1.20	0.85	0.90	0.79
28	1.20	0.88	0.92	0.76
29	1.20	0.91	0.95	0.74
30	1.20	0.94	0.97	0.71
31	1.20	0.97	0.99	0.67
32	1.20	1.01	1.01	0.64
33	1.20	1.04	1.03	0.61
34	1.20	1.07	1.05	0.58
35	1.20	1.10	1.07	0.54
36	1.20	1.13	1.09	0.51
37	1.20	1.16	1.10	0.48
38	1.20	1.19	1.12	0.44
39	1.20	1.23	1.13	0.41
40	1.20	1.26	1.14	0.37
41	1.20	1.29	1.15	0.33
42	1.20	1.32	1.16	0.30
43	1.20	1.35	1.17	0.26
44	1.20	1.38	1.18	0.22
45	1.20	1.41	1.19	0.19
46	1.20	1.45	1.19	0.15
47	1.20	1.48	1.19	0.11
48	1.20	1.51	1.20	0.08
49	1.20	1.54	1.20	0.04
50	1.20	1.57	1.20	0.00
51	1.20	1.60	1.20	-0.04
52	1.20	1.63	1.20	-0.08
53	1.20	1.67	1.19	-0.11
54	1.20	1.70	1.19	-0.15
55	1.20	1.73	1.19	-0.19
56	1.20	1.76	1.18	-0.22
57	1.20	1.79	1.17	-0.26
58	1.20	1.82	1.16	-0.30
59	1.20	1.85	1.15	-0.33
60	1.20	1.88	1.14	-0.37
61	1.20	1.92	1.13	-0.41
62	1.20	1.95	1.12	-0.44
63	1.20	1.98	1.10	-0.48
64	1.20	2.01	1.09	-0.51
65	1.20	2.04	1.07	-0.54
66	1.20	2.07	1.05	-0.58
67	1.20	2.10	1.03	-0.61
68	1.20	2.14	1.01	-0.64
69	1.20	2.17	0.99	-0.67
70	1.20	2.20	0.97	-0.71
71	1.20	2.23	0.95	-0.74
72	1.20	2.26	0.92	-0.76
73	1.20	2.29	0.90	-0.79
74	1.20	2.32	0.87	-0.82
75	1.20	2.36	0.85	-0.85
76	1.20	2.39	0.82	-0.87
77	1.20	2.42	0.79	-0.90
78	1.20	2.45	0.76	-0.92
79	1.20	2.48	0.74	-0.95
80	1.20	2.51	0.71	-0.97
81	1.20	2.54	0.67	-0.99
82	1.20	2.58	0.64	-1.01
83	1.20	2.61	0.61	-1.03
84	1.20	2.64	0.58	-1.05
85	1.20	2.67	0.54	-1.07
86	1.20	2.70	0.51	-1.09
87	1.20	2.73	0.48	-1.10
88	1.20	2.76	0.44	-1.12
89	1.20	2.80	0.41	-1.13
90	1.20	2.83	0.37	-1.14
91	1.20	2.86	0.33	-1.15
92	1.20	2.89	0.30	-1.16
93	1.20	2.92	0.26	-1.17
94	1.20	2.95	0.22	-1.18
95	1.20	2.98	0.19	-1.19
96	1.20	3.02	0.15	-1.19
97	1.20	3.05	0.11	-1.19
98	1.20	3.08	0.08	-1.20
99	1.20	3.11	0.04	-1.20
100	0.60	3.14	0.00	-0.60
SUM	120.01	-	76.41	0.00

Check Total Force	120.01	OK

Figure A.9. Load input calculation - Case 19, 119, and 1019

ABAQUS Model Verificaiton **Check Load Input** 6/23/2012

Surface Pressure to Vertical Reaction Force

shaft radius (in)	4
width of loaded area (in)	12
delta theta (rad)	0.031
incremental arc length (in)	0.126
Number of increments (ea)	100
Pressure (psi)	796
Resultant on Increment Area (kip)	1.200

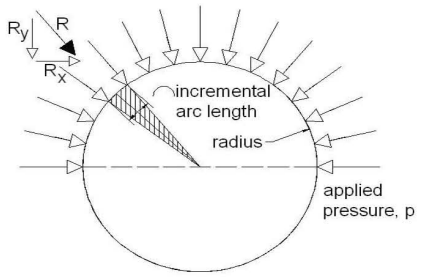

increment	R	theta	Ry	Rx
1	1.80	0.03	0.06	1.80
2	1.20	0.06	0.08	1.20
3	1.20	0.09	0.11	1.20
4	1.20	0.13	0.15	1.19
5	1.20	0.16	0.19	1.19
6	1.20	0.19	0.22	1.18
7	1.20	0.22	0.26	1.17
8	1.20	0.25	0.30	1.16
9	1.20	0.28	0.33	1.15
10	1.20	0.31	0.37	1.14
11	1.20	0.35	0.41	1.13
12	1.20	0.38	0.44	1.12
13	1.20	0.41	0.48	1.10
14	1.20	0.44	0.51	1.09
15	1.20	0.47	0.54	1.07
16	1.20	0.50	0.58	1.05
17	1.20	0.53	0.61	1.03
18	1.20	0.57	0.64	1.01
19	1.20	0.60	0.67	0.99
20	1.20	0.63	0.71	0.97
21	1.20	0.66	0.74	0.95
22	1.20	0.69	0.77	0.92
23	1.20	0.72	0.79	0.90
24	1.20	0.75	0.82	0.88
25	1.20	0.79	0.85	0.85
26	1.20	0.82	0.88	0.82
27	1.20	0.85	0.90	0.79
28	1.20	0.88	0.92	0.77
29	1.20	0.91	0.95	0.74
30	1.20	0.94	0.97	0.71
31	1.20	0.97	0.99	0.67
32	1.20	1.01	1.01	0.64
33	1.20	1.04	1.03	0.61
34	1.20	1.07	1.05	0.58
35	1.20	1.10	1.07	0.54
36	1.20	1.13	1.09	0.51
37	1.20	1.16	1.10	0.48
38	1.20	1.19	1.12	0.44
39	1.20	1.23	1.13	0.41
40	1.20	1.26	1.14	0.37
41	1.20	1.29	1.15	0.33
42	1.20	1.32	1.16	0.30
43	1.20	1.35	1.17	0.26
44	1.20	1.38	1.18	0.22
45	1.20	1.41	1.19	0.19
46	1.20	1.45	1.19	0.15
47	1.20	1.48	1.20	0.11
48	1.20	1.51	1.20	0.08
49	1.20	1.54	1.20	0.04
50	1.20	1.57	1.20	0.00
51	1.20	1.60	1.20	-0.04
52	1.20	1.63	1.20	-0.08
53	1.20	1.67	1.20	-0.11

increment	R	theta	Ry	Rx
54	1.20	1.70	1.19	-0.15
55	1.20	1.73	1.19	-0.19
56	1.20	1.76	1.18	-0.22
57	1.20	1.79	1.17	-0.26
58	1.20	1.82	1.16	-0.30
59	1.20	1.85	1.15	-0.33
60	1.20	1.88	1.14	-0.37
61	1.20	1.92	1.13	-0.41
62	1.20	1.95	1.12	-0.44
63	1.20	1.98	1.10	-0.48
64	1.20	2.01	1.09	-0.51
65	1.20	2.04	1.07	-0.54
66	1.20	2.07	1.05	-0.58
67	1.20	2.10	1.03	-0.61
68	1.20	2.14	1.01	-0.64
69	1.20	2.17	0.99	-0.67
70	1.20	2.20	0.97	-0.71
71	1.20	2.23	0.95	-0.74
72	1.20	2.26	0.92	-0.77
73	1.20	2.29	0.90	-0.79
74	1.20	2.32	0.88	-0.82
75	1.20	2.36	0.85	-0.85
76	1.20	2.39	0.82	-0.88
77	1.20	2.42	0.79	-0.90
78	1.20	2.45	0.77	-0.92
79	1.20	2.48	0.74	-0.95
80	1.20	2.51	0.71	-0.97
81	1.20	2.54	0.67	-0.99
82	1.20	2.58	0.64	-1.01
83	1.20	2.61	0.61	-1.03
84	1.20	2.64	0.58	-1.05
85	1.20	2.67	0.54	-1.07
86	1.20	2.70	0.51	-1.09
87	1.20	2.73	0.48	-1.10
88	1.20	2.76	0.44	-1.12
89	1.20	2.80	0.41	-1.13
90	1.20	2.83	0.37	-1.14
91	1.20	2.86	0.33	-1.15
92	1.20	2.89	0.30	-1.16
93	1.20	2.92	0.26	-1.17
94	1.20	2.95	0.22	-1.18
95	1.20	2.98	0.19	-1.19
96	1.20	3.02	0.15	-1.19
97	1.20	3.05	0.11	-1.20
98	1.20	3.08	0.08	-1.20
99	1.20	3.11	0.04	-1.20
100	0.60	3.14	0.00	-0.60
SUM	120.03	-	76.43	0.00

Check Total Force	120.03	OK

Figure A.10. Load input calculation - Typical for Case 20, 120, and 1020

APPENDIX B

VALIDATION – SHAFT DEFLECTION

As another validation check to the ABAQUS models, the deflection of the trunnion shaft was checked for the configuration of case 5, which modeled a 4 inch diamter trunnion shaft, spanning 8 inches between (2) 4 inch thick yoke plates.

The deflection was checked assuming a simply supported beam using hand calculaitons as well as two SAP2000 beam models. The deflection was calculated for (2) different lengths: (1) clear span of 8 inches and (2) the center to center distance between the two yoke plates, 12 inches. This was considered an acceptable range to envelope the expected deflection as modeled in ABAQUS. See the calculations below.

$P := 120kip$ *trunnion load*

$b := 8in$ *width of distributed load*

$t_{yoke} := 4in$ *thickness of supporting yoke plates*

$E := 29000ksi$ *young's modulus of steel*

$L := 8in = 8.0 \cdot in$ *effective length of shaft*

$w := \frac{P}{b} = 15.0 \cdot \frac{kip}{in}$ *distributed load*

$D := 4in$ *shaft diameter*

$I := \frac{\pi \cdot D^4}{64} = 12.6 \cdot in^4$ *moment of inertia*

$\Delta := \frac{5 \cdot w \cdot L^4}{384 \cdot E \cdot I} = 2.2 \cdot \frac{in}{1000}$ *deflection of shaft*

The hand calculations resulted in a maximum deflection of 2.2 inches, located at the center of the shaft. The simly supported beam was also inputted into SAP2000 to determine the maximum deflection.

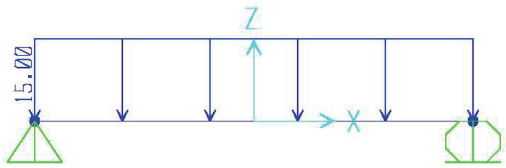

FIGURE B.1. Simply supported load diagram assuming clear span as the beam length.

The SAP2000 model of the simply suppoerted beam with a length of 8 inches resulted in a maximum deflection of 2.2/1000 inches located at the center of the span; therefore, the 2.2/1000 inches was considered the lower bound of the acceptable range of the shaft deflection.

Another SAP2000 model was created to determine the upport bound limit of the acceptable range of the trunnion shaft deflection. In the second model, the same distributed load was applied over 8 inches; however, the overal span of the shaft was increased to 12 inches, which is the center to center distance between the two supporting yoke plates.

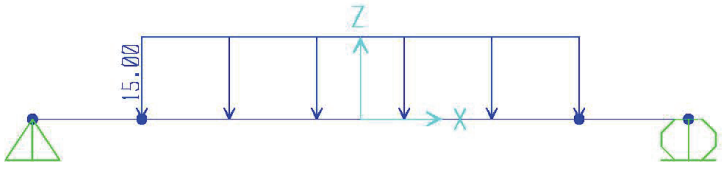

FIGURE B.2. Simply supported load diagram assuming center to center distance as the beam length.

The model produced a maximum deflection of 4.8/1000 inches, which was considered the upper bound of the acceptable range for the trunnion shaft deflection.

As shown above, the expected deflection of the trunnion shaft relative to its end is between 2.2 and 4.8 thousandths of an inch. The global deflected coordinates of the trunnion shaft were outputted from the ABAQUS model (case 5) at the centerline of the shaft and at a node located at the inboard edge of the yoke plate support.

Deformed Nodal Coordinates of A Node at Centerline of Trunnion Shaft (Node ID 10028):

$X_1 := -0.125581\text{in}$

$Y_1 := -2.0019\text{in}$

$Z_1 := 8.00\text{in}$

Deformed Nodal Coordinates of A Node at Inboard Edge of Yoke Plate (Node ID 5036):

$X_2 := 0.125544\text{in}$

$Y_2 := -1.99839\text{in}$

$Z_2 := 3.99774\text{in}$

Relative Vertical Deflection:

$$\delta := Y_2 - Y_1 = 3.5\frac{\text{in}}{1000}$$

As shown above, the ABAQUS model determined that the relative deflection of the trunnion shaft was 3.5 thousandths of an inch, which is within the expected range (2.2/1000 inch and 4.8/1000 inch) previously calculated by hand.

APPENDIX C

VON MISES CONTOUR PLOTS – NO SLEEVE

Appendix C includes a series of screenshots taken from the different ABAQUS models that were developed. For reference, table C.1 provides the specific parameters that are associated to each of the analysis cases that are documented within this appendix.

Table C.1. Summary of cases without a sleeve.

Case	Sleeve	Shaft Diameter (in)	Trunnion Load (kips)	Yoke Plate Thickness (in)	Clear Span (in)
1	None	4	120	2	2
2	None	4	120	2	4
3	None	4	120	2	6
4	None	4	120	4	4
5	None	4	120	4	8
6	None	4	120	4	12
7	None	4	120	6	4
8	None	4	120	6	8
9	None	4	120	6	12
10	None	8	240	2	8
11	None	8	240	2	12
12	None	8	240	2	16
13	None	8	240	4	8
14	None	8	240	4	12
15	None	8	240	4	16
16	None	8	240	6	8
17	None	8	240	6	12
18	None	8	240	6	16
19	None	8	240	6	20
20	None	8	240	6	4

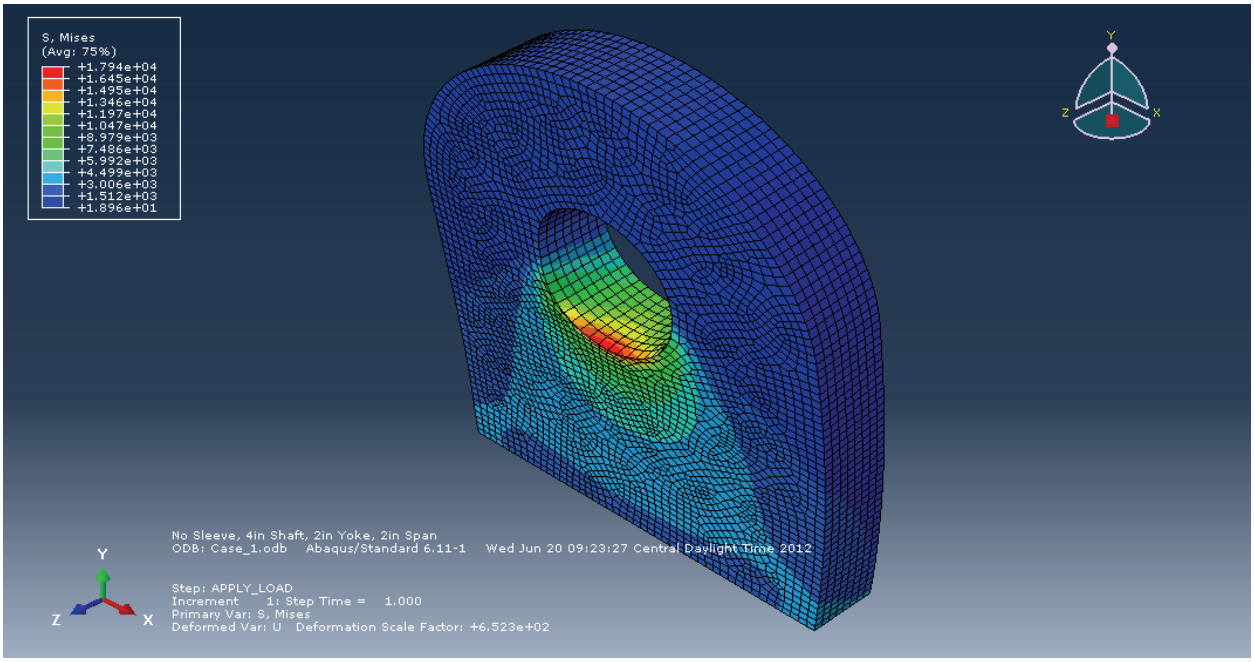

Figure C.1 – Case 1 Yoke Plate von Mises Contours (4 Inch Diameter Shaft, 2 Inch Thick Yoke, 2 Inch Span)

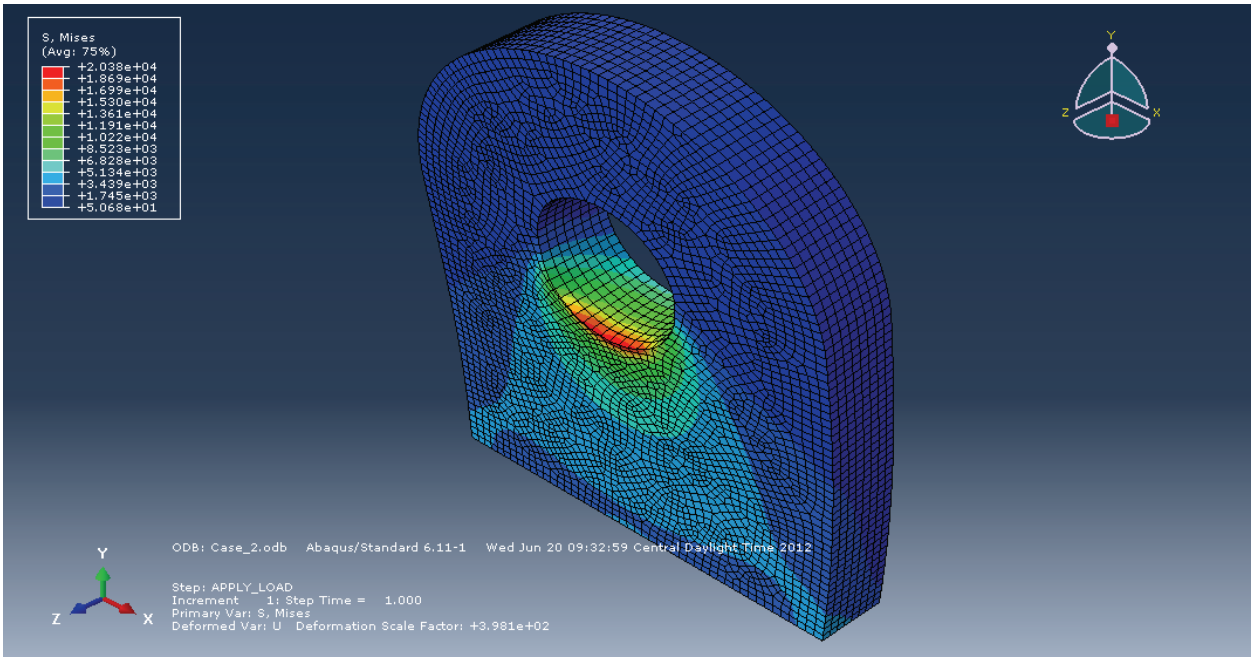

Figure C.2 – Case 2 Yoke Plate von Mises Contours (4 Inch Diameter Shaft, 2 Inch Thick Yoke, 4 Inch Span)

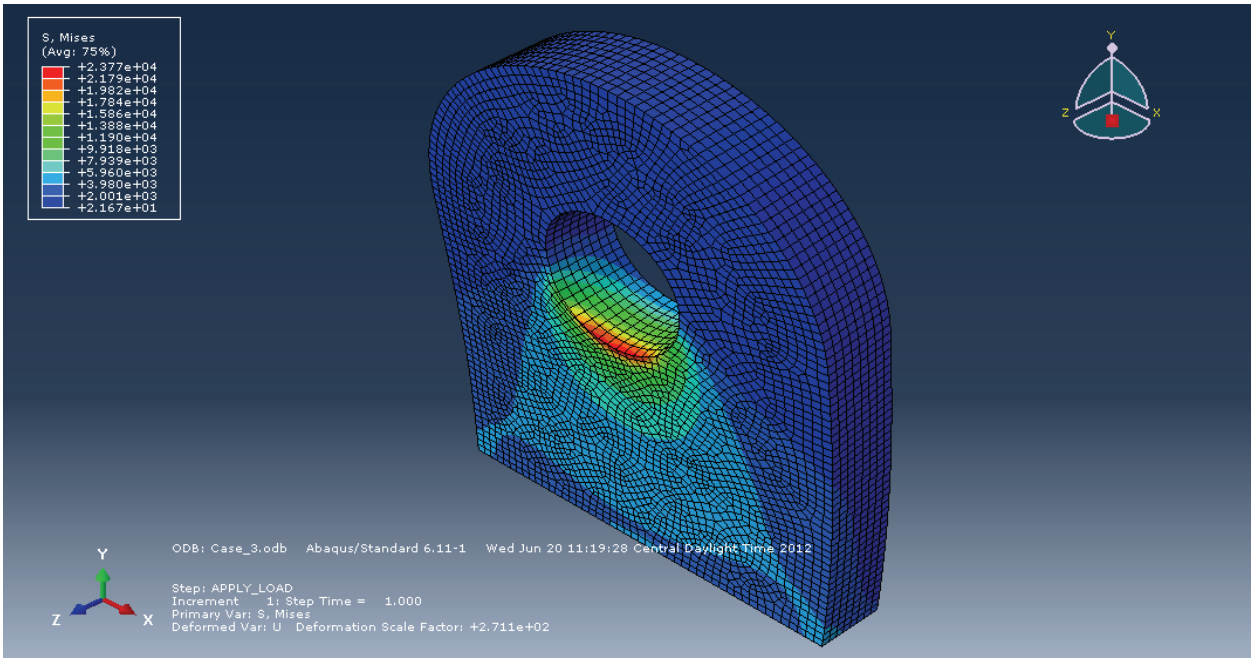

Figure C.3 – Case 3 Yoke Plate von Mises Contours (4 Inch Diameter Shaft, 2 Inch Thick Yoke, 6 Inch Span)

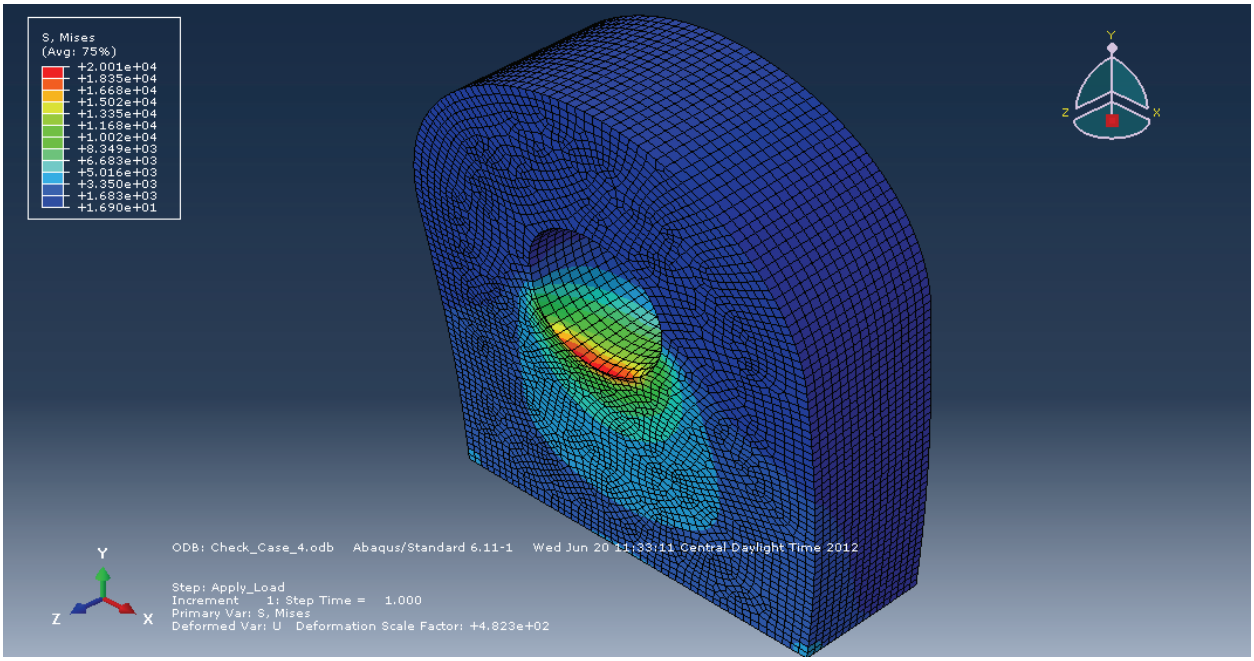

Figure C.4 – Case 4 Yoke Plate von Mises Contours (4 Inch Diameter Shaft, 4 Inch Thick Yoke, 4 Inch Span)

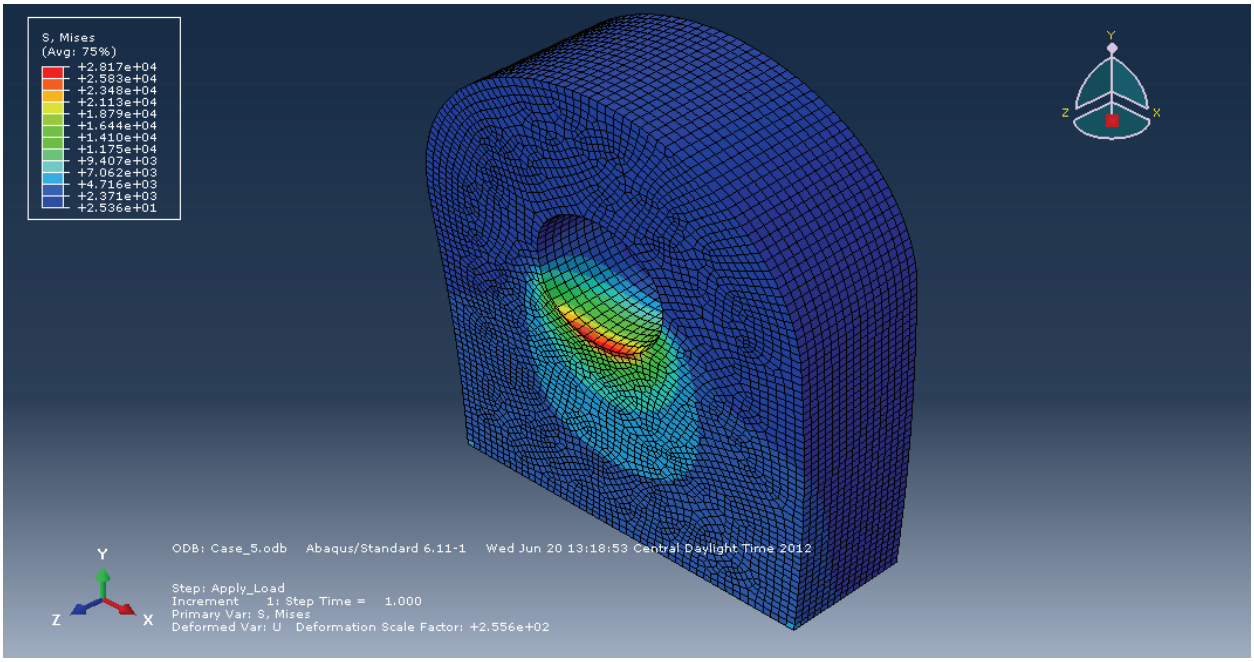

Figure C.5 – Case 5 Yoke Plate von Mises Contours (4 Inch Diameter Shaft, 4 Inch Thick Yoke, 8 Inch Span)

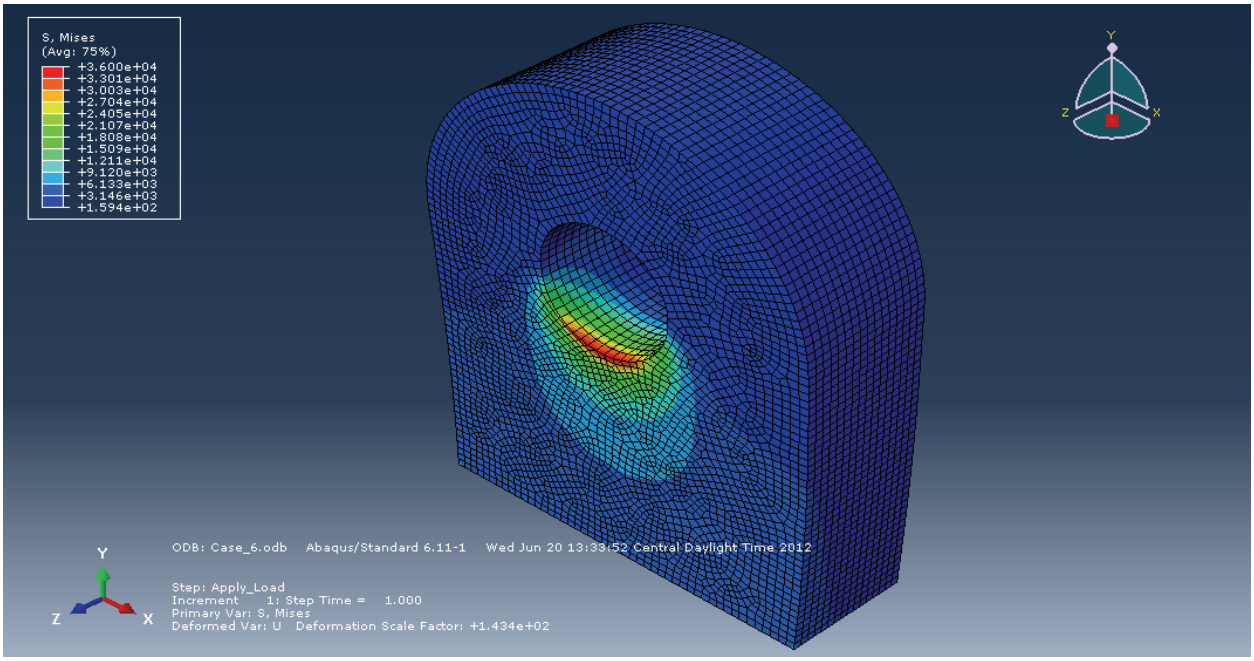

Figure C.6 – Case 6 Yoke Plate von Mises Contours (4 Inch Diameter Shaft, 4 Inch Thick Yoke, 12 Inch Span)

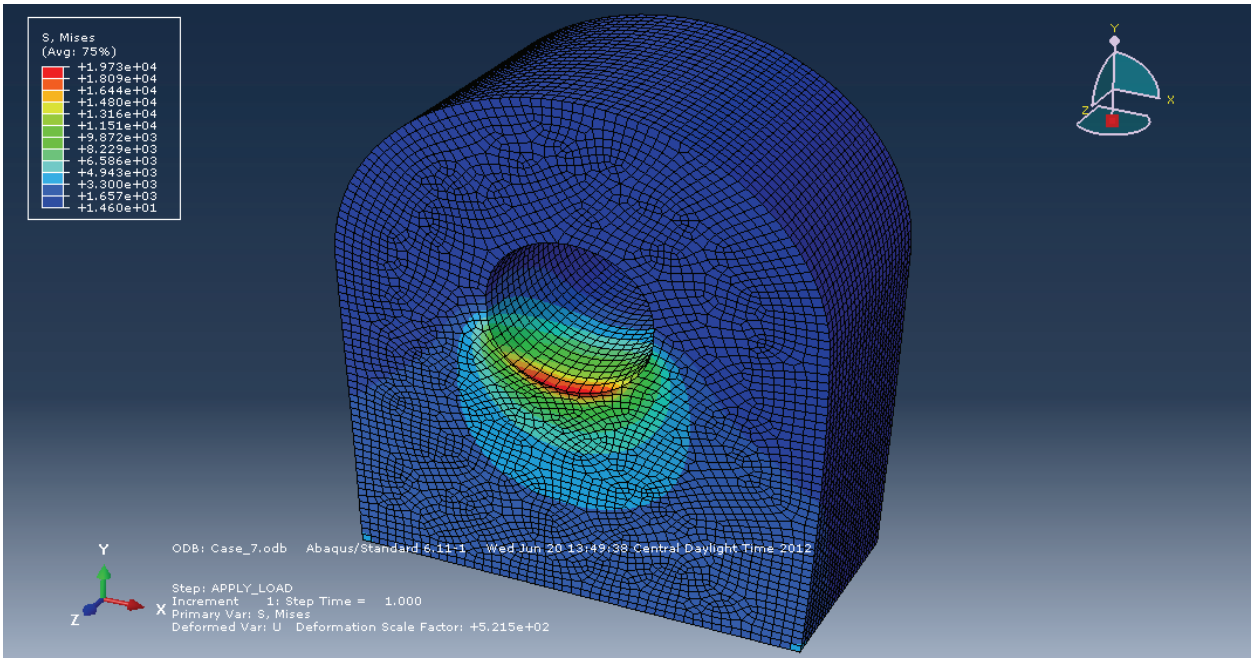

Figure C.7 – Case 7 Yoke Plate von Mises Contours (4 Inch Diameter Shaft, 6 Inch Thick Yoke, 4 Inch Span)

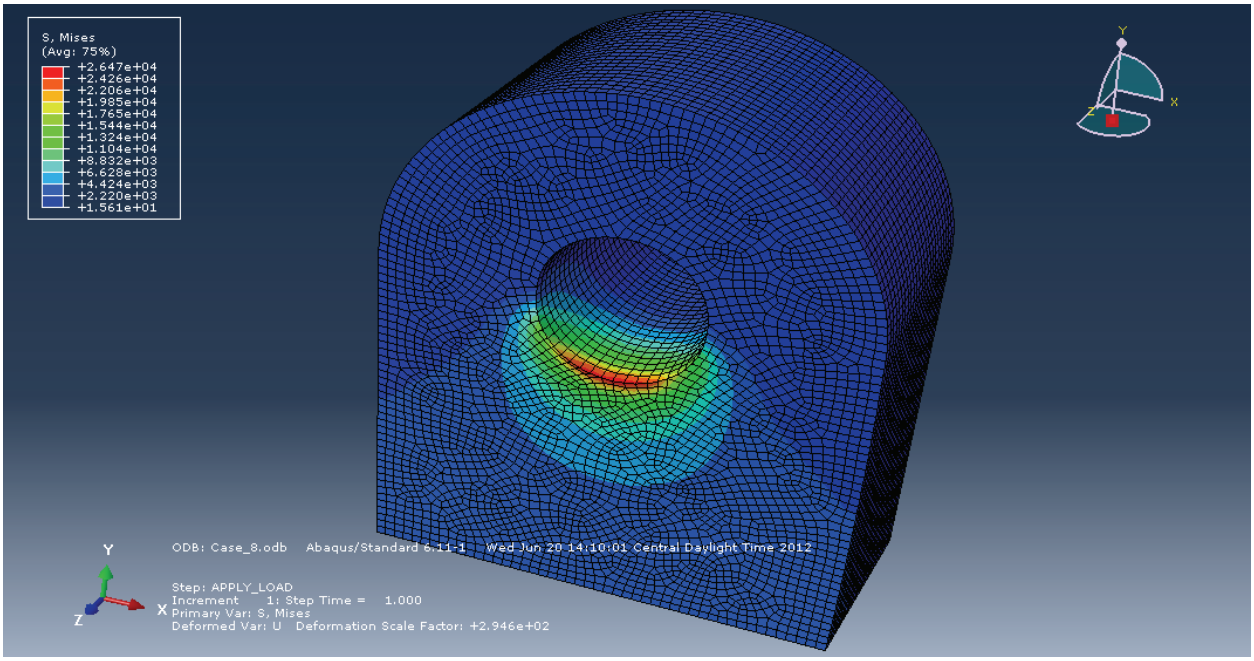

Figure C.8 – Case 8 Yoke Plate von Mises Contours (4 Inch Diameter Shaft, 6 Inch Thick Yoke, 8 Inch Span)

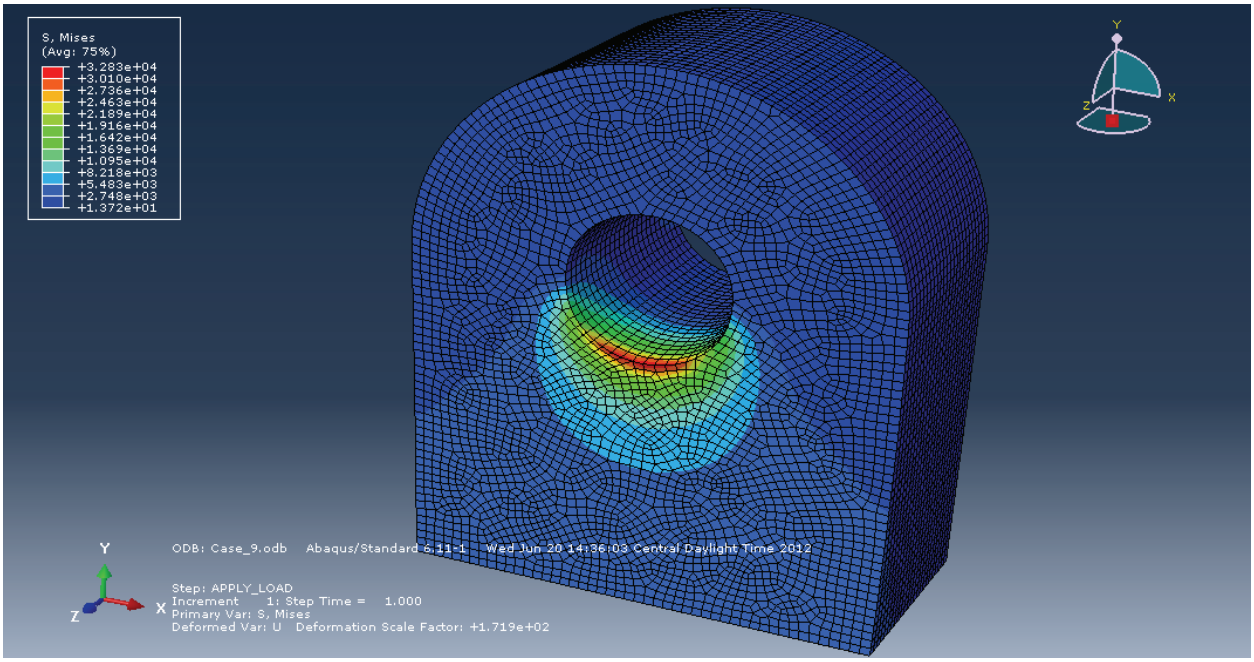

Figure C.9 – Case 9 Yoke Plate von Mises Contours (4 Inch Diameter Shaft, 6 Inch Thick Yoke, 12 Inch Span)

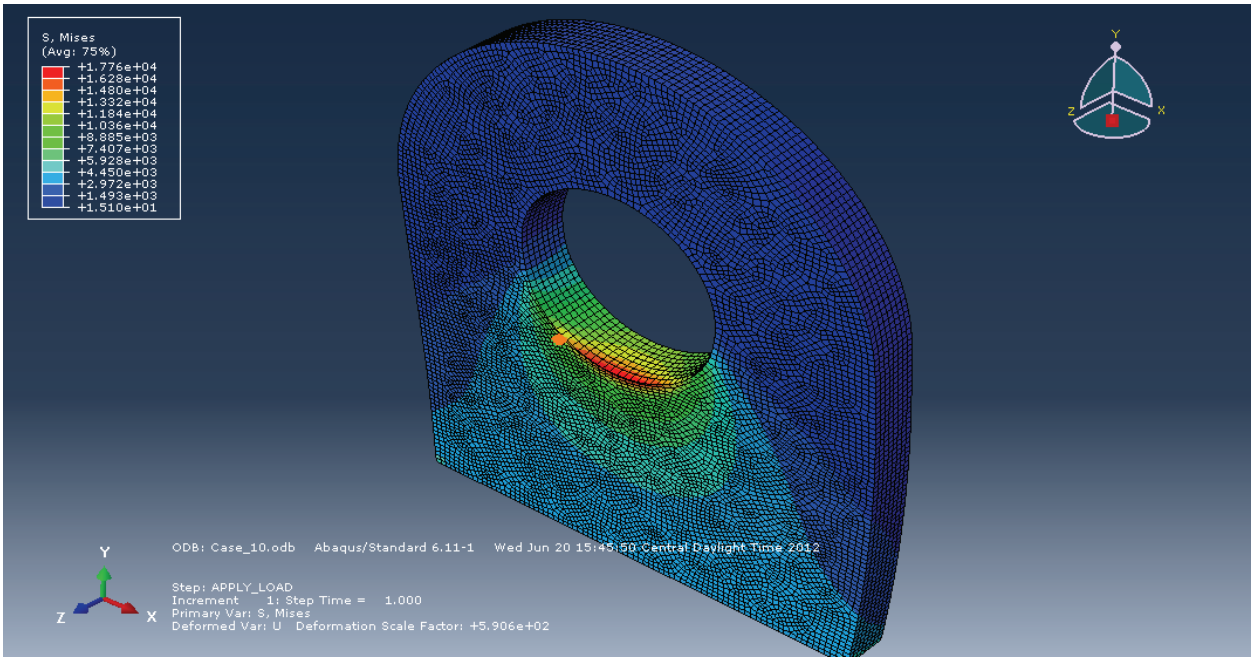

Figure C.10 – Case 10 Yoke Plate von Mises Contours (8 Inch Diameter Shaft, 2 Inch Thick Yoke, 8 Inch Span)

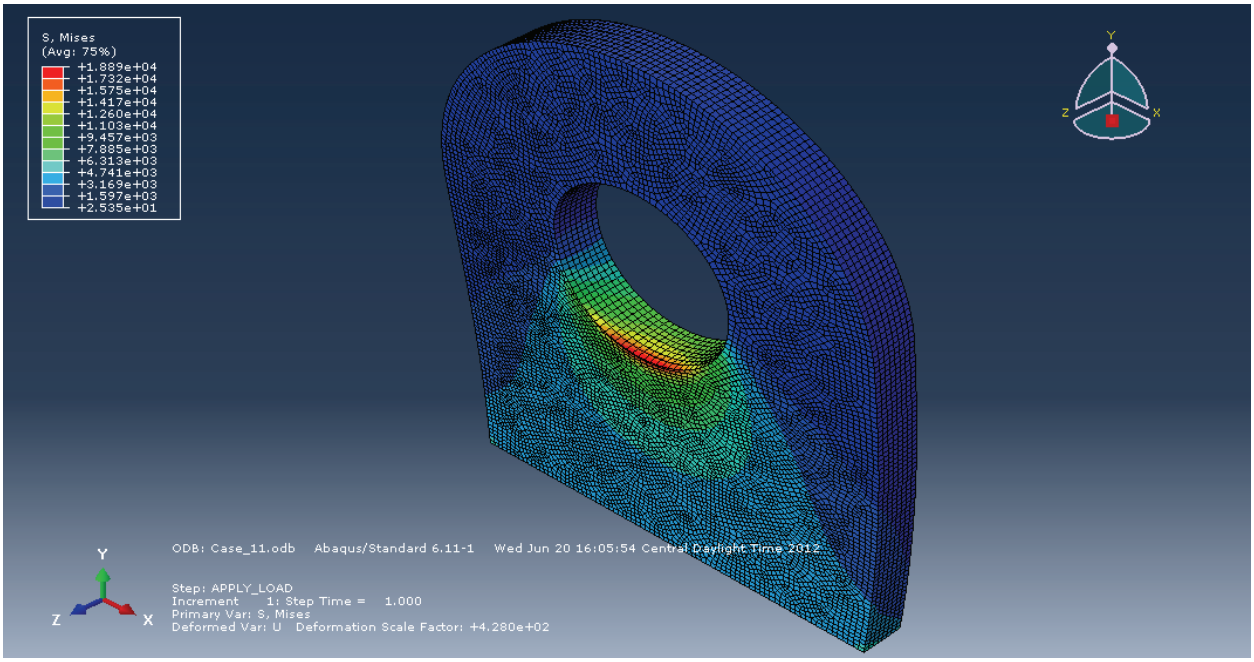

Figure C.11 – Case 11 Yoke Plate von Mises Contours (8 Inch Diameter Shaft, 2 Inch Thick Yoke, 12 Inch Span)

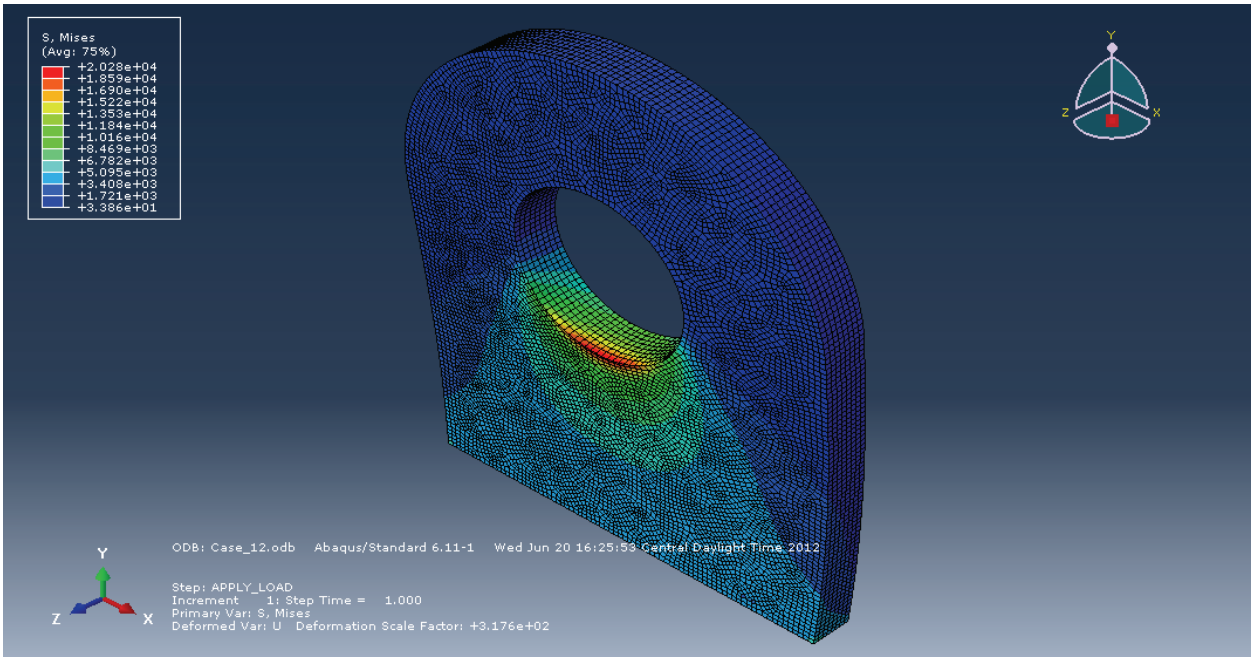

Figure C.12 – Case 12 Yoke Plate von Mises Contours (8 Inch Diameter Shaft, 2 Inch Thick Yoke, 16 Inch Span)

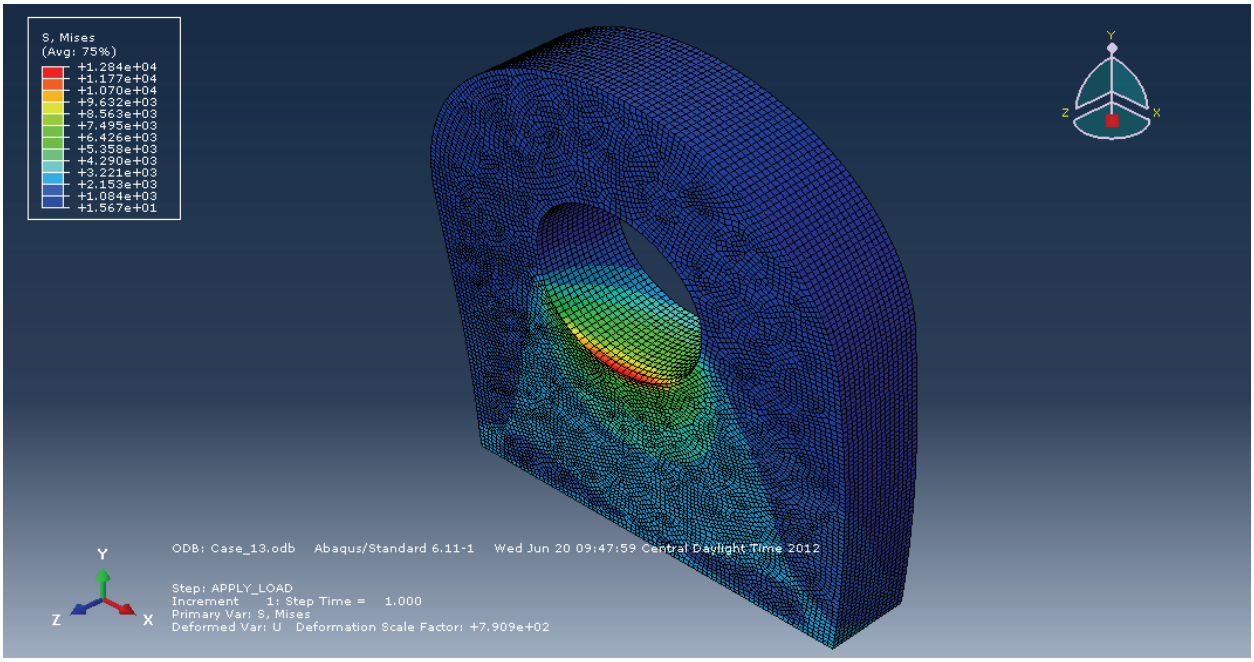

Figure C.13 – Case 13 Yoke Plate von Mises Contours (8 Inch Diameter Shaft, 4 Inch Thick Yoke, 8 Inch Span)

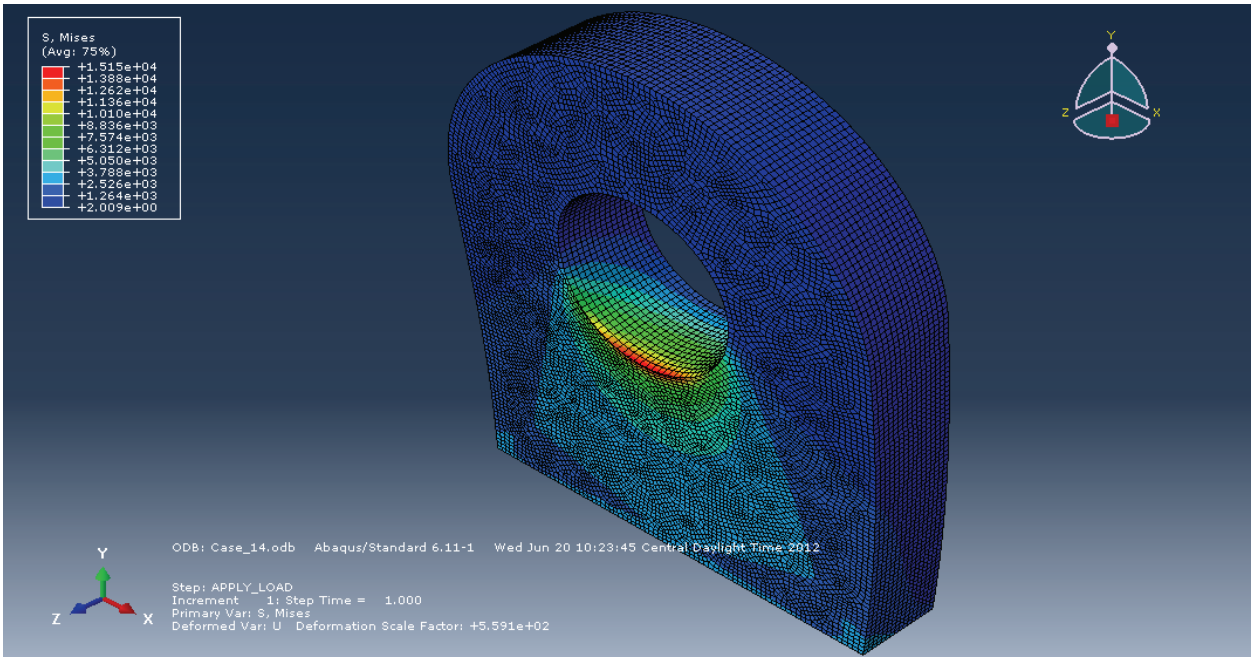

Figure C.14 – Case 14 Yoke Plate von Mises Contours (8 Inch Diameter Shaft, 4 Inch Thick Yoke, 12 Inch Span)

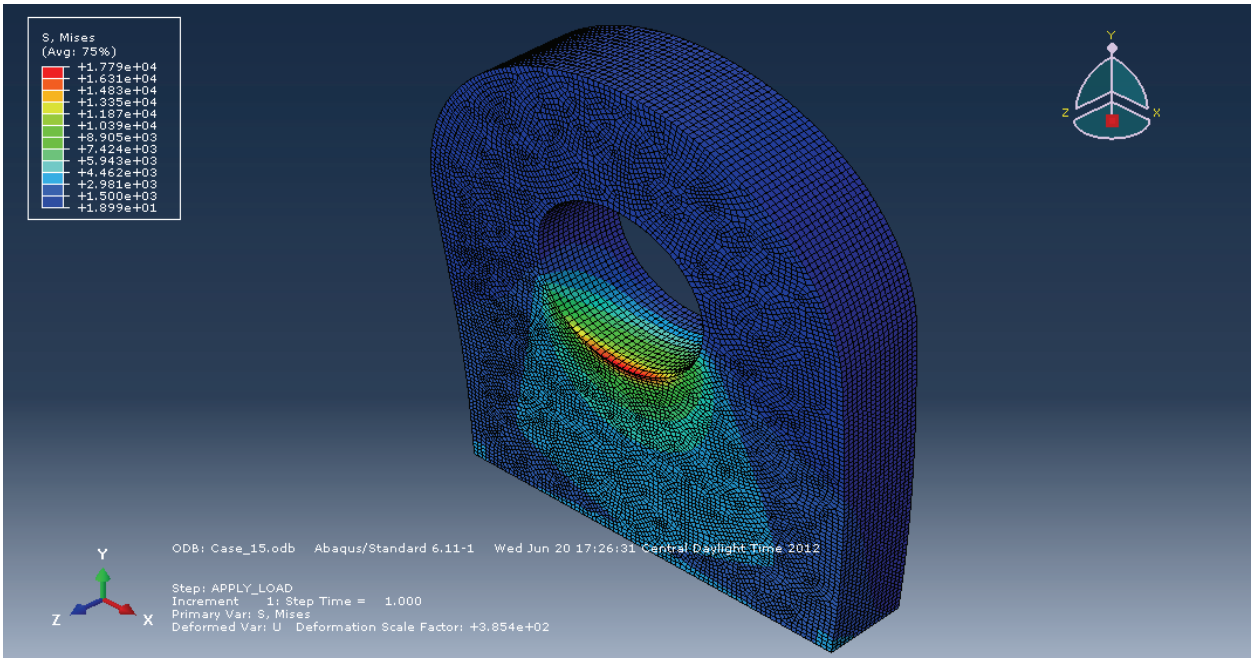

Figure C.15 – Case 15 Yoke Plate von Mises Contours (8 Inch Diameter Shaft, 4 Inch Thick Yoke, 16 Inch Span)

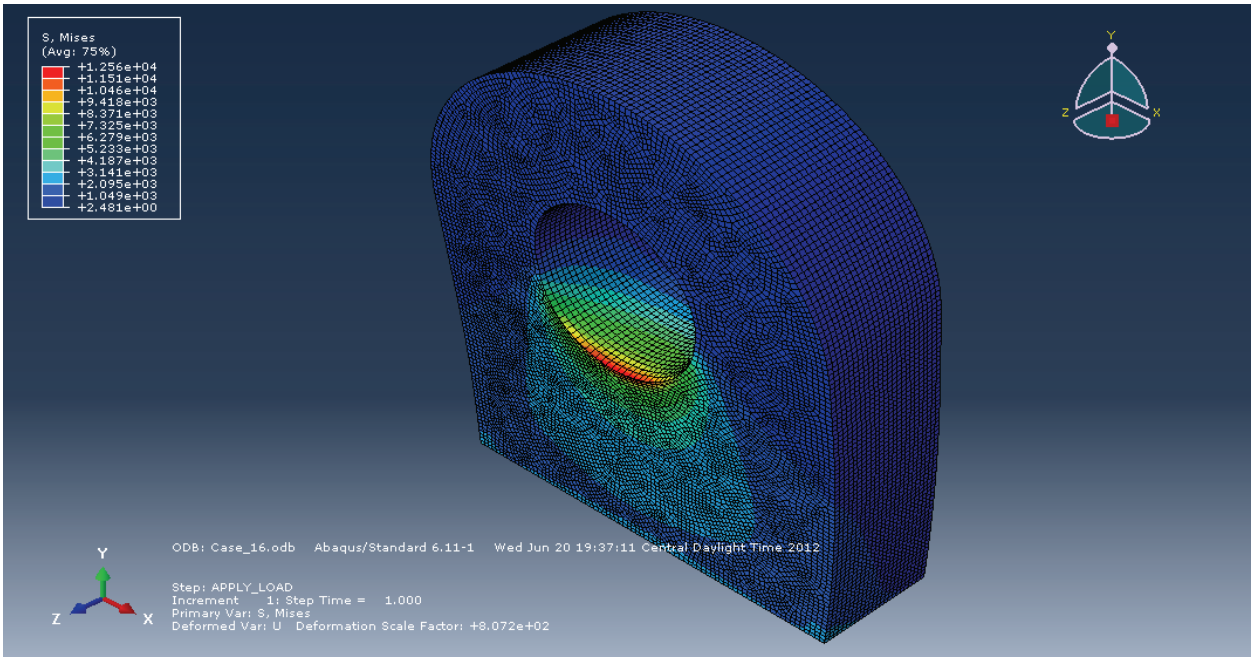

Figure C.16 – Case 16 Yoke Plate von Mises Contours (8 Inch Diameter Shaft, 6 Inch Thick Yoke, 8 Inch Span)

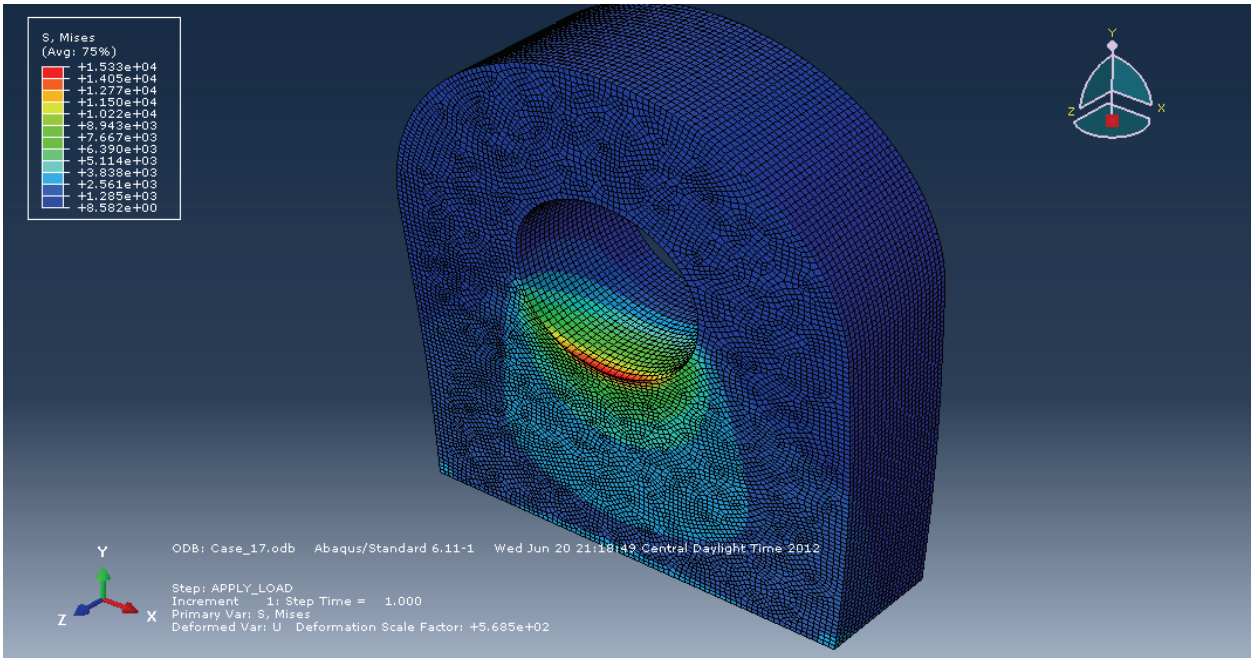

Figure C.17 – Case 17 Yoke Plate von Mises Contours (8 Inch Diameter Shaft, 6 Inch Thick Yoke, 12 Inch Span)

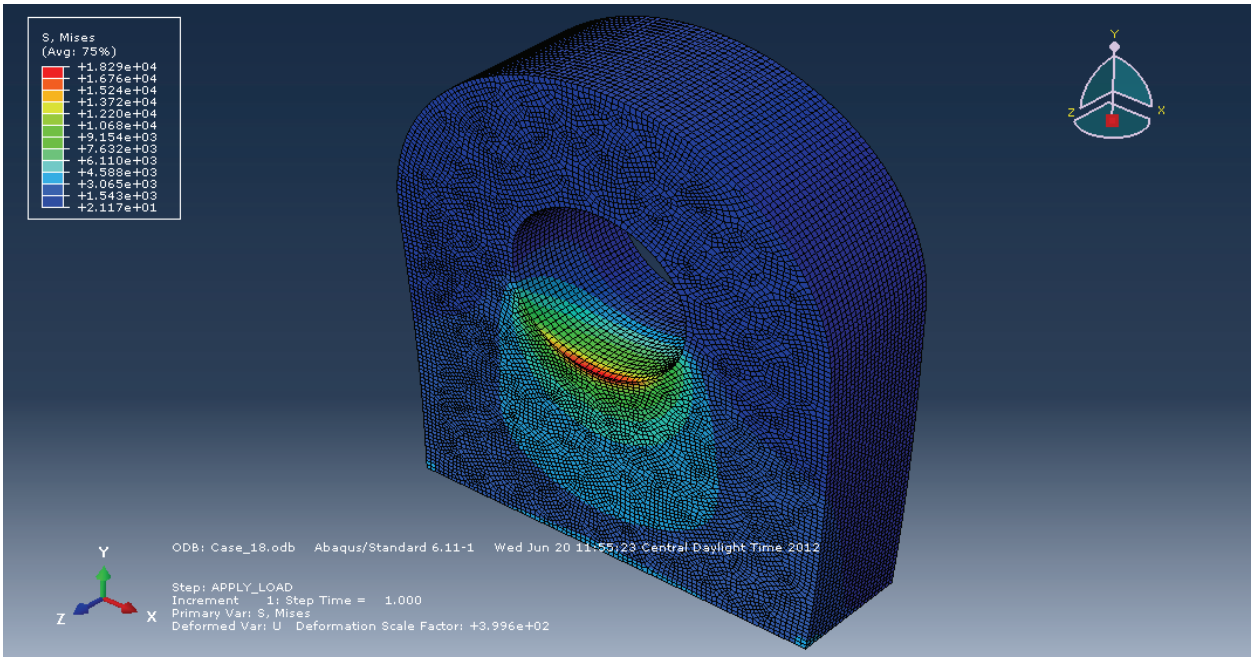

Figure C.18 – Case 18 Yoke Plate von Mises Contours (8 Inch Diameter Shaft, 6 Inch Thick Yoke, 16 Inch Span)

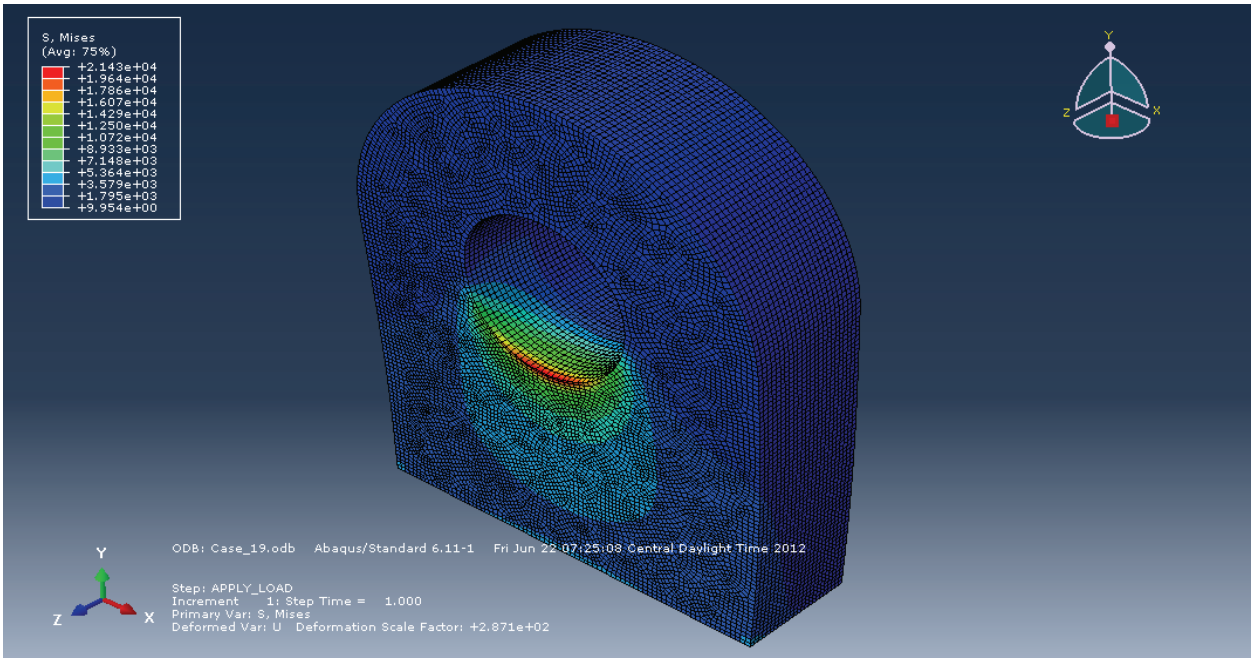

Figure C.19 – Case 19 Yoke Plate von Mises Contours (8 Inch Diameter Shaft, 6 Inch Thick Yoke, 20 Inch Span)

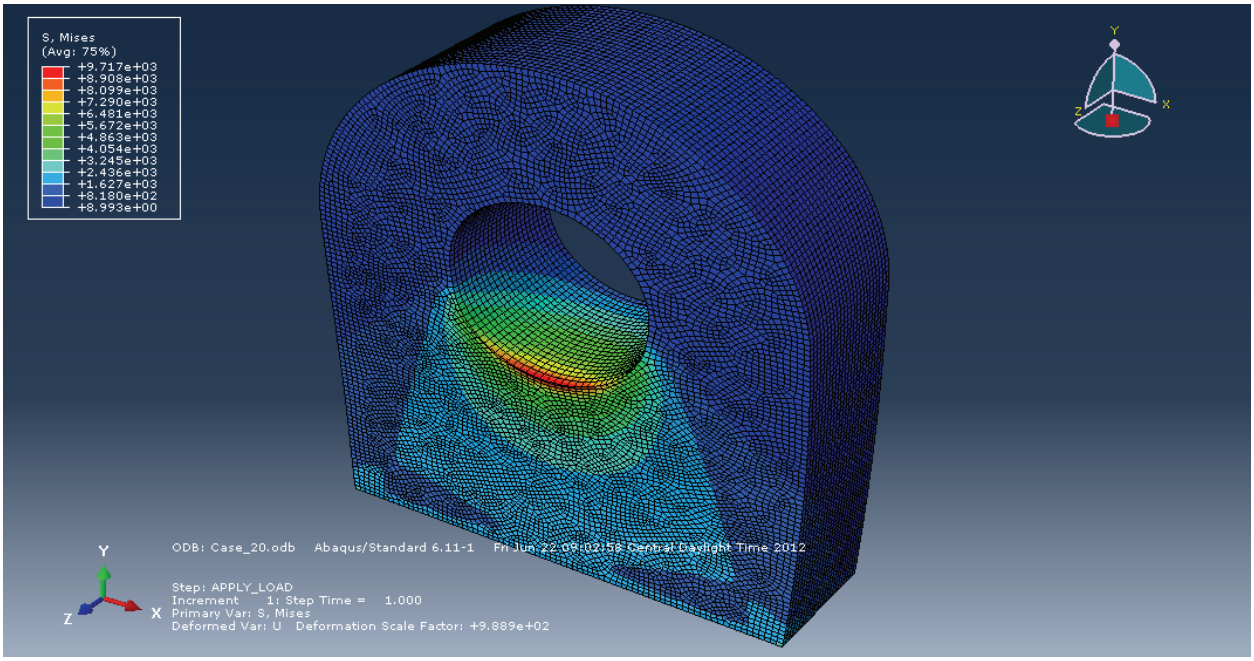

Figure C.20 – Case 20 Yoke Plate von Mises Contours (8 Inch Diameter Shaft, 6 Inch Thick Yoke, 4 Inch Span)

APPENDIX D

VON MISES CONTOUR PLOTS – BRONZE SLEEVE

Appendix D includes a series of screenshots taken from the different ABAQUS models that were developed. For reference, table D.1 provides the specific parameters that are associated to each of the analysis cases that are documented within this appendix.

Table D.1. Summary of cases with a bronze sleeve.

Case	Sleeve	Shaft Diameter (in)	Trunnion Load (kips)	Yoke Plate Thickness (in)	Clear Span (in)
101	Bronze	4	120	2	2
102	Bronze	4	120	2	4
103	Bronze	4	120	2	6
104	Bronze	4	120	4	4
105	Bronze	4	120	4	8
106	Bronze	4	120	4	12
107	Bronze	4	120	6	4
108	Bronze	4	120	6	8
109	Bronze	4	120	6	12
110	Bronze	8	240	2	8
111	Bronze	8	240	2	12
112	Bronze	8	240	2	16
113	Bronze	8	240	4	8
114	Bronze	8	240	4	12
115	Bronze	8	240	4	16
116	Bronze	8	240	6	8
117	Bronze	8	240	6	12
118	Bronze	8	240	6	16
119	Bronze	8	240	6	20
120	Bronze	8	240	6	4

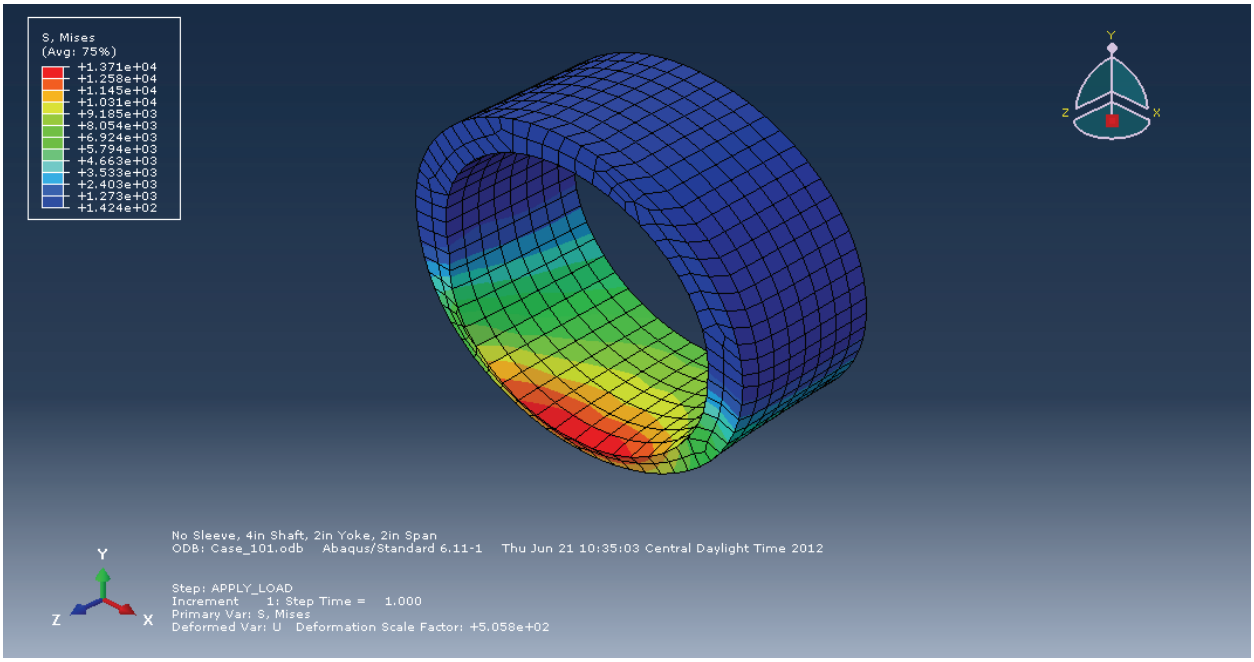

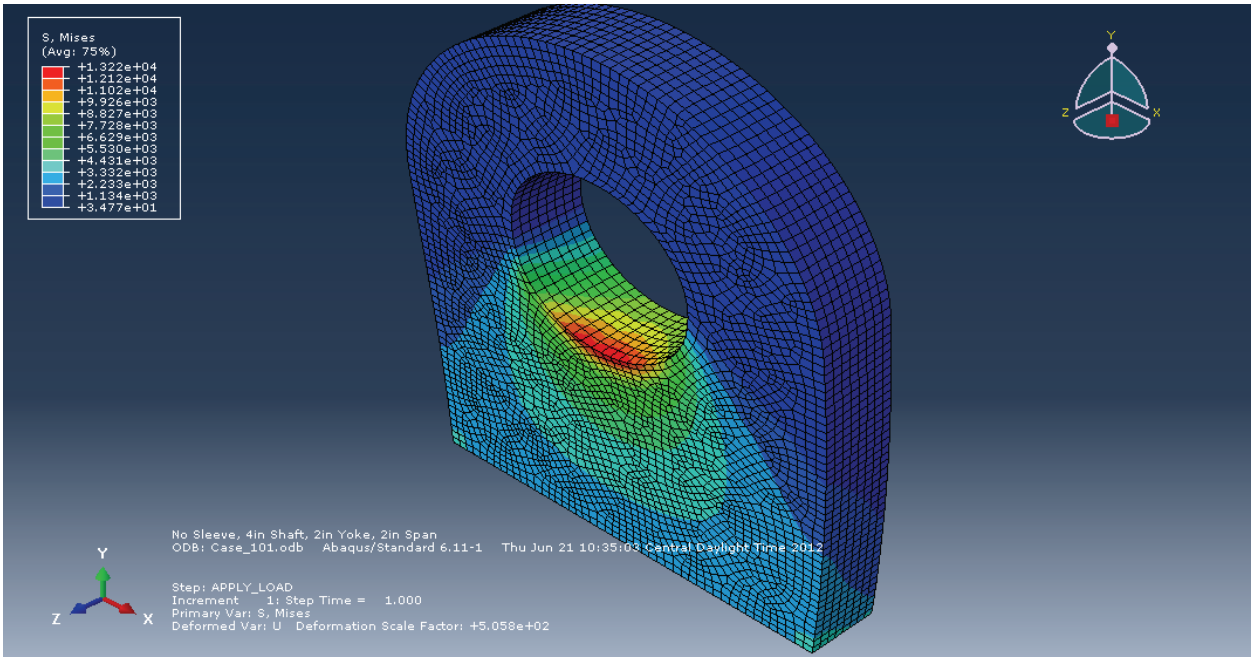

Figure D.1 – Case 100 Yoke Plate and Sleeve Von Mises Contours (4 Inch Diameter Shaft, 2 Inch Thick Yoke, 2 Inch Span)

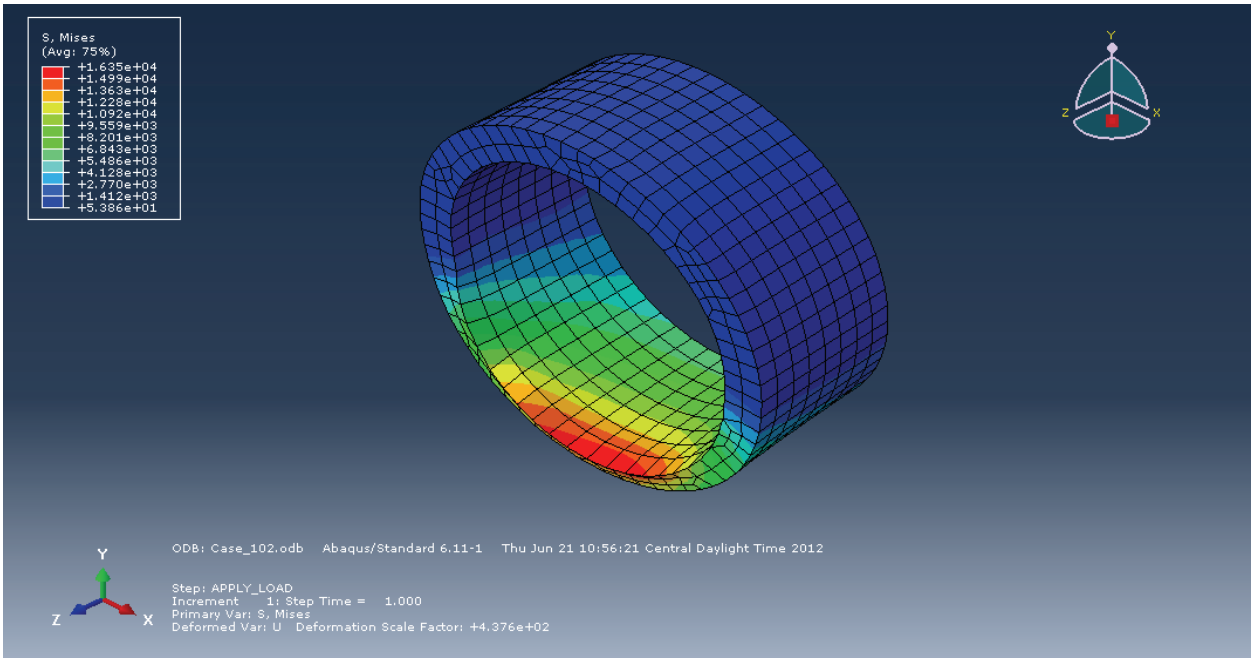

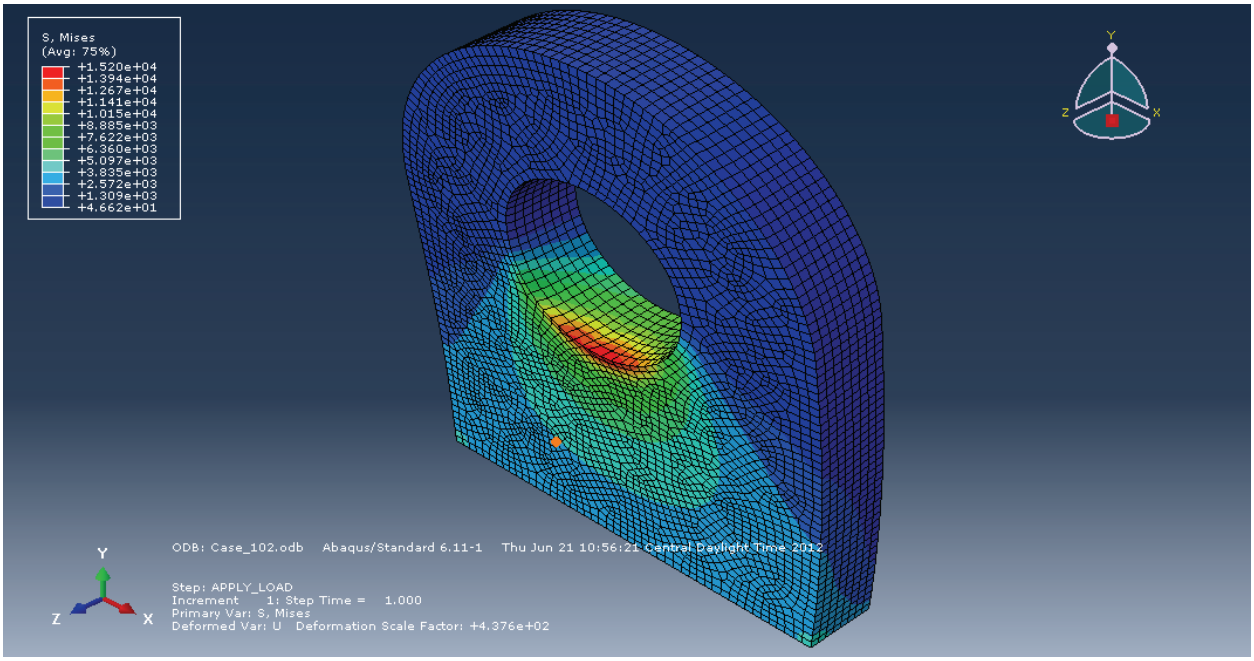

Figure D.2 – Case 102 Yoke Plate and Sleeve Von Mises Contours (4 Inch Diameter Shaft, 2 Inch Thick Yoke, 4 Inch Span)

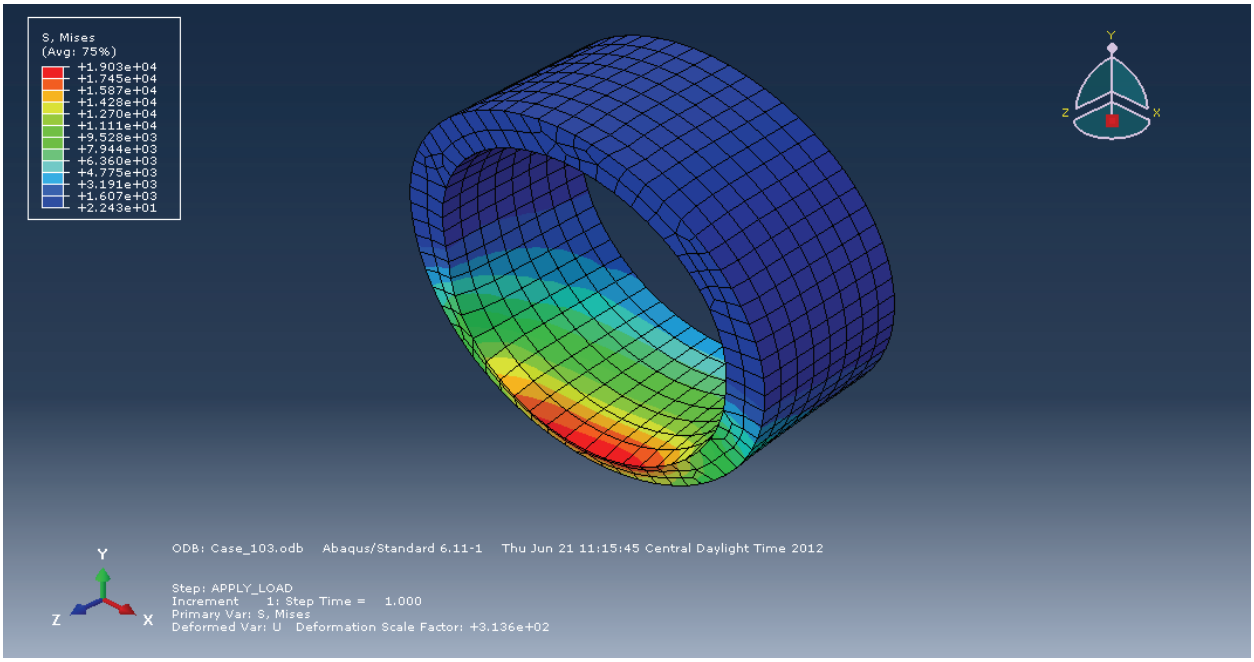

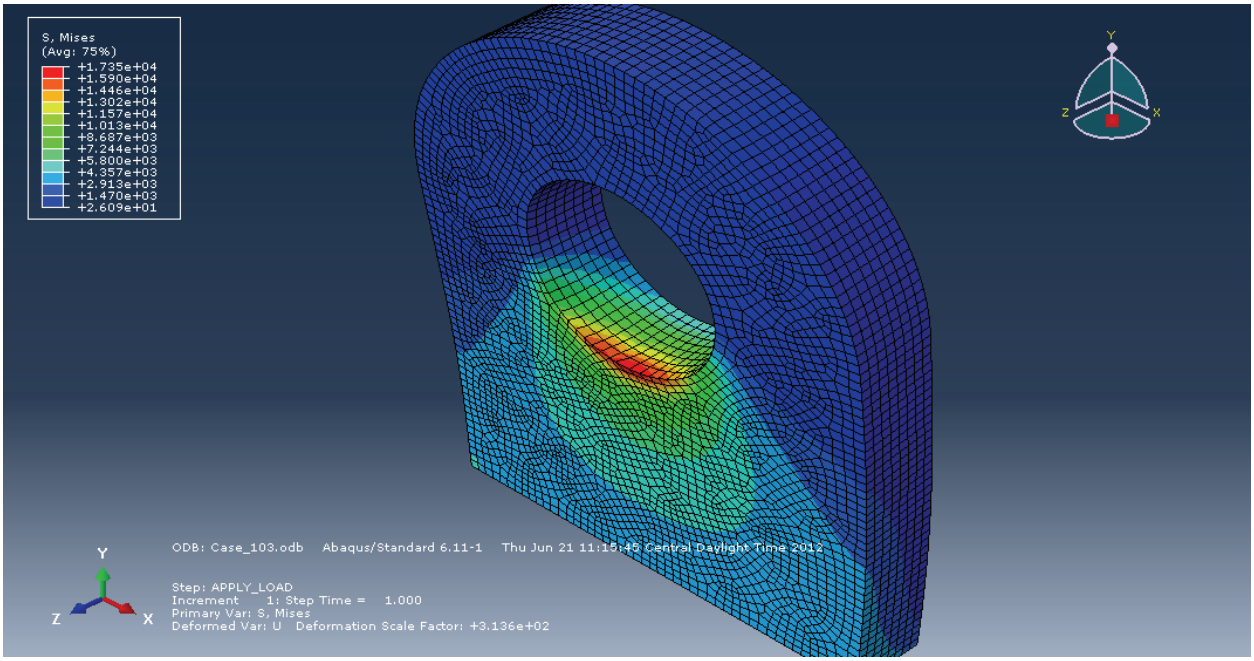

Figure D.3 – Case 103 Yoke Plate and Sleeve Von Mises Contours (4 Inch Diameter Shaft, 2 Inch Thick Yoke, 6 Inch Span)

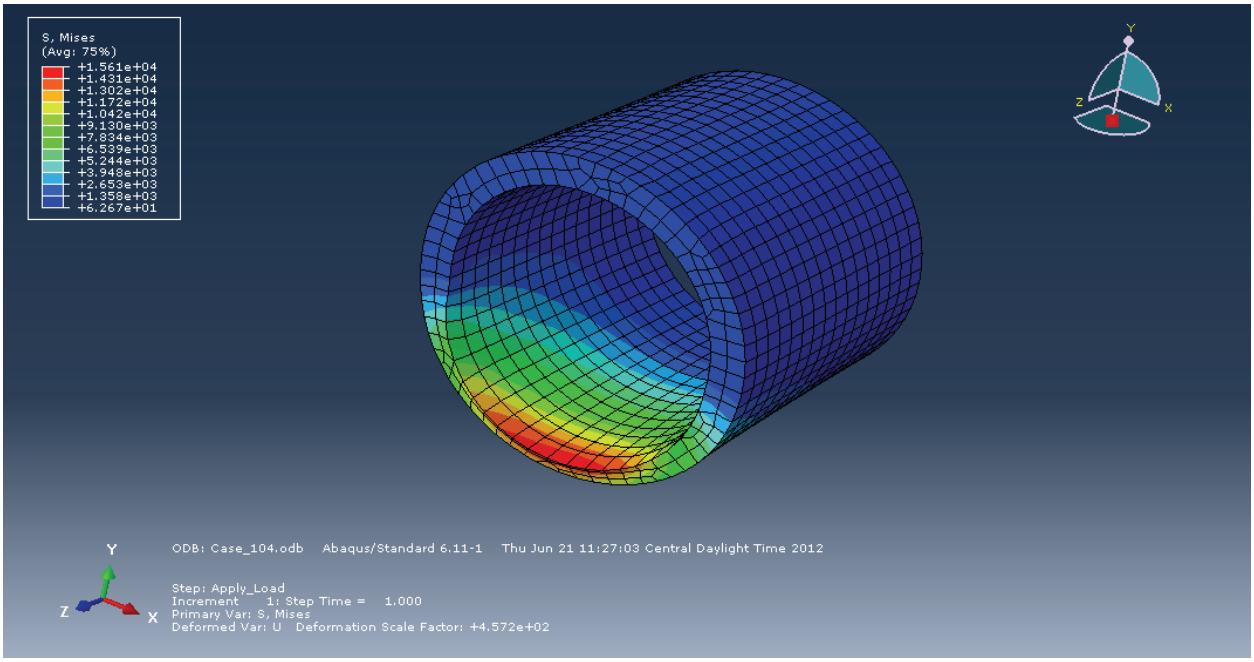

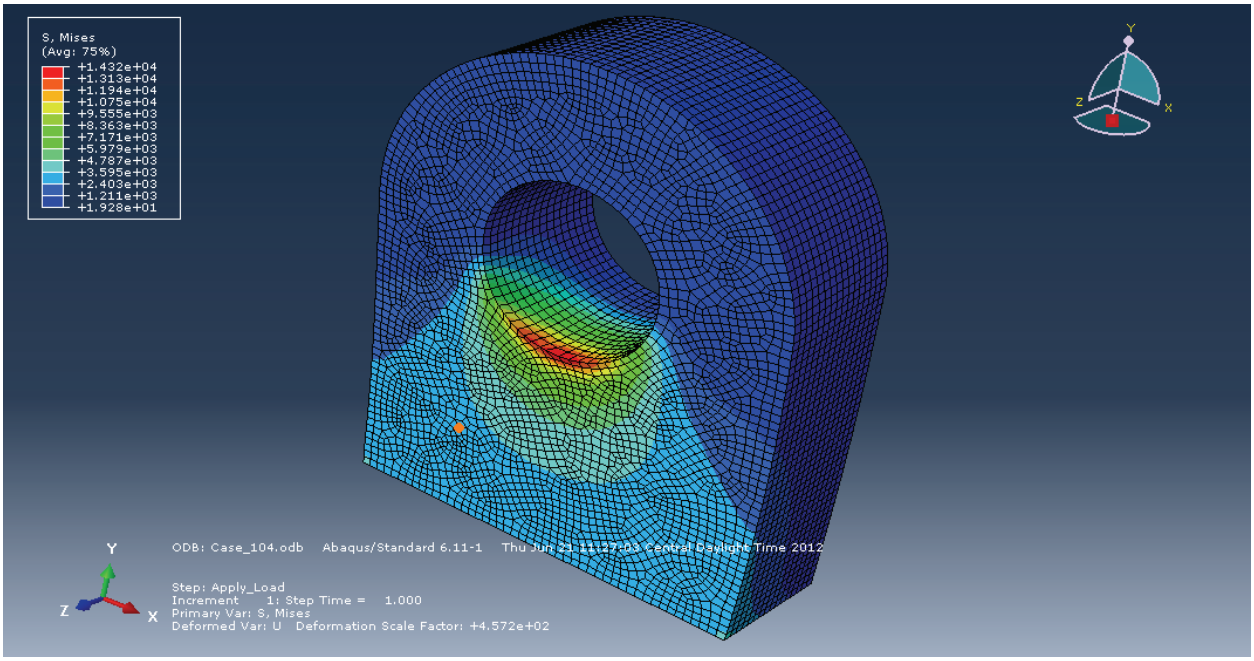

Figure D.4 – Case 104 Yoke Plate and Sleeve Von Mises Contours (4 Inch Diameter Shaft, 4 Inch Thick Yoke, 4 Inch Span)

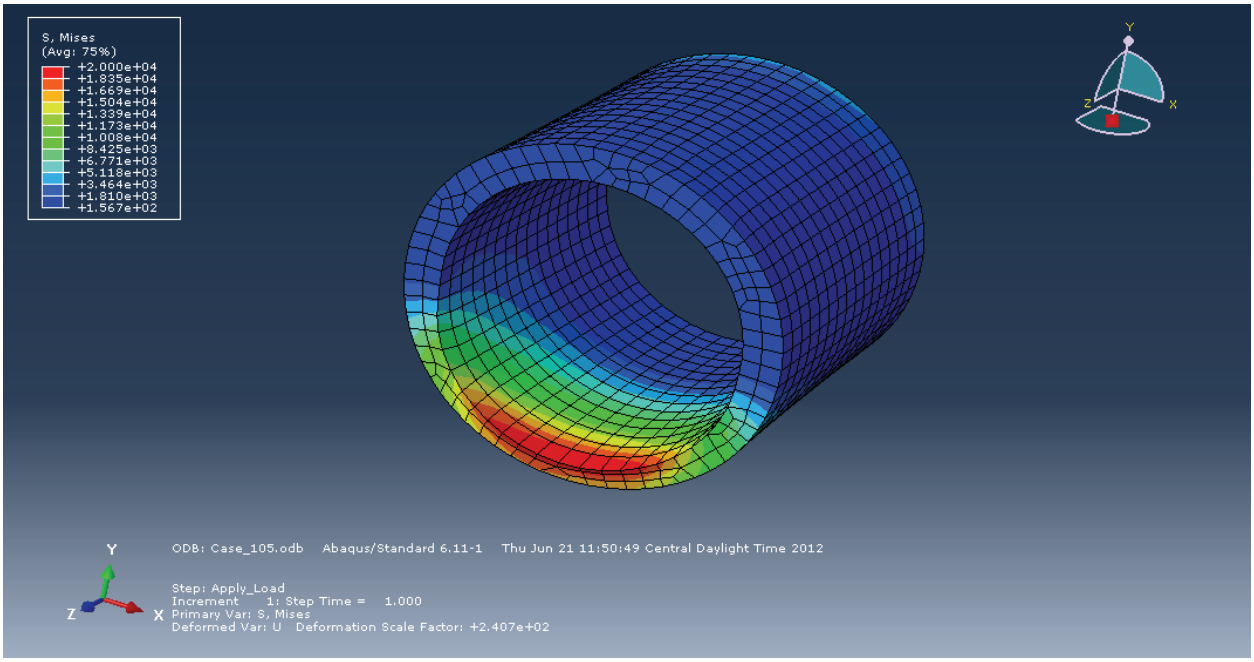

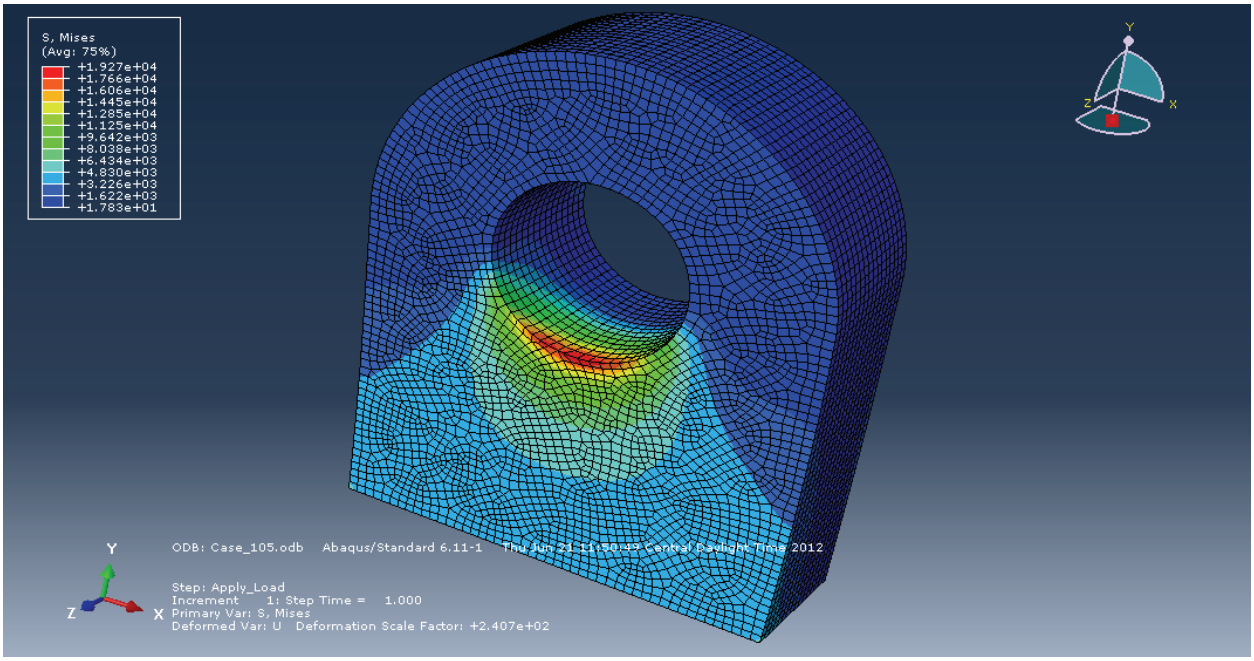

Figure D.5 – Case 105 Yoke Plate and Sleeve Von Mises Contours (4 Inch Diameter Shaft, 4 Inch Thick Yoke, 8 Inch Span)

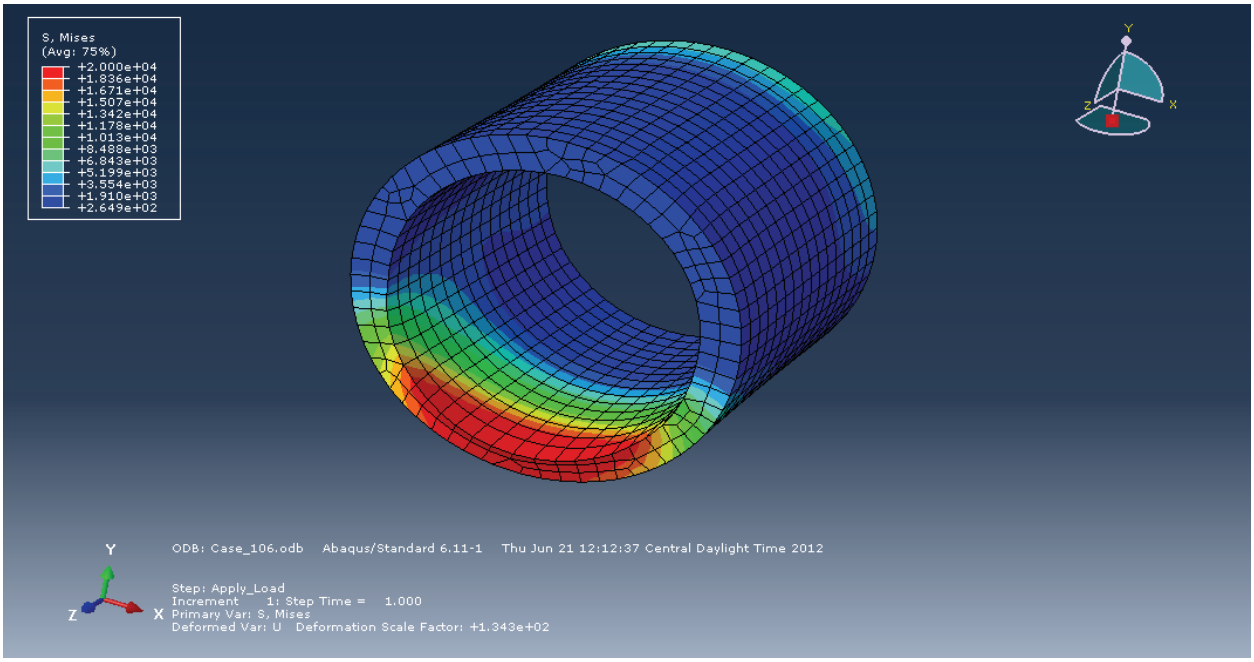

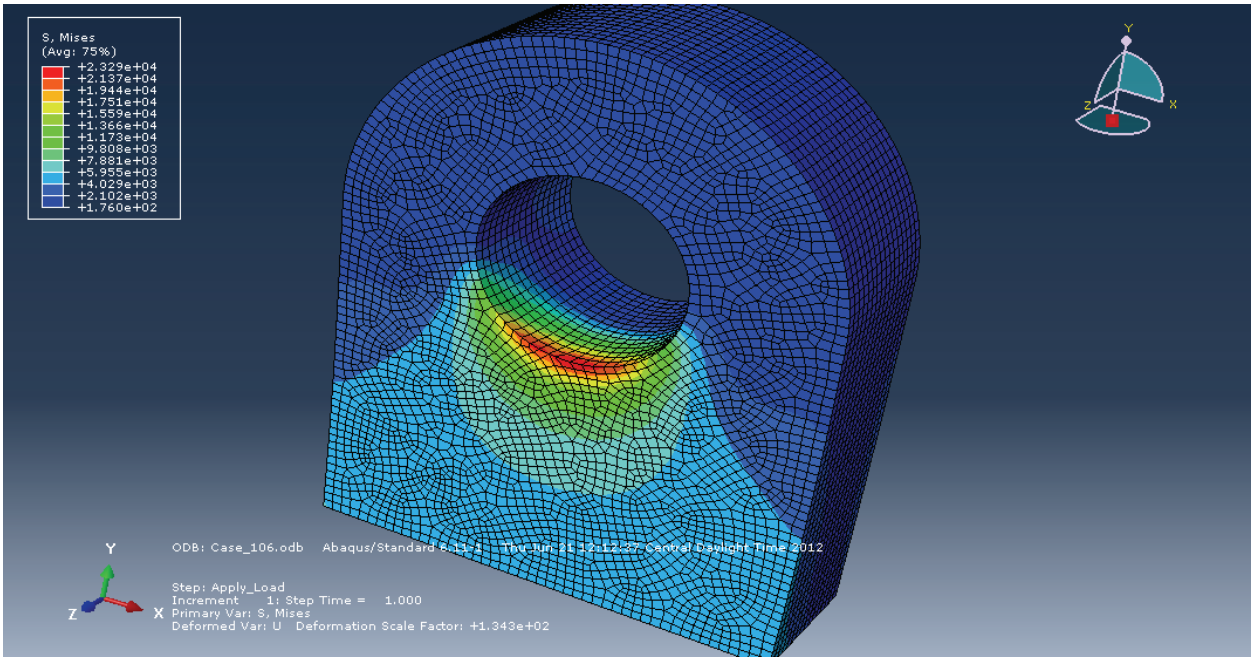

Figure D.6 – Case 106 Yoke Plate and Sleeve Von Mises Contours (4 Inch Diameter Shaft, 4 Inch Thick Yoke, 12 Inch Span)

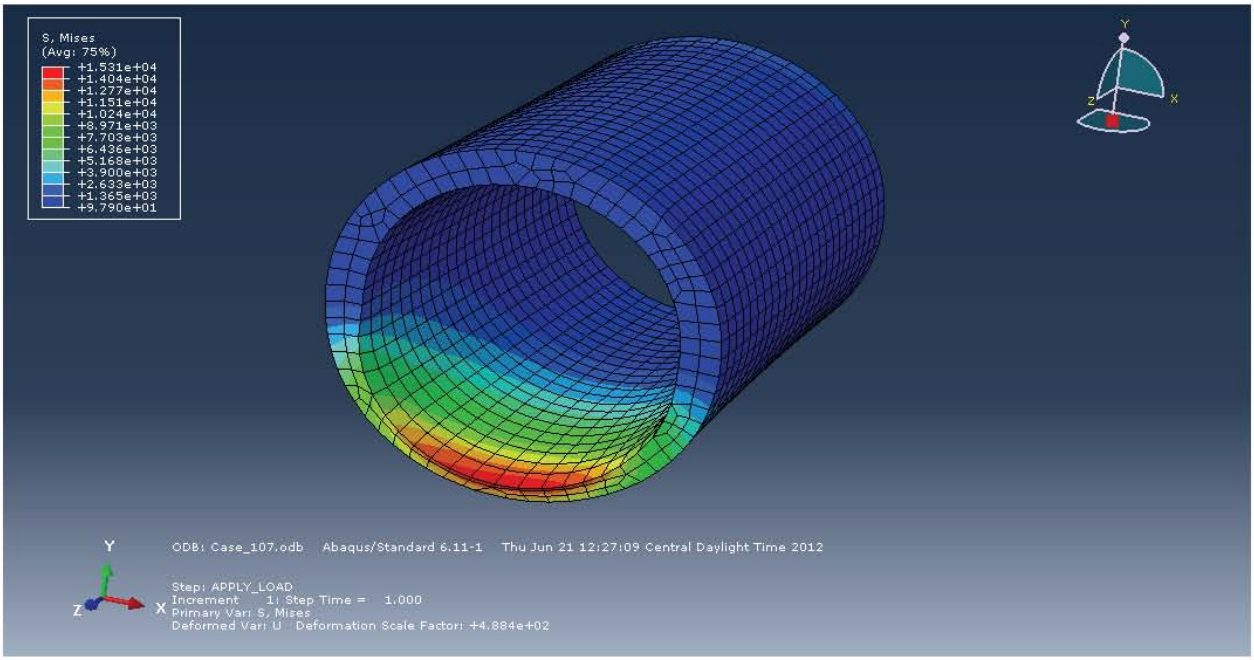

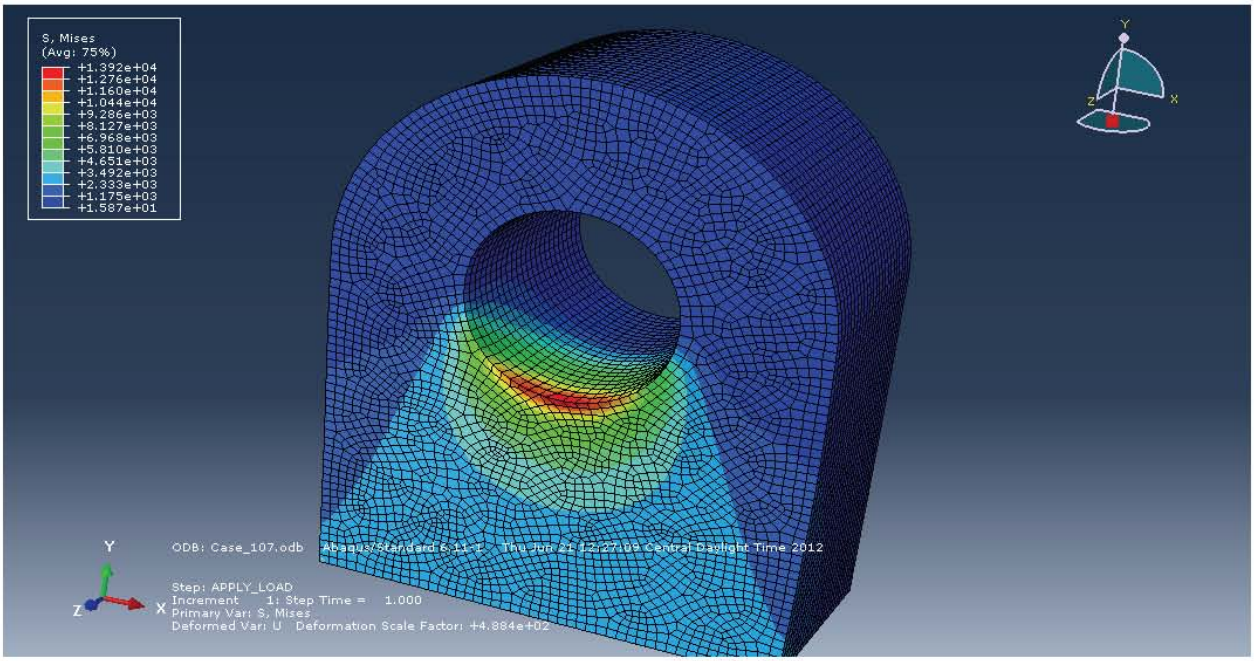

Figure D.7 – Case 107 Yoke Plate and Sleeve Von Mises Contours (4 Inch Diameter Shaft, 6 Inch Thick Yoke, 4 Inch Span)

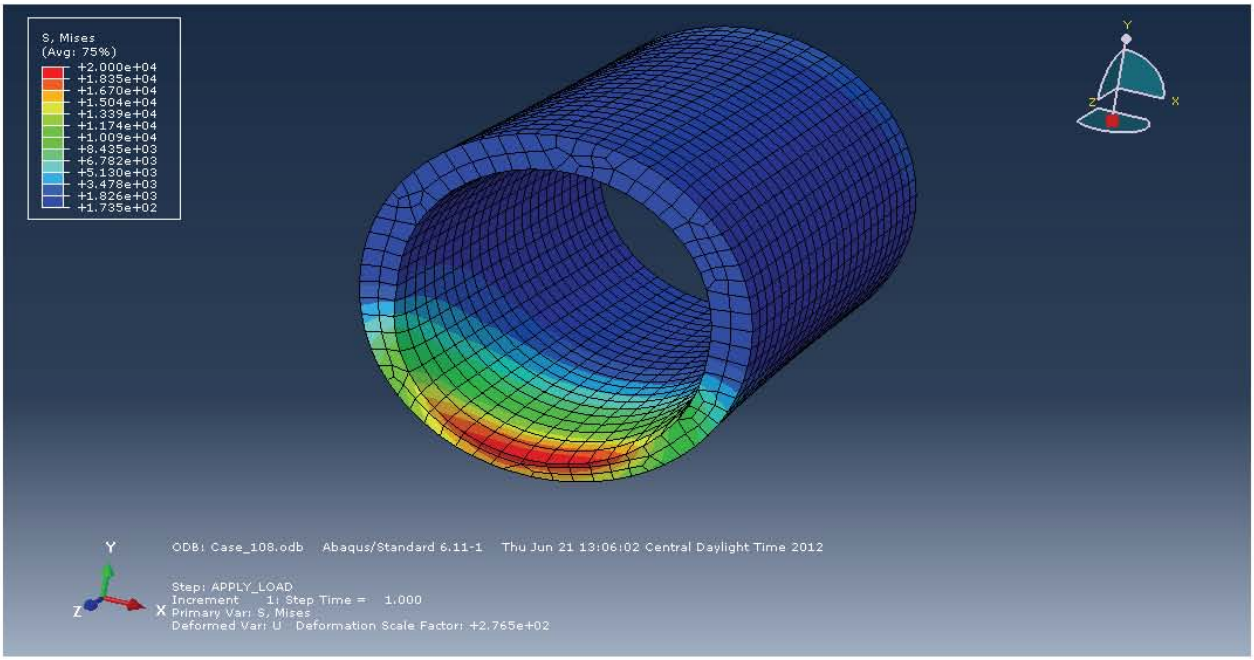

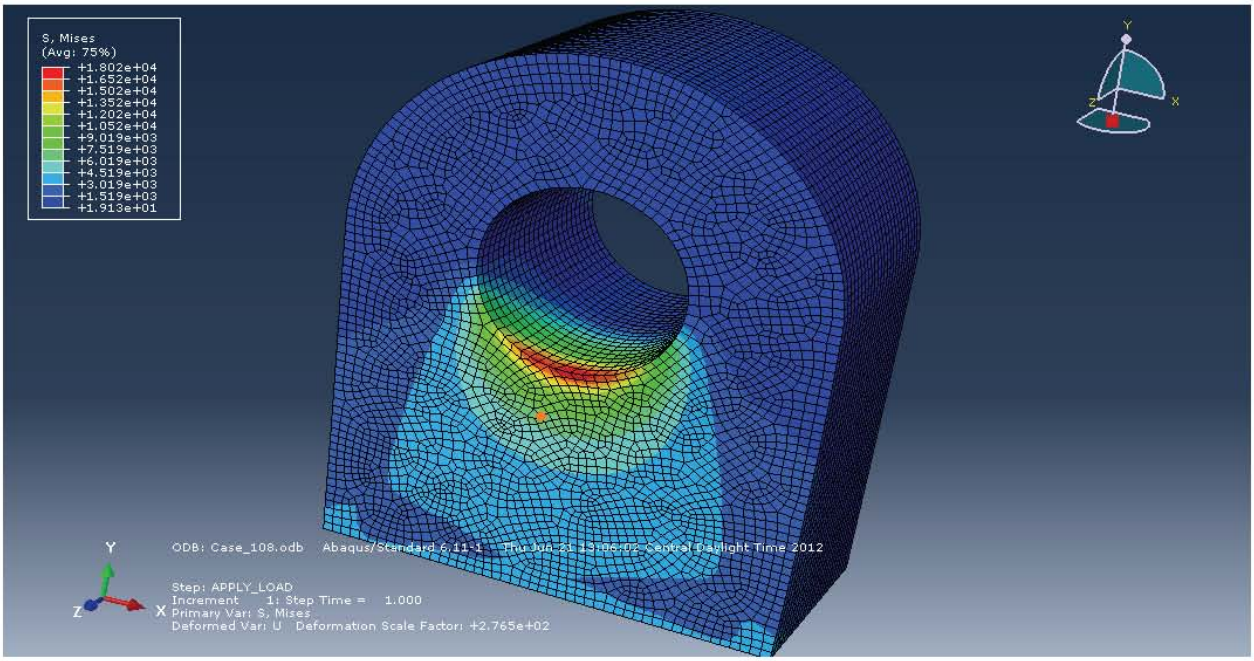

Figure D.8 – Case 8 10Yoke Plate and Sleeve Von Mises Contours (4 Inch Diameter Shaft, 6 Inch Thick Yoke, 8 Inch Span)

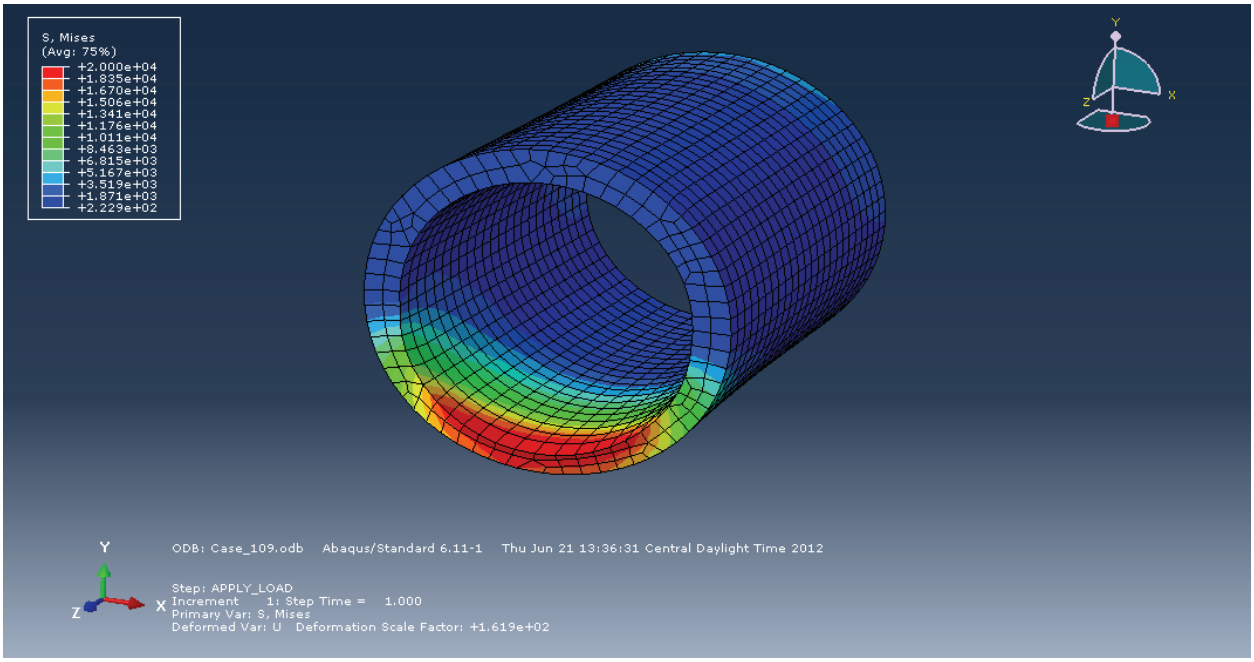

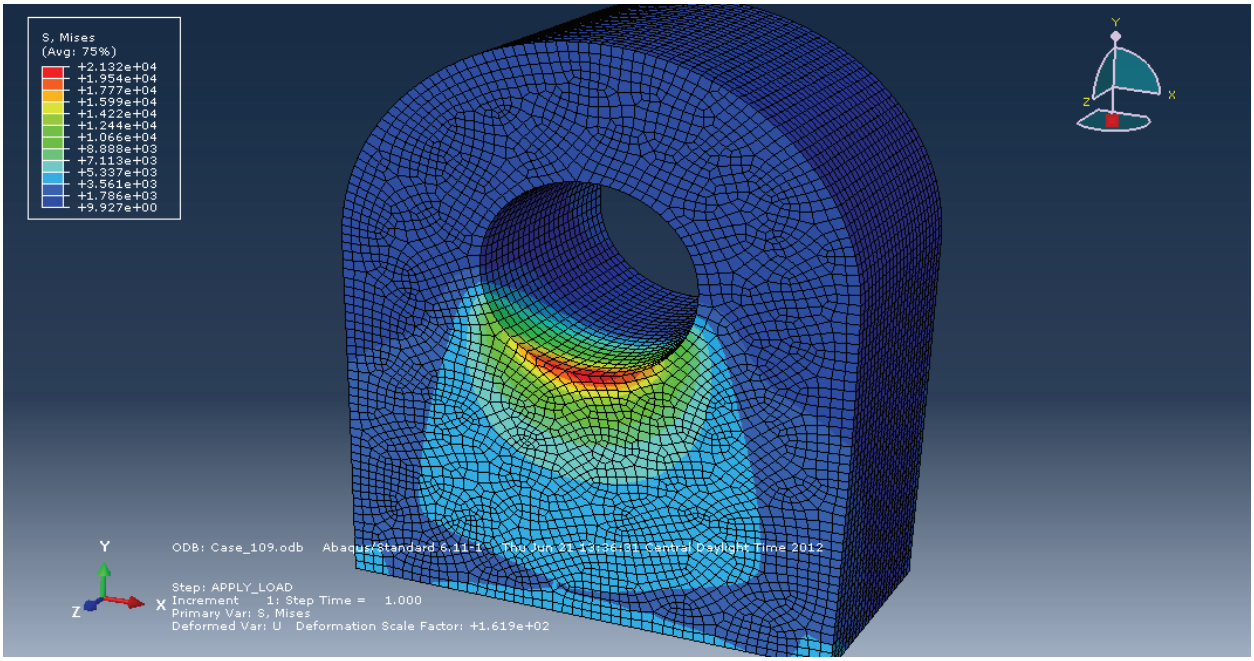

Figure D.9 – Case 109 Yoke Plate and Sleeve Von Mises Contours (4 Inch Diameter Shaft, 6 Inch Thick Yoke, 12 Inch Span)

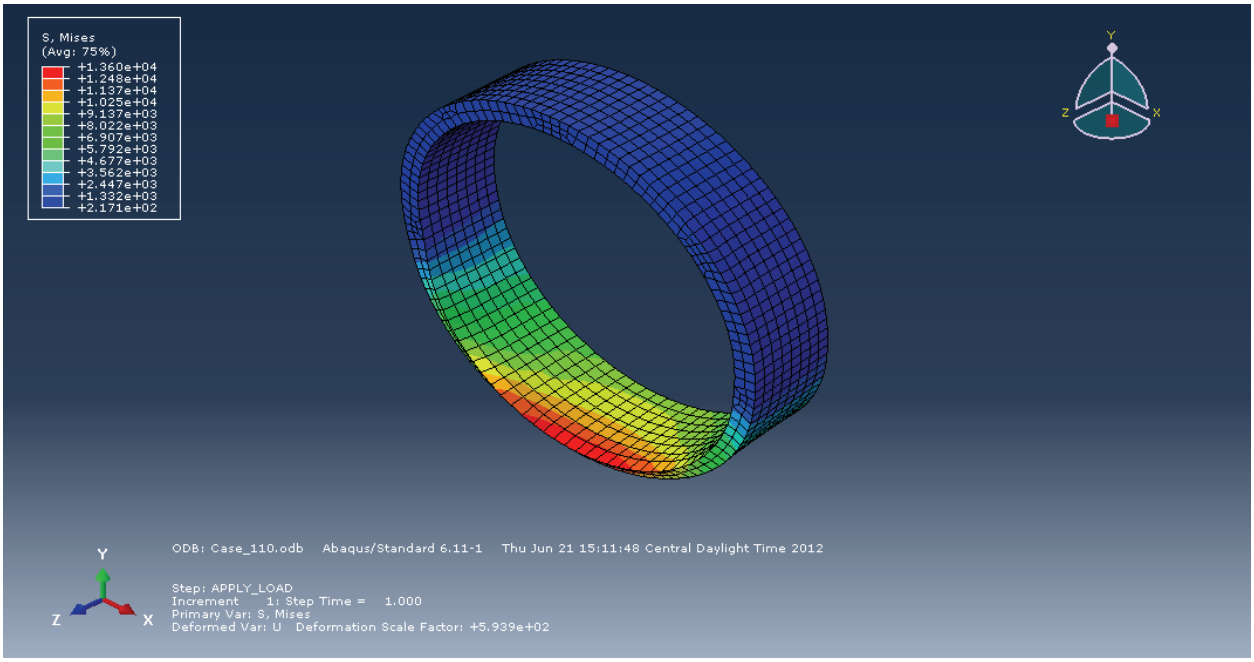

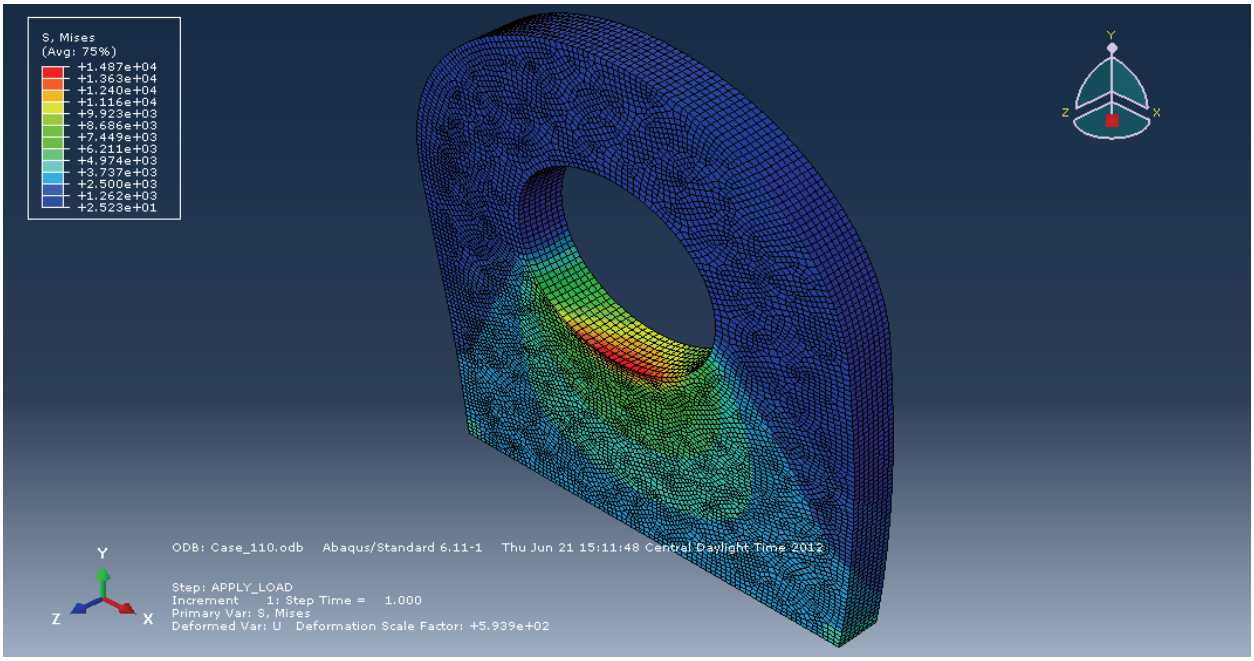

Figure D.10 – Case 110 Yoke Plate and Sleeve Von Mises Contours (8 Inch Diameter Shaft, 2 Inch Thick Yoke, 8 Inch Span)

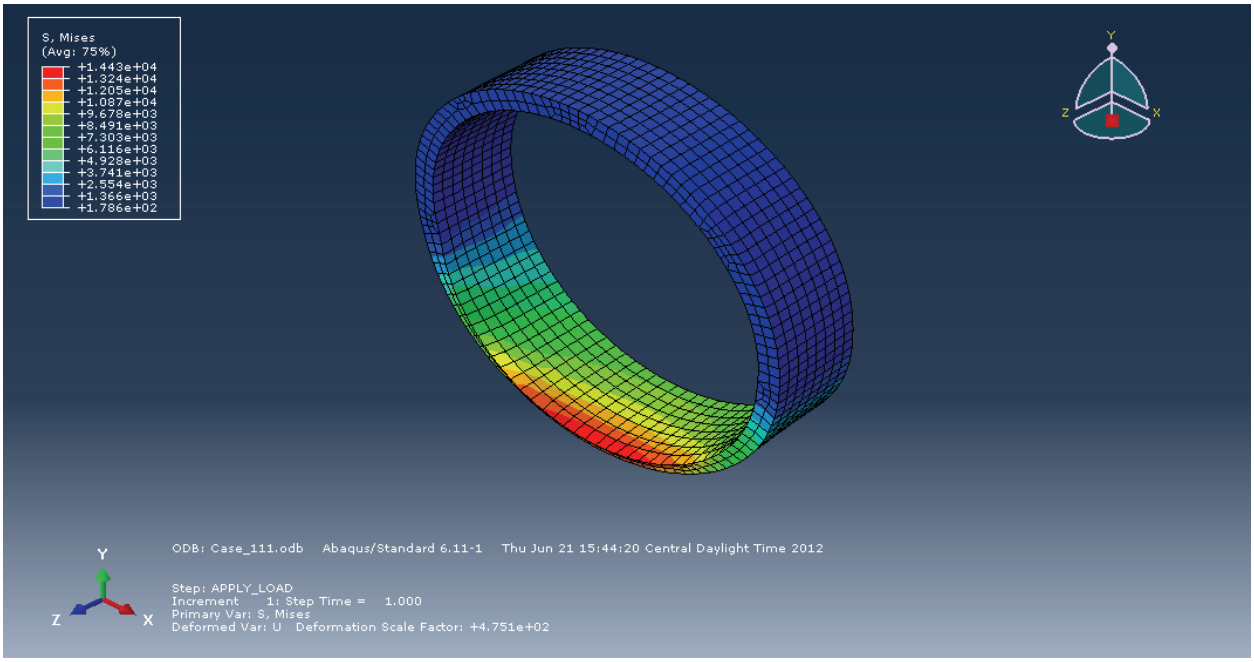

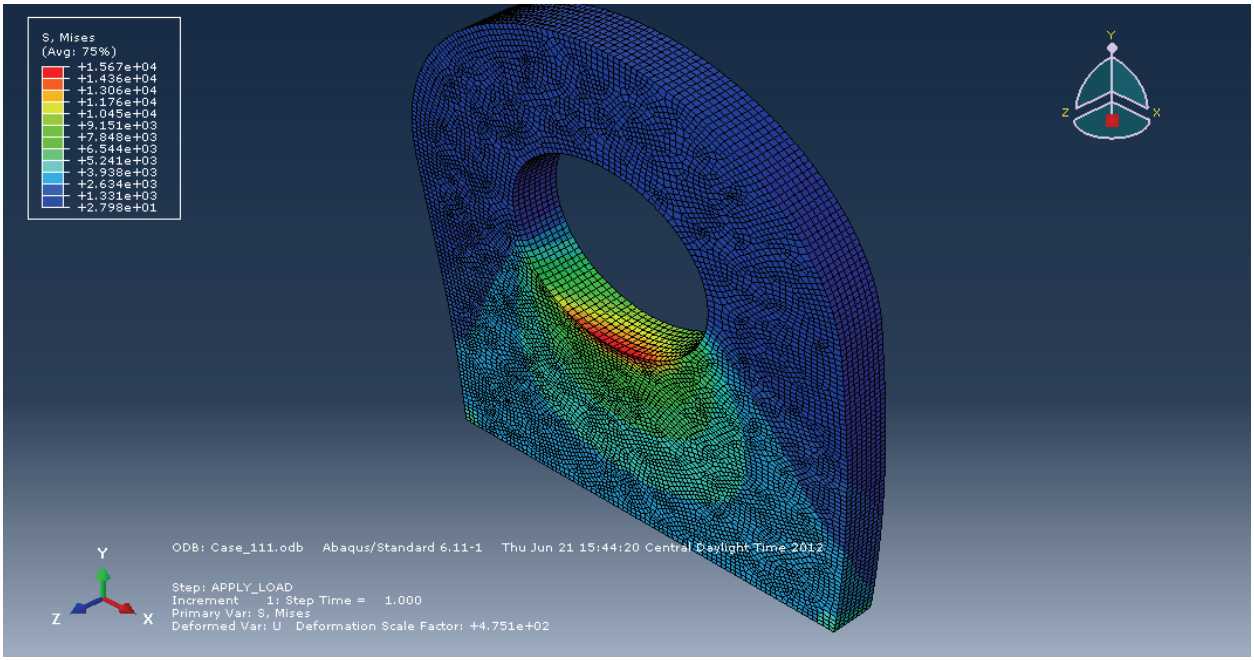

Figure D.11 – Case 111 Yoke Plate and Sleeve Von Mises Contours (8 Inch Diameter Shaft, 2 Inch Thick Yoke, 12 Inch Span)

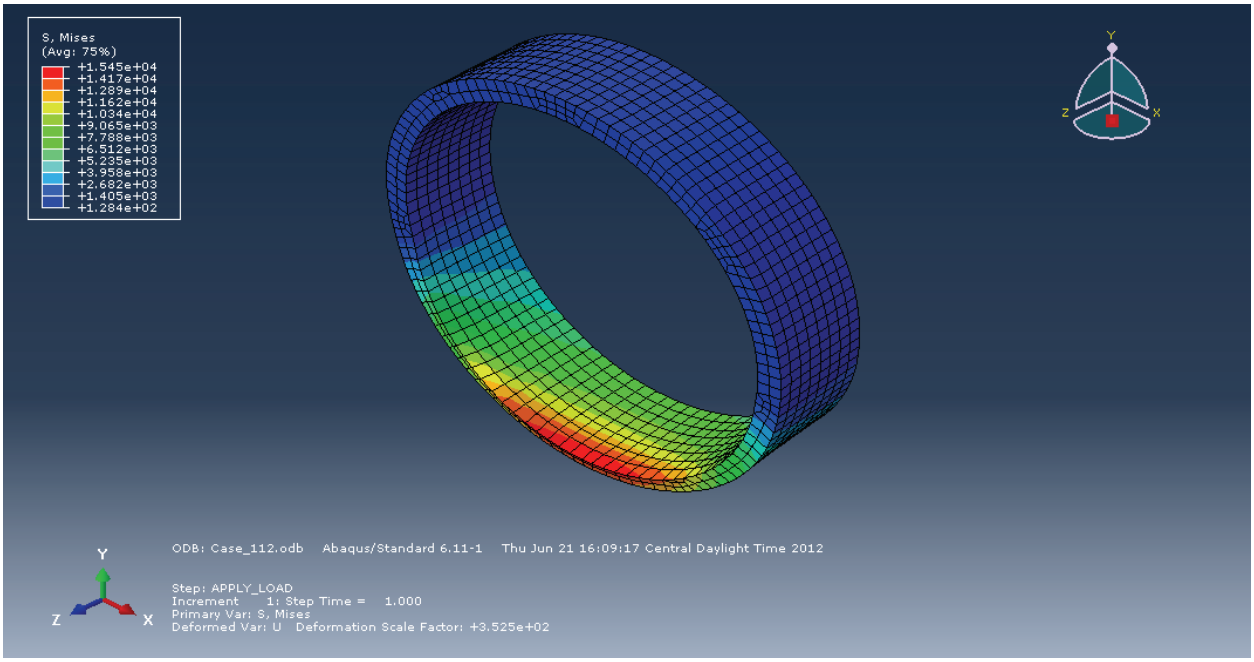

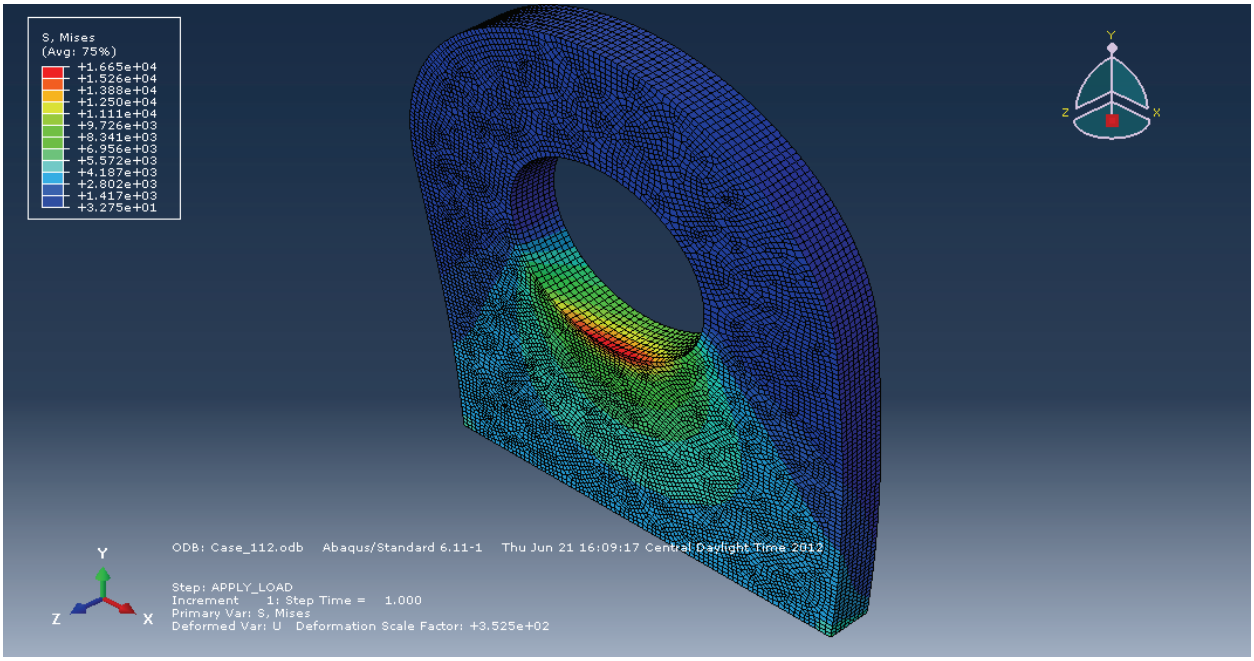

Figure D.12 – Case 112 Yoke Plate and Sleeve Von Mises Contours (8 Inch Diameter Shaft, 2 Inch Thick Yoke, 16 Inch Span)

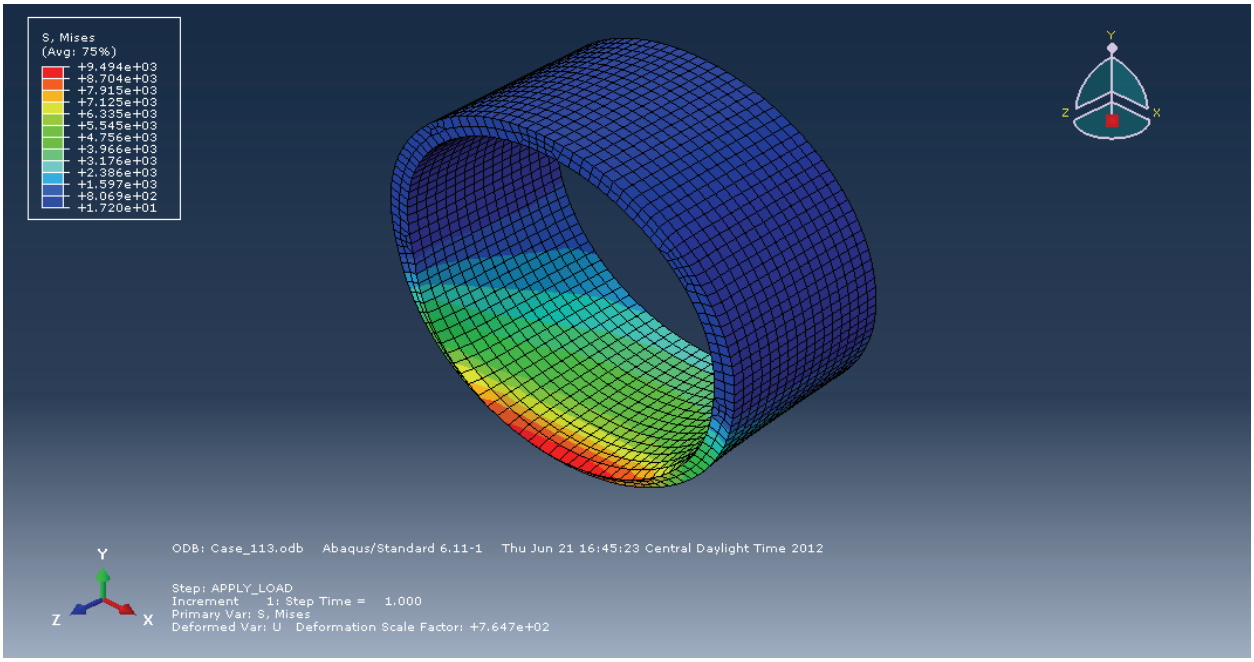

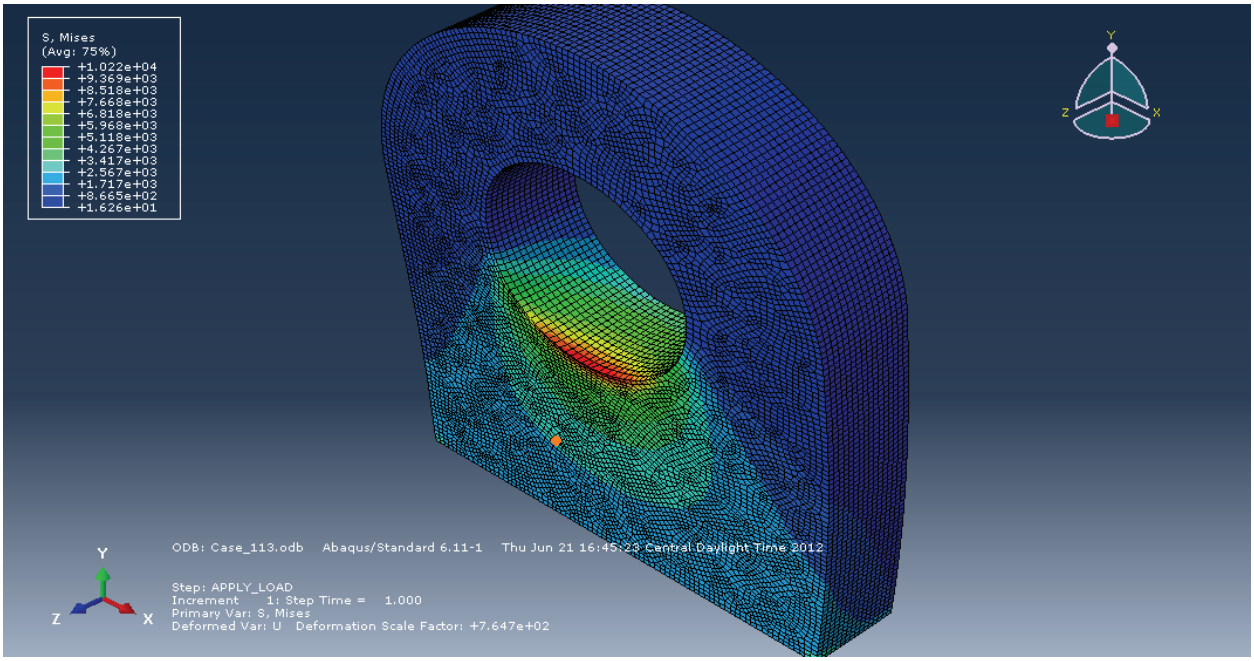

Figure D.13 – Case 113 Yoke Plate and Sleeve Von Mises Contours (8 Inch Diameter Shaft, 4 Inch Thick Yoke, 8 Inch Span)

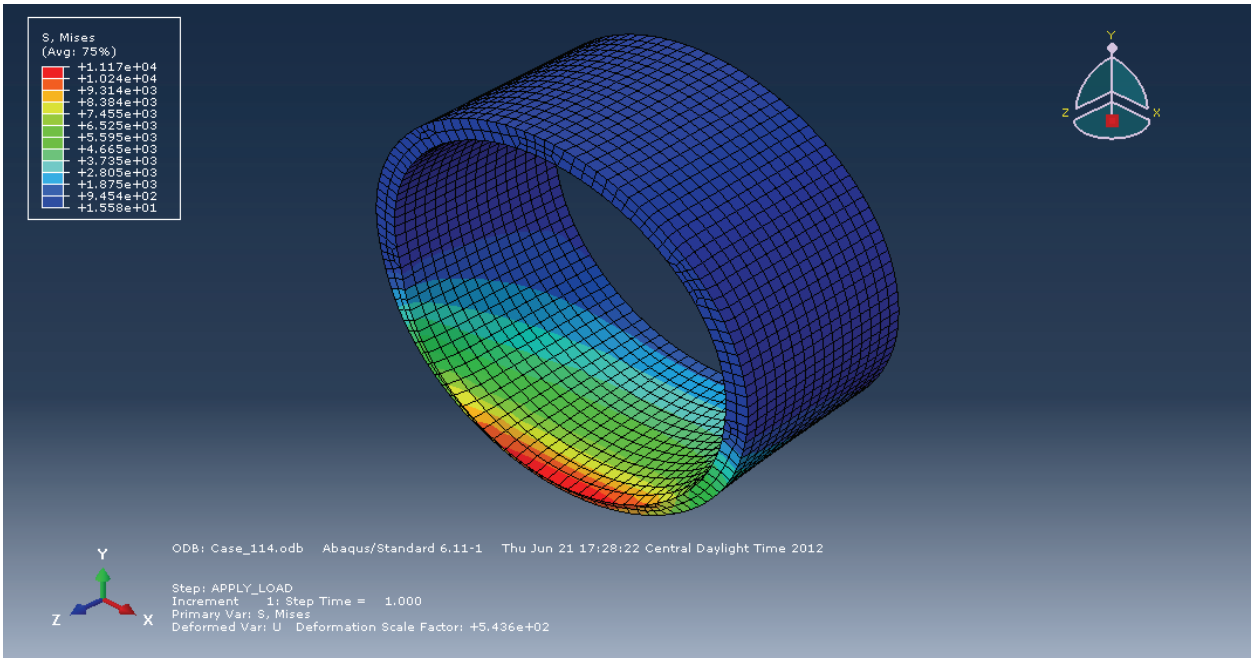

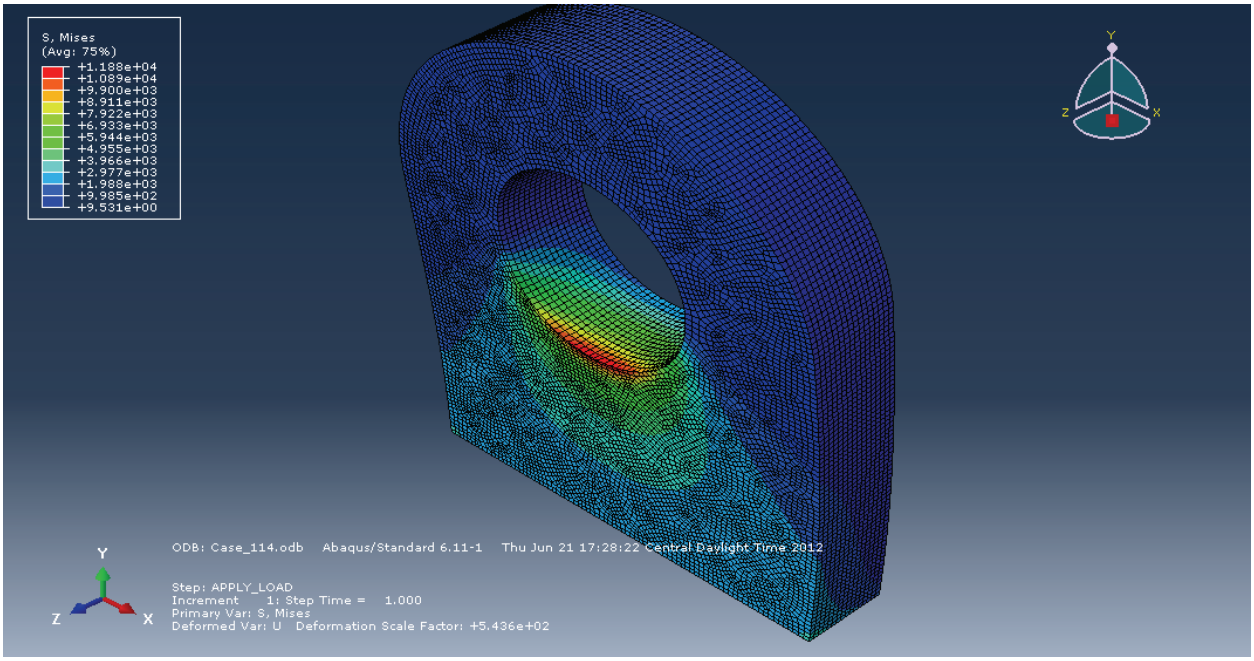

Figure D.14 – Case 114 Yoke Plate and Sleeve Von Mises Contours (8 Inch Diameter Shaft, 4 Inch Thick Yoke, 12 Inch Span)

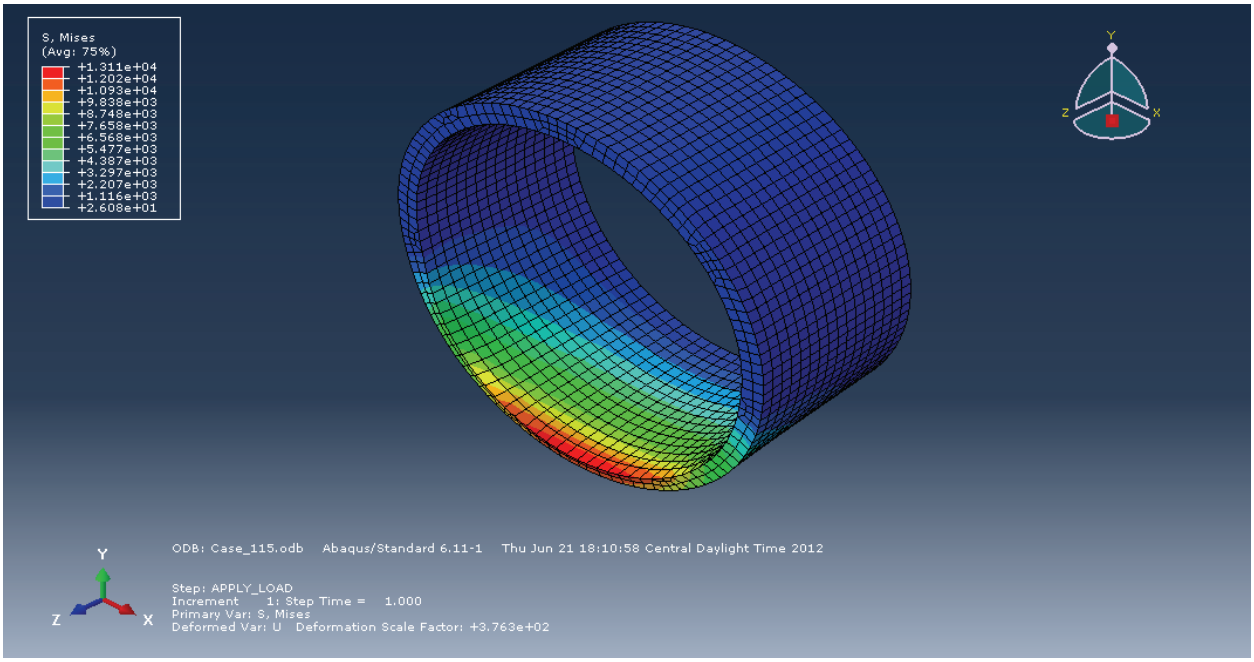

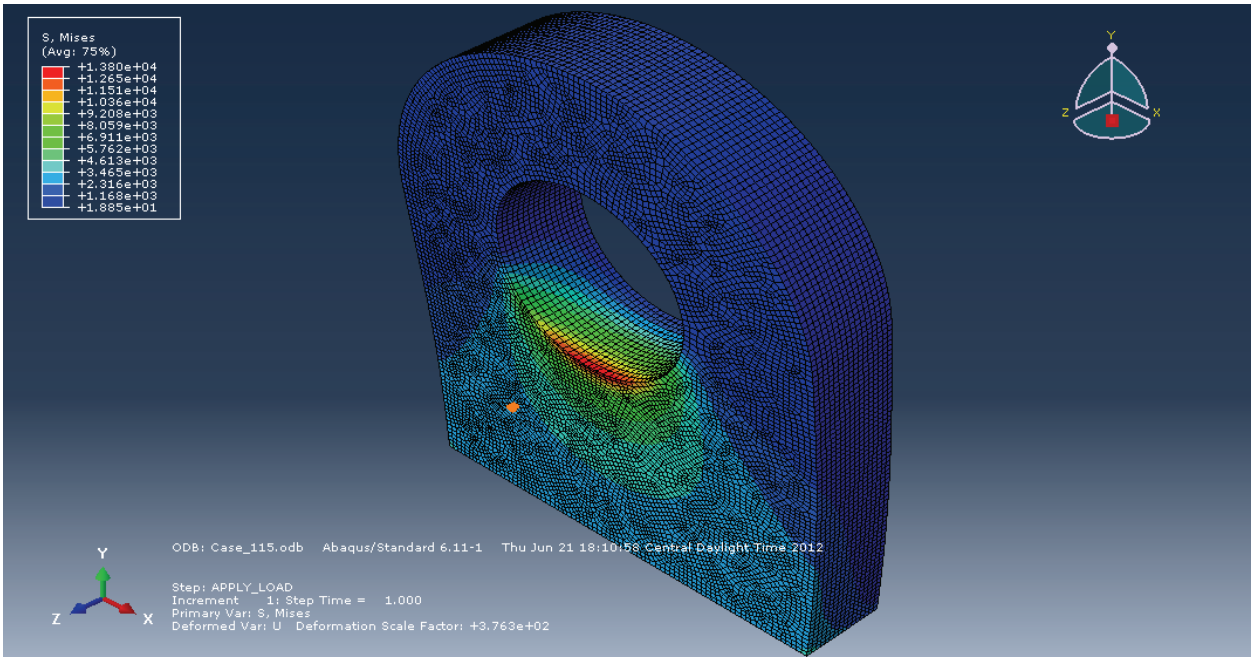

Figure D.15 – Case 115 Yoke Plate and Sleeve Von Mises Contours (8 Inch Diameter Shaft, 4 Inch Thick Yoke, 16 Inch Span)

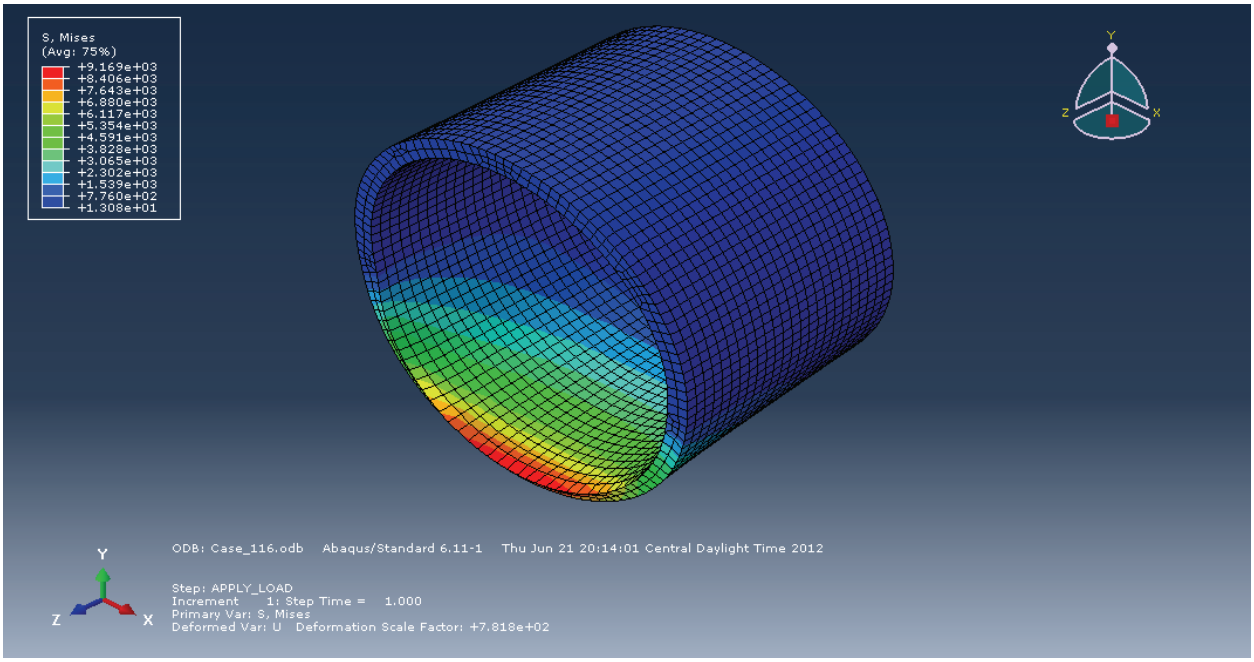

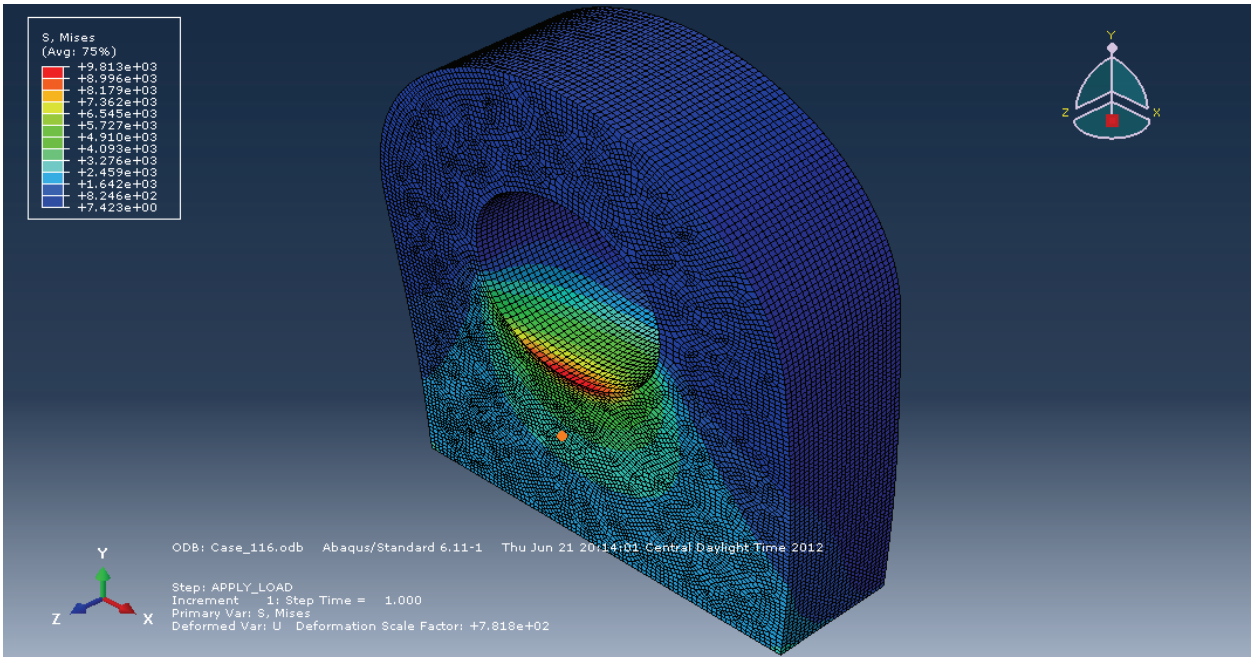

Figure D.16 – Case 16 Yoke Plate and Sleeve Von Mises Contours (8 Inch Diameter Shaft, 6 Inch Thick Yoke, 8 Inch Span)

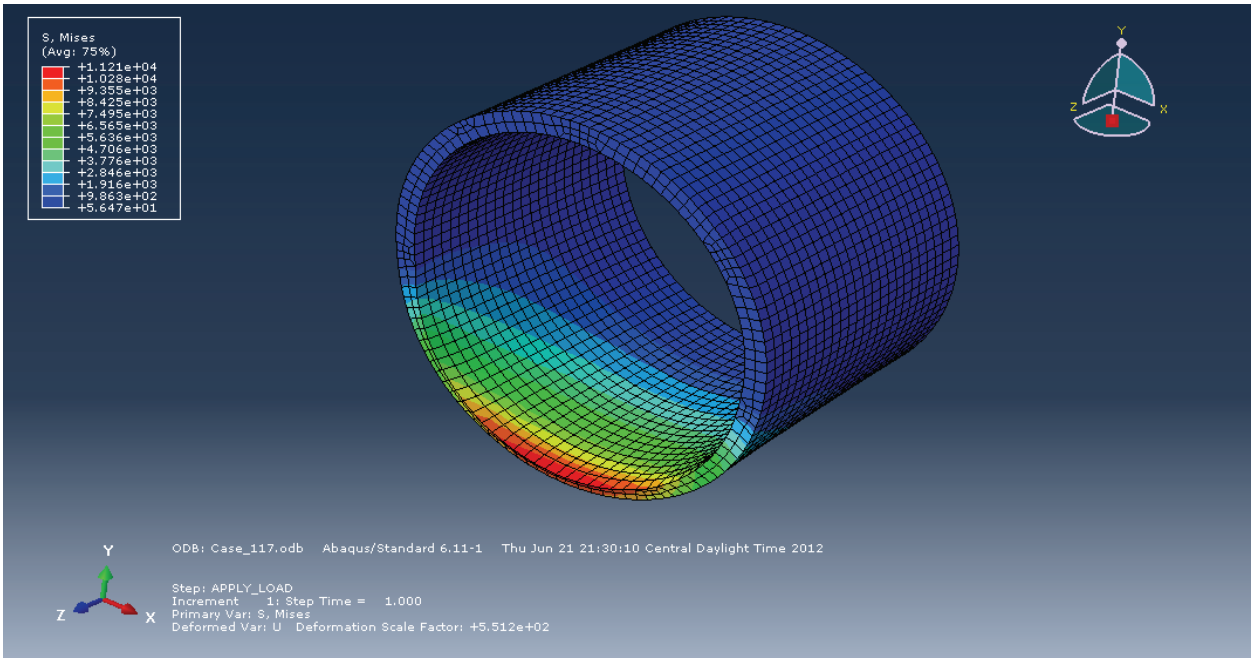

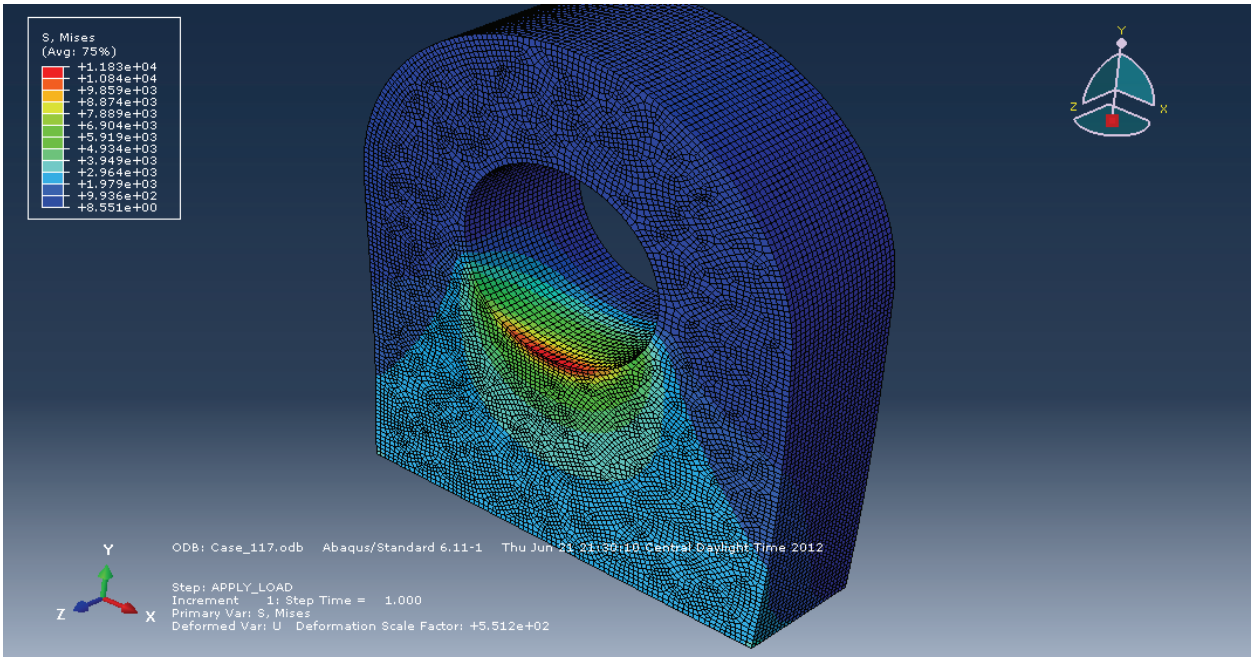

Figure D.17 – Case 117 Yoke Plate and Sleeve Von Mises Contours (8 Inch Diameter Shaft, 6 Inch Thick Yoke, 12 Inch Span)

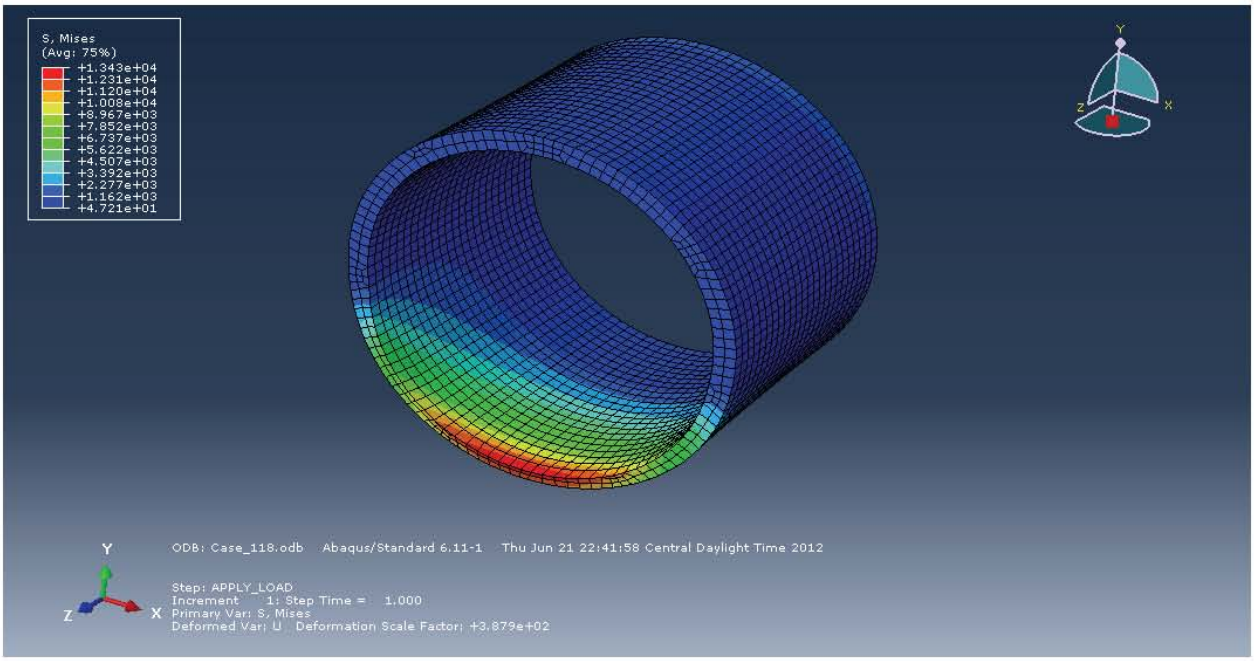

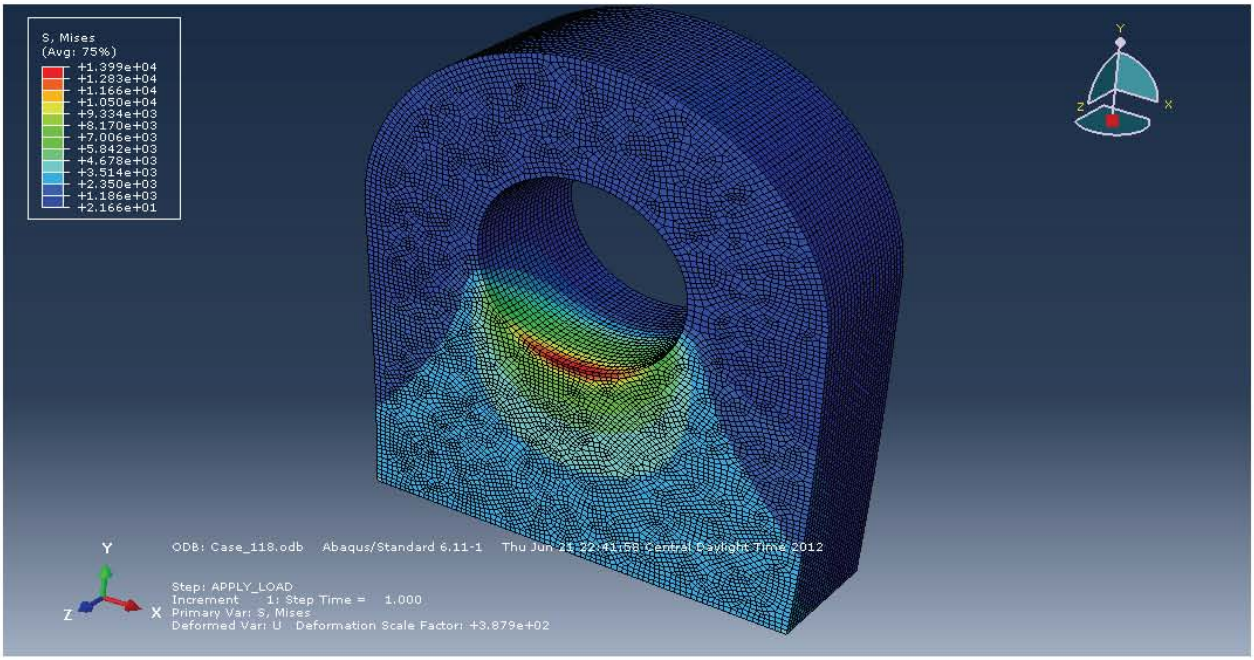

Figure D.18 – Case 118 Yoke Plate and Sleeve Von Mises Contours (8 Inch Diameter Shaft, 6 Inch Thick Yoke, 16 Inch Span)

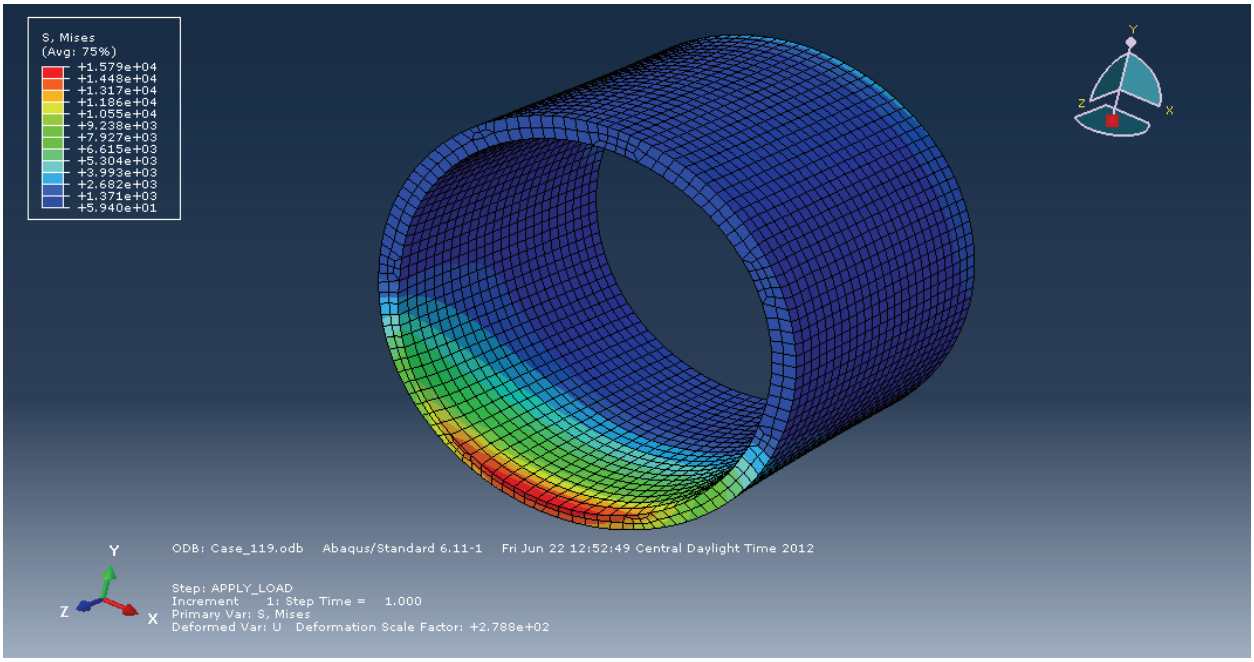

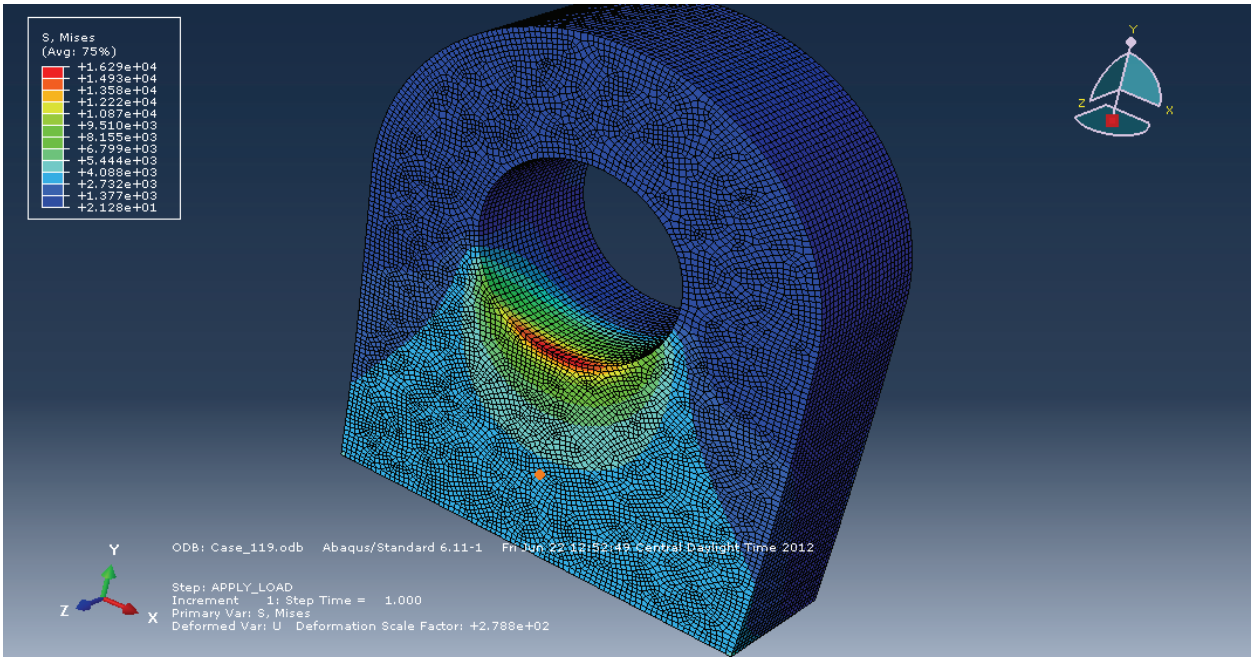

Figure D.19 – Case 119 Yoke Plate and Sleeve Von Mises Contours (8 Inch Diameter Shaft, 6 Inch Thick Yoke, 20 Inch Span)

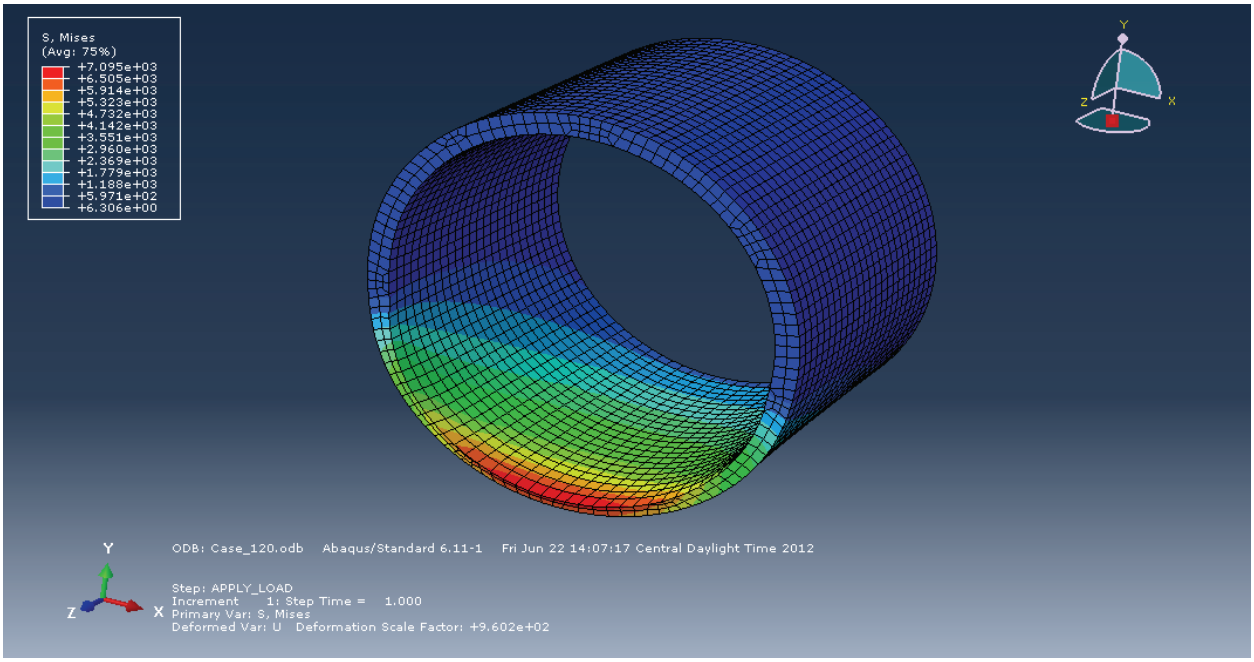

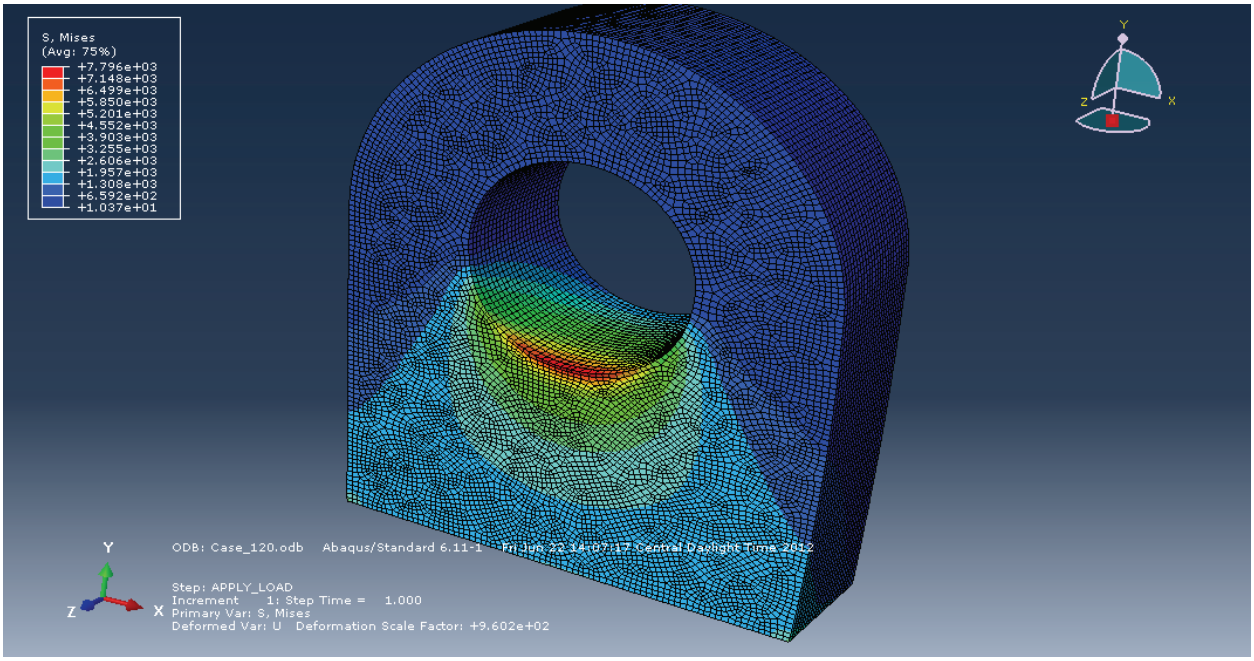

Figure D.20 – Case 120 Yoke Plate and Sleeve Von Mises Contours (8 Inch Diameter Shaft, 6 Inch Thick Yoke, 4 Inch Span)

APPENDIX E

VON MISES CONTOUR PLOTS – COMPOSITE SLEEVE

Appendix E includes a series of screenshots taken from the different ABAQUS models that were developed. For reference, table E.1 provides the specific parameters that are associated to each of the analysis cases that are documented within this appendix.

Table E.1. Summary of cases with a composite sleeve.

Case	Sleeve	Shaft Diameter (in)	Trunnion Load (kips)	Yoke Plate Thickness (in)	Clear Span (in)
1001	Composite	4	120	2	2
1002	Composite	4	120	2	4
1003	Composite	4	120	2	6
1004	Composite	4	120	4	4
1005	Composite	4	120	4	8
1006	Composite	4	120	4	12
1007	Composite	4	120	6	4
1008	Composite	4	120	6	8
1009	Composite	4	120	6	12
1010	Composite	8	240	2	8
1011	Composite	8	240	2	12
1012	Composite	8	240	2	16
1013	Composite	8	240	4	8
1014	Composite	8	240	4	12
1015	Composite	8	240	4	16
1016	Composite	8	240	6	8
1017	Composite	8	240	6	12
1018	Composite	8	240	6	16
1019	Composite	8	240	6	20
1020	Composite	8	240	6	4

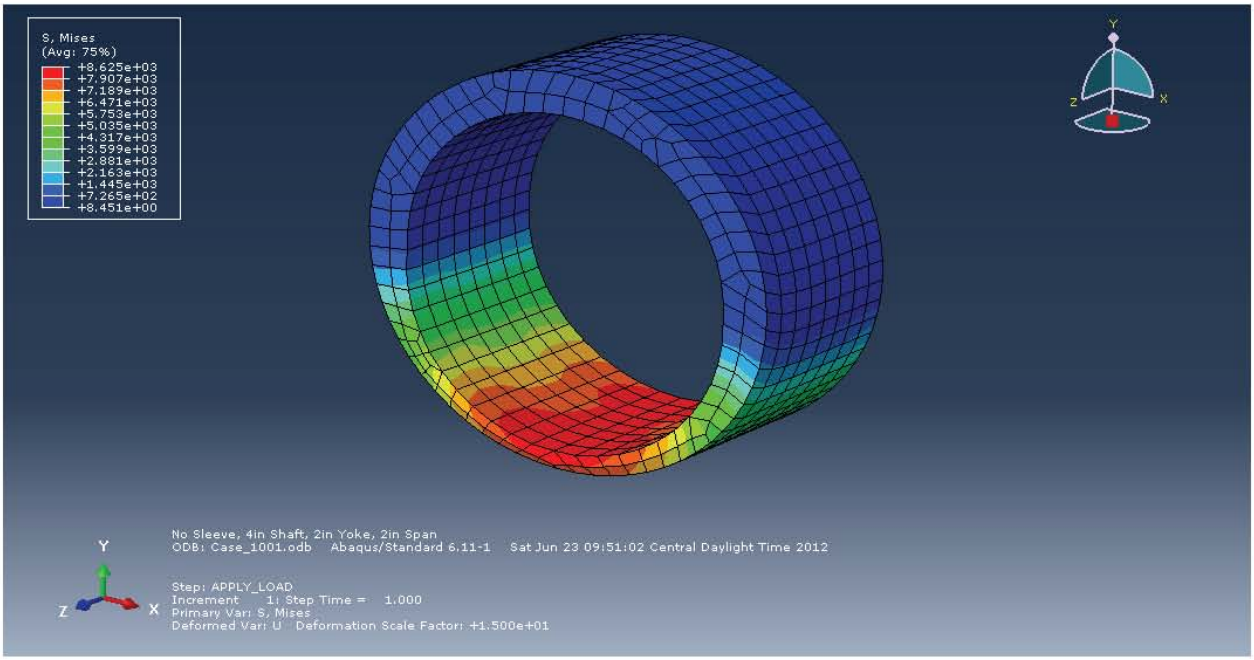

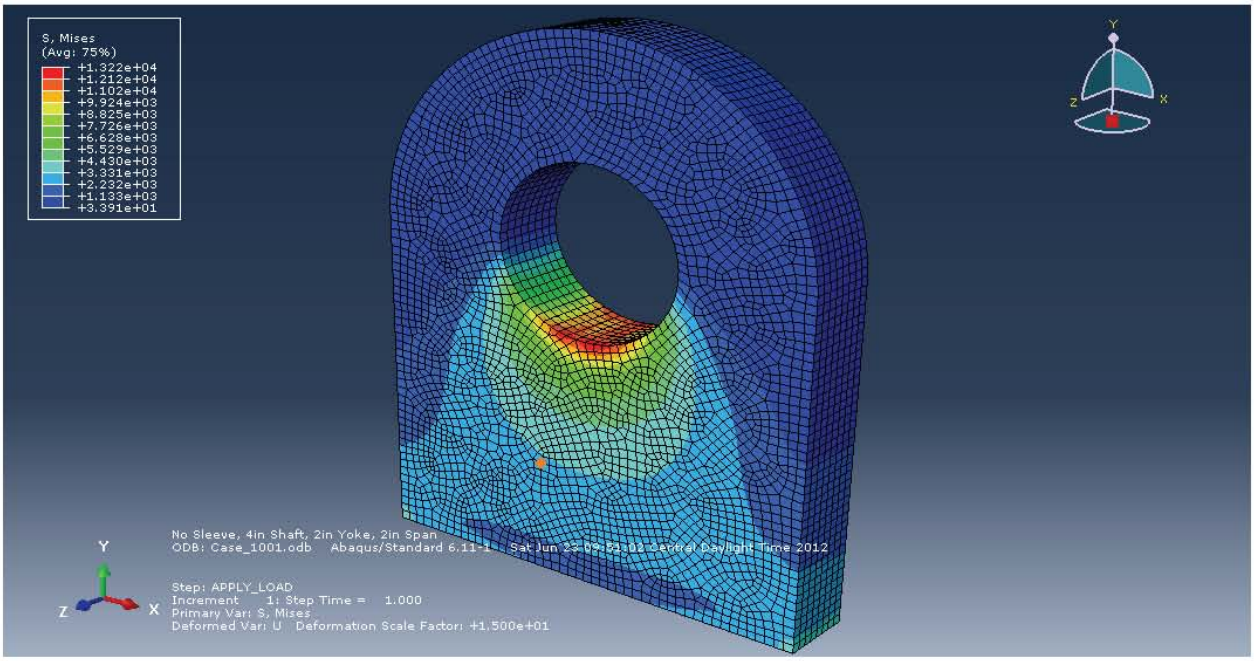

Figure E.1 – Case 1001 Yoke Plate and Sleeve Von Mises Contours (4 Inch Diameter Shaft, 2 Inch Thick Yoke, 2 Inch Span)

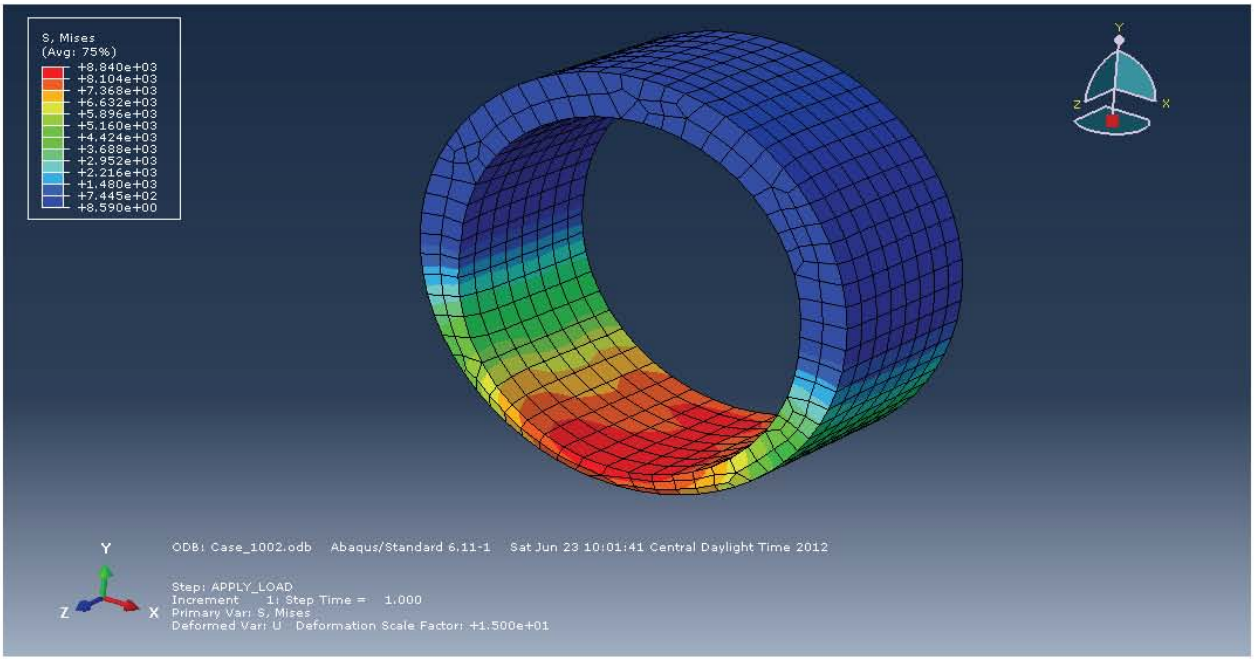

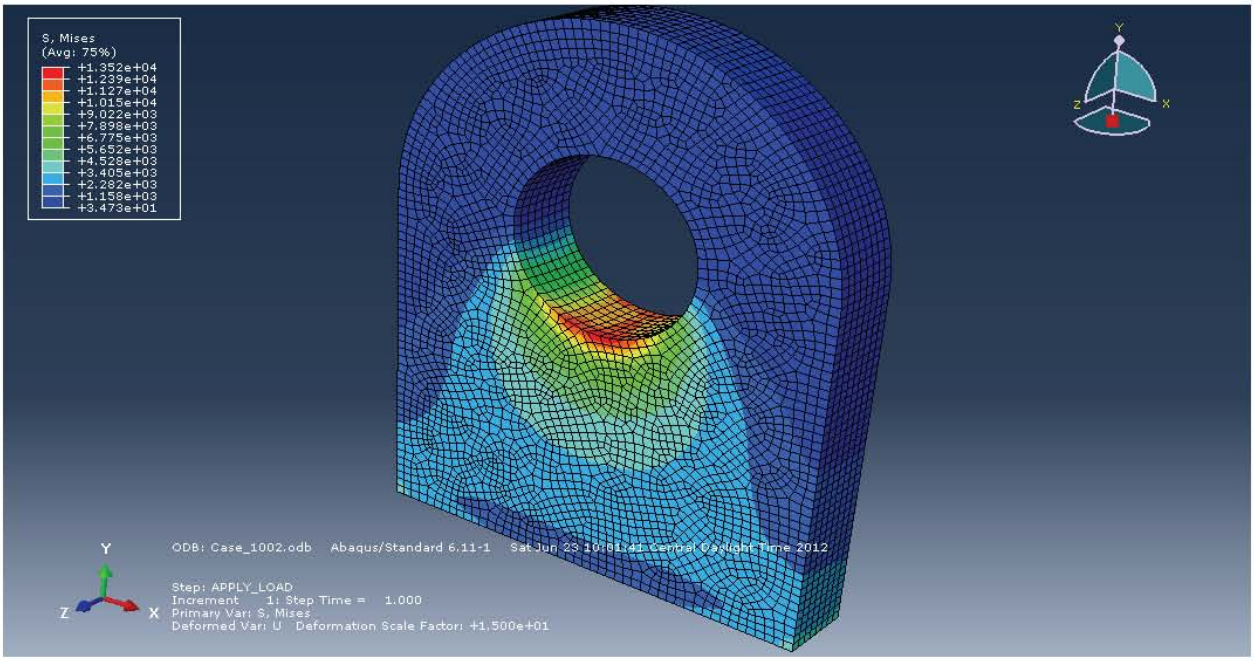

Figure E.2 – Case 1002 Yoke Plate and Sleeve Von Mises Contours (4 Inch Diameter Shaft, 2 Inch Thick Yoke, 4 Inch Span)

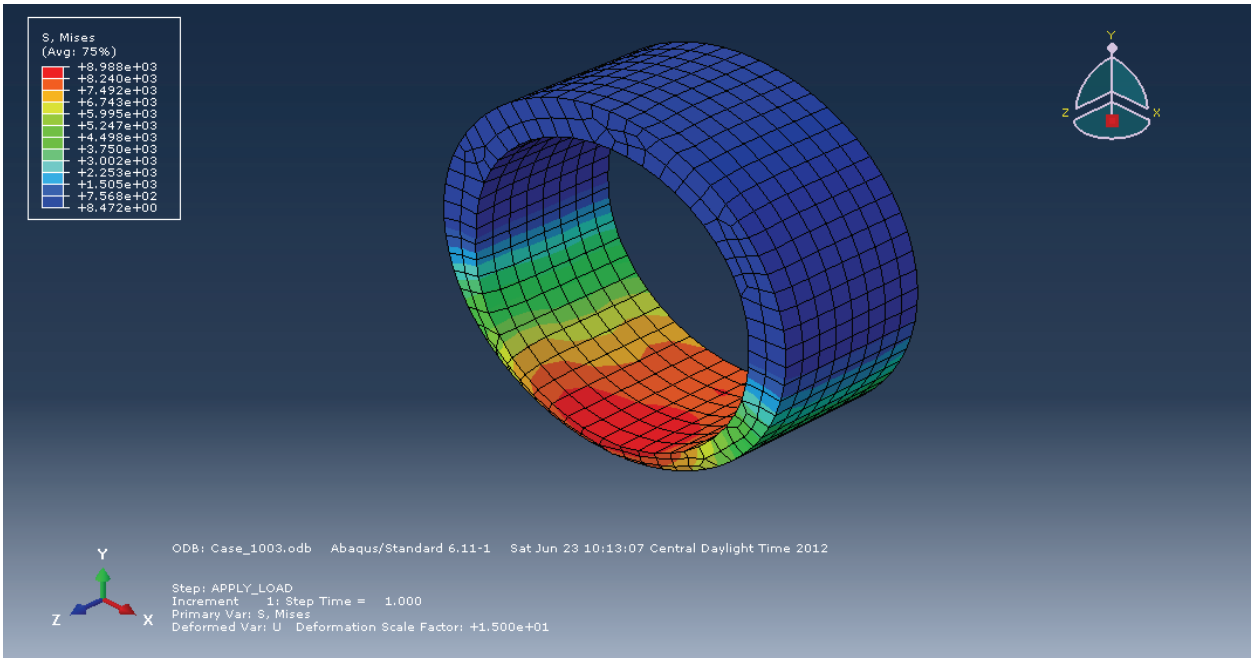

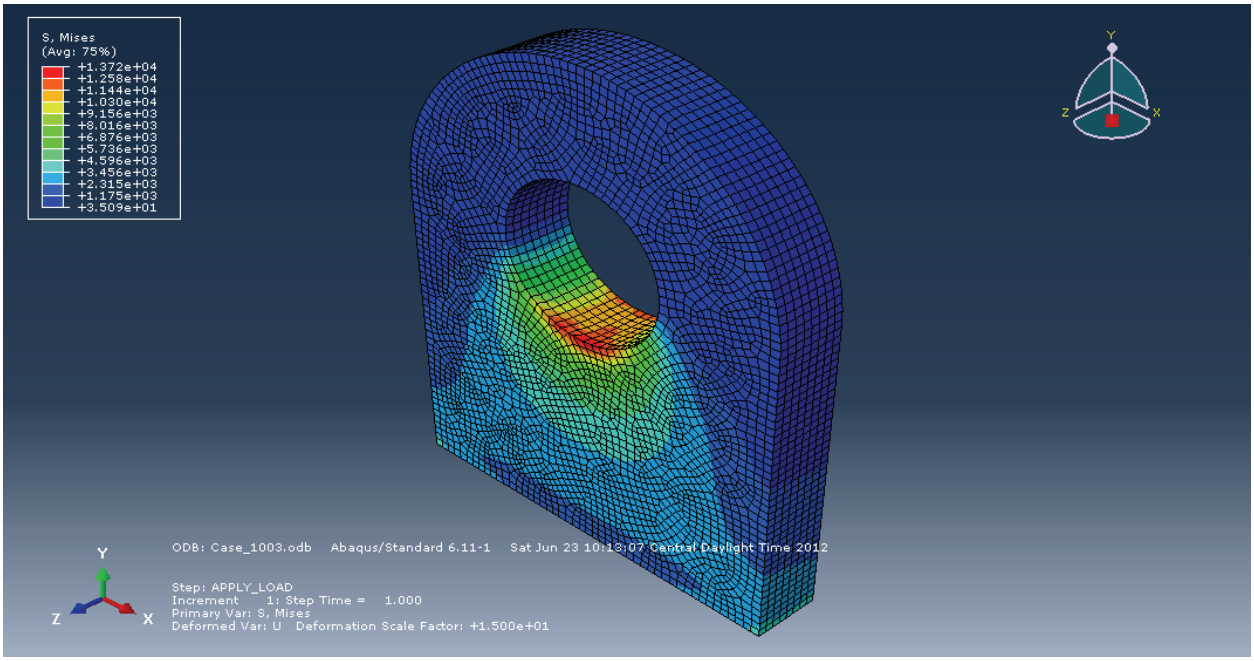

Figure E.3 – Case 1003 Yoke Plate and Sleeve Von Mises Contours (4 Inch Diameter Shaft, 2 Inch Thick Yoke, 6 Inch Span)

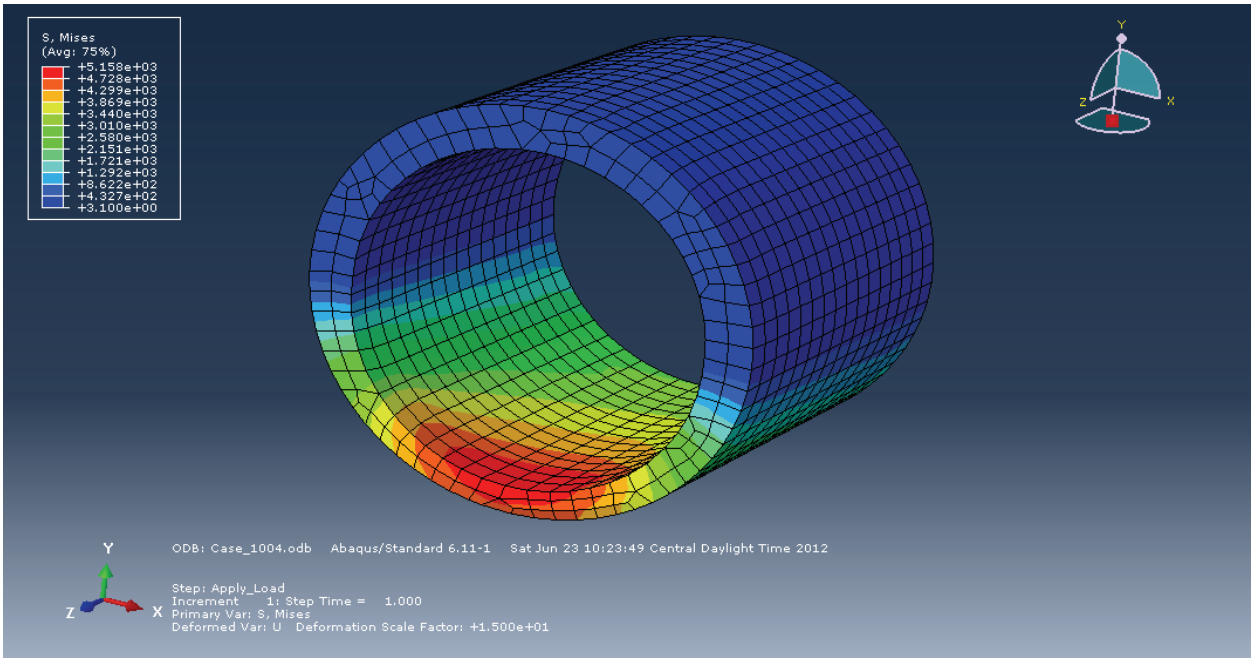

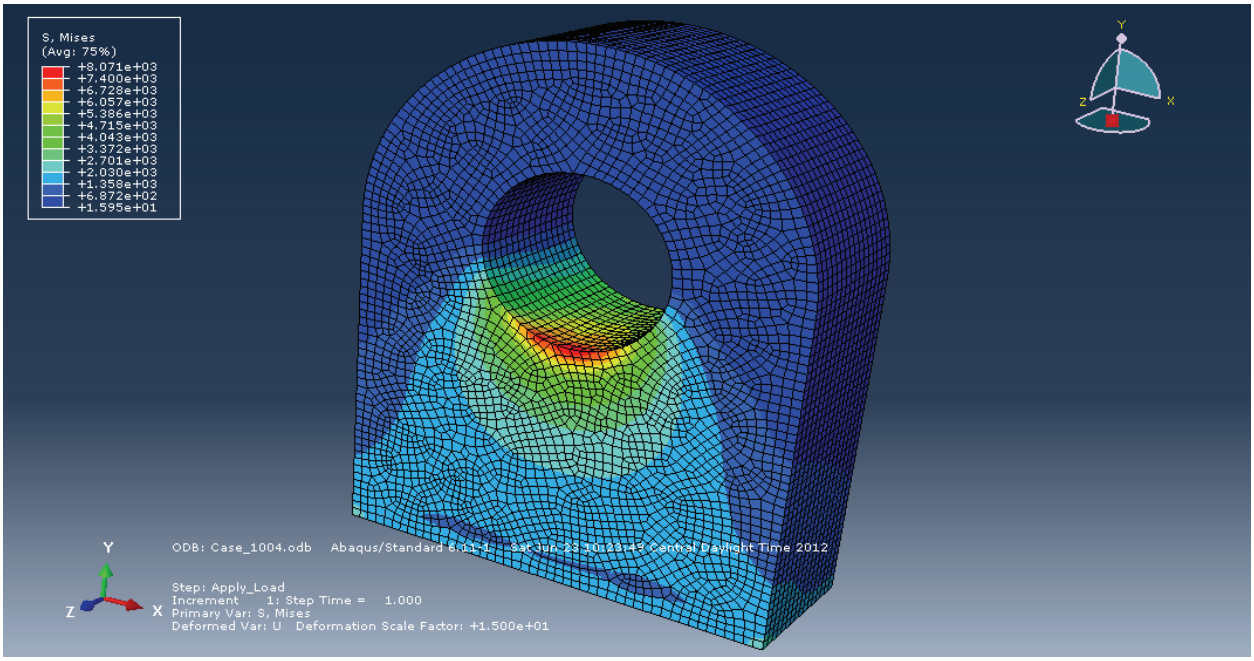

Figure E.4 – Case 1004 Yoke Plate and Sleeve Von Mises Contours (4 Inch Diameter Shaft, 4 Inch Thick Yoke, 4 Inch Span)

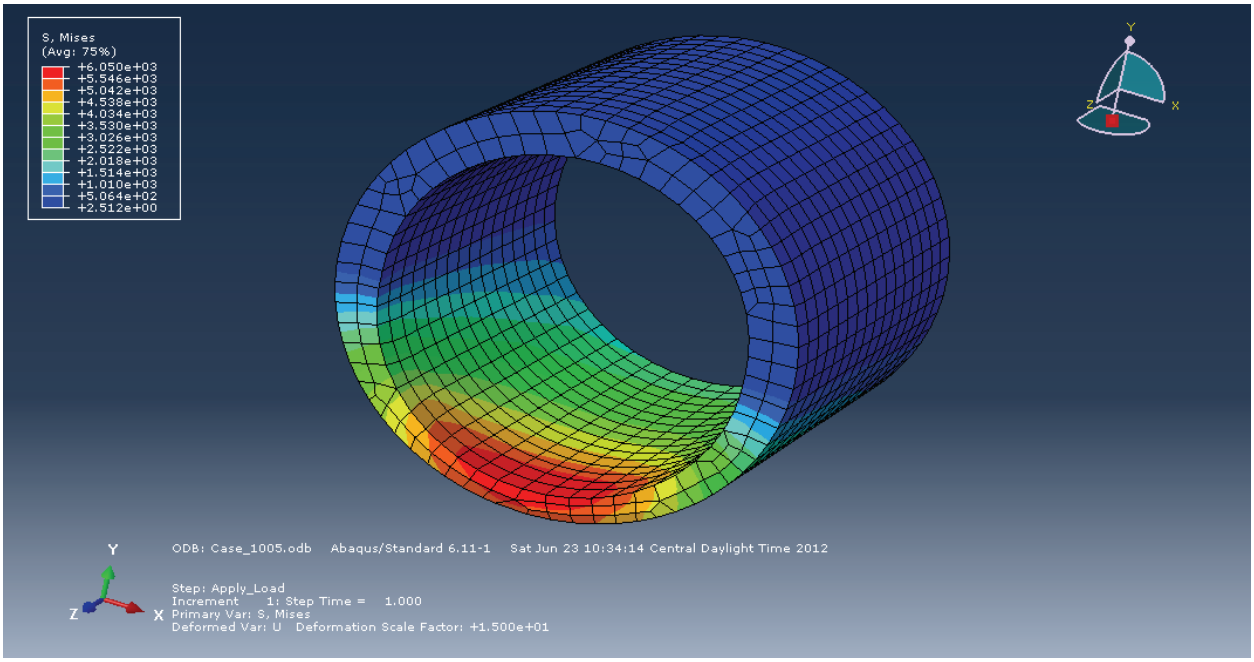

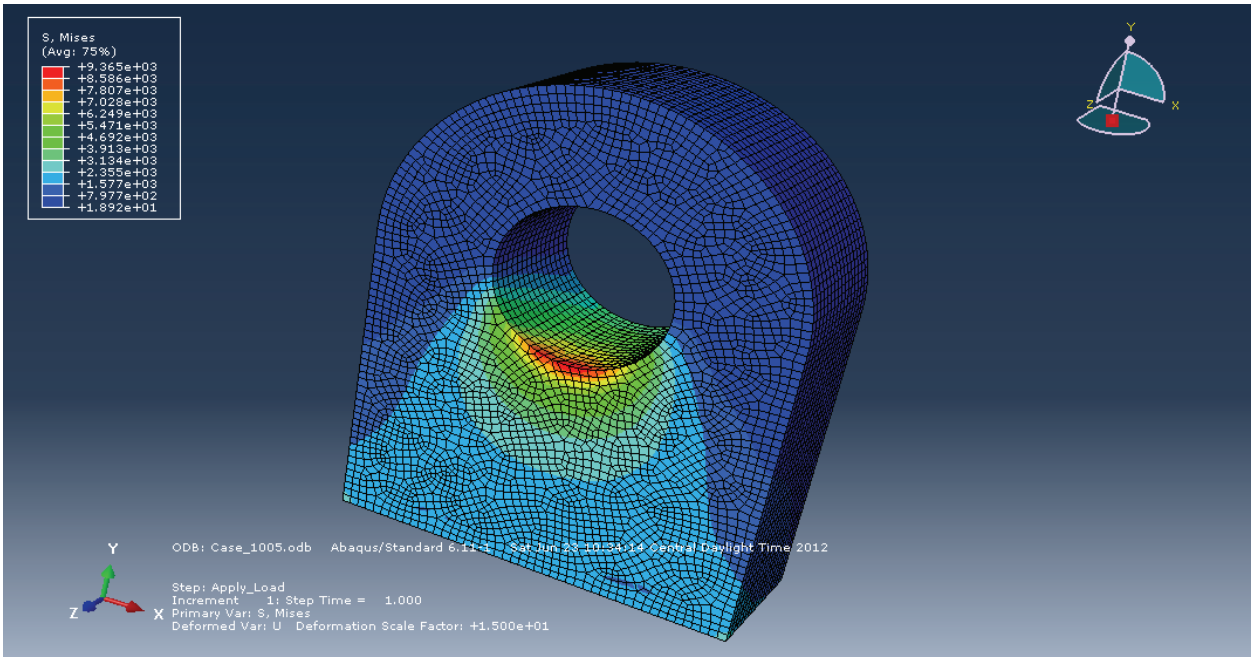

Figure E.5 – Case 1005 Yoke Plate and Sleeve Von Mises Contours (4 Inch Diameter Shaft, 4 Inch Thick Yoke, 8 Inch Span)

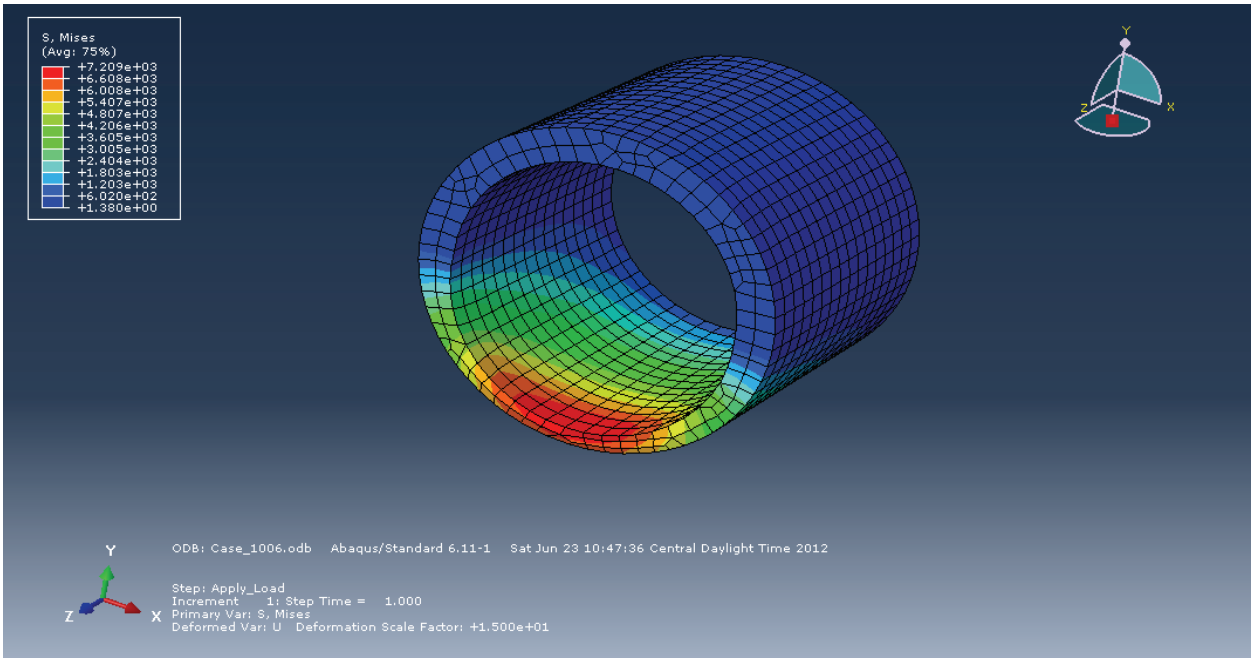

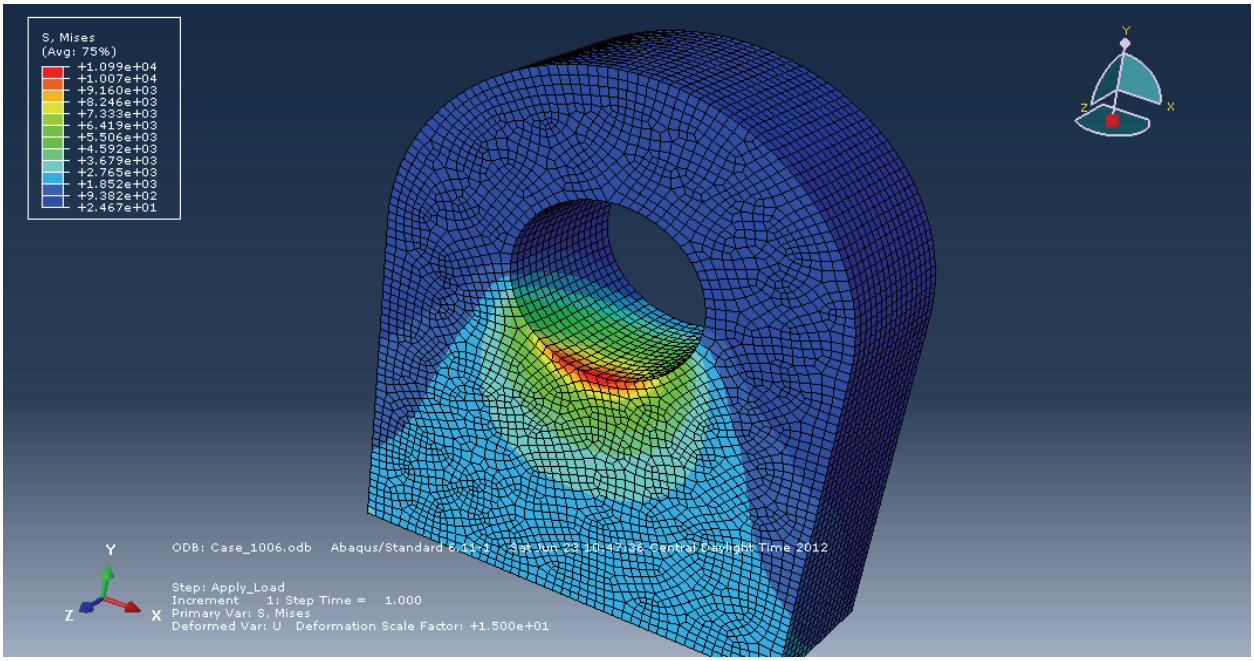

Figure E.6 – Case 1006 Yoke Plate and Sleeve Von Mises Contours (4 Inch Diameter Shaft, 4 Inch Thick Yoke, 12 Inch Span)

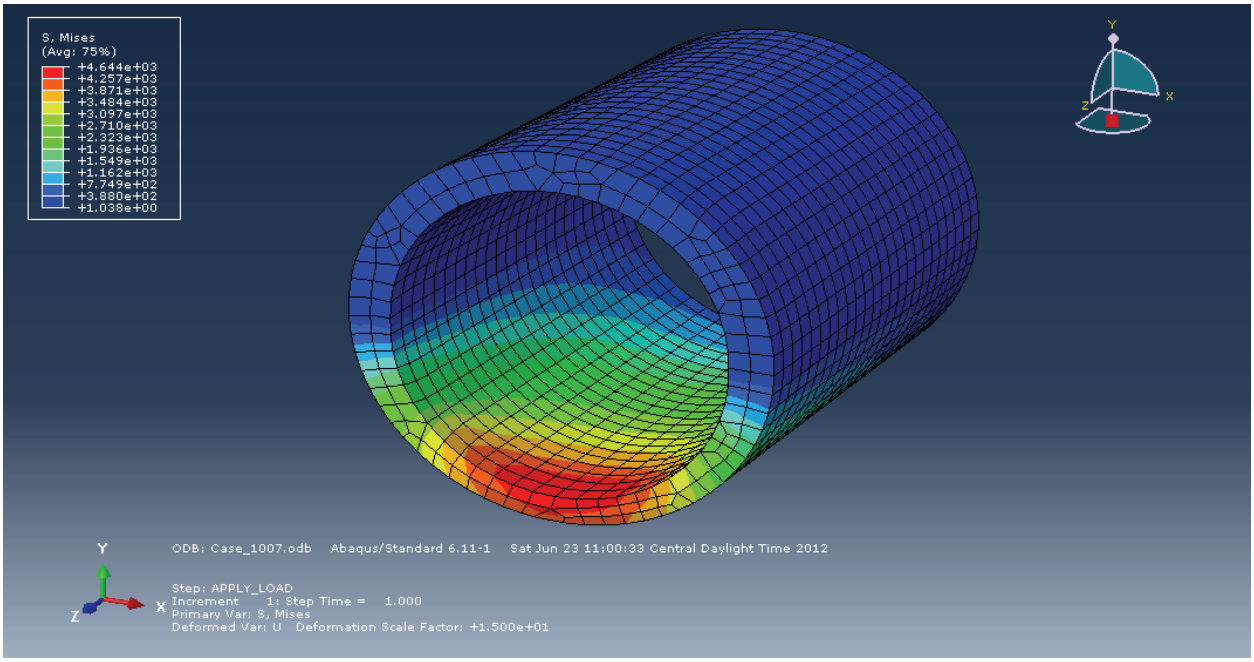

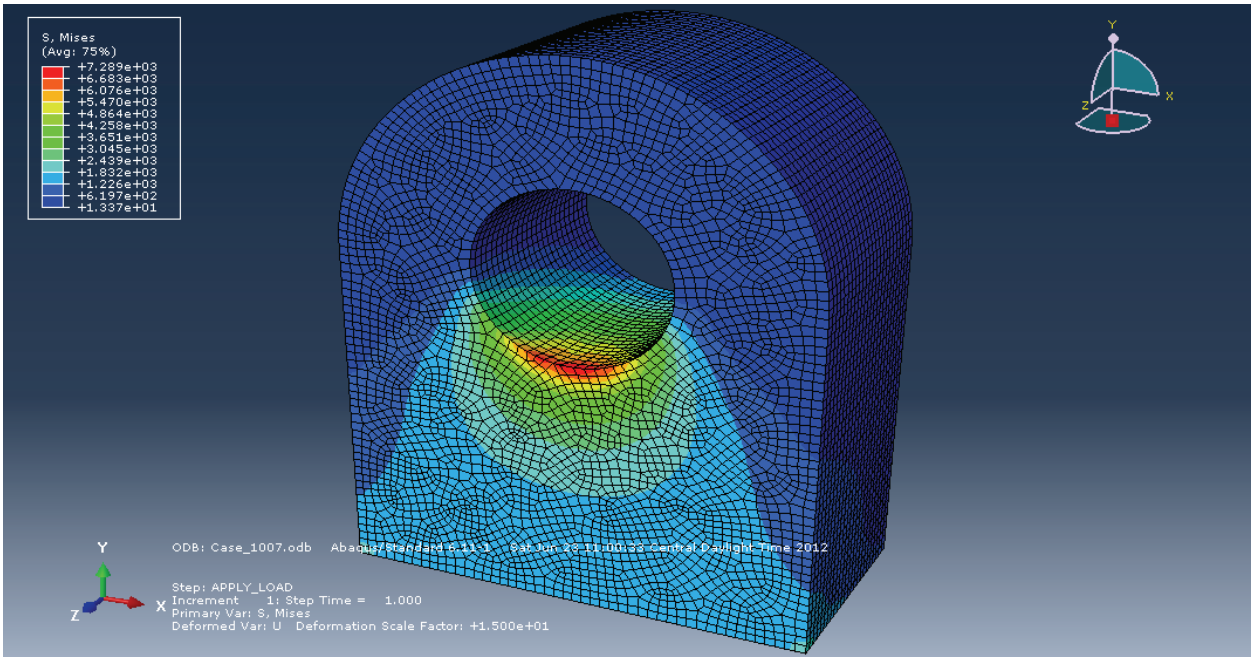

Figure E.7 – Case 1007 Yoke Plate and Sleeve Von Mises Contours (4 Inch Diameter Shaft, 6 Inch Thick Yoke, 4 Inch Span)

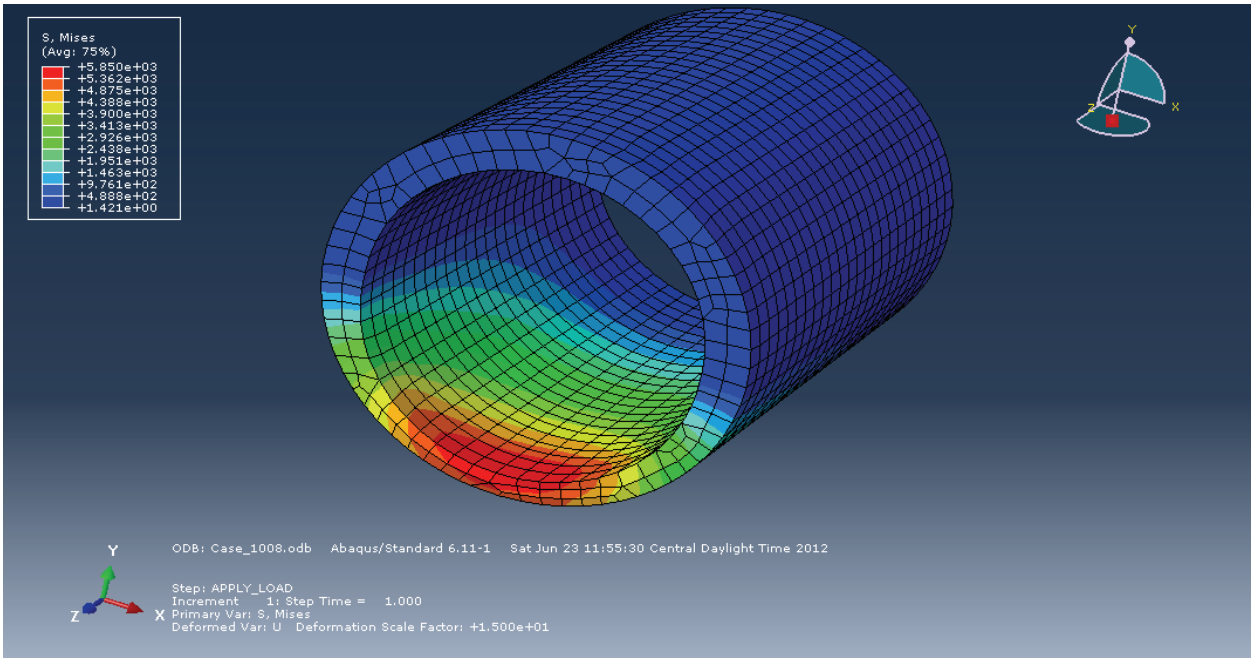

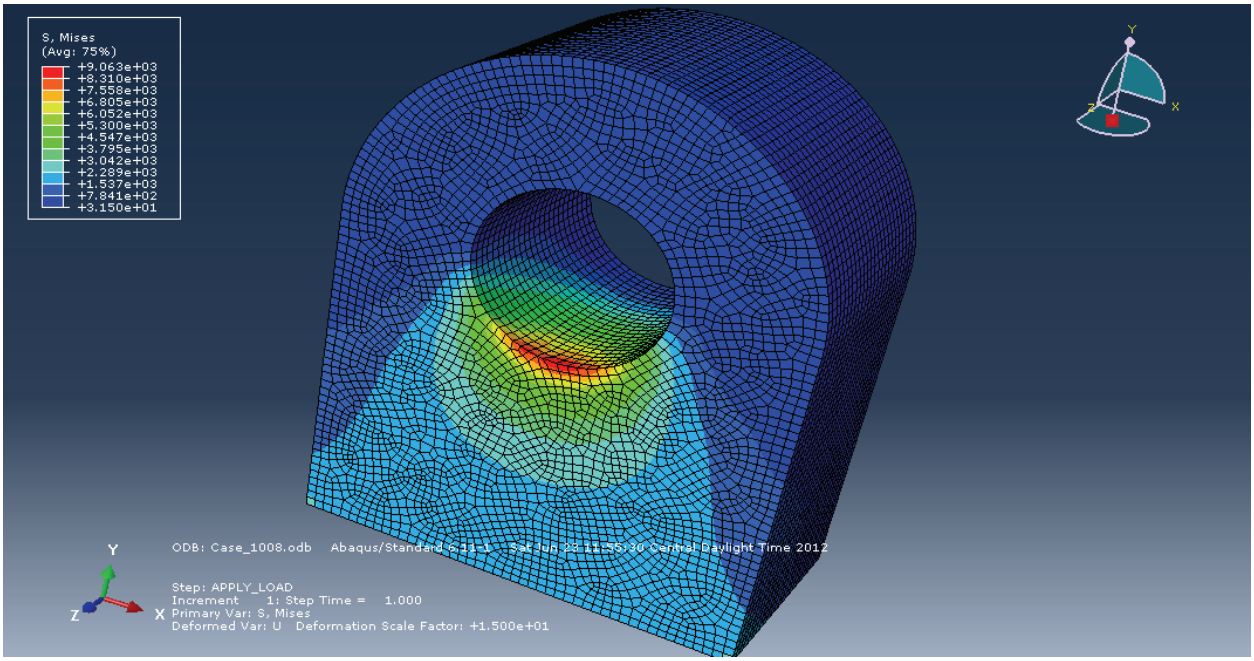

Figure E.8 – Case 1008 Yoke Plate and Sleeve Von Mises Contours (4 Inch Diameter Shaft, 6 Inch Thick Yoke, 8 Inch Span)

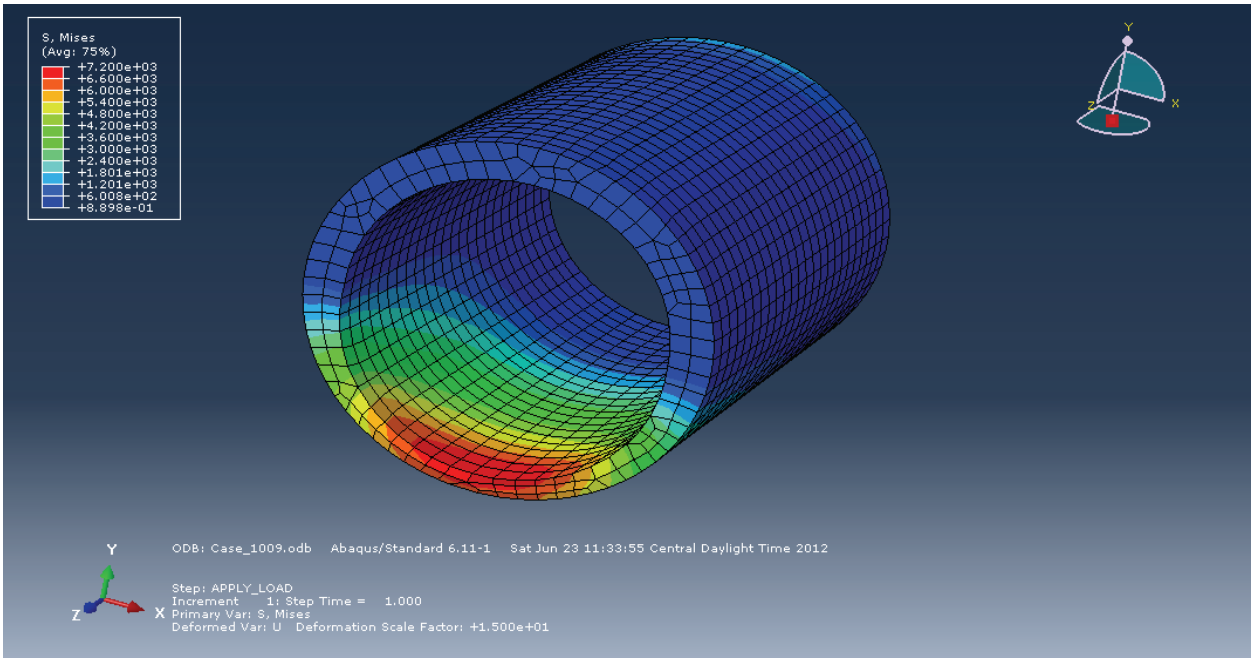

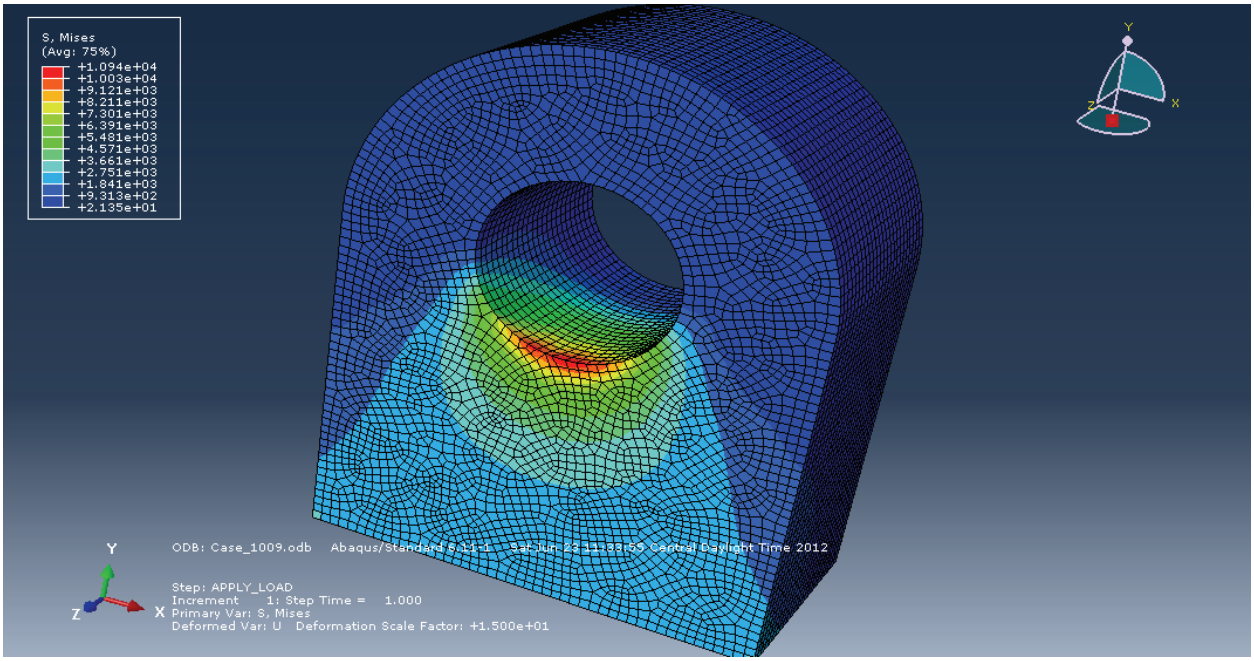

Figure E.9 – Case 1009 Yoke Plate and Sleeve Von Mises Contours (4 Inch Diameter Shaft, 6 Inch Thick Yoke, 12 Inch Span)

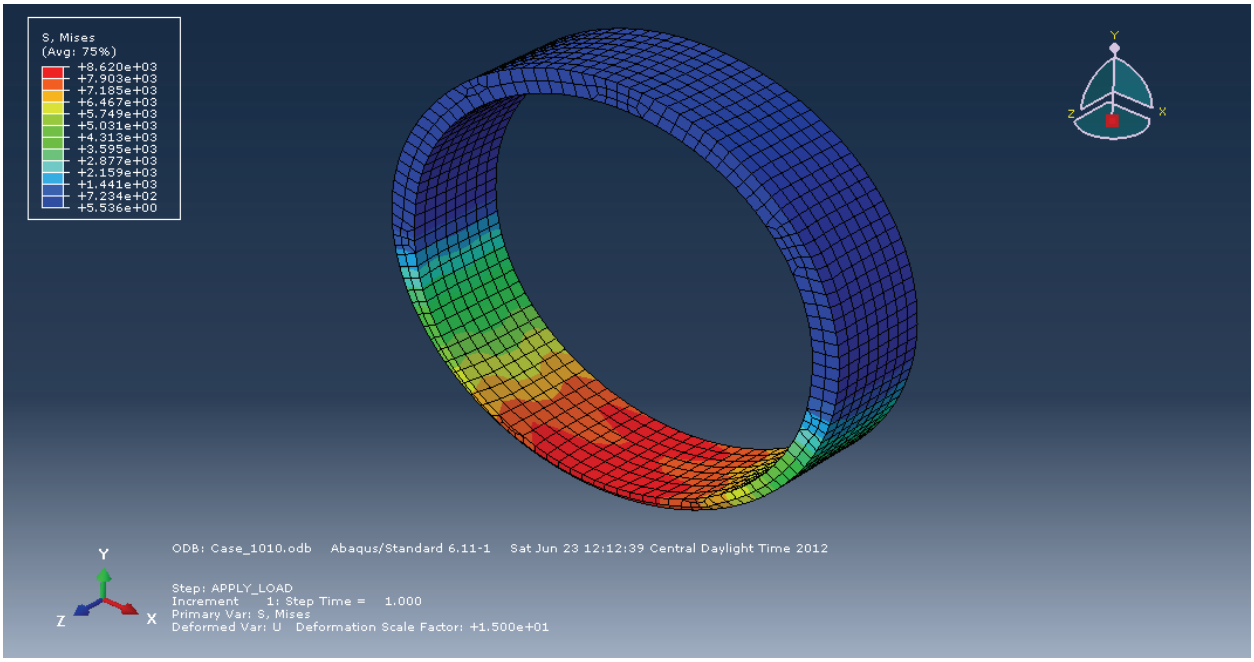

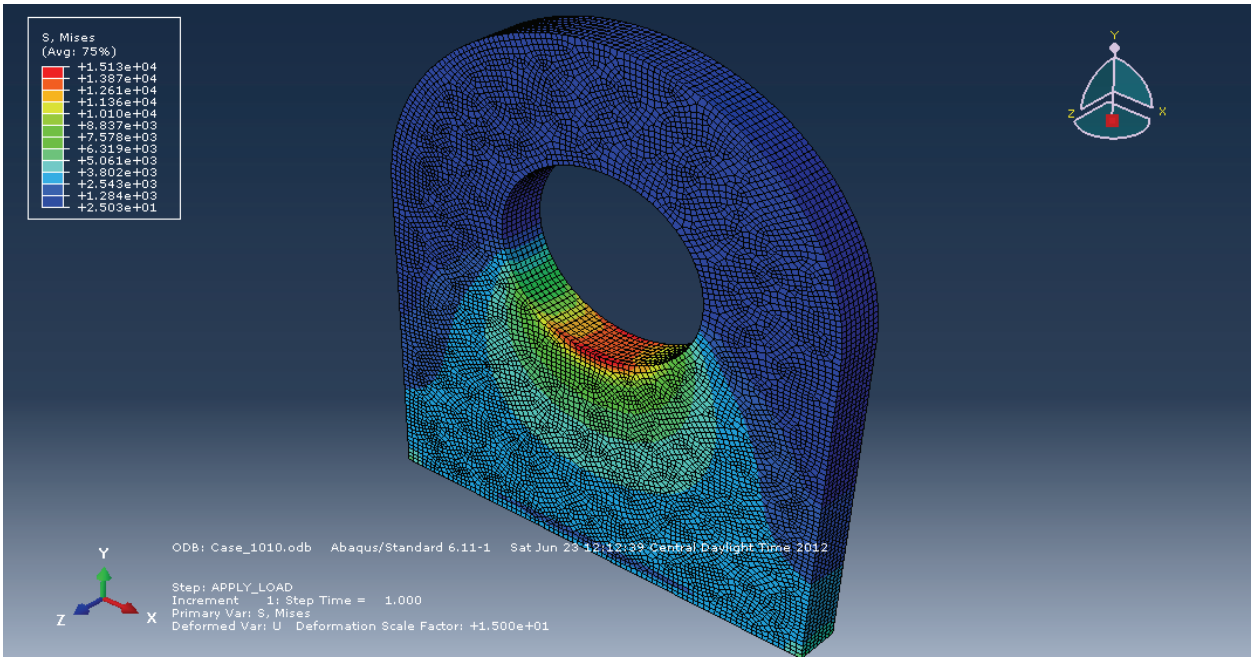

Figure E.10 – Case 1010 Yoke Plate and Sleeve Von Mises Contours (8 Inch Diameter Shaft, 2 Inch Thick Yoke, 8 Inch Span)

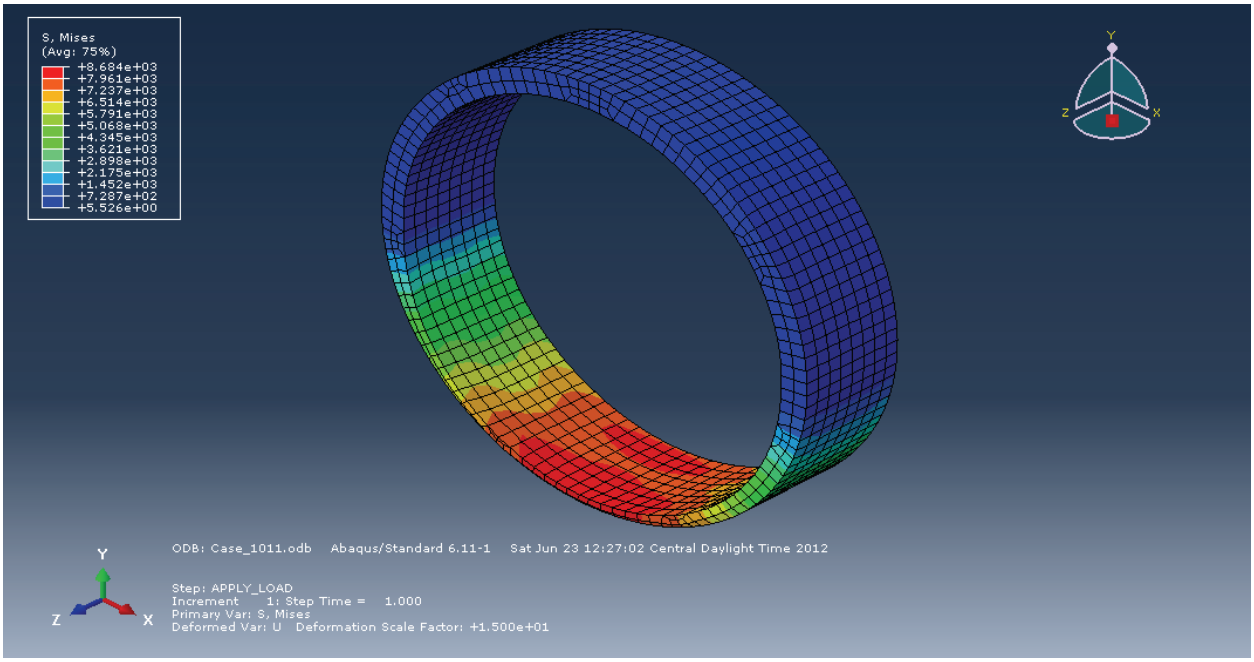

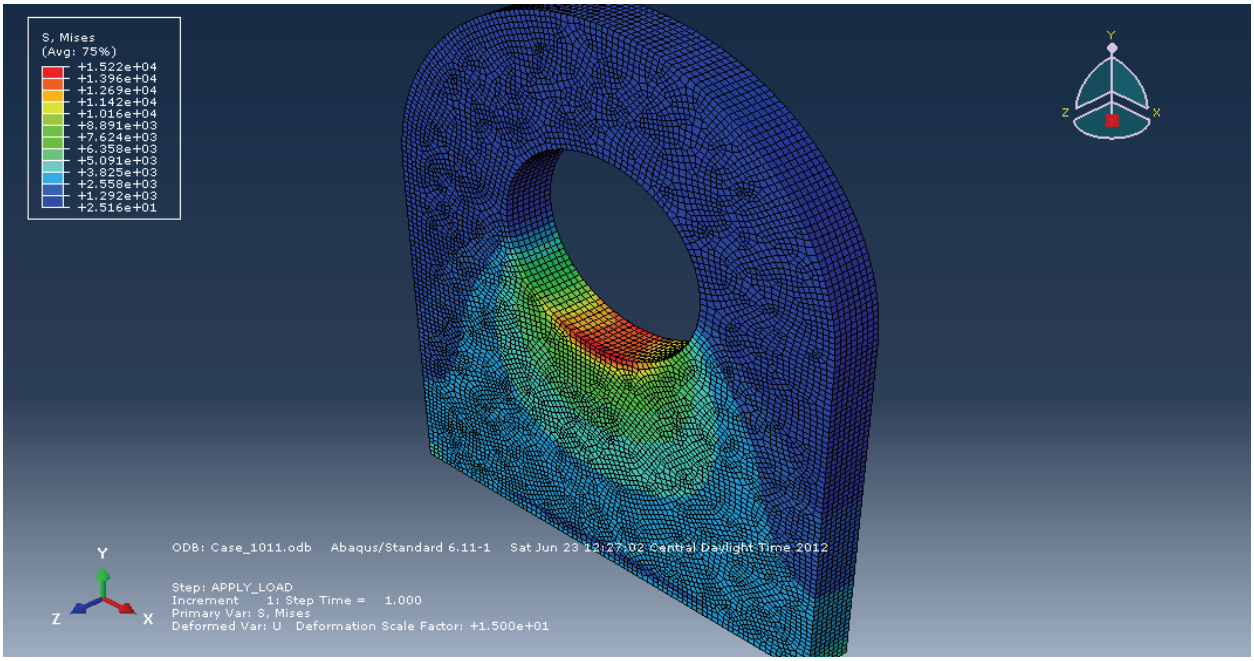

Figure E.11 – Case 1011 Yoke Plate and Sleeve Von Mises Contours (8 Inch Diameter Shaft, 2 Inch Thick Yoke, 12 Inch Span)

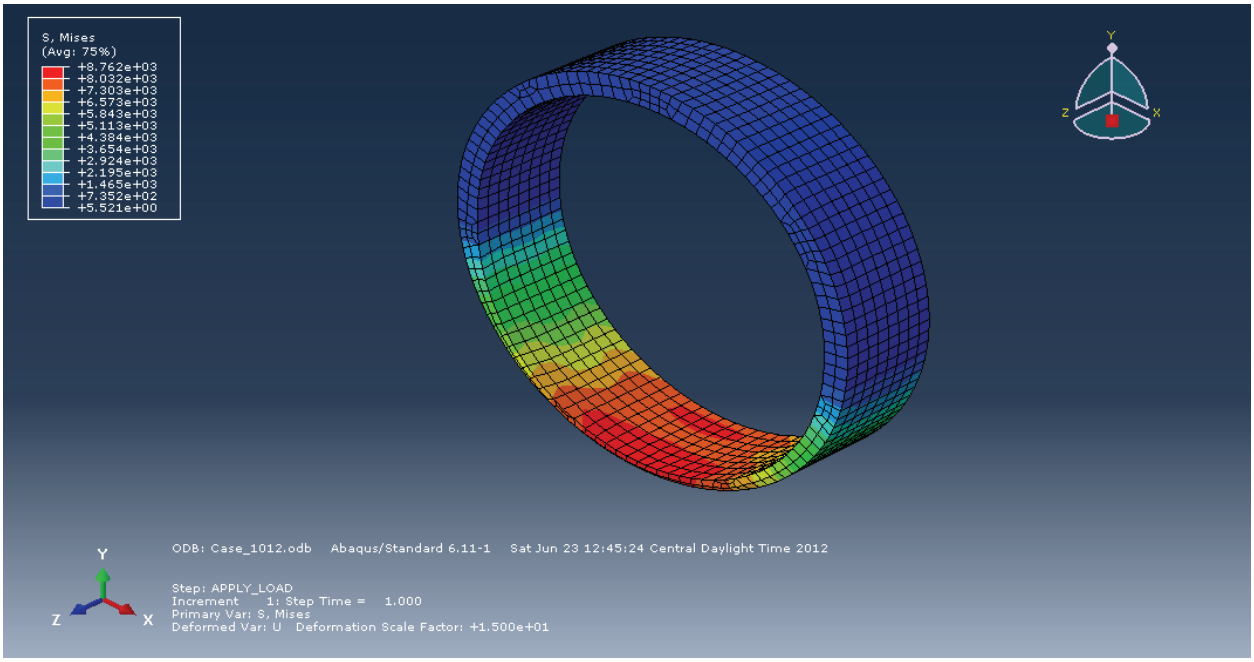

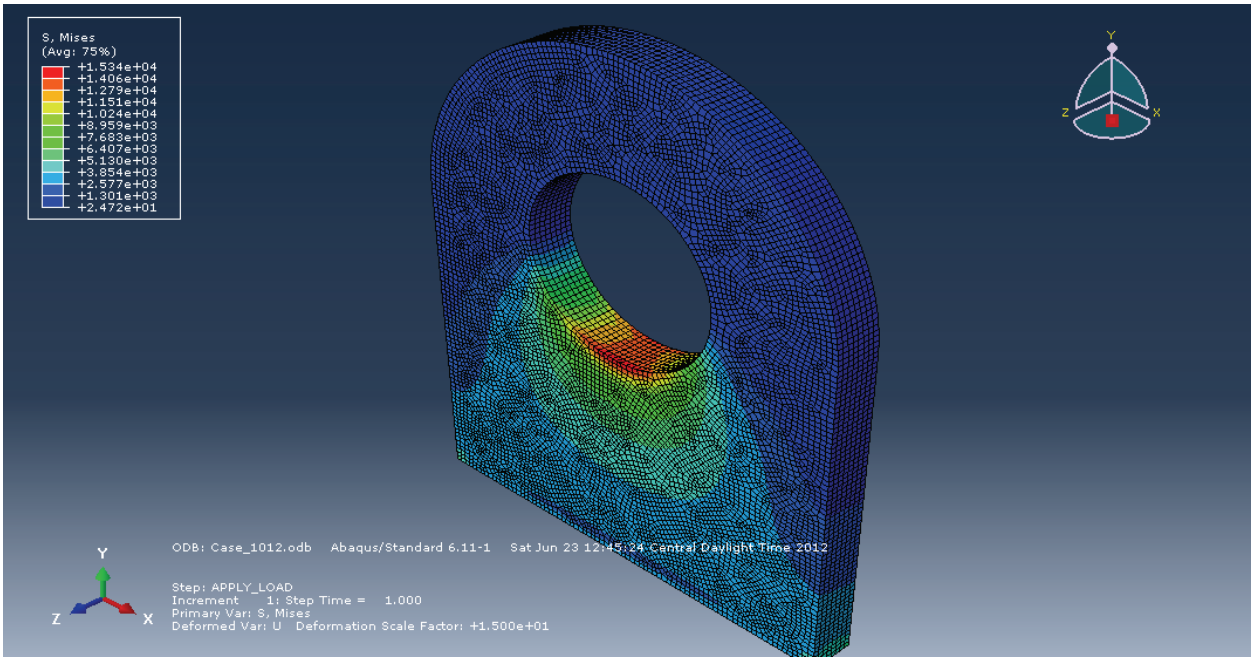

Figure E.12 – Case 1012 Yoke Plate and Sleeve Von Mises Contours (8 Inch Diameter Shaft, 2 Inch Thick Yoke, 16 Inch Span)

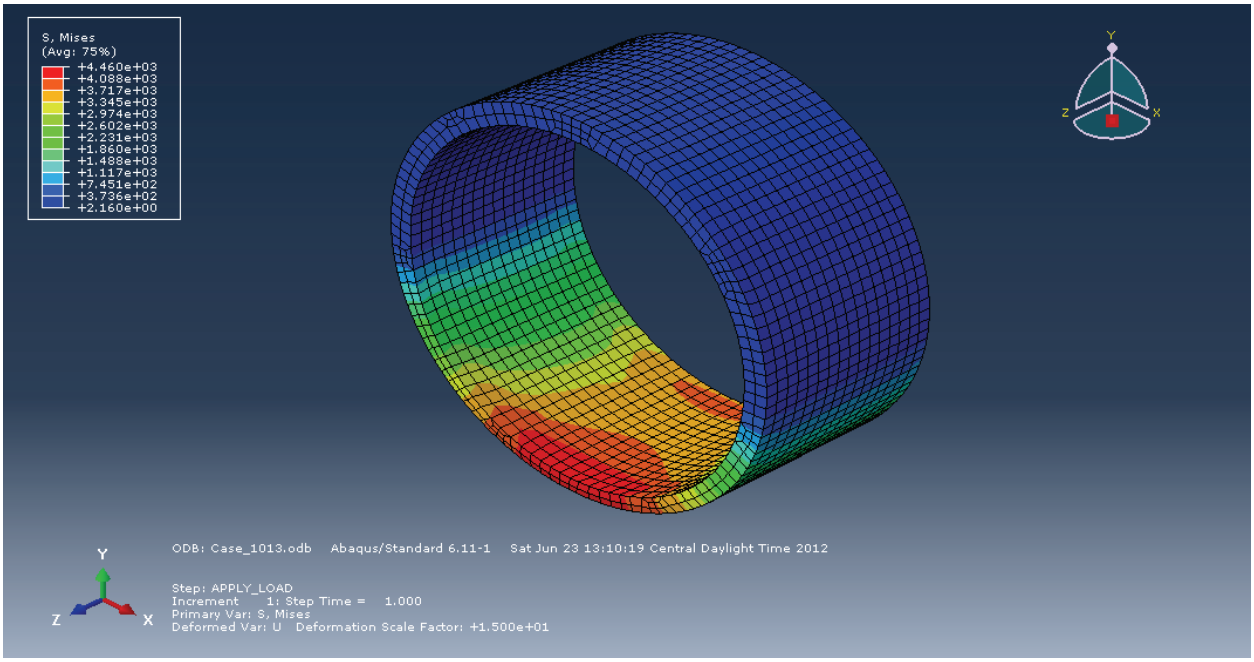

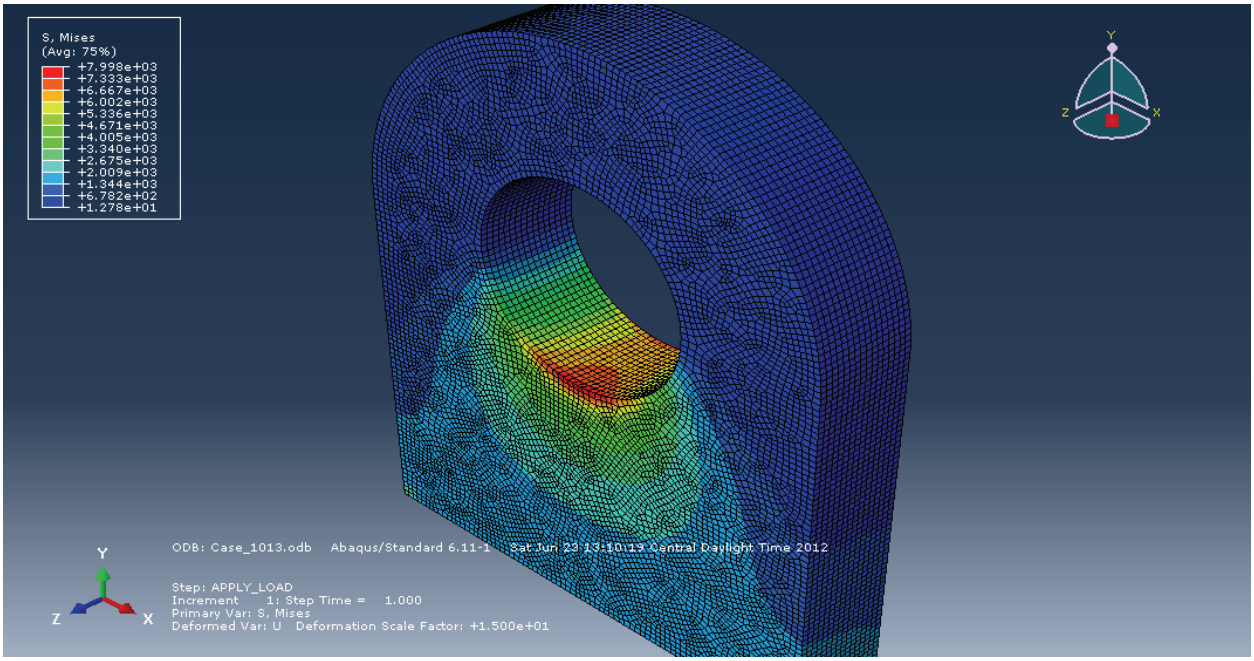

Figure E.13 – Case 1013 Yoke Plate and Sleeve Von Mises Contours (8 Inch Diameter Shaft, 4 Inch Thick Yoke, 8 Inch Span)

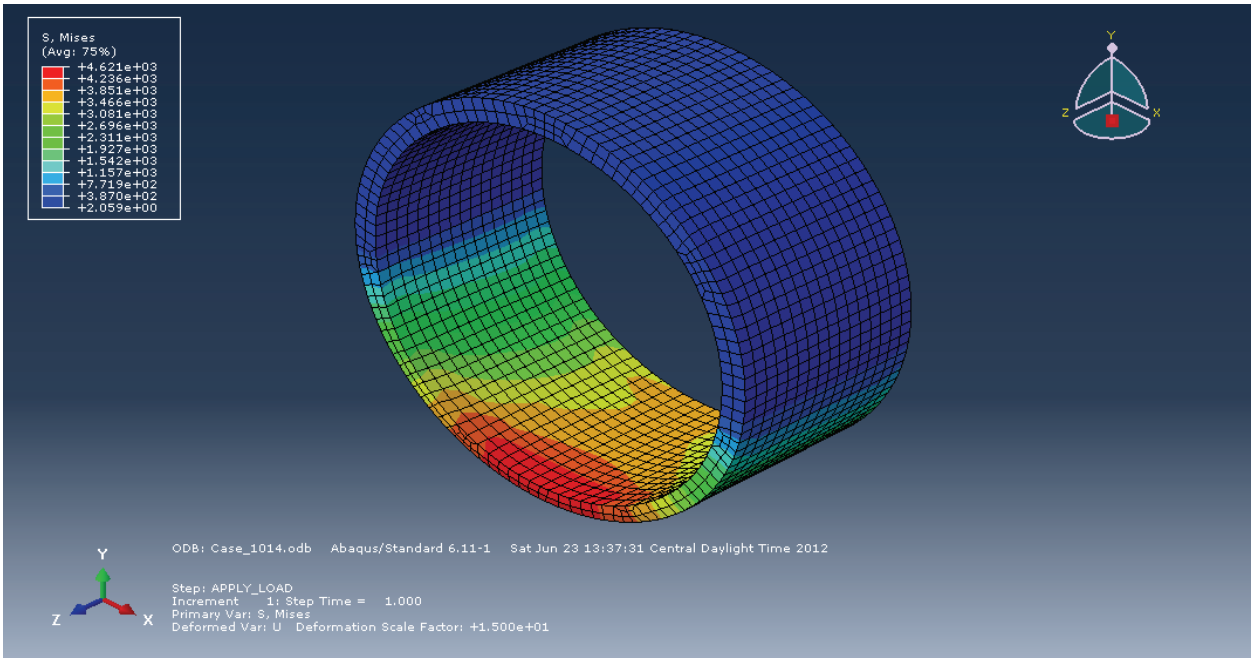

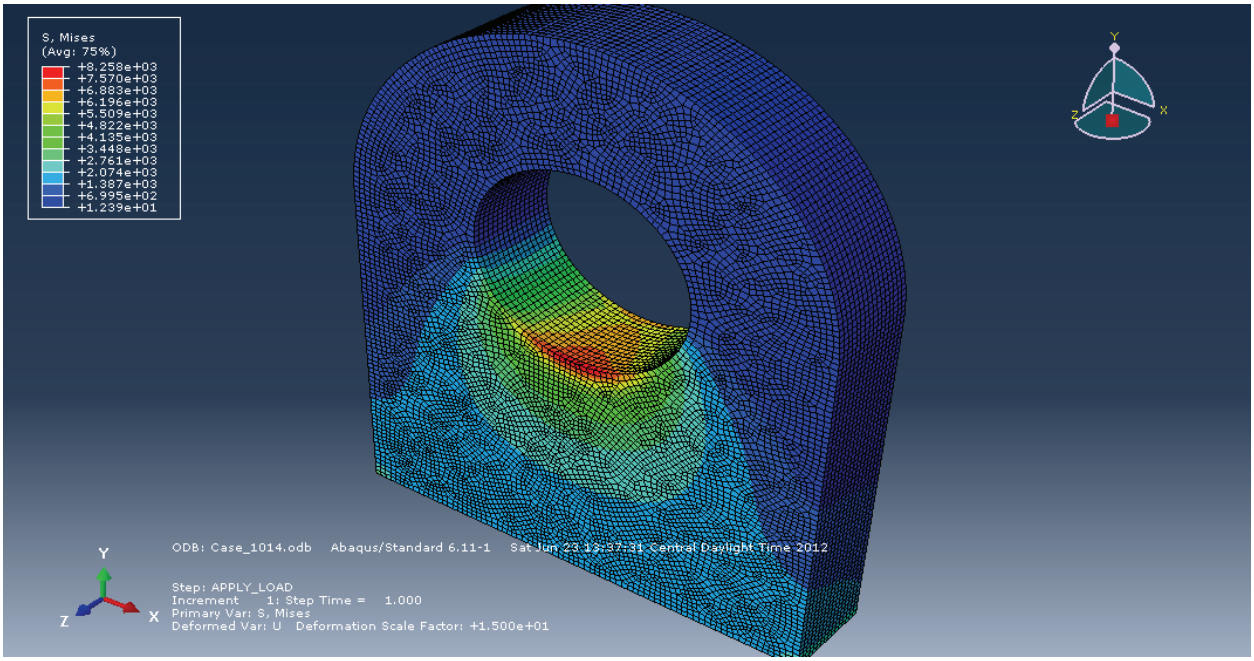

Figure E.14 – Case 1014 Yoke Plate and Sleeve Von Mises Contours (8 Inch Diameter Shaft, 4 Inch Thick Yoke, 12 Inch Span)

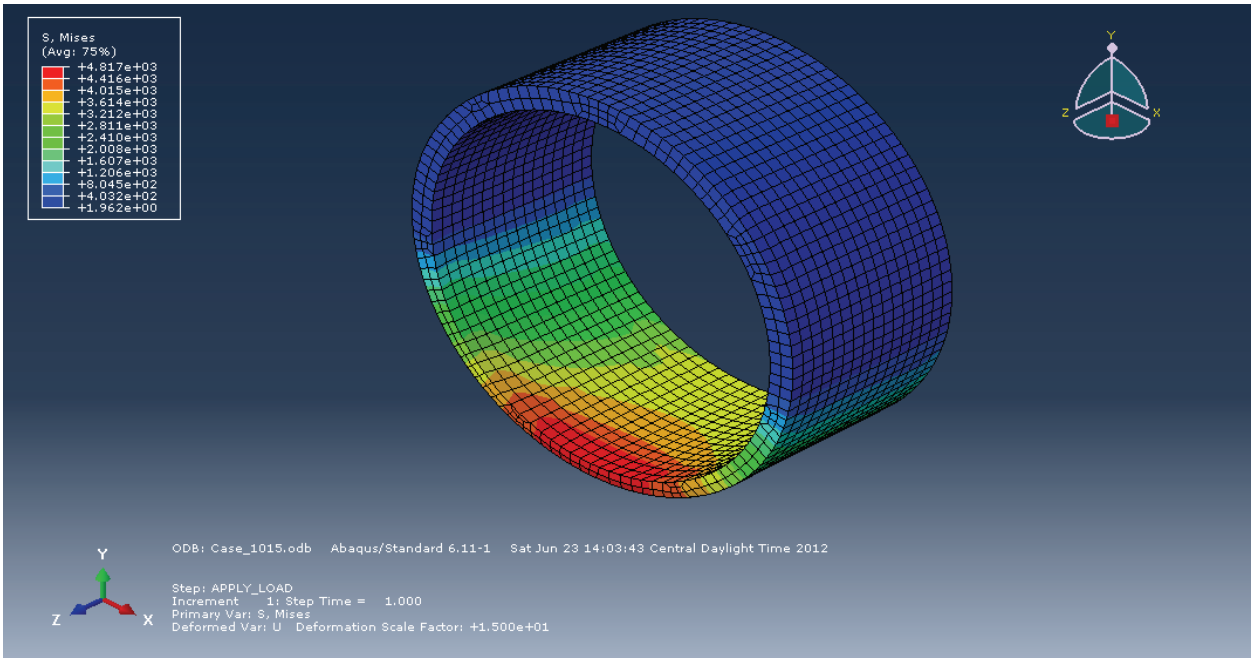

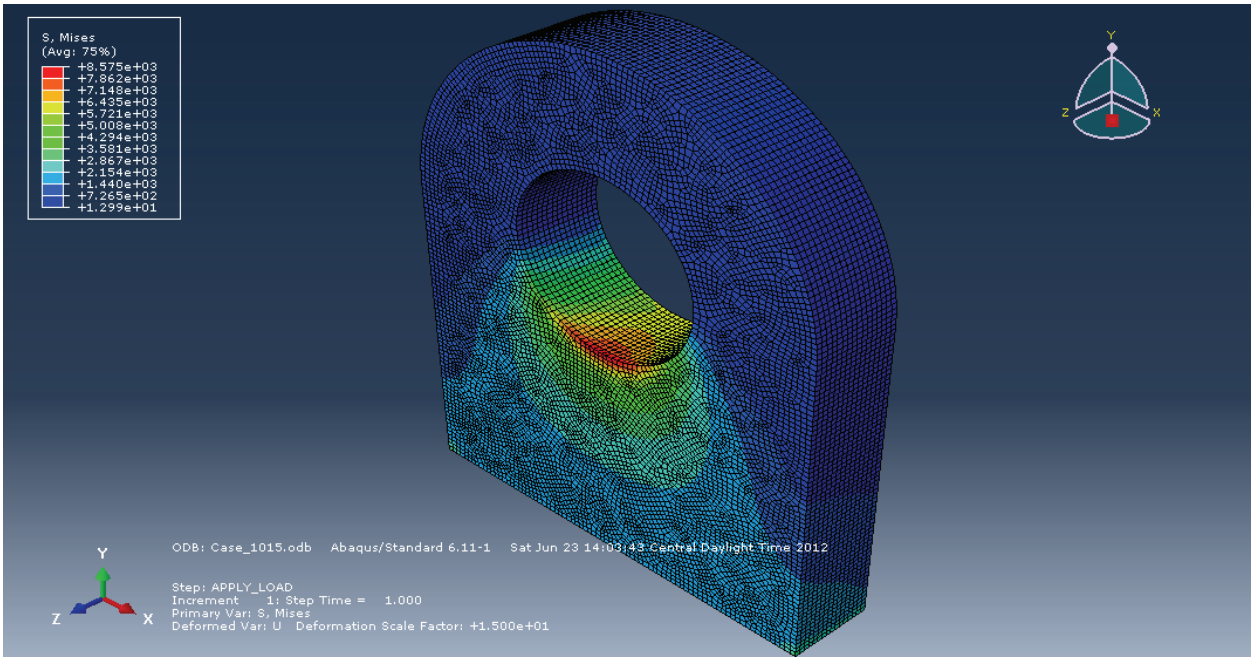

Figure E.15 – Case 1015 Yoke Plate and Sleeve Von Mises Contours (8 Inch Diameter Shaft, 4 Inch Thick Yoke, 16 Inch Span)

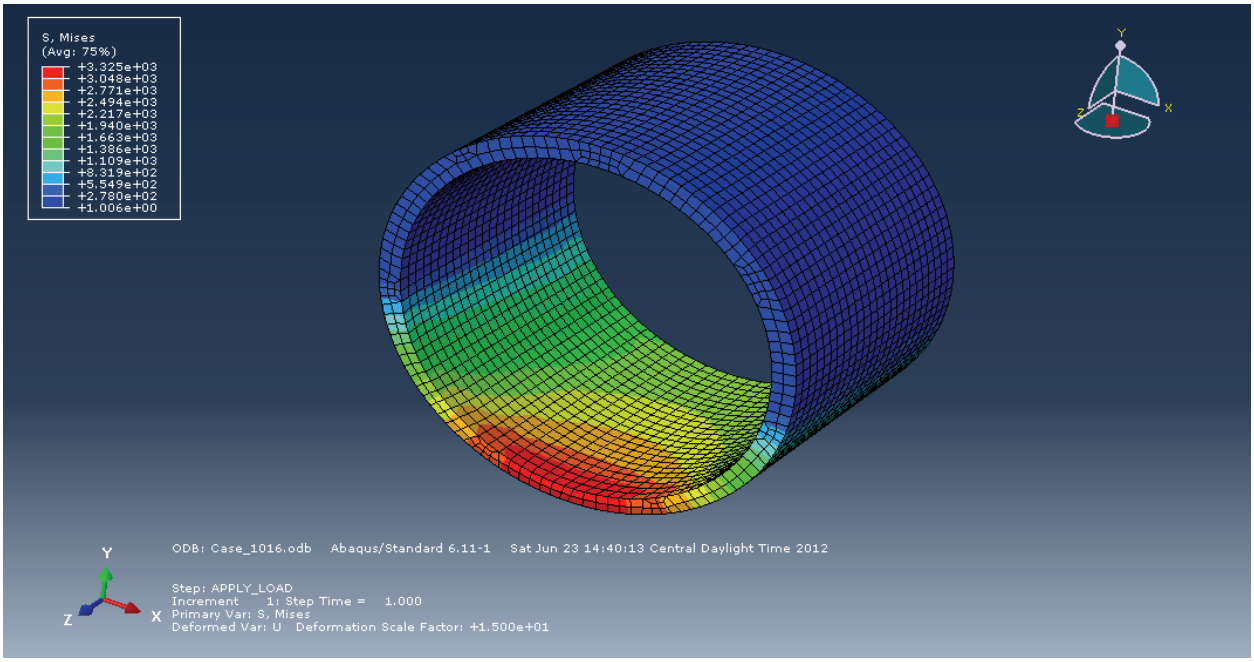

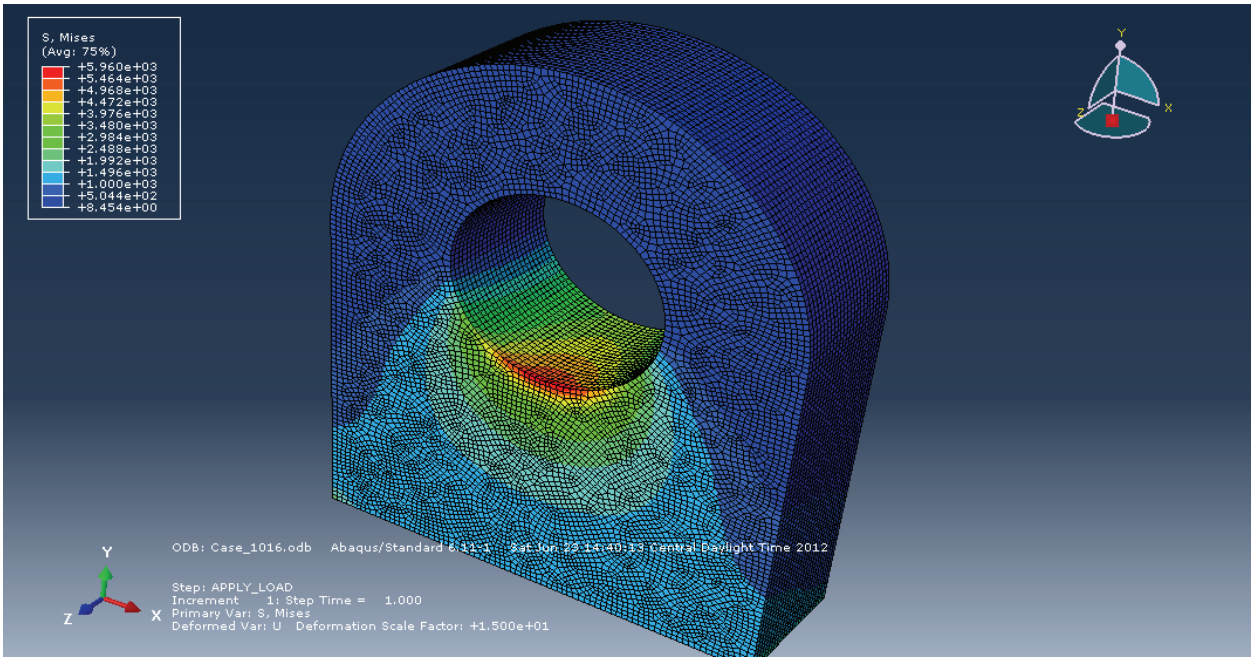

Figure E.16 – Case 1016 Yoke Plate and Sleeve Von Mises Contours (8 Inch Diameter Shaft, 6 Inch Thick Yoke, 8 Inch Span)

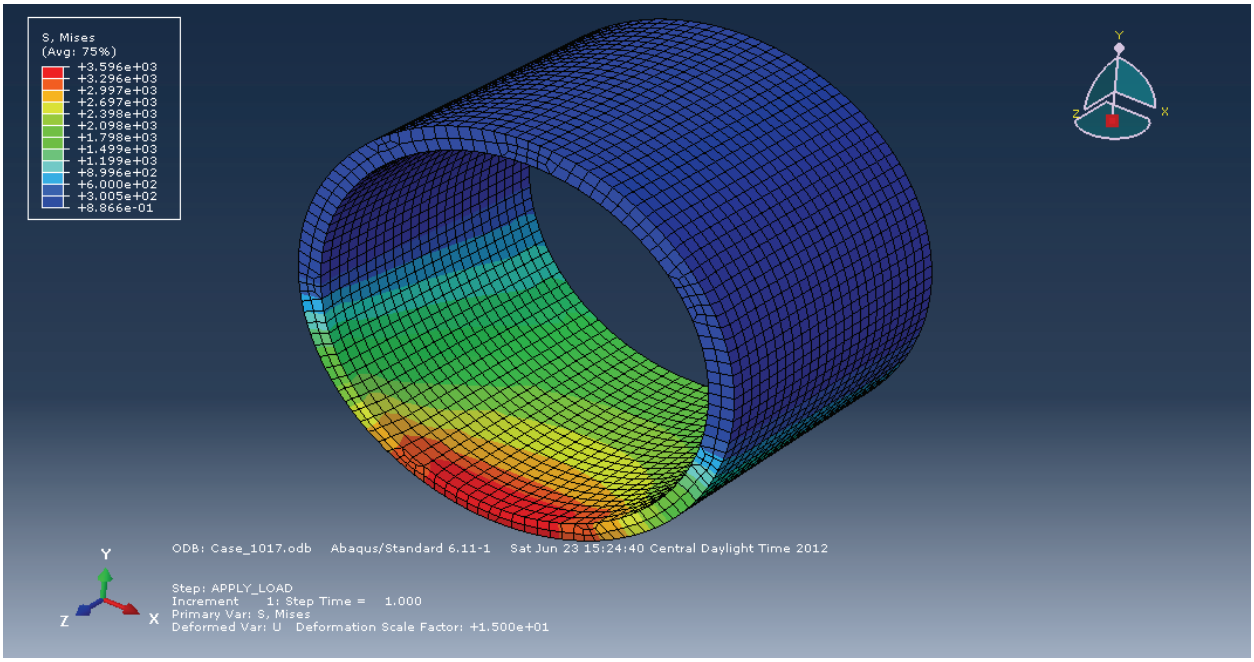

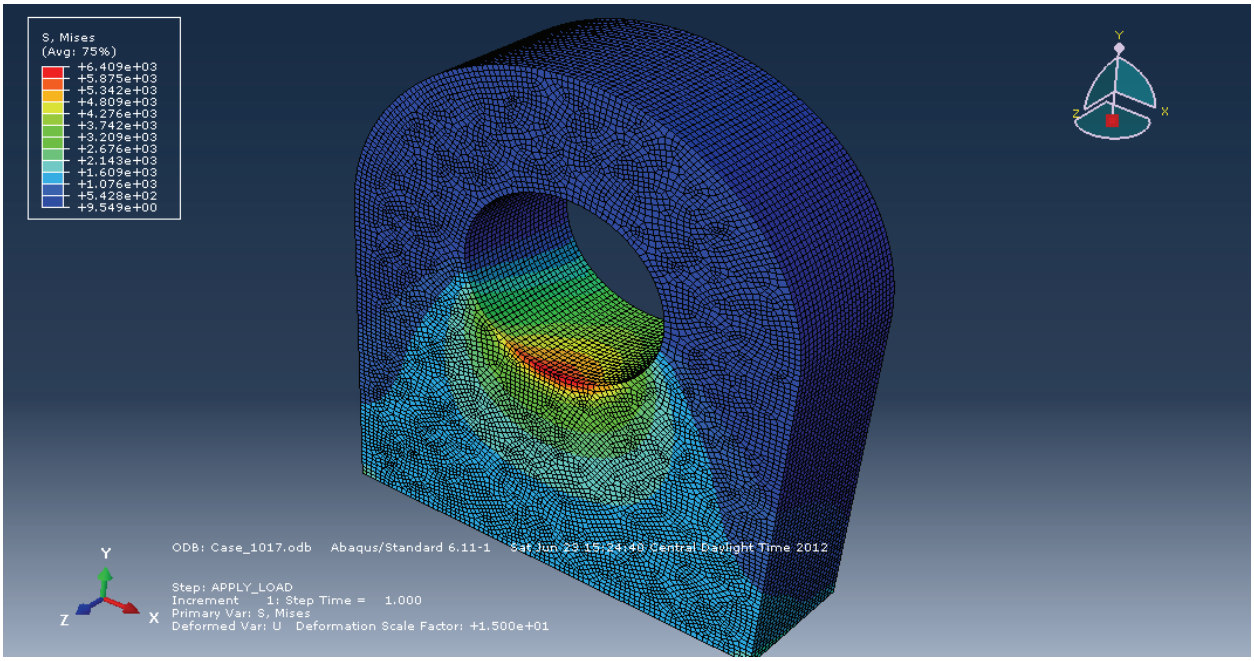

Figure E.17 – Case 1017 Yoke Plate and Sleeve Von Mises Contours (8 Inch Diameter Shaft, 6 Inch Thick Yoke, 12 Inch Span)

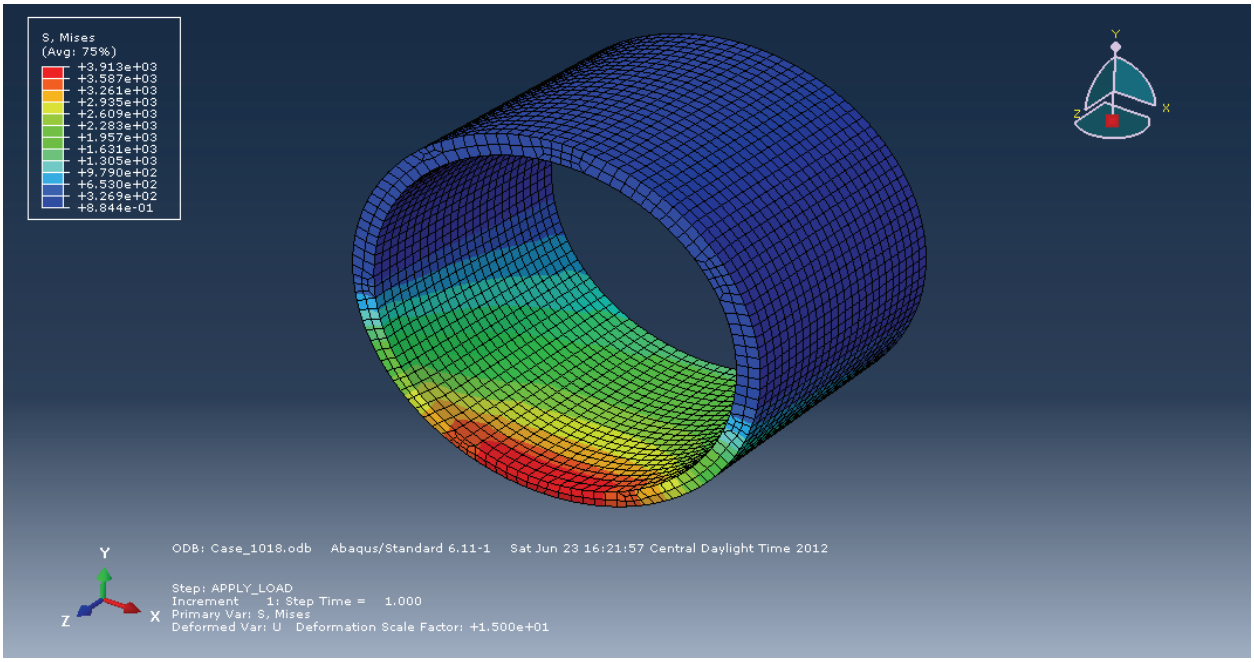

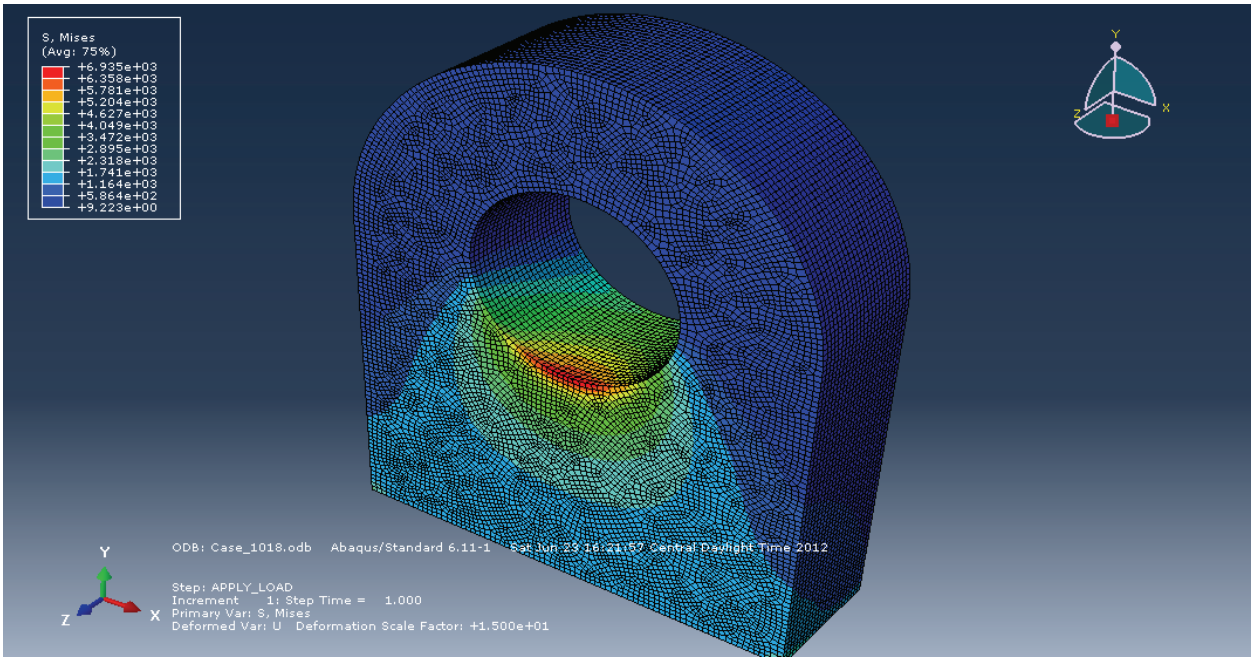

Figure E.18 – Case 1018 Yoke Plate and Sleeve Von Mises Contours (8 Inch Diameter Shaft, 6 Inch Thick Yoke, 16 Inch Span)

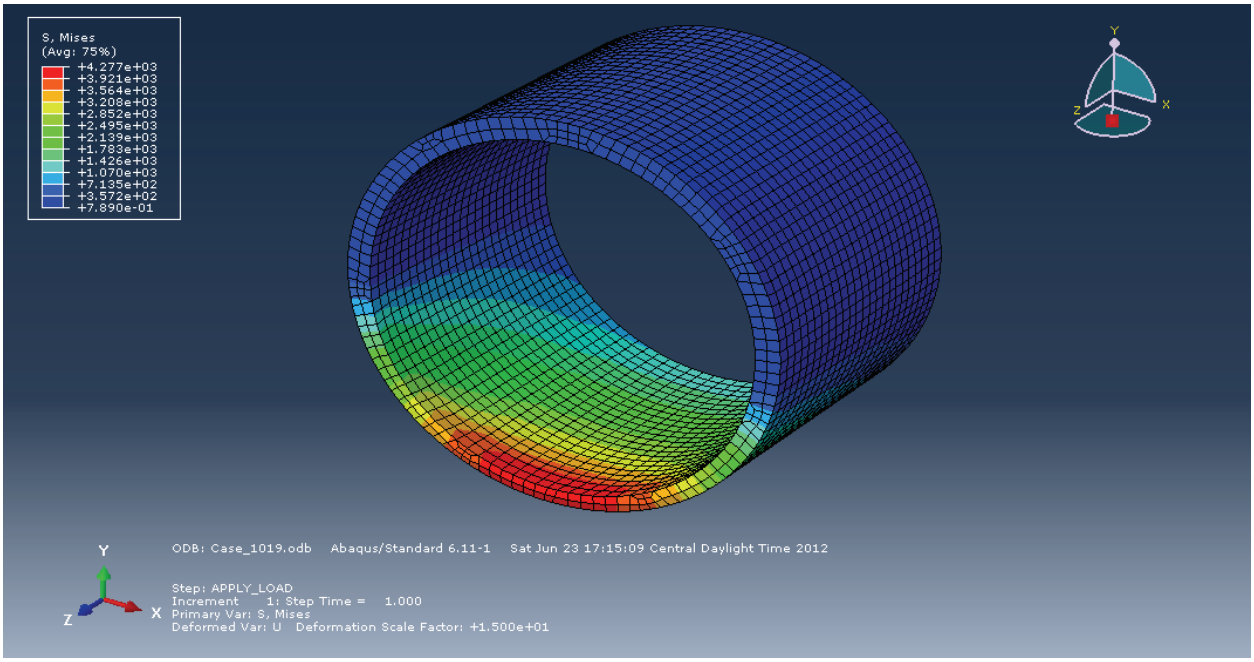

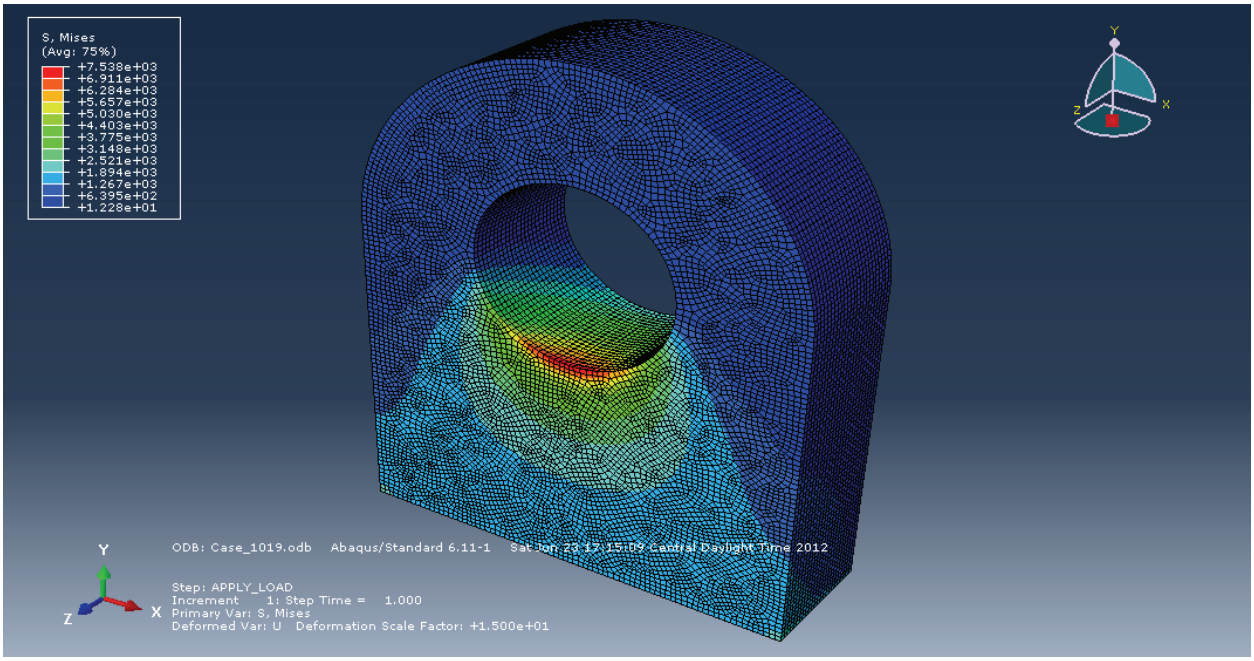

Figure E.19 – Case 1019 Yoke Plate and Sleeve Von Mises Contours (8 Inch Diameter Shaft, 6 Inch Thick Yoke, 20 Inch Span)

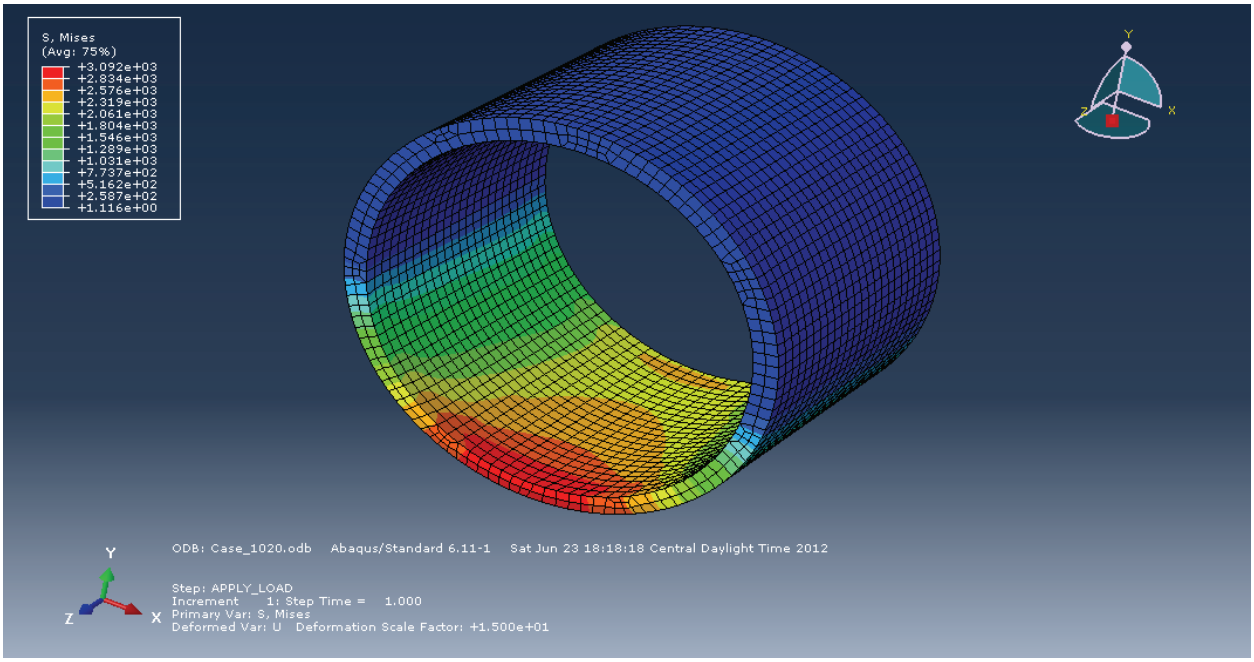

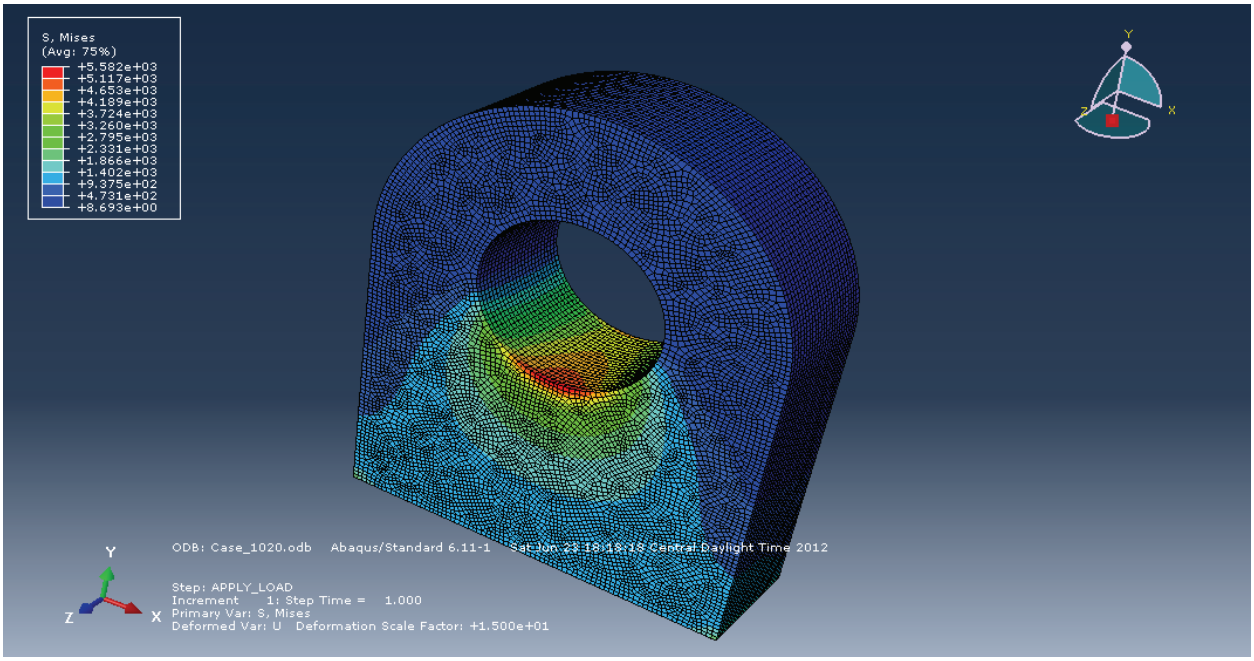

Figure E.20 – Case 1020 Yoke Plate and Sleeve Von Mises Contours (8 Inch Diameter Shaft, 6 Inch Thick Yoke, 4 Inch Span)

REFERENCES

1. U.S. ARMY CORPS OF ENGINEERS, *EM 1110-2-2702* Design *of Spillway Tainter Gates.* 2000.

2. U.S. ARMY CORPS OF ENGINEERS, *EM 1110-2-2105* Design *of Hydraulic Steel Structures.* 1993.

3. U.S. ARMY CORPS OF ENGINEERS, *EM 1110-2-2610 Lock and Dam Gate Operating and Control Systems.* 2004.

4. UNITED STATES SOCIETY ON DAMS, *2013 Annual Meeting and Conference Introduction.* http://www.ussdams.org/2013conf.html (accessed June 30, 2012).

5. SIMULA, *"Abaqus/CE User's Manual,"* http://kc-sce-31jsms1:2080/v6.11/books/usi/default.htm (accessed July 29, 2012).

6. SADD, MARTIN H., *Elasticity Theory, Applications, and Numerics, 2nd Edition. 2009.*

7. AMERICAN INSTITUTE OF STEEL CONSTRUCTION, *AISC 325 Steel Construction Manual, 13th Edition.* 2005.

8. AMERICAN STANDARD FOR TESTING MATERIALS, *ASTM A 36 The Standard Specification for Carbon Structural Steel.* 2008.

9. AMERICAN STANDARD FOR TESTING MATERIALS, *ASTM A 705 Standard Specification for Age-Hardening Stainless Steel Forgings.* 1995 (Rev. 2009).

10. ANCHOR BRONZE AND METALS, "*Copper Alloy No. C93200 SAE 660 Bearing Bronze," www.anchorbronze.com/c93200.htm.* (accessed December 4, 2011).

11. COLUMBIA INDUSTRIAL PRODUCTS, "*CIP Hydro Properties," www.cipcomposites.com/hydro.cfm/page/properties*. (accessed December 4, 2011).

VITA

Thomas Johnathan Walker was born and raised in West Sacramento, CA. He was educated in local private schools and graduated from Jesuit High School in 2000. After high school, he was accepted into the dual degree program between Saint Mary's College of CA (Moraga, CA) and Washington University in St. Louis. Per the requirements of the program, Mr. Walker studied liberal arts and physics at St. Mary's and Civil Engineering at Washington University. At the end of the 5 year program, Mr. Walker was awarded a B.A. in Liberal Arts from St. Mary's and a B.S. in Civil Engineering from Washington University in St. Louis.

Upon graduation, Mr. Walker accepted a full time position with the Sacramento District of the U.S. Army Corps of Engineers. While with the Corps, Mr. Walker gained experience with the design and construction of many large scale civil works structures including tainter gate trunnion assemblies, vertical lift gates, dams, closure structures, floodwalls, and retaining walls. In 2008, Mr. Walker became a licensed professional civil engineer in the state of California.

In 2011, Thomas Walker left his position with the Corps to pursue a career in the private sector with Black and Veatch. Thomas Walker is currently a Lead Structural Engineer with Black & Veatch, and provides structural engineering support to its clients in both the Water and Federal Special Projects Divisions.